Uppsala University
Signals and Systems

ANTI-WINDUP AND CONTROL OF SYSTEMS WITH MULTIPLE INPUT SATURATIONS

Tools, Solutions and Case Studies

Jonas Öhr

UPPSALA UNIVERSITY 2003

Dissertation for the degree of Doctor of Philosophy
in Electrical Engineering with specialization in Automatic Control at Uppsala University, 2003

ABSTRACT
Öhr, J., 2003. On Anti-Windup and Control of Systems with Multiple Input Saturations: Tools, Solutions and Case Studies, 221 pp. Uppsala. ISBN 91-506-1691-9.

Control of linear systems with saturating actuators are considered and anti-windup compensators for multiple-input multiple-output systems, and robust, almost time-optimal controllers for double integrators with input amplitude saturations, are proposed.

Windup effects are defined and anti-windup compensators aiming at minimizing the windup effects are propoaed. The design is based on 1) linear quadratic (LQ) optimization techniques and 2) heuristic design using Nyquist-like techniques and pole-placement techniques.

A root-locus like technique that can, approximately, foretell possible *directional problems* that may be present in MIMO systems with input saturations, and that can be used for design of anti-windup compensators and for selection of appropriate *static directional compensators*, is proposed.

The problem of control of double integrators via saturating inputs is addressed and a robust piece-wise linear controller that gives almost time-optimal performance is suggested. It is shown that time optimal control of a double integrator via an input amplitude limiter, is equivalent to time-optimal control of a single integrator having a rate limiter at the input. This result is expected to make the proposed controllers useful in many industrial applications. One such application, concerning control of hydraulic cylinders in container crane systems, is presented. An extension of the controller, allowing synchronous control of two integrators with input rate limitations, is proposed.

Keywords: Anti-windup compensator, saturating actuator, amplitude limiter, rate limiter, path anti-windup, double integrator, time-optimal control, container crane, spreader, hydraulic cylinder.

Jonas Öhr, Signals and Systems, Uppsala University, P O Box 528,
SE-751 20 Uppsala, Sweden. Email: jonas.ohr@signal.uu.se.

ISBN 91-506-1691-9
Printed in Sweden by Elanders Gotab, Vällingby, Sweden
Distributed by Signals and Systems, Uppsala University, Uppsala, Sweden

To my parents Anders and Marina and to my family
Helena, Harry, Hanna and Hedvig

Contents

Acknowledgments

I have many people to thank for the knowledge and experiences I have gained during my years as a Ph.D. student. Among them, I especially like to express my sincere gratitude to the following people.

To my supervisors, Prof. Anders Ahlén and Prof. Mikael Sternad. To Mikael for his uncompromising view of high scientific quality and to Anders for his uplifting spirit and because he personifies the slogan by Pirelli: *Power is nothing without Control*. May it be automatic or manual. Anders and Mikael have both shown great patient and understanding for my situation, in particular my strong attraction to large industrial plants and processes. They have both been of great, great help in the work of finishing this thesis.

To Dr. Claes Tidestav for being a good friend and for sharing his knowledge, experience and XO-cognac with me and for helping me out of the LaTeX-swamp all the way until the final moments. If I hade listen more to him, maybe this thesis hade been finished *in time*.

To Dr. Stefan Rönnbäck, who introduced me to the anti-windup problem, for believing in my ability to solve industrial control problems. When it comes to automatic control Stefan has been, and still is, my greatest source of inspiration. I wish we can work together again in the future.

I also want to thank all the people at the Signals and Systems Group and although not many of them share my interest in automatic control, they all contribute to the inspiring environment.

During the time as a PhD student I also had the pleasure working with many talented people in the industry. Among them I especially like to thank Stig Moberg, Sören Quick and Mats Isaksson and all the other people at the motion control group at ABB Robotics in Västerås, Andy Lewis at Bromma Conquip in Vällingby, Ken Lindfors and Hans Svanfelth at CC-systems in Uppsala, the people at Optimation AB in Luleå and Piteå, Per Lundqvist at NAF AB in Linköping, Ulf Magnussson at Pharmacia Biosciences in Uppsala and Mats Andersson and Nilo C. Ericsson and all the other colleges at Magasin1 AB in Uppsala.

I also want thank the Ph.D. students and the Professors at S3, Royal Institute of Technology in Stockholm, and at the Systems and Control Group, Uppsala University for good cooperation in graduate courses.

I am also grateful to John Erik Larsson, former PhD student at Luleå University of Technology, for helping me out with the case study concerning control of a paper machine headbox.

I also want to thank Prof. Petar Kokotovic and Prof. Andrew Teel for their hospitality during my short visit at UCSB.

Finally, I want to thank my dear wife and children for letting me use much of the time that was meant for them, to finish this thesis.

Jonas Öhr
Uppsala, August 2003.

Remarks on the notation

System descriptions
Most of the concepts and techniques discussed in this thesis hold for both continuous-time systems and discrete-time systems. In order to make this clear without having to present every thing twice, we use the same notation for discrete-time systems and continuous-time systems.

In continuous time, the system can be in state space form:

$$\begin{aligned} \frac{dx(t)}{dt} &= \mathbf{F}x(t) + \mathbf{G}u(t) \\ y(t) &= \mathbf{C}x(t) + \mathbf{D}u(t) \end{aligned} \tag{1}$$

or in polynomial form:

$$\boldsymbol{B}(s)\boldsymbol{A}^{-1}(s) \tag{2}$$

where s is the Laplace transform variable. In discrete time the system can be represented in state space form:

$$\begin{aligned} x(k+1) &= \mathbf{F}x(k) + \mathbf{G}u(k) \\ y(k) &= \mathbf{C}x(k) + \mathbf{D}u(k) \end{aligned} \tag{3}$$

or by the pulse transfer function:

$$\boldsymbol{B}(z)\boldsymbol{A}^{-1}(z). \tag{4}$$

When considering signals in time passing in and out of systems, the reader should think of the Laplace transform variable to be replace by the *differential operator*

$$p = d/dt \tag{5}$$

and

$$y(t) = \boldsymbol{B}(p)\boldsymbol{A}^{-1}(p)u(t) \; . \tag{6}$$

Similar in the discrete time case, the z-operator is replaced by the forward-shift operator q, defined by

$$qy(k) = y(k+1) \; . \tag{7}$$

The signal model in discrete time is then

$$y(k) = \boldsymbol{B}(q)\boldsymbol{A}^{-1}(q)u(k) \; . \tag{8}$$

We will use the simple notation

$$\begin{bmatrix} \nu x \\ x \end{bmatrix} = \left[\begin{array}{c|c} \mathbf{F} & \mathbf{G} \\ \hline \mathbf{C} & \mathbf{D} \end{array}\right] \begin{bmatrix} x \\ u \end{bmatrix} \tag{9}$$

for both the continuous time and the discrete time state space representations. Here, ν is either one of the operators

$$\nu = \begin{cases} p = \frac{d}{dt} & \text{continuous time case} \\ q = \text{forward shift} & \text{discrete time case .} \end{cases} \tag{10}$$

Similarly the notation

$$\boldsymbol{B}\boldsymbol{A}^{-1} \tag{11}$$

is used for both the continuous time and the discrete polynomial representations.

For polynomial models described in terms of a state space description, i.e.,

$$\boldsymbol{B}\boldsymbol{A}^{-1} = \begin{cases} \mathbf{C}(s\mathbf{I} - \mathbf{F})^{-1}\mathbf{G} + \mathbf{D} & \text{continuous time case} \\ \mathbf{C}(z\mathbf{I} - \mathbf{F})^{-1}\mathbf{G} + \mathbf{D} & \text{discrete time case,} \end{cases} \tag{12}$$

we will use the simple notation

$$\boldsymbol{B}\boldsymbol{A}^{-1} \sim \left[\begin{array}{c|c} \mathbf{F} & \mathbf{G} \\ \hline \mathbf{C} & \mathbf{D} \end{array}\right] \; . \tag{13}$$

Operators and functions
For a matrix $\mathbf{R} \in \Re^{nxn}$, the expression $\mathbf{R} > 0$ means that $\mathbf{R}$ is positive definite.

The suffix $*$ represents transpose-conjugate of a polynomial matrix $\boldsymbol{H}$. In the continuous time case, $\boldsymbol{H} = \boldsymbol{H}(s)$, we then have that

$$\boldsymbol{H}^*(s) \triangleq \boldsymbol{H}^T(-s). \tag{14}$$

In the discrete time case, $\boldsymbol{H} = \boldsymbol{H}(z)$, we then have that

$$\boldsymbol{H}^*(z) \triangleq \boldsymbol{H}^T(z^{-1}). \tag{15}$$

CHAPTER 1

Introduction

CO ntrol of a dynamic system requires manipulable inputs. The manipulation is usually transmitted (or transferred) to the system via *constrained actuators*. In many technical systems actuators are *transducers* which transforms a low power signal, usually electric, into high power ”action”. Examples are valves for flow control and high power electronics for electric power control. The latter can in a second step e.g. be used for torque control of an electric motor. In most cases, properly dimensioned actuators will *saturate* even under normal operation.

What happens if, or when, actuators saturate depends critically on the ability of control strategy (the controller) to handle a saturation event as well as on the properties of controlled system. Some systems are easier to control via constrained actuators than others. Some controllers are better suited to handle saturation events than others. The following example illustrates this.

EXAMPLE 1.1: LINEAR CONTROLLERS AND SATURATION EFFECTS

Consider three equal linear systems given by

$$\mathcal{G} = \frac{1}{s+1} \tag{1.1}$$

controlled by the three different controllers shown in Figure 1.1. The first system is controlled by a pure feed-forward controller, the second by a PI-controller and the third by a P-controller. By ignoring the saturation in the loops, the transfer functions from the reference to the output are, however, the same in the three cases namely

$$\tag{1.2}$$

$$\mathcal{G}_r = \frac{5}{s+5} \; . \tag{1.3}$$

Consequently, the reference-step responses of the three systems are identical as shown in Figure 1.2.

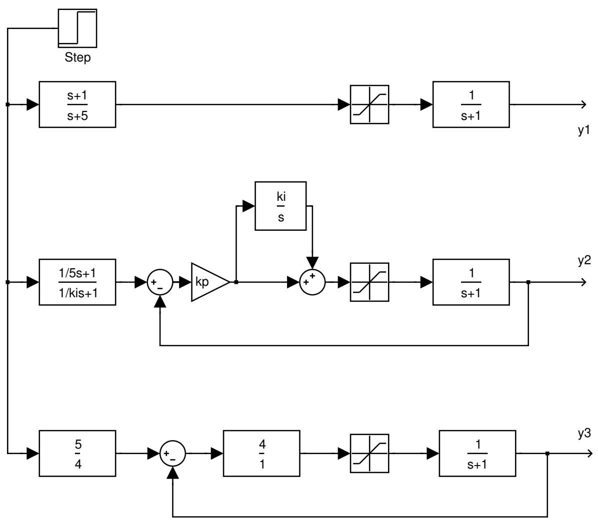

Figure 1.1: Three different systems having equal linear response but different saturation effects. Here, $kp = 9,\ ki = 2.8$.

But in the real case, when the inputs saturate, they behave quite differently from each other. See Figure 1.3. Loosely speaking one could say that the first system (y_1) needs more feedback the second (y_2) needs less and the third (y_3) behaves well (at least what saturation concerns). The second system suffer from *integrator windup*, a phenomenon which has been discussed in the literature for many decades. The first system suffers from the fact that not enough energy was put into the system sufficiently fast. We say that such systems do not *recover from saturation* sufficiently fast. Or, we say that the *de-saturation transient* does not decay sufficiently fast. These undesired phenomena and what causes them, and how to overcome them, are discussed in this thesis.

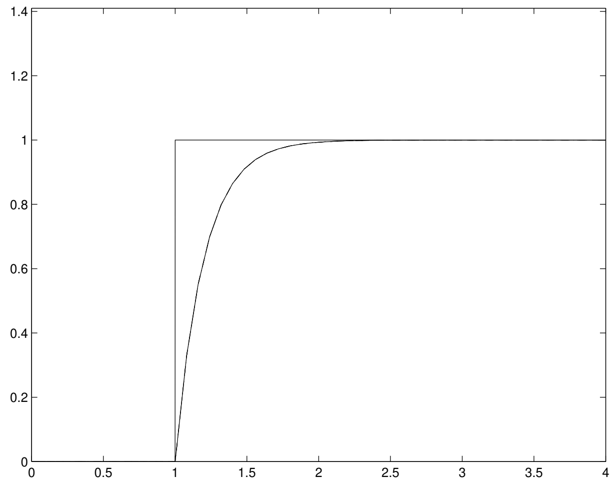

Figure 1.2: Equal linear response.

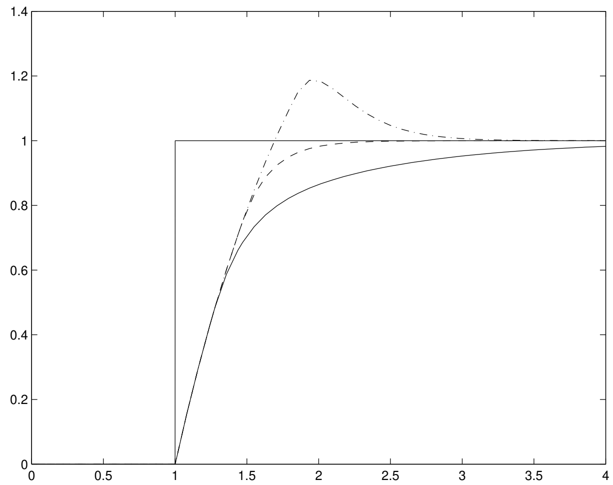

Figure 1.3: Different saturation effects. The solid line represents the response of the feed-forward control system, the dash-dotted line the response of the PI-control system, and the dashed line represent the response of the P-control system. Here, the saturation limits are ± 2.

1.1 Control of linear systems

Seen from a control engineering perspective, one of the main purposes of describing a dynamic system by a linear dynamic model is that this should simplify the design and the implementation of a controller. Whether such a controller will perform well or not depends much on how well the linear model captures the most important dynamic properties of the real system. Theory and design of linear control systems are discussed in many textbooks on control. A representative reference on linear systems theory is Kailath [1]. Design of linear controllers in general are discussed in e.g. [2][3][4][5][6][7] and design of linear optimal controllers are discussed in [8][9][10][11]. Representative texts on design of linear MIMO controllers are [12][13]. Detailed discussions exclusively devoted to theory, design and tuning of PID controllers are provided in [14].

Many dynamic systems behave as ”almost” linear, under certain operating conditions, and therefore linear control theory is widely applicable in reality. But quite often, e.g. when operating a system on its limits, different kinds of nonlinearities make them self known and may degrade the stability and performance properties to such an extent that they are no longer acceptable. These nonlinearities must then be taken into account when designing and implementing the controller. Actuator nonlinearities, such as amplitude- and rate limiters, appearing at the plant input, are examples of such nonlinearities. By introducing amplitude- and/or rate limiters at the input of an otherwise linear model, one will be able to describe a significantly larger class of dynamic systems in such a way that the controller design results in good performance.

1.2 Control of linear systems with saturating actuators

Control of linear systems with saturating actuators have been studied for many decades and the research activity has increased dramatically during the last decade. A chronological bibliography reaching up to 1995 is presented in [15] and a more recent overview is provided in [16]. The least demand we put on any control system is that it is stable under under normal operation. Stability of control systems with saturating actuators, and design of controllers where input saturations are taken into account *a priori*, are discussed in e.g [17][18][19][20][21][22][23][24][25][26][27][28][29]. See also the articles in [16]. In some cases, when global stability can not be achieved, it is desirable to know the domain of attraction (region where the system is stable). Estimation of such domains are discussed in e.g. [30]. See also the references therein.

Among the proposed control concepts, we can distinguish three that are used more often than others in practice, namely

- Constrained Model Predictive Control (CMPC)
- Scheduled controllers (i.e. gain scheduling or piecewise-linear control)
- Anti-Windup Compensators (AWC)

Model Predictive Controllers are, besides simple SISO PI-controllers, the most land-winning regulators used in chemical industries for the control of MIMO systems with saturations. Overviews and references can be found in Qin and Badgwell (1997) [31] and Roberts (1999) [32]. Connections to adaptive control are, with a humble attitude, provided by Bitmead et'al in [33]. Recent results on MPC solutions, allowing heavy computations to be carried out offline, i.e. not in real-time, are presented in Bemporad et'al in [34]. Recent results on connections between anti-windup compensators and MPC are presented in [35].

Scheduled controllers (also called piecewise-linear controllers or gain scheduling schemes) are also often used in practice and can be used to handle different kinds of nonlinearities. Scheduled controllers are e.g. widely used in the aerospace industry. Discussions concerning design of scheduled controllers for input saturation systems can be found in e.g. [23][25][36][37].

Anti-windup compensators are widely used in practice for the control of systems with saturating actuators. Design of anti-windup compensators can be carried out using linear design methods which explains its usefulness and popularity among control engineers. We will now focus our attention to anti-windup compensators.

1.3 Anti-windup compensation: an overview

An *anti-windup compensator* consists of a *nominal* (most often linear) controller appended with anti-windup compensation. An important property of anti-windup compensation is that it leaves the loop unaffected as long as saturation does not occur. Consequently, the control action provided by the anti-windup compensator is identical to that of the nominal controller, as long as the control signals operate within the saturation limits. The design can be split into two parts where the first part concerns the linear controller and the second the anti-windup modification. Hence, when designing anti-windup compensators in this way, input saturations are taken into account *a posteriori*.

Anti-windup techniques have been discussed in the academic literature for many decades and have probably been used in industrial applications at least as long. Important work on anti-windup techniques can be found in e.g. Fertik and Ross [38], Hanus [39],[40], Glattfelder and Schaufelberger [41], Åström and Wittenmark [2], Doyle et'al [42], Åström and Rundqwist [43], Walgama and Sternby [44], Rönnbäck et'al [45], Rundqwist [46], Sternad and Rönnbäck [47], Kothare et'al [48], Öhr et'al [49][50], Teel and Kapoor [51][52], Edwards and Postlethwaite [53], Kapoor and Teel [54], Hippe and Wurmthaler [55].

Anti-windup was originally used for preventing the integrator state in PID controllers from growing large and cause overshoots and limit cycles. An early contribution to the academic research reports on automatic control, concerning anti-windup, is the one by Fertik and Ross from 1967 [38]. Other representative reports on anti-windup for PID controllers are [2][14][43][46]. See also [41]. Anti-windup for PID controllers are also discussed in many textbooks on automatic control.

Whenever a linear controller has been designed under the assumption that its output will affect the plant input directly and unaltered, then, any input nonlinearity, such as rate- and/or amplitude saturation, causing deviation between the controller output and the plant input, almost always degrades the performance, and stability of the closed loop system may be put at risk. [1] Anti-windup compensation is the simplest and most commonly used modification of a linear controller, aiming at retaining stability and most of the performance in such a system. In this thesis we will show how reliable anti-windup compensators can be designed by the use of linear methods.

Even though the underlying design intentions may have been the same when developing many of the proposed anti-windup compensators, namely to make the constrained-input closed-loop system behave well even when the inputs saturate, the proposed techniques and modifications have been motivated by different design goals. The early proposed anti-windup techniques consider windup as a phenomenon that occurs only in the states of the controller. Therefore, most of the early proposed designs of anti-windup compensators take only the properties of the input limiters, the properties of the nominal controller, and the desired proper-

[1] One example of an exception is when a linear stable controller and a linear stable plant would form an unstable linear closed loop due to e.g. plant variations. Then, amplitude saturation of the control signal will result in a closed-loop system with bounded states.

ties of the resulting anti-windup compensator, into account. The properties of the controlled plant are often ignored. Reliable design methods take all components in the feedback loop, i.e. *controller-limiters-plant*, into account. It should be pointed out, however, that such design methods require a reliable plant model to be known. In case reliable models are difficult to find, methods that do not take the plant into consideration may be preferable.

Next, some of the anti-windup compensators proposed over the years will be discussed in more detail. Similar, but in some aspects more detailed explanations of connections between different schemes and proposed designs, are provided in the theses by Rundqwist [46], Rönnbäck [56], Kothare [57] and Bak [58].

1.3.1 Observer based anti-windup compensators

The observer based anti-windup compensator (OBSAWC), as a general structure, was proposed in 1984 by Åström & Wittenmark [2]. Many of the anti-windup compensators that have been proposed over the years can be cast into the OBSAWC structure. Some of them were actually proposed even before the OBSAWC structure was formally defined in [2], see [44]. All anti-windup compensators discussed in this subsection can be cast in to the OBSAWC structure.

In Åström and Wittenmark (1984) [2] the authors provide some design guidelines and they propose the dead-beat observer anti-windup compensator for discrete-time controllers. The design goal is to adjust the states of the anti-windup compensator so that its output, u, tracks the the saturated ditto, v, with dead-beat dynamics.[2] The method ignores the properties of the plant as well as the properties of the nominal controller. This anti-windup compensator gives nice performance in some systems whereas it destabilizes others.[3]

One of the most frequently discussed anti-windup compensators is based on the so called *Conditioning technique* suggested by Hanus (1987) [59]. The design goal is the same as in the case of the dead-beat observer anti-windup compensator, namely to adjust the states of the anti-windup compensator so that its output, u, tracks the the saturated ditto, v. In this case, however, this tracking depends on the dynamics of the reference pre-filter. The method ignores the properties of the

[2] Note that we denote the controller output by u and its saturated ditto by v. This notation is used in some reports whereas in others, e.g. in [2], the notation is reversed.

[3] The method with dead-beat compensation is probably more suitable for bumpless transfer than for anti-windup. When used for bumpless transfer, the output from the latent controller tracks the output from the active with dead-beat dynamics.

plant. Unfortunately, this compensator suffers from the drawback that anti-windup is accomplished by feedback of the possible saturated plant input, via the plant-output reference filter. Such a reference filter is most often tuned for improving the servo properties of the linear system and sometimes *happens also* to be appropriate for anti-windup compensation. Some problems associated with this drawback are discussed in [60].

In Campo & Morari [61], the researches propose an anti-windup compensator having the special property that when saturation occurs, the controller states are no longer driven by the control error. The researchers also show that in the case of error-feedback, i.e., when not using a reference pre-filter, their proposed design is equivalent to the conditioning technique discussed above. This strategy is also discussed in [5]. The method ignores the properties of the plant. The researches also provide conditions for when this compensator can not be used. Furthermore, they show a case where these basic conditions for usefulness are fulfilled, but where the compensator gives an unstable system due to plant directionality problems. Such problems where discussed by Doyle et'al (1987) [42]. In [61] the researches suggest that directionality compensation can be used to overcome the problems. The idea is to preserve the direction of the controller output, $u(t)$, in the plant input, $v(t)$. By this modification, MIMO systems that are not stable when having the standard, decentralized, amplitude limiter in the loop, may become stable. Direction compensation will be discussed and used later later in this thesis, and one of the examples from [61] is used to illustrate the abilities of the design strategies proposed in this thesis.

In [48] and also in [57], the authors suggest a unified framework for observer-based anti-windup designs and interprets many earlier proposed anti-windup compensators in terms of there framework.

A rigorous investigation of what OBSAWC:s can accomplish is provided by Kapoor et'al in [54]. There, the researchers give sufficient conditions for when observer-based anti-windup compensation can stabilize the system and a new design is proposed. This design does not guarantee stability, which still depends on the plant dynamics and the gain of the nominal controller. However, it is shown, also in [54], how the gain of the nominal controller can be adjusted in order to achieve stability.

1.3.2 General linear anti-windup compensators

The *general linear anti-windup compensator* (GLAWC) was, to my knowledge, first proposed by Rönnbäck 1991 [45] for SISO systems. The GLAWC can be regarded as an extension of the OBSAWC. This anti-windup compensator is sometimes named *dynamic compensator* in the literature. The reason for this is that the anti-windup *modification* takes the form of a filter where, in a polynomial representation, both the numerator and the denominator can be selected independently of each other. The corresponding modification of the OBSAWC is a polynomial and, hence, the OBSAWC lacks half degree of freedom compared to the GLAWC.

Many anti-windup compensators that have been proposed lately belong to GLAWC class and most of the proposed design methods for general linear anti-windup compensators, in fact, take the whole system (controller-limiters-plant) into consideration. Some representative reports are [62][56][49][53][50][51][52][63][55].

1.3.3 Anti-windup and bumpless transfer

Many control systems consists of several alternative controllers and it is often desirable to obtain smooth transfers when switching between the controllers. In other words, it is desirable to obtain a *bumpless transfer*. Anti-windup compensators can sometimes be used to obtain bumpless transfers in such systems. Such controller schemes are discussed and proposed in e.g. [59][2][64][65][66].

1.4 Anti-windup compensation: a second step in controller design or a separate problem ?

Most often, when discussed in the literature and also in this thesis, anti-windup design is considered as a second step in the design of a controller used for the control of a system with saturating inputs. However, if the nominal controller was designed, let us say, by someone else at an earlier stage and if it works very well, except when saturation occurs, then anti-windup compensation can be considered as a separate control problem.

For example, assume that a simple decentralized PI controller is used for control of a MIMO system with saturating actuators and that the system performs well except when saturation occur. In many cases it may be undesirable to replace the whole controller by a more sophisticated controller. However, a sophisticated anti-windup modification may be an option in such a situation. This sometimes motivates the use of anti-windup modifications that are more complex than the nominal controller itself.

1.5 Outline of the thesis

The analysis and design methods discussed and presented in this thesis are rather simple in the sense that most engineers with a basic knowledge in linear systems, pole-placement techniques, frequency domain techniques, root-locus techniques, linear quadratic control methods, and simple logic operators will be able to understand, and hopefully use, the techniques.

We open the discussion in Chapter 2 by presenting some standard limiters causing control signal saturations when present at the plant inputs in the systems considered in later chapters. The notation ψ will be used to represent these limiters.

In Chapter 3, windup effects are defined, as deviations between the input- and the output signals in a linear (ideal) closed loop system, and a closed loop system having a limiter ψ at the plant input. The degree of windup depends on the degree of feedback in the system with ψ at the input, on the properties of the limiter ψ itself, and on how the system is operated.

The degree of feedback around ψ, in the sequel often characterized by the *loop gain*, can be controlled by the anti-windup compensator. In addition to the loop gain, we will investigate the properties of the dynamics controlling de-saturation transients. In Chapters 5 and 6 we discuss design of anti-windup compensators, aiming at adjusting the loop gain and the transient dynamics so that windup effects are minimized.

In Chapter 4 we propose one OBSAWC scheme and one GLAWC scheme for MIMO system, both in polynomial form. The main part of this chapter is concerned with processes, controllers and compensators represented in polynomial (input-output) form. However, connections to state-space descriptions will be discussed. After presenting the OBSAWC and the GLAWC we will proceed discussing design strategies which we split into two categories: 1) design based linear quadratic (LQ) optimization techniques and 2) heuristic design using Nyquist-like techniques, pole-placement techniques and a root-locus like technique.

The heuristic design is quite craftsman-like and it is here treated more in terms of a discussion than a stringent design methodology. What motivates this discussion is that it is, in some applications, highly desirable to keep windup effects on an acceptable level by making as small adjustments as possible to the controller. The heuristic design strategy is therefore appropriate, e.g. in applications where low complexity is a critical issue. Furthermore, as we pointed out earlier, it requires only basic knowledge on linear control systems. We also show that more general directional compensators than the one discussed in Campo and Morari [61], can be used for stabilization of systems having "directional problems". Furthermore, we propose a simple "root-locus like" method that foretell *possible* directional problems and that can be used for the selection of appropriate directional compensators. This method is used in some of the examples in Chapters 5-8.

The LQ-design technique is characterized by the property that one part of the compensator decouples the system with saturating inputs, into one linear part, and one nonlinear part. The linear part, and the nonlinear part of the system having saturations in the loop, can then be design and tuned separately and (more of less) independently of each other. Nominal underlying design goals such as disturbance attenuation are taken into consideration only in the linear system design. Control of the nonlinear part takes the form of control to the origin of an input-saturating system and most of the nominal design goals can be disregarded in this design. The LQ-design technique is discussed in Chapter 5. The directionally problems mentioned above, are implicitly taken care of when using the LQ-design method. The LQ-design method requires a model of the plant.

The discussion in the last two chapters, i.e. Chapter 9 and 10 do not concern anti-windup compensators.

In Chapter 9 control of double integrators via saturating inputs are discussed and a piece-wise linear controller that gives almost time-optimal performance is proposed. The proposed controller combines the excellent performance of a true time-optimal controller with the almost unbeatable robustness properties of a simple PD-controller. We also show that time optimal control of a double integrator with an input amplitude limiter, is equivalent to time-optimal control of a single integrator having a rate limiter at the input. This chapter also includes a comparative study along the lines of [67].

In Chapter 10, we present a real case where the proposed almost time-optimal controller is used for the control of hydraulic cylinders in container handling systems. Furthermore, we propose an extension of the controller allowing us to control two cylinders synchronously. The controller is, at present time, in use in approximately fifty container cranes and spreaders all over the world, all performing very well [68].

1.6 Conference papers

- J. Öhr, Mikael Sternad and Anders Ahlén, ”Systematic Anti-Windup Compensator Design for Multivariable Systems”, *Proceedings of the Swedish Control Meeting'96*, Luleå, Sweden, June 6-7, p. 168-172, 1997.
- J. Öhr, Mikael Sternad and Anders Ahlén, ”Anti-windup Compensators for Multivariable Systems”, *Proceedings of the ECC'97*, Brussels, Belgium, July 1-4, paper 496, 1997.
- J. Öhr, Stefan Rönnbäck and Mikael Sternad, ”H_2-optimal anti-windup performance in siso control systems”, SIAM'98, Jacksonville, FL, USA, 1998.
- J. Öhr and Mikael Sternad, ”LQ-baserad anti-windup kompensering via tillståndsåterkoppling i MIMO system”, *Proceedings of the Swedish Control Meeting'98*, Lund, Sweden, July 11-12, p. 227, 1998.
- J. Öhr, ”Control of a Paper Machine Headbox with Saturating Inputs”, *Proceedings of the* 1^{st} *Europoly Workshop on Polynomial Systems Theory and Applications*, Glasgow, UK, April 15-16, p. 127-129, 1999.
- J. Öhr, Jan-Olov Olsson, Andreas Stattin and Stefan Sundström, ”Tryckreglering i Starklutsaccumulator med Varierande ångflödesbegränsning”, *Proceedings of the Swedish Control Meeting'2000*, Uppsala, Sweden, Juni 7-8, p. 270-271, 2000.
- S. Moberg, M. Isaksson, J. Öhr, G. Hovland, S. Quick and S. Hansen, ”Automatisk trimning av industrirobot”, *Proceedings of the Swedish Control Meeting'2002*, Linköping, Sweden, May 29-30, p. 88-91, 2002.

CHAPTER 2

Linear systems with input rate- and amplitude saturation

We open the discussion in this chapter by presenting the *nominal system* which we in the sequel will define as a linear feedback controller used for the control of a linear plant having amplitude- and/or rate limiters at the input. Then, models commonly used for describing the functionality of amplitude- and rate limiters, [14],[69] will be defined and described. We will also discuss a simple and commonly used technique for compensating other static input nonlinearities so that the standard rate- and/or amplitude limiter can replace the more complicated nonlinearity. The terms *input constrained* and *input saturation* are often used in the text of this thesis whenever an amplitude and/or rate limiter, as they are defined in this chapter, appear at the plant input.

2.1 The nominal system

Both the continuous-time and the discrete-time cases will be treated simultaneously. The reader should think of polynomial arguments as being either the derivative operator $p = d/dt$, the forward shift operator q or there transform variables s and z respectively. The δ-operator form proposed by Middleton & Goodwin in [70] and also discussed in [5], and the backward shift operator q^{-1} can also be used. Whenever we use the expression ”causal/proper”, then causal refers to discrete-time systems whereas proper refers to continuous-time systems.

Plant

We will consider a class of linear time-invariant (LTI) systems with m outputs, which are controlled by p inputs, $v = \psi(u)$ where u is the control action and $\psi(\cdot)$ represents rate- and/or amplitude limited actuators, discussed and defined later in this chapter. These systems are here most often represented by a right matrix fraction description

$$y = \boldsymbol{B}\boldsymbol{A}^{-1}(\psi(u) + \beta) \; . \tag{2.1}$$

Here y is the $m|1$ vector of outputs whereas the $p|1$ vector β represent external input disturbances. The plant is assumed to be stable or marginally stable.[1] This means, in particular, that we allow single integrators and double integrators in the plant dynamics. In the following we will often say that control signals *saturate*. We thereby mean that the actuator operates outside its ideal region so that $\psi(u) \neq u$. The notation v is often used instead of $\psi(u)$.

Nominal Controller

As a starting point of our discussion, a *nominal* linear feedback controller

$$\boldsymbol{R}u = -\boldsymbol{S}y + \boldsymbol{T}r \tag{2.2}$$

is assumed to be designed to fulfill goals specified for the linear closed loop system. In the sequel we call this the *nominal design* problem. In (2.2), r represents the reference for the plant output y. We require that the controller is causal/proper but not necessarily strictly causal/proper.

Linear closed loop system

The closed loop linear system, obtained by connecting (2.2) to the plant (2.1) when $\psi(u) \equiv u$, is assumed to be asymptotically stable. Its plant output and controller output, are given by

$$\begin{aligned} y_l &= \boldsymbol{B}\boldsymbol{\alpha}^{-1}(\boldsymbol{T}r + \boldsymbol{R}\beta) \\ u_l &= \boldsymbol{A}\boldsymbol{\alpha}^{-1}(\boldsymbol{T}r - \boldsymbol{S}\boldsymbol{B}\boldsymbol{A}^{-1}\beta) \\ \boldsymbol{\alpha} &\stackrel{\Delta}{=} \boldsymbol{R}\boldsymbol{A} + \boldsymbol{S}\boldsymbol{B} \end{aligned} \tag{2.3}$$

respectively. The expressions (2.3) are derived in Appendix A.1.1.

We assume the plant (2.1) and the controller (2.2) to be such that large values, or rapid changes, in the reference r and/or in the disturbances β may (or will) force the input to saturate.

[1]Marginally stable means that poles can be located on the stability margin.

2.2 Input rate- and/or amplitude limiters

The class of input limiters considered in this thesis will be divided in three subclasses denoted as follows:

$$\psi(u(t)) \;=\; \begin{cases} \sigma_a^b(u(t)) & \text{amplitude limiter,} \\ \rho_c^d(u(t)) & \text{rate limiter,} \\ \rho_c^d[\sigma_a^b(u(t))] & \text{amplitude and rate limiter .} \end{cases} \tag{2.4}$$

These limiters will be defined next.

2.2.1 Amplitude limiter

For the scalar $u(t)$, the corresponding amplitude-saturated value, denoted $\sigma_a^b(u(t))$, is defined by

$$\sigma_a^b(u) \triangleq \begin{cases} b & \text{if } \; u \geq b, \\ a & \text{if } \; u \leq a, \\ u & \text{otherwise .} \end{cases} \tag{2.5}$$

This amplitude-limiter function can also be obtained and described by

$$\sigma_a^b(u(t)) = \max[a, \min(b, u(t))] \; . \tag{2.6}$$

For a vector u having p elements the de-centralized (individual) saturation function is given by

$$\sigma(u(t)) \triangleq \begin{pmatrix} \sigma_{a_1}^{b_1}(u_1(t)) \\ \vdots \\ \sigma_{a_p}^{b_p}(u_p(t)) \end{pmatrix} \; . \tag{2.7}$$

When the limits a and b are not important for the discussion they will sometimes be omitted and amplitude limiters will be denoted simply by σ.

2.2.2 Rate limiter

A rate limited (or rate saturated) signal $u(t)$, denoted $v(t)$, will according to (2.4) be written as

$$v(t) \;=\; \rho_c^d(u(t)) \; . \tag{2.8}$$

A simple and commonly used rate limiter model consists of an integrator controlled by a high gain feedback via an amplitude limiter and is defined by the following equations:

$$\begin{aligned} \dot{v}(t) &= \sigma_c^d(w(t)) \\ w(t) &= K(u(t) - v(t)) \ . \end{aligned} \tag{2.9}$$

See also Figure 2.1. The value of the constant K should be selected sufficiently

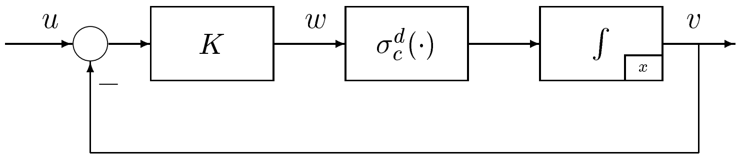

Figure 2.1: A simple model of a rate-limiter

large with respect taken to expected frequencies in the input u under normal operation. Too high values of K imply noise sensitivity. [2] Note that this type of rate limiter has the property that v ramps-up (or down) with a rate d (or c) until it reaches the value of u, i.e., $v = u$ in steady-state. This type of rate limiter model has its real counterpart in e.g. a DC-motor servo, where the input $\sigma_c^d(\cdot)$ could be voltage and the output is the motor-shaft angle, controlled by a high gain feedback.

2.2.3 Combined rate- and amplitude saturation

Most physical rate limiters are also limited in amplitude. We therefore introduce the combined rate- and amplitude limiter and we present two slightly different models. These are shown in the Figures 2.2 and 2.3 respectively. The one in Figure 2.2 has an amplitude limiter σ_a^b inside the integrator. A discrete time version of such a limiter is described in more detail in (2.10)-(2.11). In the figure this is indicated by the σ-symbol in the upper-right corner of the integrator. The one in Figure 2.3 limits the amplitude before it enters the rate limiter. The rate limits are c and d for down-ramping and up-ramping respectively.

[2] A typical value used by SAAB in the control design for the fighter JAS 39 Gripen is $K \approx 10$ [71].

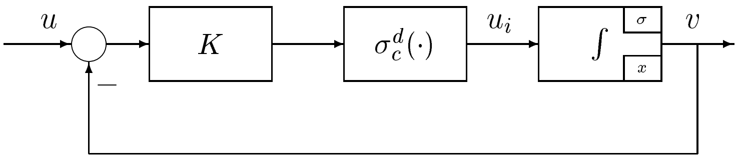

Figure 2.2: Model of an amplitude and rate-limiter. The amplitude of v is limited inside the integrator. This is indicated by the σ-symbol in the upper-right corner of the integrator. These amplitude limits are $a,\ b$.

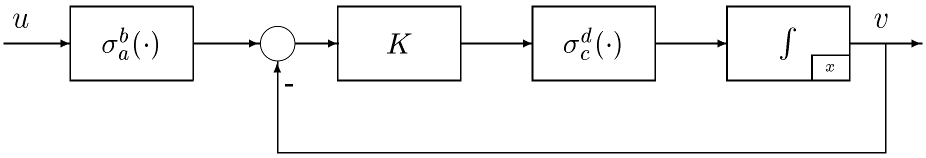

Figure 2.3: Alternative model of an amplitude and rate-limiter. The amplitude of the input u is limited before entering the rate limiter.

The difference in the behavior of these two limiter models is that the one having the amplitude limiter at the input has, in some situations, a slightly slower response. This can be understood in the following way: Assume that the systems depicted in Figures 2.2 and 2.3 are at rest, such that $v = u$. Let u be a step from, say, zero to ten and the amplitude limit is $b = 5$. Then the rate limiter in Figure 2.3 will ramp-up with full speed d since $\sigma_c^d(\cdot)$ is at its upper limit. This will go on until $K(5 - v(t)) < d$. From now on, and until $v = u$, this rate limiter will act as a low-pass filter having a pole (continuous time) in $-K$. The rate limiter in Figure 2.2, however, will ramp-up with full speed d until $K(10 - v(t)) < d$ and then, act as a low-pass filter having a pole in $-K$. But since this limiter has an inner state saturation that limits $v(t) \leq b$, it will ramp up at full speed all the way to b, thus resulting in a faster response. The larger K, the smaller is this difference between the two models. We leave it up to the user to decide which of the two models would be best for a given application.

We will in the sequel denote the rate- and amplitude limiters of both Figure 2.2 and Figure 2.3 according to (2.4), i.e. $\rho_c^d[\sigma_a^b(\cdot)]$.

Examples of physical systems that could be fairly well described by such rate- and amplitude limiters are: a hydraulic cylinder where the input is flow and the output is cylinder position (hydraulic servo), and a tank where the input is flow and the output is the level of the liquid pumped into (and out from) the tank. Whenever such a system is controlled in closed loop and operated so that the input saturates ”often” and for a ”long” time, which may be the case if the controller is aggressively tuned, the closed loop system can often be considered to constitute a rate- and amplitude limiter. Consequently, if such a system actuates a second system, then it can be modelled as an input rate- and amplitude limiter to that second system. Aircrafts were the control surfaces are actuated by hydraulic cylinders, which are position-controlled by feedback, are examples of such systems.

Rate- and amplitude limiter models used in controllers are often referred to as *software rate limiters*. Software rate limiters are useful not only as models representing limiters present in the real system, but also as components used to purposely introduce rate limits on, e.g., reference- and control signals for ”ramping up” the reference signal and/or the controller output (and thereby the actuator). This is a commonly used technique in some process control applications where, e.g., the flow through a valve must be increased slowly. Otherwise the liquid- or gas flow may rupture the pipe it flows in when it encounters the first bend of the pipe, causing a highly dangerous and costly accident. Another application that utilizes this technique is in the flight control system in the Swedish fighter JAS 39 Gripen. Here, both the pitch-angle and the pitch-angle velocity is limited and the latter especially for pitch-down in order to limit the G-force acting on the aircraft for such manoeuvres. One of the reasons for limiting the G-force is that the pilot would otherwise be put in the unpleasant situation of hanging in his belt [71]. This technique is also used in the application concerning control of hydraulic cylinders discussed in Chapter 10. However, there the goal is to limit acceleration so that oscillations are avoided.

A discrete-time rate- and amplitude limiter

Next, a discrete-time version of the limiter shown in Figure 2.2 is presented. Here we have chosen the simple backward-Euler approximation of the derivative[3]. The integrator with limited output (last block in Figure 2.2) is given by

$$v(t) \;=\; \sigma_a^b(v(t-1) + T_s u_i(t)) \tag{2.10}$$

[3] $\dot{v}(t) \approx (v(t) - v(t-1))/T_s$ where T_s is the sampling interval

where T_s is the sampling interval, and u_i is given by

$$u_i(t) \;=\; \sigma_c^d\left(\frac{u(t)-v(t-1)}{T_s}\right) \;. \tag{2.11}$$

It is straight forward to derive a discrete-time model for the other rate- and amplitude limiter in a similar way.

2.3 Combined feedback and feed-forward control of systems with input saturations

In this section we show that, when two signals are first added and then passed through a combined rate- and amplitude limiter, the limits of the limiter will vary with one of the signals, as seen from the perspective of the other signal. Here, we assume that an external feed forward control signal changes the saturation limits, as seen from the perspective of a feedback control signal.

Consider control of the system (2.1) where

$$\psi(u) = \;\rho_c^d[\sigma_a^b(u)] \tag{2.12}$$

and

$$u \;=\; u_{fb} + v_{ff} \;. \tag{2.13}$$

Here, u_{fb} represents the feedback control signal whereas v_{ff} represents the external feed-forward control signal. We assume that v_{ff} is limited in advance such that

$$v_{ff} \;=\; \rho_{cf}^{df}[\sigma_{af}^{bf}(u_{ff})] \;, \tag{2.14}$$

for some u_{ff}. In case the limits of the feed forward action are selected by the control designer, a typical choice would be

$$\begin{aligned} cf \;&\geq\; c,\; df \;\leq\; d \\ af \;&\geq\; a,\; bf \;\leq\; b\,. \end{aligned} \tag{2.15}$$

The main purpose of selecting the feed forward limits smaller than the limits of ψ is that it guarantees that some control authority is always left for the feedback controller.

We can now present the following Result:

Result 2.1 Varying saturation limits
By using the model (2.10)-(2.11) of the limiter (2.12) in discrete time, the plant input v can be expressed as

$$\begin{aligned}
v(t) &= v_{fb}(t) + v_{ff}(t) \\
v_{fb}(t) &= \sigma_{\bar{a}(t)}^{\bar{b}(t)} \left(v_{fb}(t-1) + T_s \sigma_{\bar{c}(t)}^{\bar{d}(t)} \left(\frac{u_{fb}(t) - v_{fb}(t-1)}{T_s} \right) \right) \\
\bar{a}(t) &\triangleq a - v_{ff}(t) \\
\bar{b}(t) &\triangleq b - v_{ff}(t) \\
\bar{c}(t) &\triangleq c - \frac{\Delta v_{ff}(t)}{T_s} \\
\bar{d}(t) &\triangleq d - \frac{\Delta v_{ff}(t)}{T_s}
\end{aligned} \tag{2.16}$$

where $\Delta v_{ff}(t) \triangleq v_{ff}(t) - v_{ff}(t-1)$.

For a detailed derivation of the expressions in Result 2.1 see Appendix A.1.2 and A.1.3 respectively.

Thus, the feed forward signal v_{ff} shifts both the rate and the amplitude saturation limits, as seen from the perspective of the feedback control signal u_{fb}.

Remark 2.1 In case the output from the limiter, v, is used by an anti-windup compensator that uses the Mechanism 2 defined in Section 3.1, then the feed forward signal must be removed and the signal $v - v_{ff}$ should be fed back to the anti-windup compensator. If not removed, the anti-windup compensator will interpret *any* feed forward control actions, $v_{ff} \neq 0$, as saturation events.

Note that the limiter in (2.16) does not have to be realized when used for, e.g. anti-windup compensation. The expressions in (2.16) is only derived here to illustrate the effect of having a feed forward signal mixed with the feedback signal.

2.4 Plant-input saturation models in controllers

An anti-windup compensator uses feedback of the possibly saturated plant input $\psi(u)$. In case an exact model of ψ is available, it can be used inside the controller to saturate the controller output before it saturates at the real plant input,

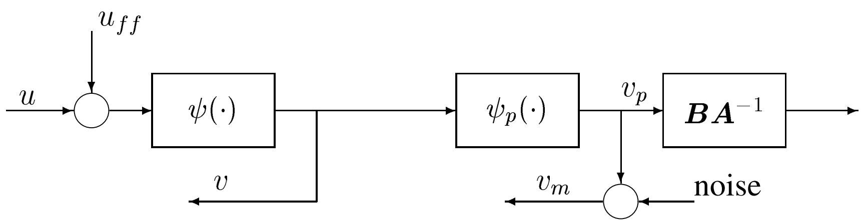

Figure 2.4: Model of an input nonlinearity (ψ) implemented in series with the real plant-input nonlinearity (ψ_p).

see Figure 2.4. Then the output from the model (v in Figure 2.4) can be used in the anti-windup feedback loop. This is, to my knowledge, the most common way to estimate the plant input when used for implementing anti-windup. However, if the real input saturation (ψ_p in Figure 2.4) varies and/or if its limits are unknown, then it might be better to use the measured real plant input (v_p in Figure 2.4) if it is measurable. This may, on the other hand, involve another problem. A noisy measurement v_m will trigger the anti-windup mechanism even when saturation does not occur. A compromise could be to use the measured signal v_m for adjusting (or adapting) the limits of the saturation model ψ and then use the model output v for anti-windup compensation. Such an adaption procedure will be quite application specific and therefore we leave it up to the designer to find out exactly how this can be done in the best way.

2.5 Static directional compensation

When one or a few of the control signal components $v(t) = \sigma(u(t))$, defined in (2.7), saturates, this may drastically change the direction of the vector $v(t)$ in relation to the direction of u. The change of direction may have very unsatisfactory consequences in the control of some types of plants in which an appropriate control action depends on a delicate balance between the components of the control vector, [72]. Such a plant is often referred to as an *ill-conditioned* plant. Improved stability and performance properties can then be obtained by introducing an artificial saturation on all components of $u(t)$. The aim is to avoid *critical directions* of $v(t)$, i.e., directions that will drive the plant outputs far away from desirable and acceptable levels. We will here discuss an artificial limiter that preserves the direction of the control signal. Later in Section 6.2.1 a novel root-locus like analysis method for MIMO systems with amplitude saturations will be proposed and demonstrated. This method allows us to select artificial limiters avoiding only the critical directions.

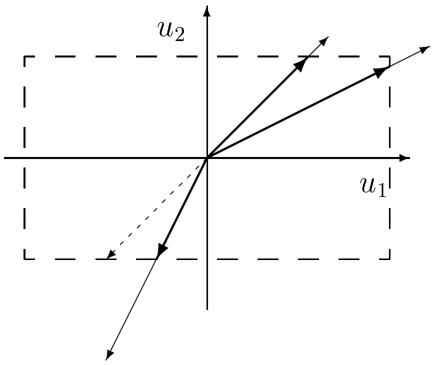

Figure 2.5: Controller outputs u (thin) and saturated and directional compensated plant-inputs γu (thick). If the decentralized amplitude limiter $\sigma(u)$ in (2.7) operates on the control vector u shown in the lower-left part of the figure, then the result becomes the dashed vector in the lower-left part of the figure. To keep the figure clear, we have not drawn the corresponding σ-saturated (dashed) vectors in the upper-right part of the figure.

2.5.1 Directional preservation

The aim is to adjust the components of $u(t)$ so that the direction is preserved in $v(t)$. This can be accomplished by scaling $u(t)$ by γ so that

$$v(t) = \gamma u(t)$$

where

$$\gamma = \begin{cases} \min_i \left| \frac{\sigma(u_i)}{u_i} \right| & \text{when saturating}, \\ 1 & \text{otherwise}. \end{cases} \qquad (2.17)$$

Hence, γ is a scalar, memoryless, but time-varying scaling factor taking values in the interval $(0\ 1]$.

Remark 2.2 Consider the situation in Figure 2.4 (for $u_{ff} = 0$). Assume that $\psi_p = \sigma$, i.e., a decentralized amplitude limiter. Then selecting $\psi(u) = \gamma u$ makes the action of the decentralized limiter $\psi_p = \sigma$ insignificant, i.e., $v_p = \gamma u$.

The situation is illustrated in Figure 2.5. This type of compensation is discussed, e.g., in [61] and we will discuss it further, and use it in some of the examples, in the chapters that follow. When discussed in the literature, the directional preserving limiter (2.17) may be expressed in other ways, for instance as

$$v = \frac{u}{\max\limits_i(|u_i|, 1)}, \tag{2.18}$$

where all the components of u saturate at ± 1. In case the components of u saturate at other limits than ± 1, use of the function (2.18) as a directional preserving amplitude limiter, requires pre-scaling of u before it enters the limiter (2.18), and then re-scaling of v afterwards.

2.6 Local linearization of amplitude-limited actuators

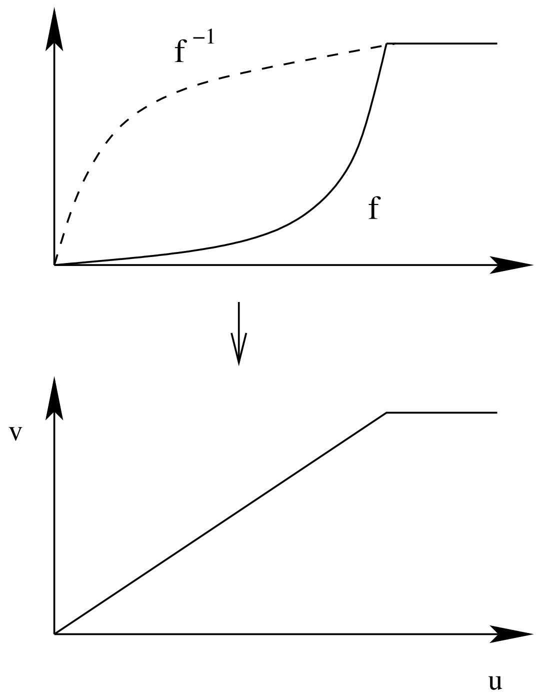

Figure 2.6: Static, nonlinear relation $f(\cdot)$ between the actuator input and output (solid curve in the upper picture). By letting its inverse (dashed curve in the upper picture) operate on the controller output, the ideal and simple amplitude limiter is obtained (lower picture)

Most physical actuators have constrained output amplitude. Some are almost linear when operating within the limits and some are not. Actuators used in industry are most often transducers that convert a low power signal, usually electrical, into a high power ”action”, may it be of the same physical dimension or not. This transformation can, in addition to the saturation nonlinearity, sometimes be described by a static but nonlinear relation between the input and the output, see Figure 2.6. For example, a control valve controlling a flow can often be described in this way. In such a case the input is the desired valve-opening angle and the output is flow. As argued earlier, it is easier to design a well performing controller when the actuator response can be described by a pure amplitude limiter σ. The aim of *local linearization* is to *linearize* the response of the actuator so that the relation between the *linearizer* input and the actuator output (e.g. flow) can fairly well be described by a simple amplitude limiter σ. In practice this can be done in two different ways:

- feedback control of the actuator output (e.g. flow feedback control) or
- static pre-compensation.

The feedback solution will typically be able to handle unknown variations better whereas the pre-compensator does not require the output to be measured. In the valve-and-flow case, this means that flow must be measured when using the feedback approach whereas the pre-compensator approach requires the (in some cases) static and nonlinear valve angle-to-flow relation to be known.

Based on several tests where the actuator input and the output response is measured, the function $\hat{f}^{-1}$ can be estimated. One can either implement this inverse function as a table or fit a simple model, such as a piece-wise linear model or a polynomial model, to the data. A short but illustrating discussion can be found in Section 9.3 of [73].

Some modern control valves, having a small ”built-in” DP-cell[4] and a micro-controller, in fact, support both the feedback- and the pre-compensation technique to be realized in the control valve itself.

Control valves used in the process industry are quite often over-dimensioned [74]. Such valves give a highly nonlinear relation between the valve opening and the flow and, furthermore, the flow will typically saturate long before the valve is fully opened. Compensation of such a valve is, of course, extra important in order to obtain satisfactory flow control.

[4]DP stands for Differential Pressure and DP-cells are often used to measure flow.

CHAPTER 3

Anti-windup compensation techniques

The most essential part of this chapter is the definition of *windup effects* and the formulation of design goals, in terms of dynamic properties of the system, based on our definition of windup effects. Thereafter, we introduce the idea that forms the fundament of the design strategy developed and discussed in Chapters 5 and 6. This design strategy, together with the anti-windup compensator proposed in Chapter 4, constitute the main contribution to anti-windup compensation of this thesis.

We open this chapter by presenting the basic concept of an *anti-windup modification* resulting in an *Anti-Windup Compensator* (AWC). We then proceed by making a definition of *windup effects* followed by a discussion on what influences them. The main objectives of anti-windup compensation are then listed. The chapter is closed by a brief discussion about the *impact of saturation*, a property that can help sort out wether anti-windup techniques can be expected to be appropriate or not, for the control of linear systems having input saturations.

3.1 The anti-windup mechanism

An *anti-windup compensator* (AWC) consists of a nominal linear controller (2.2) having *windup compensation* (or *windup modification*). One of the characterizing properties of windup compensation is that the possibly saturated plant input $\psi(u)$, defined in (2.1) and (2.4), is fed back to the controller. Hence, the states of the controller will then be driven by $\psi(u)$. This is highly desirable since the controller states, such as e.g. an integrator state, can be adjusted with respect to $\psi(u)$ thus preventing the integrator from ”winding up”. See also the discussion in the introduction to this thesis.

One of the key properties of AWC is that the feedback of ψ is such that when the control signal operates in the linear region, i.e. $\psi(u(t)) = u(t)$, the controller states are updated as usual and the controller will behave according to the underlying design intensions. In other words, the windup compensator does not affect the controller, and thereby not the system, unless saturation occurs. A feedback having this property can be accomplished in two alternative ways:

Mechanism 1: Feedback of the difference between the controller output and the plant input $\psi(u(t)) - u(t)$. This signal equals zero when $\psi(u(t)) = u(t)$, and hence, does not affect the states of the controller. This mechanism is the one used in the Figure 3.1 below, and also in the AWC:s (4.6) and (4.9) in Chapter 4.

Mechanism 2: A nominal *dynamic* controller uses feedback of its output, u, to update its states. This is so wether an anti-windup modification is used or not! Anti-windup can then be accomplished by using the saturated value $\psi(u(t))$ in this update instead of $u(t)$. This mechanism is used in the AWC:s (4.8) and (4.15) in Chapter 4.

Remark 3.1 When using **Mechanism 2**, any component of u that can be considered as ”external” e.g. a pure input feed forward signal which is not generated by the nominal controller, must be subtracted from $\psi(u)$ before $\psi(u)$ is used in the controller feedback loop. This was pointed out earlier in Section 2.3. How these mechanisms are used in AWC:s will be shown later in Chapter 4.

As mentioned in Chapter 1, many anti-windup compensators that have been proposed by researchers in the academic control society over the years, can be cast into one of the two categories *Observer-based anti-windup compensators* (OBSAWC) or *General Linear Anti-Windup Compensators* (GLAWC). The term *general linear anti-windup compensator* is proposed in this thesis for the first time and can as far as the author is aware not be found elsewhere in the literature. We use the term because we believe that it reflects the most important properties of the compensators in this class of AWC:s. The above mentioned compensator categories will be discussed in more detail in Chapter 4.

3.2 Definition of the term windup

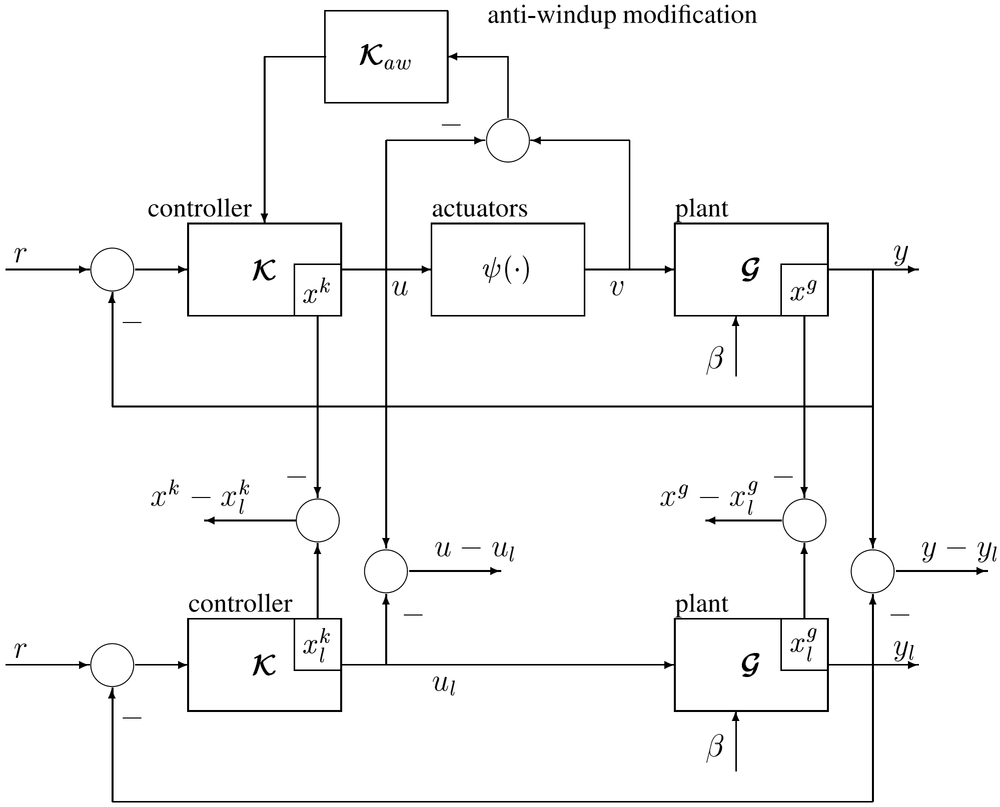

Figure 3.1: Illustration of the windup effects and the basic principles of anti-windup compensation. Ideal linear system (lower part) and the real system with constrained actuators, ψ, having anti-windup compensation (upper part).

As a qualitative definition of windup we shall here adopt the view expressed by Rönnbäck in [56]. In the words of the author:

We will say that a state variable is 'winding up' when the deviation from its nominal performance increases, and that it is 'unwinding' when the deviation decreases. That is, we have adopted the terminology commonly used to describe similar changes in the integral part of a PID-controller subject to 'integrator windup'. These terms can also be used when considering different linear combinations of the *state variables, e.g. the process output y(t). However, for the sake of simplicity, we define windup as a general concept referring to all these undesirable changes, irrespectively of their directions. The task of the AWC is to operate so that the windup phenomenon becomes as 'small' as possible. In the literature, windup is usually defined with respect only to the state of the controller, and the concept 'controller windup' is used by some authors to accentuate this. This probably explains why different anti-windup methods deal mostly with the stabilization of the controller modes during saturation. Our definition is obviously more general, as we define windup with respect to the state of the whole system. Hence, according to our definition it is possible that windup will occur even when a static controller is used, e.g. a simple P-controller which obviously does not contain any state variables that can 'wind up'.*

Figure 3.1 describes the situation. The controller structure shown here is, however, not the same as the ones discussed and proposed later in this thesis. By denoting the states in the linear system by x_l^g and x_l^k, for the plant and the controller respectively, and the states of the system with input constraints by x^g and x^k, as in Figure 3.1, we now make the following definitions:

Definition 3.1 Windup effects in state-space systems
Windup effects in the plant and in the controller are characterized by the properties of

$$\begin{aligned} x_\delta^g(t) &\triangleq x^g(t) - x_l^g(t) \\ x_\delta^k(t) &\triangleq x^k(t) - x_l^k(t) \end{aligned} \tag{3.1}$$

respectively.

Definition 3.2 Windup effects in input-output systems
Windup effects in the plant and in the controller are characterized by the properties of

$$\begin{aligned} y_\delta(t) &\triangleq y(t) - y_l(t) \\ u_\delta(t) &\triangleq u(t) - u_l(t) \end{aligned} \tag{3.2}$$

respectively.

Here we have distinguished between systems represented by state-space models and systems represented by input-output models.

Definitions similar to Definition 3.1 and Definition 3.2, in the sense that they consider windup in the whole system, are used in [42][56] and [52]. Definitions 3.1 and 3.2 are based on comparing the behavior of a system having constrained actuators to that of a linear (unrealistic) system having unconstrained actuators, see Figure 3.1. It can be argued that this is in some sense not relevant. Why compare to something that can never be achieved ? Many anti-windup strategies that strive to make the difference between the linear system and the real system "small" do, in fact, work well, see e.g. [56], [49],[52]. This will also be demonstrated throughout this thesis and we take these results as a motivation for working with the definitions. [1]

3.3 Factors influencing the degree of windup

For any given control system consisting of a linear plant having input limiters ψ (2.1), controlled by a linear controller, with or without windup compensation, the windup effects according to Definition 3.1 and 3.2 are influenced by

1. the degree of capacity reduction caused by the limiter, ψ, present at the plant input
2. the properties of the linear plant such as dynamics, gains, cross-couplings (MIMO), and
3. the properties of the feedback loop around ψ.

See Example 1.1 in the introduction.

Remark 3.2 The "immediate" capacity reduction caused by a saturation event in a single-input system, can not be influenced by any controller. It can only be changed by physical redesign. In systems having multiple-inputs, however, saturation in some of the components of u can, sometimes, be compensated for by the other components of u.

[1] Another measure of windup effects would be to compare the control system under consideration with the performance of a system controlled by a nonlinear controller obtained from solving a *constrained optimal* control problem. The performance of the system under consideration, which in this part of the thesis is a linear plant controlled by a nominal controller usually having anti-windup compensation, is then compared to what is, at least mathematically, possible instead of what a linear, unrealistic, system could provide. But even though such a performance measure would be relevant and interesting for the sake of comparison, it is not clear how it should be used as an aid for the design of *linear* anti-windup compensators.

Remark 3.3 Notice that the properties of the linear closed loop system will affect windup. For example if the controller has low gain such that saturation never occurs, then the windup effects are always zero. If, on the other hand, the nominal controller is aggressively tuned so that the response of the linear closed loop system is fast, saturation effects will be large. This is true no matter how well the real system with saturating inputs, actually performs in terms of the "original" and "actual" performance measure. This indicates that windup effects, as they are measured in terms of x_δ, are meaningful only when comparing different anti-windup strategies for a *given nominal system* that performs well when operating in the linear region.

Loosely speaking, the degree of feedback around ψ should be such that it compensates for the immediate capacity reduction, caused by saturation,

- as soon as possible after de-saturation of u_l in single-input systems, and
- as soon as possible after saturation of u_l in multiple-input systems.

In both cases this must be a gentle operation so that large overshoots, repeated re-saturations and limit-cycles are avoided. These properties are often referred to as "stability properties". It is well known that the stability properties of a feedback system are given by the properties of the loop transfer function (or the loop gain) taken around ψ. According to the Figure 3.1 the loop transfer function around ψ, which in the sequel will be denoted by $\boldsymbol{\mathcal{L}}_v$, is given by

$$\begin{aligned} u &= -\boldsymbol{\mathcal{L}}_v v \\ v &= \psi(u) \\ r &= \gamma = 0 \,. \end{aligned} \tag{3.3}$$

When using only the nominal controller in (2.2) ($\boldsymbol{\mathcal{K}}_{aw} \equiv \mathbf{0}$ in Figure 3.1) for controlling the plant (2.1), the loop transfer function is given by

$$\begin{aligned} \boldsymbol{\mathcal{L}}_v &= \boldsymbol{R}^{-1}\boldsymbol{S}\boldsymbol{B}\boldsymbol{A}^{-1} = \boldsymbol{R}^{-1}(\boldsymbol{S}\boldsymbol{B}+\boldsymbol{R}\boldsymbol{A}-\boldsymbol{R}\boldsymbol{A})\boldsymbol{A}^{-1} \\ &= \boldsymbol{R}^{-1}\boldsymbol{\alpha}\boldsymbol{A}^{-1} - \mathbf{I} \,. \end{aligned} \tag{3.4}$$

We shall discuss the implications of $\boldsymbol{\mathcal{L}}_v$ for the windup effects below.

A quantitative *measure* of the loop gain can be obtained by evaluating $\boldsymbol{\mathcal{L}}_v$ in the frequency domain. For $\boldsymbol{\mathcal{L}}_v(s)$, its frequency domain representation is obtained by setting $s = j\omega$, and for $\boldsymbol{\mathcal{L}}_v(z)$ its is obtained by setting $z = e^{j\omega T_s}$, where T_s is the sampling time.

Notice that if saturation has never occurred before time t_s say, then $u(t) \equiv u_l(t), \ \forall t < t_s$. Now, if the loop transfer function is identically zero, $\boldsymbol{\mathcal{L}}_v \equiv \mathbf{0}$, then $u(t) \equiv u_l(t), \ \forall t$ even if saturation occurs ($v(t) \neq u(t)$) at some time instant $t > t_s$. Thus, u must be independent of v and, hence, $u_\delta \equiv \mathbf{0}$. This leads us to highlight the following property:

Property 1 The windup effects u_δ in the *controller* can be avoided completely by selecting $\boldsymbol{\mathcal{L}}_v \equiv 0$.

When using the nominal controller (2.2) without any anti-windup modification, we can see in (3.4) that $\boldsymbol{\mathcal{L}}_v \equiv \mathbf{0}$ could only be attained by the choice $\boldsymbol{S} \equiv \mathbf{0}$. This is most often certainly not an acceptable choice considering the overall control objectives. Such a nominal controller has no feedback from y. By using the general linear anti-windup compensator (GLAWC), that will be introduced in the next chapter, $\boldsymbol{\mathcal{L}}_v \equiv \mathbf{0}$ can be accomplished without affecting the choice of $\boldsymbol{S}$. However, as we will show, $\boldsymbol{\mathcal{L}}_v \equiv \mathbf{0}$ is seldom an appropriate design goal even though it can be obtained without affecting the nominal controller. The reason is that the windup effects y_δ in the *plant* has not been accounted for in an appropriate way.

The windup effects in the plant, y_δ, of Definition 4.2 are given by

$$y_\delta \triangleq y - y_l \ = \ \boldsymbol{B}\boldsymbol{A}^{-1}(v - u_l). \tag{3.5}$$

When using the nominal controller (2.2) for the control of (2.1), y_δ can also be written as

$$y_\delta \ = \ \boldsymbol{B}\boldsymbol{\alpha}^{-1}\boldsymbol{R}(v - u), \tag{3.6}$$

see Appendix B.1.1. The transfer function from the difference between the plant input and the controller output

$$v - u \triangleq \delta \tag{3.7}$$

to y_δ will be analyzed and discussed frequently in the upcoming discussions, and it will be denoted by $\boldsymbol{\mathcal{H}}_\delta$, i.e.,

$$y_\delta \ = \ \boldsymbol{\mathcal{H}}_\delta \delta. \tag{3.8}$$

Hence, when using the nominal controller (2.2) for the control of the plant (2.1), we obtain the following relations:

System description when using the nominal controller

$$
\begin{aligned}
y &= y_l + y_\delta \;=\; y_l + \boldsymbol{\mathcal{H}}_\delta \delta \\
u &= -\boldsymbol{\mathcal{L}}_v v + \boldsymbol{R}^{-1} w \\
w &\triangleq \boldsymbol{T} r - \boldsymbol{S}\boldsymbol{B}\boldsymbol{A}^{-1}\beta \\
&\text{where} \\
\boldsymbol{\mathcal{L}}_v &= \boldsymbol{R}^{-1}\boldsymbol{S}\boldsymbol{B}\boldsymbol{A}^{-1} = \boldsymbol{R}^{-1}\boldsymbol{\alpha}\boldsymbol{A}^{-1} - \mathbf{I} \\
\boldsymbol{\mathcal{H}}_\delta &= \boldsymbol{B}\boldsymbol{\alpha}^{-1}\boldsymbol{R}\,.
\end{aligned}
\tag{3.9}
$$

The transfer function $\boldsymbol{\mathcal{H}}_\delta$ represents the dynamics that describes the recovery at the plant output back to linear performance, after de-saturation. If $\boldsymbol{\mathcal{H}}_\delta$ has fast dynamics, then the recovery *may* be fast. On the other hand, when $\boldsymbol{\mathcal{H}}_\delta$ has fast dynamics, then $\boldsymbol{\mathcal{L}}_v$ may have a large norm and the stability properties may therefore be poor. This fact indicates that a proper trade-off is needed. However, such trade-offs implies that we have to *de-tune the nominal controller, i.e., change* $\boldsymbol{S}$, $\boldsymbol{R}$. This is often undesirable. However, as will be shown in the next chapter, anti-windup compensation ($\boldsymbol{\mathcal{K}}_{aw} \neq \mathbf{0}$) introduces an extra degree of freedom allowing the designer to build in some properties of $\boldsymbol{\mathcal{H}}_\delta$ and $\boldsymbol{\mathcal{L}}_v$ which are independent of the design choices of the nominal controller.

The selection of properties of $\boldsymbol{\mathcal{H}}_\delta$ and $\boldsymbol{\mathcal{L}}_v$, aiming at keeping the windup effects small, constitute the basis for the design strategy proposed later in Chapter 6, and it requires the use of the GLAWC proposed in Chapter 5. More heuristic design concepts useful for the design of OBSAWC:s as well as GLAWC:s, that also involve this trade-off, are presented in Chapter 7.

3.4 The objectives of anti-windup compensation

Our qualitative definition of windup stated in Section 4.2, contains the line "*The task of the AWC is to operate so that the windup phenomena become as 'small' as possible*". The term "windup phenomena" is here considered to be the same as the term "windup effects" used in the Definitions 3.1 and 3.2. This suggests the aim of anti-windup compensation, in MIMO-systems, to be the following:

Objective 1 Leave the original linear behavior unchanged

Objective 2 Provide a graceful degradation of the system performance during saturation

Objective 3 Provide a fast recovery back to linear behavior after de-saturation

Objective 1 is guaranteed by using one of the standard anti-windup mechanism described earlier in Section 4.1.

The other two objectives require, at least, that the closed loop system consisting of (2.1) and a controller with anti-windup compensation, is asymptotically stable. But one can usually do more than that. According to the discussion in the previous section the recovery back to linear performance can be controlled by selecting $\mathcal{H}_\delta$ in an appropriate way. Hence, Objective 3 can be controlled in this way. Objective 2 is more difficult to quantify in terms of properties of linear transfer functions. It is our experience though, that a decent trade-off between stability properties of the closed loop system and fast dynamics of $\mathcal{H}_\delta$ will satisfy Objective 2 to an acceptable level. This will be demonstrated by the examples in Chapters 5 and 6. In some cases, and especially when the plant is ill-conditioned, using the directional compensator described in Section 2.5 may help fulfilling Objective 2.

3.5 Strong or weak impact of limiters

As we mentioned briefly in the beginning of Chapter 2, inherent nonlinearities in a process limit how well linear control design methods will succeed. In a similar way, one can say that the extent of input saturation in an otherwise linear system, places limits on the overall behavior of the system when using linear controllers having anti-windup compensation. Before this is discussed further, we make the following definitions[2]:

Definition 3.3 Strong impact of saturations
We say that the impact of saturation, caused by an input-limiter, represented by ψ, is *strong* when a system (2.1) must be operated in such a way that the input saturates often and "deeply" and maybe for a long period of time, in order to fulfil the operating goals.

Definition 3.4 Weak impact of saturations
We say that the impact of saturation, caused by an input-limiter, represented by ψ, is *weak* when a system (2.1) is operated in such a way that the input rarely saturates, and it still fulfills the operating goals.

[2]These definitions are inspired by the short discussion at the introduction of [16].

Remark 3.4 The properties strong- and weak impact of saturation are fundamentally related to the operating conditions and the physical properties of the process, such as the input limiters and the plant dynamics.

In [16] the researchers point out that the understanding of analysis and design of control systems where the saturation impact is strong, ”is at its infancy”. With reference to, e.g., other papers in the same volume, they also point out that in systems where the impact of saturation is weak, anti-windup ”can successfully be employed”. Although we agree with this, we would like to point out that anti-windup techniques also work well in some applications where the impact of saturation is strong.

Based on my experiences from industrial control applications, my experiences from research in the field of anti-windup compensation and with the use of common sense, I dare to present the following hunches concerning strong- and weak impact of saturation:

Hunch 3.1 Strong impact of saturation
In these situations there is probably a greater need for other nonlinear controllers than linear controllers having anti-windup compensation. In case linear controllers with anti-windup compensation have a potential to do well, one can expect that it is more often acceptable to adapt the *nominal* linear controller to the nonlinear loop and use the more simple OBSAWC to obtain satisfactory performance, than compared to the case of weak impact. In other words, the Objective 1 is less relevant when the impact of saturation is strong compared to when it is weak.

Hunch 3.2 Weak impact of saturation
Anti-windup compensation is expected to work well in many cases. When so is the case, one would expect that it is desirable to adapt and tune the nominal controller with respect to the underlying design goals of the linear system (u operating exclusively in the linear region of ψ), and hence, not with respect to the nonlinear loop. In other words, the Objective 1 is relevant and we can expect that it is desirable to fulfill it. In this endeavour, an OBSAWC may be sufficient but if not, the GLAWC improves the odds to succeed.

CHAPTER 4

Controller structures with anti-windup compensation

Anti-windup compensation of the nominal controller (2.2) is here considered for multiple-input multiple-output (MIMO) systems. The first anti-windup compensator discussed here is the well known *observer-based anti-windup compensator* (OBSAWC) suggested by Åström & Wittenmark in [2] for SISO-polynomial systems and for MIMO state-space systems. A MIMO-polynomial OBSAWC will, however, be discussed here and an augmented version of that compensator is proposed. It will be named the *general linear anti-windup compensator* (GLAWC).

4.1 Observer-based anti-windup compensation (OBSAWC)

The observer-based anti-windup compensator (OBSAWC) for MIMO-systems can be obtained by introducing the polynomial matrix $\boldsymbol{A}_o$, and the possibly saturated plant input, v,[1] into the nominal controller (2.2) according to

$$\begin{aligned} \boldsymbol{A}_o u_o &= (\boldsymbol{A}_o - \boldsymbol{R})v - \boldsymbol{S}y + \boldsymbol{T}r \\ v &= \psi(u_o) \ . \end{aligned} \tag{4.1}$$

The controller is depicted in Figure 4.1 where the signal u_a is zero in the case of observer anti-windup compensation. This signal will however be used by the GLAWC presented in the next section. To keep the expressions clear in the sequel,

[1]Note that we denote the controller output by u and its saturated ditto by v. This notation is used in some reports whereas in others, e.g. in [2], the notation is reversed.

we denote

$$\boldsymbol{A}_o - \boldsymbol{R} \triangleq \boldsymbol{R}_o. \tag{4.2}$$

We proceed by imposing the following requirements on $\boldsymbol{R}$, $\boldsymbol{A}_o$, and $\boldsymbol{R}_o$:

Requirement 4.1 The transfer function $\boldsymbol{A}_o^{-1}$ is asymptotically stable.

Requirement 4.2 The transfer functions

$$\boldsymbol{R}^{-1}\boldsymbol{R}_o \tag{4.3}$$

and

$$\boldsymbol{A}_o^{-1}\boldsymbol{R}_o \tag{4.4}$$

are both strictly causal/proper.

Requirement 4.1 is necessary (but not sufficient) to retain stability in the system when the inputs saturate. Requirement 4.2 guarantees the absence of algebraic loops in the OBSAWC. It requires $\boldsymbol{A}_o$ and $\boldsymbol{R}$ to have the same highest degree coefficient matrices.

Remark 4.1 Requirement 4.2 is sufficient but not necessary for the avoidance of algebraic loops in systems having multiple inputs. If $\{\mathbf{F}, \mathbf{G}, \mathbf{C}, \mathbf{D}\}$ is a discrete time state space realization of $\boldsymbol{R}^{-1}\boldsymbol{R}_o$, say, where $\mathbf{D}$ has zeros on the diagonal and above, or zeros on the diagonal and below, then we can allow the rest of the elements in $\mathbf{D}$ to be nonzero. Such a system is not strictly causal yet algebraic loops are avoided if the components u_i of the control signal vector u are calculated in a particular order. For example, if $\mathbf{D}$ has zeros on the diagonal and above, then one must begin calculating u_1 and then u_2 and so on. The order is reversed in case $\mathbf{D}$ has zeros on the diagonal and below. Notice that for systems having a single input, Requirement 4.2 is sufficient *and* necessary for the avoidance of algebraic loops.

The OBSAWC has the following property:

Property 2 The OBSAWC in (4.1) fulfills Objective 1 defined in Section 3.4. See Appendix B.2.1 for details.

The OBSAWC in (4.1) uses Mechanism 2 defined in the Section 3.1. One can also use Mechanism 1 in order to build an OBSAWC. By using (4.2), the expression (4.1) can be rewritten as

$$\boldsymbol{A}_o u_o \;=\; \boldsymbol{R}_o v - \boldsymbol{S} y + \boldsymbol{T} r \;. \tag{4.5}$$

It is straightforward to show that

$$\boldsymbol{R} u_o = \boldsymbol{R}_o (v - u_o) + \boldsymbol{T} r - \boldsymbol{S} y \tag{4.6}$$

provides the same control action as (4.5). This controller is depicted in Figure 4.2 ($u_a \equiv 0$).

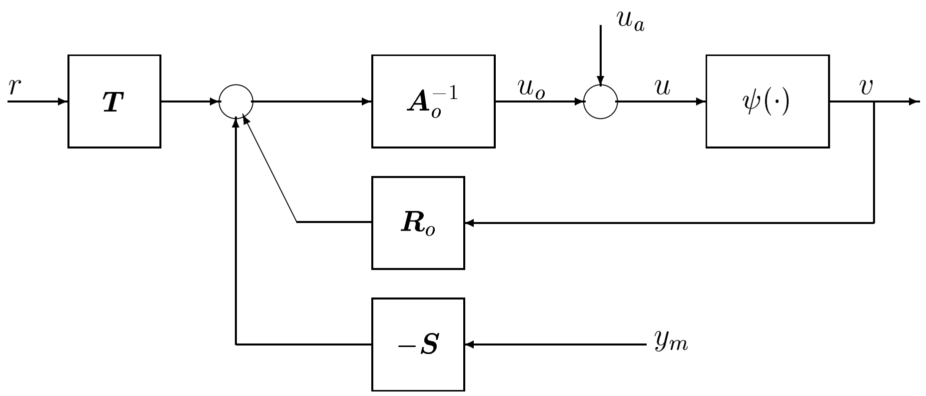

Figure 4.1: The block diagram represents the observer-based anti-windup compensator (OBSAWC) for $u_a \equiv 0$ and the GLAWC for u_a given by (4.9).

When discussed in the literature, the OBSAWC is often represented by a state-space description. Connections between such representations and the polynomial representations proposed here are discussed in Appendix B.2.2.

The class of observer-based anti-windup compensators (OBSAWC) was defined and proposed by Åström & Wittenmark in [2]. It was shown later by Walgama & Sternby in [44] that most anti-windup modifications proposed earlier could be cast into the OBSAWC class. In Kothare et al [48], the researchers present what they call ”A Unified Framework for the Study of Anti-windup Designs” where they also cast many of the known designs into their framework. This framework does not, however, offer more generality than the already known OBSAWC except from introducing the possibility of using direct terms in the anti-windup feedback path. This extra ”possibility” must be used with care since it may introduce algebraic

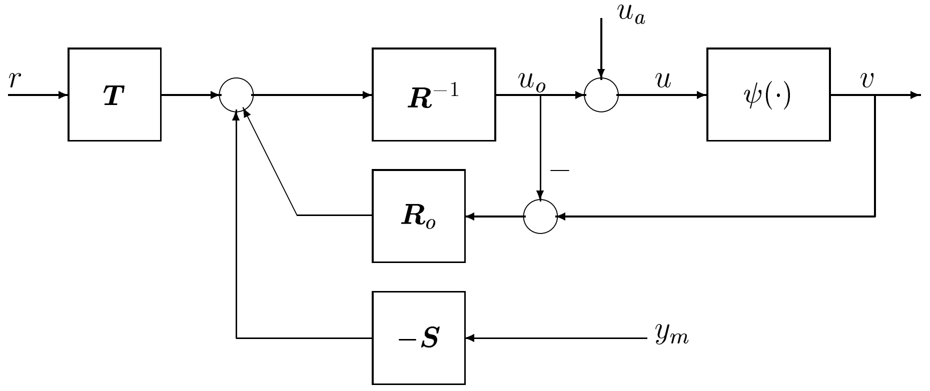

Figure 4.2: Alternative representation of the OBSAWC for $u_a \equiv 0$ and the GLAWC for u_a given by (4.9).

loops. See our Remark 5.1. The GLAWC proposed in the next section is more general, and thereby also more useful in some situations, than the framework proposed in [48]. Properties of the GLAWC will be discussed in this and in the next chapter, and its usefulness will be demonstrated by examples in Chapters 6 and 7.

In Sections 3.3 and 3.4, we argued that it is often desirable, and sometimes necessary, to adjust the properties of the loop transfer function, $\boldsymbol{\mathcal{L}}_v$, and the transfer function representing the desaturation transients, $\boldsymbol{\mathcal{H}}_\delta$, so that the windup effects (see Definition 3.1 and 3.2) could be controlled and kept small. We will now show how the OBSAWC, when used for the control of (2.1), allows some adjustments of $\boldsymbol{\mathcal{L}}_v$ and $\boldsymbol{\mathcal{H}}_\delta$ to be made without changing the nominal controller (2.2). By using (4.5) or (4.6) for the control of (2.1), the control signal $u = u_o$, the loop transfer function, taken around $\psi(u)$, and the transient dynamics represented by $\boldsymbol{\mathcal{H}}_\delta$, are given by the following set of relations:

System description when using the OBSAWC

$$
\begin{aligned}
y &= y_l + \boldsymbol{\mathcal{H}}_\delta \delta \\
u &= -\boldsymbol{\mathcal{L}}_v v + \boldsymbol{A}_o^{-1} w \\
w &\triangleq \boldsymbol{T} r - \boldsymbol{S}\boldsymbol{B}\boldsymbol{A}^{-1}\beta \\
\delta &= v - u \\
&\text{where} \\
\boldsymbol{\mathcal{L}}_v &= \boldsymbol{A}_o^{-1}\boldsymbol{\alpha}\boldsymbol{A}^{-1} - \mathbf{I} \\
\boldsymbol{\mathcal{H}}_\delta &= \boldsymbol{B}\boldsymbol{\alpha}^{-1}\boldsymbol{A}_o
\end{aligned}
\tag{4.7}
$$

respectively. For a detailed derivation of (4.7), see Appendix B.2.4 and B.2.6. By comparing (4.7) with (3.9) it is evident that the observer-based anti-windup modification has replaced $\boldsymbol{R}$ by $\boldsymbol{A}_o$ as they appear explicitly in $\boldsymbol{\mathcal{L}}_v$ and $\boldsymbol{\mathcal{H}}_\delta$. Notice, however, that the denominator of the closed loop, $\boldsymbol{\alpha} = \boldsymbol{RA} + \boldsymbol{SB}$, is unchanged and independent of $\boldsymbol{A}_o$.

According to the design philosophy presented in Chapter 4, the polynomial matrix $\boldsymbol{A}_o$ shall be selected and tuned with respect to Objectives 2 and 3 respectively, of Section (3.4). However, since $\boldsymbol{A}_o$ is a *polynomial* matrix, and not a *rational transfer function* matrix, the loop transfer function, $\boldsymbol{\mathcal{L}}_v$, lacks an adjustable *numerator* and $\boldsymbol{\mathcal{H}}_\delta$ lacks the corresponding adjustable *denominator*. This shortcoming is sometimes crucial when it comes to fulfilling Objectives 2 and 3. This will be demonstrated in some of the examples in Chapter 6. The GLAWC proposed next provides such an extra degree of freedom to the structure.

4.2 General linear anti-windup compensation (GLAWC)

The OBSAWC discussed in the previous section will here be appended to provide more flexibility to the structure. This can be accomplished by adding a signal u_a to the control signal u_o from the OBSAWC according to:

GLAWC

$$\begin{aligned} u &= u_o + u_a \\ v &= \psi(u) \ , \end{aligned} \tag{4.8}$$

where

$$\begin{aligned} u_a &= (\boldsymbol{P}_1 - \boldsymbol{P}_2)\boldsymbol{P}_2^{-1}(v - u) \\ &= (\boldsymbol{P}_1 - \boldsymbol{P}_2)\boldsymbol{P}_1^{-1}(v - u_o) \ . \end{aligned} \tag{4.9}$$

Here, as before, the signal v represents the input to the plant (2.1). Figures 4.1 and 4.2 show the two versions of general linear anti-windup compensator GLAWC, whereas Figures 4.3 and 4.4 show two different ways of how to obtain the signal u_a, given by the first and the second lines of (4.9), respectively. It is easy to verify that the expressions in (4.9) both gives the same signal u_a. Using that $u = u_o + u_a$, the expression on the first line can be written as

$$\begin{aligned} u_a &= (\boldsymbol{P}_1 - \boldsymbol{P}_2)\boldsymbol{P}_2^{-1}(v - u_o - u_a) \\ &= (\boldsymbol{P}_1 - \boldsymbol{P}_2)\boldsymbol{P}_2^{-1}(v - u_o) - (\boldsymbol{P}_1 - \boldsymbol{P}_2)\boldsymbol{P}_2^{-1}u_a \\ &= (\boldsymbol{P}_1 - \boldsymbol{P}_2)\boldsymbol{P}_2^{-1}(v - u_o) - \boldsymbol{P}_1\boldsymbol{P}_2^{-1}u_a + u_a \ . \end{aligned} \tag{4.10}$$

Hence, collecting the u_a-terms on the left hand side gives

$$\boldsymbol{P}_1\boldsymbol{P}_2^{-1}u_a \;=\; (\boldsymbol{P}_1-\boldsymbol{P}_2)\boldsymbol{P}_2^{-1}(v-u_o)\;. \tag{4.11}$$

Multiplying this equation from the left by $\boldsymbol{P}_2\boldsymbol{P}_1^{-1}$ finally gives that

$$\begin{aligned} u_a &= (\mathbf{I}-\boldsymbol{P}_2\boldsymbol{P}_1^{-1})(v-u_o) \\ &= (\boldsymbol{P}_1-\boldsymbol{P}_2)\boldsymbol{P}_1^{-1}(v-u_o)\;. \end{aligned} \tag{4.12}$$

In (4.9), $\boldsymbol{P}_1$ and $\boldsymbol{P}_2$ are both polynomial matrices, which we must place the following restrictions on:

Requirement 4.3 The transfer functions

$$(\boldsymbol{P}_1-\boldsymbol{P}_2)\boldsymbol{P}_i^{-1},\;\; i=1,2 \tag{4.13}$$

are strictly causal/proper.

Requirement 4.4 The transfer functions

$$\boldsymbol{P}_i^{-1},\;\; i=1,2 \tag{4.14}$$

are asymptotically stable.

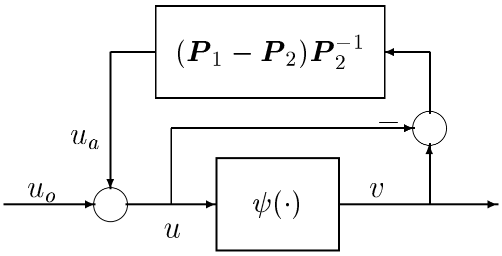

Figure 4.3: Appended observer anti-windup compensator

Requirement 4.4 is necessary (but not sufficient) to retain stability in the system when the inputs saturate, whereas Requirement 4.3 together with Requirement 4.2 guarantees the absence of algebraic loops in the GLAWC. Both Requirement 4.2 and Requirement 4.3 are sufficient (but in the MIMO-case not necessary) conditions, see Remark 4.1. Note that Requirement 4.3 restricts the highest degree coefficient matrices of $\boldsymbol{P}_1$ and $\boldsymbol{P}_2$ to be equal.

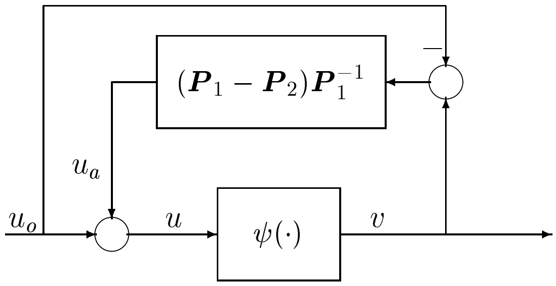

Figure 4.4: Appended observer anti-windup compensator

We can establish the fact that the GLAWC has the following property:

Property 3 The GLAWC in (4.8)-(4.9) fulfills Objective 1 of Section 3.4.

The control output from the GLAWC in (4.8)-(4.9) is expressed as a sum of two signals $u = u_o + u_a$. However, the the signal u_a can be eliminated and the GLAWC can be expressed in more compact forms. It is easy to verify that

$$\begin{aligned} u &= (\mathbf{I} - \boldsymbol{\mathcal{W}}\boldsymbol{R})v + \boldsymbol{\mathcal{W}}(\boldsymbol{T}r - \boldsymbol{S}y) \\ \boldsymbol{\mathcal{W}} &= \boldsymbol{P}_2\boldsymbol{P}_1^{-1}\boldsymbol{A}_o^{-1} \end{aligned} \tag{4.15}$$

gives the same control action as (4.8)-(4.9). A derivation of (4.15) can be found in Appendix B.2.3.

The controller (4.15), proposed in [49] and discussed in [50], was inspired by the controller proposed by Rönnbäck in [45] for SISO-systems. That controller is also discussed in [3] and [56]. The GLAWC was, to our knowledge, first proposed by Rönnbäck in [45] for SISO-systems, and can be regarded as an extension of the OBSAWC.

By using the GLAWC (4.8),(4.9) (or (4.15)) for the control of (2.1), the system can be described by the following set of relations

System description when using the GLAWC

$$
\begin{aligned}
y &= y_l + \boldsymbol{\mathcal{H}}_\delta \delta \\
u &= -\boldsymbol{\mathcal{L}}_v v + \boldsymbol{P}_2 \boldsymbol{P}_1^{-1} \boldsymbol{A}_o^{-1} w \\
w &\triangleq \boldsymbol{T} r - \boldsymbol{S}\boldsymbol{B}\boldsymbol{A}^{-1}\beta \\
\delta &= v - u \\
&\text{where} \\
\boldsymbol{\mathcal{L}}_v &= \boldsymbol{P}_2 \boldsymbol{P}_1^{-1} \boldsymbol{A}_o^{-1} \boldsymbol{\alpha} \boldsymbol{A}^{-1} - \mathbf{I} \\
\boldsymbol{\mathcal{H}}_\delta &= \boldsymbol{B}\boldsymbol{\alpha}^{-1} \boldsymbol{A}_o \boldsymbol{P}_1 \boldsymbol{P}_2^{-1} \ .
\end{aligned} \tag{4.16}
$$

For a detailed derivation, see Appendix B.2.5 and B.2.7. Comparing the expressions (4.16) with the expressions obtained by using the OBSAWC (4.7), we can see that the polynomial matrix $\boldsymbol{A}_o$ in (4.7) has been replaced by the rational transfer function $\boldsymbol{A}_o \boldsymbol{P}_1 \boldsymbol{P}_2^{-1}$. [2] Thus by introducing u_a according to (4.8)-(4.9) we now have the freedom to modify both the numerator and the denominator of the transfer functions $\boldsymbol{\mathcal{L}}_v$ and $\boldsymbol{\mathcal{H}}_\delta$.

Let us summarize the most important results of this chapter so far:

- We have proposed a general linear anti-windup compensator, GLAWC, that fulfills Objective 1
- The GLAWC allows us to shape $\boldsymbol{\mathcal{L}}_v$ and $\boldsymbol{\mathcal{H}}_\delta$ according to (4.16) with respect to the Objectives 2 and 3 of Section 3.4, without having to change the nominal controller (2.2).
- The GLAWC can be regarded as an extension of the observer based anti-windup compensator OBSAWC.

We will now present a special class of designs having the property of, to some extent, separating the windup effects from the linear system.

4.3 Cancellation of the nominal controller action

In this section a special class of GLAWC:s will be discussed. This class is defined by the property that the loop transfer function, $\boldsymbol{\mathcal{L}}_v$, and the desaturation

[2] This is probably the reason why similar AWC structures, when discussed in the literature, sometimes are referred to as "dynamic" anti-windup compensators. We do not adopt this notation simply because the OBSAWC is, indeed, a "dynamic" anti-windup compensator.

transient dynamics, represented by $\boldsymbol{\mathcal{H}}_\delta$, become independent of the nominal controller. In the literature, similar schemes are proposed in Sternad and Rönnbäck [47], Rönnbäck [56], Öhr [49] and Öhr et.al. [50] with polynomial representations, and in Teel and Kapoor [52] with state-space representations.

Using the GLAWC scheme proposed in Section 4.2, this is accomplished by selecting

$$\boxed{\boldsymbol{A}_o\boldsymbol{P}_1 = \boldsymbol{\alpha} = \boldsymbol{R}\boldsymbol{A} + \boldsymbol{S}\boldsymbol{B}} \tag{4.17}$$

For this choice, the controlled system in (4.16) is given by:

System description after cancellation of $\boldsymbol{\alpha}$

$$\begin{aligned}
y &= y_l + \boldsymbol{\mathcal{H}}_\delta\delta \\
u &= -\boldsymbol{\mathcal{L}}_v v + \boldsymbol{P}_2\boldsymbol{\alpha}^{-1}w \\
w &\triangleq \boldsymbol{T}r - \boldsymbol{S}\boldsymbol{B}\boldsymbol{A}^{-1}\beta \\
\delta &= v - u \\
&\text{where} \\
\boldsymbol{\mathcal{L}}_v &= \boldsymbol{P}_2(\boldsymbol{A}_o\boldsymbol{P}_1)^{-1}\boldsymbol{\alpha}\boldsymbol{A}^{-1} - \mathbf{I} \\
&= \boldsymbol{P}_2\boldsymbol{A}^{-1} - \mathbf{I}, \\
\boldsymbol{\mathcal{H}}_\delta &= \boldsymbol{B}\boldsymbol{\alpha}^{-1}(\boldsymbol{A}_o\boldsymbol{P}_1)\boldsymbol{P}_2^{-1} \\
&= \boldsymbol{B}\boldsymbol{P}_2^{-1}\,.
\end{aligned} \tag{4.18}$$

Since the linear system behavior is unaffected by the anti-windup compensator (Property 3), and the dynamics of $\boldsymbol{\mathcal{L}}_v$ and $\boldsymbol{\mathcal{H}}_\delta$ are here made independent of the nominal controller $\boldsymbol{R}$, $\boldsymbol{S}$ in (2.2), the linear and the nonlinear system behavior, and thereby the design problem, has been split-up. This separation is accomplished by the cancellation of $\boldsymbol{\alpha}$ in (4.18), using a *model* of $\boldsymbol{\alpha}$.

Since $\boldsymbol{A}_o$ and $\boldsymbol{P}_1$ appear separately in the controller (4.8)-(4.9) one must, first factorize $\boldsymbol{\alpha}$ according to

$$\boldsymbol{\alpha} = \boldsymbol{\alpha}_1\boldsymbol{\alpha}_2 \tag{4.19}$$

and then select

$$\begin{aligned}\boldsymbol{A}_o &= \boldsymbol{\alpha}_1 \\ \boldsymbol{P}_1 &= \boldsymbol{\alpha}_2 \; .\end{aligned} \tag{4.20}$$

This factorization must, of course, fulfill Requirements 5.1-5.4. This restricts $\boldsymbol{\alpha}_1$ to have the same highest degree coefficient matrix as $\boldsymbol{R}$. This, in turn, results in the following requirement:

Requirement 4.5 The polynomial matrices $\boldsymbol{\alpha}_2$, $\boldsymbol{P}_1$ and $\boldsymbol{P}_2$ must all have the same highest degree coefficient matrix, as the plant denominator $\boldsymbol{A}$ has.

An investigation that motivates this requirement is provided in Appendix B.2.8.

The complete AWC obtained by using (4.6) and the second expression in (4.9) for the design choice (4.20) is depicted in Figure 4.5.

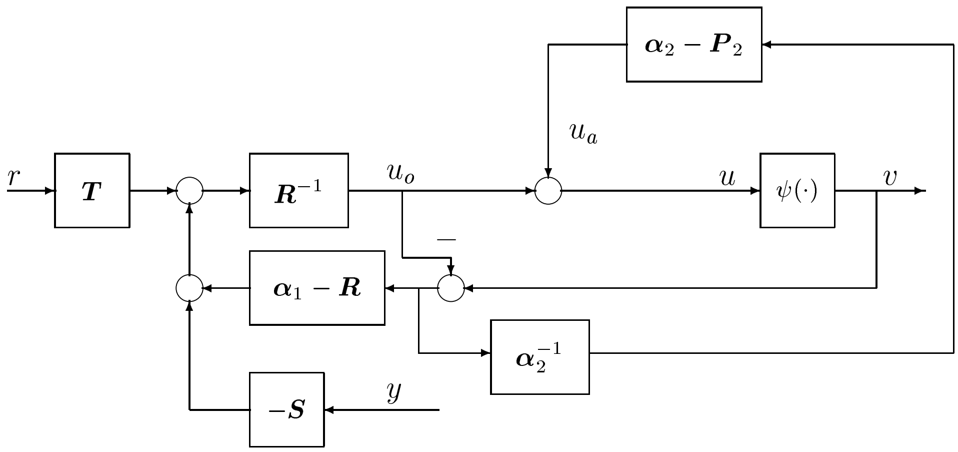

Figure 4.5: The complete AWC obtained by using the OBSAWC (4.6), the compensator given by the second expression in (4.9) for the design choice (4.20).

In Chapter 3 we stated that the aim of anti-windup compensation is to minimize the windup effects y_δ and u_δ. It was shown there that the signals y_δ and u_δ are intimately connected to the transfer functions $\boldsymbol{\mathcal{L}}_v$ and $\boldsymbol{\mathcal{H}}_\delta$. For our purpose it is convenient to describe the saturation effects in two slightly different ways. In both the cases we want to express y_δ and u_δ as signals in a dynamic system although in the first case the dynamics are driven by the difference between the plant input $v = \psi(u)$ and the control signal in the linear system u_l, i.e., $v - u_l$, and in the second case as driven by the difference between the plant input $v = \psi(u)$ and the control signal u from the AWC, i.e. $v - u = \delta$. The reason for doing this is that it allows us to formulate the anti-windup design problem as a simple linear design problem in an illustrative way.

From (4.18) we have that

$$\begin{aligned} u &= -\boldsymbol{\mathcal{L}}_v v + \boldsymbol{P}_2\boldsymbol{\alpha}^{-1}w \\ &= (\mathbf{I} - \boldsymbol{P}_2\boldsymbol{A}^{-1})v + \boldsymbol{P}_2\boldsymbol{\alpha}^{-1}w. \end{aligned} \tag{4.21}$$

By introducing $\boldsymbol{A}^{-1}\boldsymbol{A} = \mathbf{I}$ in between the matrices $\boldsymbol{P}_2$ and $\boldsymbol{\alpha}^{-1}$ in the last term of (4.21), u can be expressed as

$$\begin{aligned} u &= (\mathbf{I} - \boldsymbol{P}_2\boldsymbol{A}^{-1})v + \boldsymbol{P}_2\boldsymbol{A}^{-1}\boldsymbol{A}\boldsymbol{\alpha}^{-1}w \\ &= (\mathbf{I} - \boldsymbol{P}_2\boldsymbol{A}^{-1})v + \boldsymbol{P}_2\boldsymbol{A}^{-1}u_l \\ &= (\mathbf{I} - \boldsymbol{P}_2\boldsymbol{A}^{-1})(v - u_l) + u_l. \end{aligned} \tag{4.22}$$

Here we have used that $u_l = \boldsymbol{A}\boldsymbol{\alpha}^{-1}w$, see (2.3).

According to (4.22) and Definition 3.2, the windup effects in the controller can be described by the following signal

$$u_\delta \triangleq u - u_l = (\mathbf{I} - \boldsymbol{P}_2\boldsymbol{A}^{-1})(v - u_l). \tag{4.23}$$

An expression for the windup effects present in the plant, y_δ, generated from a dynamic system driven by $v - u_l$, is already given in (3.5). Let us summarize the expressions describing windup effects

Result 4.1 Windup effects described as a separate system
For the choice $\boldsymbol{A}_o\boldsymbol{P}_1 = \boldsymbol{\alpha} \triangleq \boldsymbol{R}\boldsymbol{A} + \boldsymbol{S}\boldsymbol{B}$ the windup effects according to the Definition 4.2 can be described by

$$\begin{aligned} y_\delta &= \boldsymbol{B}\boldsymbol{A}^{-1}(v - u_l) \\ u_\delta &= (\mathbf{I} - \boldsymbol{P}_2\boldsymbol{A}^{-1})(v - u_l) = -\boldsymbol{\mathcal{L}}_v(v - u_l)\ . \end{aligned} \tag{4.24}$$

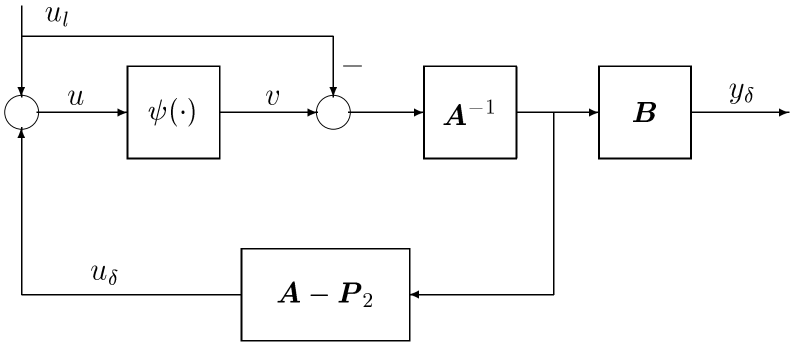

Figure 4.6: Split up of the system into one pure linear loop and a loop containing the input limiters. The linear system affects the nonlinear loop via the control signal in the linear system, u_l.

This system is depicted in Figure 4.6. The same situation is illustrated in Figure 5.1 for systems represented by state-space models.

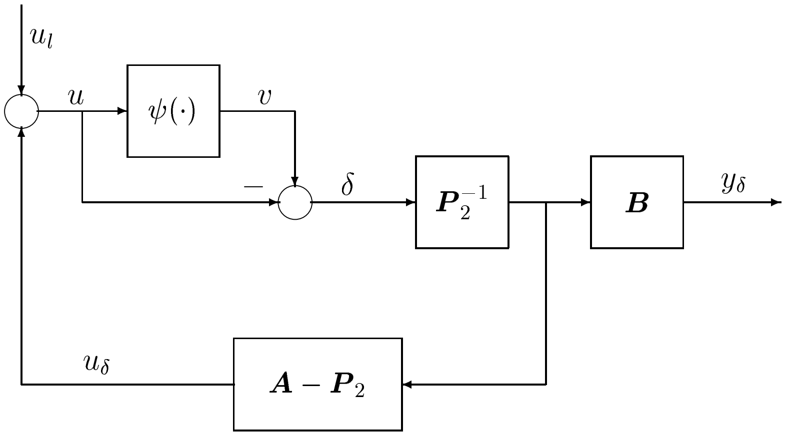

Figure 4.7: Same situation as in Figure 4.6 apart from the fact that we consider the difference $\delta = v - u$ to drive the saturation effects.

We will now proceed by deriving the second description of the windup effects.

By adding and subtracting u_δ inside the bracket in the expression for u_δ of Result 4.1, we can express u_δ as

$$\begin{aligned} u_\delta &= -\boldsymbol{\mathcal{L}}_v(v - u_l + u_\delta - u_\delta) \\ &= -\boldsymbol{\mathcal{L}}_v(v-u) - \boldsymbol{\mathcal{L}}_v u_\delta \\ &\Longleftrightarrow \end{aligned} \tag{4.25}$$

$$\begin{aligned} (\mathbf{I} + \boldsymbol{\mathcal{L}}_v)u_\delta &= -\boldsymbol{\mathcal{L}}_v(v-u) \\ &= -(\boldsymbol{\mathcal{L}}_v + \mathbf{I} - \mathbf{I})(v-u)\ . \end{aligned} \tag{4.26}$$

Then we have that

$$\begin{aligned} u_\delta &= -(\mathbf{I} - (\boldsymbol{\mathcal{L}}_v + \mathbf{I})^{-1})(v-u) \\ &= -(\boldsymbol{P}_2 - \boldsymbol{A})\boldsymbol{P}_2^{-1}(v-u). \end{aligned} \tag{4.27}$$

A description of y_δ as generated by a dynamic system driven by the difference $v-u$ is already given in (4.18). We thus obtain:

Result 4.2 Windup effects described as a separate system
For the choice $\boldsymbol{A}_o\boldsymbol{P}_1 = \boldsymbol{\alpha}$ the windup effects defined in the Definition 3.2 can be described by

$$\begin{aligned} y_\delta &= \boldsymbol{B}\boldsymbol{P}_2^{-1}(v-u) \;=\; \boldsymbol{\mathcal{H}}_\delta\delta \\ u_\delta &= (\boldsymbol{A}\boldsymbol{P}_2^{-1} - \mathbf{I})\delta \;=\; -(\mathbf{I} - (\boldsymbol{\mathcal{L}}_v + \mathbf{I})^{-1})\delta \\ \delta &= v-u. \end{aligned} \tag{4.28}$$

This description is depicted in Figure 4.7.

The anti-windup design problem is now reduced to finding an appropriate polynomial matrix $\boldsymbol{P}_2$ that accomplishes a proper trade-off between the loop transfer function $\boldsymbol{\mathcal{L}}_v$ and the desaturation transient dynamics $\boldsymbol{\mathcal{H}}_\delta$ in (4.18), which both now have become independent of the nominal controller.

Notice that if we have a perfect model of $\boldsymbol{\alpha}$ the cancellation can be interpreted as separating the linear and the nonlinear loop so that external disturbance and references can be seen as if they enter the linear system and are taken care of by the nominal controller and then, enter the nonlinear loop only via u_l.

Seen from the perspective of the nonlinear loops in Figure 4.6 and Figure 4.7, the control signal u_l acts as an external "disturbance" that excites the dynamics in the nonlinear loop when it exceeds the saturation limits. Furthermore, u_l moves the saturation limits as seen from the perspective of u_δ. This situation is similar to the one we described in Chapter 2 when having external feed forward control added to the controller output. From the perspective on the system in this section (as separate linear and nonlinear loops), a consequence of this property is that, when u_l operates close to a saturation limit after entering into the linear region of ψ, after a saturation event, not much control authority is left to the AWC for control and reduction of the saturation effects.

Notice that minimizing the loop transfer function, measured in some standard system norm, will make $|u_\delta| \triangleq |u - u_l|$ small. The minimum norm is zero and obtained for $\boldsymbol{P}_2 = \boldsymbol{A}$. Minimizing $|y_\delta|$ requires feedback, i.e., $u_\delta \neq 0$, see Figures 4.6 and 4.7. LQ-optimization based design procedures that allow a reasonable trade-off between these often contradictory requirements, were presented in [47] and [56] for SISO-systems and in [49],[50] for MIMO-systems. Similar design methods will be discussed in detail in Section 5.1. Notice that the systems described by Results 4.1 and 4.2 has the following property:

Property 4 If the plant denominator $\boldsymbol{A}$ and the anti-windup compensator $\boldsymbol{P}_2$ are selected diagonal, then the loop transfer function $\boldsymbol{\mathcal{L}}_v$ becomes diagonal and the MIMO-loop transfer function is thereby split-up in p separate SISO-loops.

This decoupling allows us to use SISO methods for the design of $\boldsymbol{P}_2 = \mathrm{diag}(P_{2i})$. Such design methods are discussed in Chapters 5 and 6.

4.3.1 The scheme by Teel & Kapoor

In [52], and also in [51], the researchers suggest an anti-windup compensator scheme for controllers and plants represented by state-space models. In case linear state feedback via a constant gain matrix $\mathbf{L}_\delta$, i.e., for the special choice of $\kappa(x_\delta) = \mathbf{L}_\delta x_\delta$ in the scheme proposed in [52], the AWC in [52] becomes very similar to the AWC we proposed in this section. The cancellation of the nominal controller effect in the expressions $\boldsymbol{\mathcal{H}}_\delta$ and $\boldsymbol{\mathcal{L}}_v$, which we obtained by selecting $\boldsymbol{A}_o\boldsymbol{P}_1 = \boldsymbol{\alpha}$ is, however, accomplished in another, and in some sense more elegant way in [52]. It is obviously so that the output u from the nominal controller (2.2) is always $u = u_l$ if its input y is always $y = y_l$. The trick is to estimate y_l and substitute it for y in the nominal controller. Such an estimate is, in fact, already available. We know from before that $y_l = y - y_\delta$ where

$$y_\delta = \boldsymbol{B}\boldsymbol{P}_2^{-1}(v - u) = \boldsymbol{B}\boldsymbol{A}^{-1}(v - u_l). \tag{4.29}$$

Hence, the following controller gives the same control action u as the one described earlier in this section:

A polynomial version of the AWC proposed by Teel & Kapoor

$$\begin{aligned} \boldsymbol{R}u_l &= -\boldsymbol{S}(y - y_\delta) + \boldsymbol{T}r \\ \xi_\delta &= \boldsymbol{A}^{-1}(v - u_l) \\ y_\delta &= \boldsymbol{B}\xi_\delta \\ u_\delta &= (\boldsymbol{A} - \boldsymbol{P}_2)\xi_\delta \\ u &= u_l + u_\delta \\ v &= \psi(u). \end{aligned} \tag{4.30}$$

Here ξ_δ are *partial states*. For an explanation of the concept *partial state*, see e.g. Kailath [1].

The situation is depicted in Figure 4.8. This AWC cancels input saturation effects y_δ present in the plant output y, before they affect the controller. By doing so, the nominal controller will always operate as if the systems was linear and consequently the nominal controller output will be u_l. The signal u_δ represents the feedback around ψ and it can, as we have argued many times in our discussions, be used to reduce the windup effects y_δ.

The anti-windup compensator scheme proposed in [52] can be used for nonlinear anti-windup modifications and in [75] the researchers propose an anti-windup modification design based on recent results on explicit linear quadratic regulators for constrained systems [76].

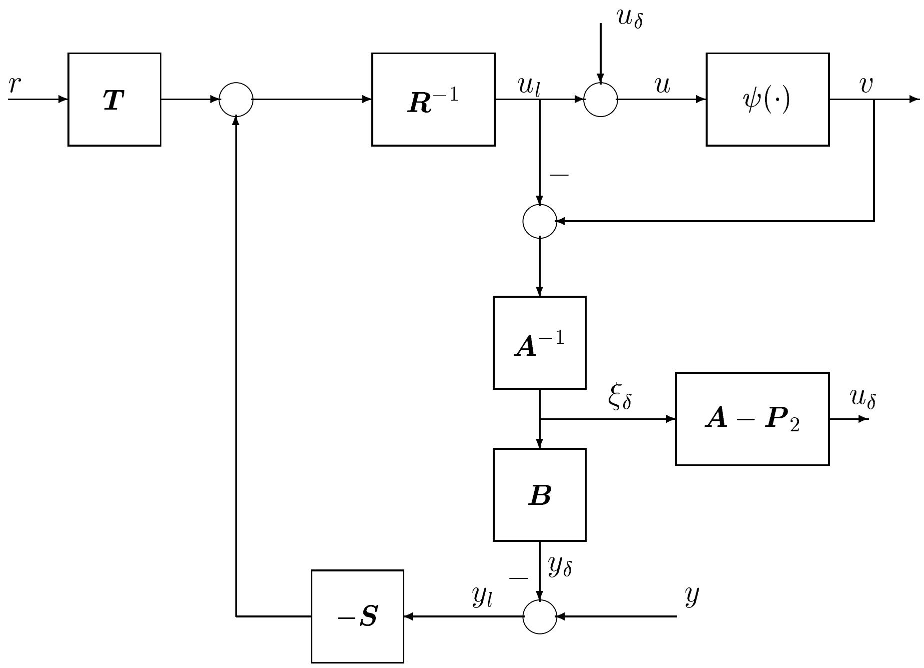

Figure 4.8: A polynomial version of the AWC proposed by Teel & Kapoor

CHAPTER 5

MIMO AWC design: $\mathcal{H}_2$ and LQR methods

Design of anti-windup compensators for MIMO systems is an important and non-trivial issue. Although there exist exact methods for analysis and synthesis concerning *stability*, it is not clear how performance can be achieved in such a system. One of the reasons for this gap is of fundamental character namely that linear AWC:s are comparatively simple controller structures, used for the control of a MIMO-system with input limiters. However, as we argued in Section 3.5, in systems where the *impact of saturations* are *weak*, we can expect linear AWC:s to work quite well. If properly designed, that is.

In this chapter we will present model-based design methods that take both performance and stability into consideration. The anti-windup compensator design problem is formulated as a *Linear Quadratic Regulator* (LQR)-optimization problem.

We open the chapter by presenting the LQR design methods and the corresponding solutions. Then, anti-windup designs that decouples the loop are proposed and discussed. A short presentation of some stability analysis methods follows after that and we close the chapter by illustrating the performance of our proposed design methods by a number of comparative examples.

5.1 LQR AWC design: a state-space approach

The separation of windup effects from the linear behavior, allowing us to expressed them as two different systems in the Section 4.3, will be used here. Recall that the separation requires that the polynomial matrices $\boldsymbol{A}_o$ and $\boldsymbol{P}_1$ are selected as in (4.17) and the LQR-design concerns only the polynomial matrix $\boldsymbol{P}_2$.

For our purpose it is appropriate to use the system description of windup effects of Result 4.1 in this, and in the first part of the next, section. In this section, however, we will represent the windup effects of Result 4.1 by a state-space description and the anti-windup design problem is, as we will show, then to be solved by finding a state-feedback gain matrix that minimizes a quadratic criterion. Once obtained, this matrix can be used for calculating the polynomial matrix $\boldsymbol{P}_2$.

Before we proceed, it should be pointed out, however, that by the use of a state-space description of the plant, the state-feedback gain matrix, which will be denoted by $\mathbf{L}_\delta$, can be used directly in order to obtain the additional control action u_a (4.9). Such a scheme is used in Chapter 8.

Let a state space representation of the plant (2.1) be described by

$$\begin{aligned} \nu x(t) &= \mathbf{F}x(t) + \mathbf{G}(v(t) + \beta(t)) \\ y(t) &= \mathbf{C}x(t) \end{aligned} \tag{5.1}$$

where ν may represent the derivative operator $\frac{d}{dt}$ or the forward shift operator q. From linear systems theory we know that the representation is by no means unique. However, regardless of the representation, (2.1) and (5.1) are two ways to describe the input-output behavior. In the sequel we shall use a "$\sim$" to indicate that (2.1) and (5.1) correspond to one another by writing

$$\boldsymbol{B}\boldsymbol{A}^{-1} \sim \left[\begin{array}{c|c} \mathbf{F} & \mathbf{G} \\ \hline \mathbf{C} & \mathbf{0} \end{array}\right] . \tag{5.2}$$

Given a state space description (5.1) of (2.1) the windup effects in the plant given by Result 4.1 can now be represented by

$$\begin{aligned} \begin{bmatrix} \nu x_\delta \\ x_\delta \end{bmatrix} &= \left[\begin{array}{c|c} \mathbf{F} & \mathbf{G} \\ \hline \mathbf{I} & \mathbf{0} \end{array}\right] \begin{bmatrix} x_\delta \\ (v - u_l) \end{bmatrix} \\ y_\delta &= \mathbf{C}x_\delta \, . \end{aligned} \tag{5.3}$$

For an explanation of the nomenclature see also the Remarks on the notations at the beginning of the thesis.

Assume that the plant input v is given by

$$
\begin{aligned}
v &= \psi(u) \\
u &= u_l \ ,
\end{aligned}
\tag{5.4}
$$

where u_l is, as before, the control signal in the ideal linear system not affected by saturation. Then, according to the Results 4.1 and 4.2, we have that

$$
\begin{aligned}
\boldsymbol{\mathcal{H}}_\delta &= \boldsymbol{B}\boldsymbol{A}^{-1} \sim \left[\begin{array}{c|c} \mathbf{F} & \mathbf{G} \\ \hline \mathbf{C} & \mathbf{0} \end{array}\right] \\
\boldsymbol{\mathcal{L}}_v &= \mathbf{0} \ .
\end{aligned}
\tag{5.5}
$$

respectively.
Now, we *create* the control signal u_δ from state feedback of the states x_δ, i.e.

$$
u_\delta = -\mathbf{L}_\delta x_\delta \ , \tag{5.6}
$$

and add it to u_l in order to obtain the control signal u as

$$
u = u_l + u_\delta \ . \tag{5.7}
$$

Hence, the state space description of the windup effects, that corresponds to the polynomial description of Result 4.1, is given by (5.3), (5.6) and (5.7). We summarize these expressions as a Result:

> **Result 5.1 Windup effects described as a separate system**
> The windup effects in the state space system (5.1), according to the Definition 4.2, can be described by
>
> $$
> \begin{aligned}
> \begin{bmatrix} \nu x_\delta \\ x_\delta \end{bmatrix} &= \left[\begin{array}{c|c} \mathbf{F} & \mathbf{G} \\ \hline \mathbf{I} & \mathbf{0} \end{array}\right] \begin{bmatrix} x_\delta \\ (v - u_l) \end{bmatrix} \\
> y_\delta &= \mathbf{C} x_\delta \\
> u_\delta &= -\mathbf{L}_\delta x_\delta \ .
> \end{aligned}
> \tag{5.8}
> $$

This system is shown in the Figure 5.1.

The anti-windup design problem, aiming at minimizing the windup effects, is then to be solved by finding an appropriate state-feedback gain matrix $\mathbf{L}_\delta$. We will soon show how this can be done by the use of LQR-design but first, we will derive state space descriptions for $\boldsymbol{\mathcal{H}}_\delta$ and $\boldsymbol{\mathcal{L}}_v$, which, in turn, allow us to express a new Result that corresponds to Result 4.2 where the difference $v - u$ is the input to the system describing the windup effects. At this point it is important to point out that many of the design methods that takes saturations into account *a priori* can be used here. References where such design methods are proposed were given in Section 1.2.

By subtracting and adding u_δ to the input of the system of Result 5.1, we have that

$$\begin{aligned} \nu x_\delta &= \mathbf{F}x_\delta + \mathbf{G}(v - u_l - u_\delta + u_\delta) \;=\; \mathbf{F}x_\delta + \mathbf{G}(v - u + u_\delta) \\ &= \mathbf{F}x_\delta + \mathbf{G}\delta + \mathbf{G}u_\delta \;, \end{aligned} \tag{5.9}$$

where $\delta = v - u$ as before. Now, we insert $u_\delta = -\mathbf{L}_\delta x_\delta$ which gives that

$$\begin{aligned} \nu x_\delta &= \mathbf{F}x_\delta + \mathbf{G}\delta - \mathbf{G}\mathbf{L}_\delta x_\delta \\ &= (\mathbf{F} - \mathbf{G}\mathbf{L}_\delta)x_\delta + \mathbf{G}\delta \;. \end{aligned} \tag{5.10}$$

We thus obtain:

Result 5.2 Windup effects described as a separate system
The windup effects in the state space system (5.1), according to the Definition 4.2, can be described by

$$\begin{aligned} \begin{bmatrix} \nu x_\delta \\ x_\delta \end{bmatrix} &= \left[\begin{array}{c|c} \mathbf{F} - \mathbf{G}\mathbf{L}_\delta & \mathbf{G} \\ \hline \mathbf{I} & \mathbf{0} \end{array}\right] \begin{bmatrix} x_\delta \\ (v - u) \end{bmatrix} \\ y_\delta &= \mathbf{C}x_\delta \\ u_\delta &= -\mathbf{L}_\delta x_\delta \;. \end{aligned} \tag{5.11}$$

According to the expression for y_δ of Result 4.2, and the expression for u_δ of Result 4.1, the transfer function $\boldsymbol{\mathcal{H}}_\delta$ and the loop transfer function $\boldsymbol{\mathcal{L}}_v$ of the polynomial system are related to the state space ditto as

$$\boldsymbol{\mathcal{H}}_\delta = \boldsymbol{B}\boldsymbol{P}_2^{-1} \sim \left[\begin{array}{c|c} \mathbf{F} - \mathbf{G}\mathbf{L}_\delta & \mathbf{G} \\ \hline \mathbf{C} & \mathbf{0} \end{array}\right]$$

$$\boldsymbol{\mathcal{L}}_v = (\boldsymbol{P}_2 - \boldsymbol{A})\boldsymbol{A}^{-1} \sim \left[\begin{array}{c|c} \mathbf{F} & \mathbf{G} \\ \hline \mathbf{L}_\delta & \mathbf{0} \end{array}\right] \tag{5.12}$$

respectively. It should clear also from Figure 5.1 that $\mathcal{L}_v$ is given by the state space description in (5.12).

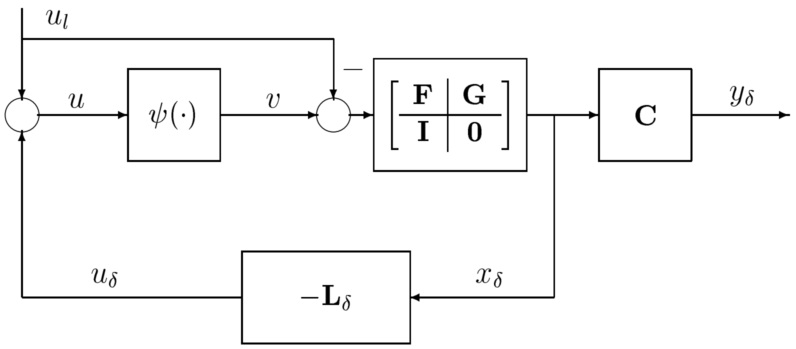

Figure 5.1: A state-space description of the system in Figure 4.6.

According to Definition 3.1, windup effects in a state space system may be present in all of the states x_δ. We will, however, in the sequel only be interested in the windup effects given by the two linear combinations $y_\delta = \mathbf{C}x_\delta$ and $u_\delta = -\mathbf{L}_\delta x_\delta$ of x_δ. This is a reasonable choice when y_δ and u_δ are the only linear combinations of states that have a direct physical interpretation.

With our definition of windup effects (Definition 3.1 and 3.2) in mind, let us now formalize Objectives 2 and 3 of Section 3.4 as a LQR design problem. A basic reason for considering LQR is that this solution has nice robustness properties with respect to input failures (which saturation events can be considered as to be from a linear perspective). See e.g. Grimble [9] Section 2.6.3 and Anderson & Moore [11] Chapters 5 and 8. We will motivate this further after presenting the following two results:

Result 5.3 The LQR anti-windup problem and solution for continuous time systems
Let $\mathbf{F}$, $\mathbf{G}$ and $\mathbf{C}$ be matrices in a continuous time state space description of Result 5.1. The LQR cost function to be minimized is given by

$$J_c \;=\; \int (y_\delta^T(t)\mathbf{Q}y_\delta(t) \;+\; u_\delta^T(t)\mathbf{Q}_u u_\delta(t))\; dt \tag{5.13}$$

where $\mathbf{Q} \;=\; \mathbf{Q}^T \;\geq 0$ and $\mathbf{Q}_u \;=\; \mathbf{Q}_u^T \;> 0$ are constant symmetric matrices. The steady-state solution to (5.13) is given by

$$\mathbf{L}_\delta \;=\; \mathbf{Q}_u^{-1}\mathbf{G}^T\mathbf{P}_c \tag{5.14}$$

where $\mathbf{P}_c$ satisfies the algebraic Riccati equation

$$\mathbf{F}^T\mathbf{P}_c + \mathbf{P}_c\mathbf{F} - \mathbf{P}_c\mathbf{G}\mathbf{Q}_u^{-1}\mathbf{G}^T\mathbf{P}_c + \mathbf{C}^T\mathbf{Q}\mathbf{C} = 0\ . \tag{5.15}$$

Notice that when selecting the penalty matrix $\mathbf{Q}_u = \rho\mathbf{I} > 0$ we have that

$$\mathbf{L}_\delta = \mathbf{G}^T\mathbf{P}_c\frac{1}{\rho}\ . \tag{5.16}$$

Since the LQR-solution guarantees $\mathbf{P}_c = \mathbf{P}_c^T \geq 0$, then, according to the stability conditions given in [52] which we have summarized in the Lemma 6.1 below, stability is guarantied if

$$\mathbf{P} = \mathbf{P}_c\frac{1}{\rho} \tag{5.17}$$

satisfies the Lyapunov equation $\mathbf{F}^T\mathbf{P} + \mathbf{P}\mathbf{F} < 0$.

Result 5.4 The LQR anti-windup problem and solution for discrete time systems
Let $\mathbf{F}$, $\mathbf{G}$ and $\mathbf{C}$ be matrices in a discrete time state space description of Result 5.1. The LQR cost function to be minimized is given by

$$J_d = \sum_{t=0}^{T} (y_\delta^T \mathbf{Q} y_\delta + u_\delta^T \mathbf{Q}_u u_\delta) \tag{5.18}$$

where $\mathbf{Q} = \mathbf{Q}^T \geq 0$ and $\mathbf{Q}_u = \mathbf{Q}_u^T \geq 0$ are constant symmetric matrices. The steady-state solution is given by

$$\mathbf{L}_\delta = (\mathbf{Q}_u + \mathbf{G}^T \mathbf{P}_d \mathbf{G})^{-1} \mathbf{G}^T \mathbf{P}_d \mathbf{F} \tag{5.19}$$

where $\mathbf{P}_d$ is obtained from the discrete time algebraic Riccati equation

$$\mathbf{F}^T \mathbf{P}_d \mathbf{F} - \mathbf{P}_d - \mathbf{F}^T \mathbf{P}_d \mathbf{G} (\mathbf{Q}_u + \mathbf{G}^T \mathbf{P}_d \mathbf{G})^{-1} \mathbf{G}^T \mathbf{P}_d \mathbf{F} + \mathbf{C}^T \mathbf{Q} \mathbf{C} = 0 \, . \tag{5.20}$$

Although Results 5.3 and 5.4 are somewhat novel when used for the design of anti-windup compensators, aiming at reducing windup effects $y_\delta, \; u_\delta$, the LQ design tools themselves are well known and can be found in many standard textbooks on control, see e.g. [8][9][10][11][12].

A motivation for why we use LQR methods for the design of anti-windup compensators will be given next and we choose to discuss the discrete-time case by considering the criterion (5.18).

Assume that the controller output, $u = u_l + u_\delta$, de-saturates at time $t = 0$ and that it stays unsaturated thereafter (at least for a while). In case the elements in the matrix $\mathbf{Q}$ are selected large (or the elements in $\mathbf{Q}_u$ small), then the LQR solution will make the sum of squares of y_δ small, by making the transient dynamics $\boldsymbol{\mathcal{H}}_\delta$ (5.12) become fast (and stable). *However, if the elements of $\mathbf{Q}$ are selected too large, then the loop gain $|\boldsymbol{\mathcal{L}}_v|$ (5.12), may become too large and u_δ may tend to repeatedly re-saturate due to this. As a consequence, the sum of squares of the saturation effects y_δ may not become small although that was what we aimed for.* The problem we want to highlight here is caused by a too aggressive control action provided by $u_\delta = -\mathbf{L}_\delta x_\delta$ (which represents windup effects in the controller but also helps reducing the effects in the plant). If the elements of $\mathbf{Q}$ are selected small, then the loop gain reduces and the stability properties will improve and the tendency of u_δ (and thereby also $u = u_l + u_\delta$) to repeatedly re-saturate will reduce. However, as a consequence, the transient dynamics $\boldsymbol{\mathcal{H}}_\delta$ will approach the dynamics of the uncompensated plant which may be slow or poorly damped. The LQR-design provides a tool to manage these (most often contradictory) goals via proper selection of $\mathbf{Q}$ and $\mathbf{Q}_u$.

The stability properties are of such great importance that we make the following remarks concerning them:

Remark 5.1 It is a well known fact that the LQR-solution $\mathbf{L}_\delta$ guarantees $\boldsymbol{\mathcal{H}}_\delta$ in (5.12) to be asymptotically stable. The solutions $\mathbf{L}_\delta$ of the Result 5.3 and 5.4 does not guarantee stability of the nonlinear system (5.3) for all $\mathbf{Q}_u$. However, in case the plant is asymptotically stable, large elements of $\mathbf{Q}_u$ will make $\boldsymbol{\mathcal{L}}_v \to \mathbf{0}$ and the system will eventually become stable as the elements in $\mathbf{Q}_u$ are increased by the designer (or perhaps by some automatized design procedure).

Remark 5.2 The passivity-based stability condition, given for the continuous time case in [52] (summarized in the Lemma 6.1), which places restrictions on the solution $\mathbf{P}_c$ of the continuous time Riccati equation, does not hold for the solution $\mathbf{P}_d$ of the discrete time Riccati equation.

Remark 5.3 Notice that the robustness problems related to observers and state estimation for the LQG-solution, pointed out by Doyle in [42], are not present here. We perform feedback from the states of a model that is driven exclusively by inputs!

We can expect the solution to give nice performance for properly selected penalty matrices $\mathbf{Q},\ \mathbf{Q}_u$. This is due to the fact that we can disregard the objectives of the *underlying design* problem regarding the *nominal controller*, i.e., objectives such as disturbance attenuation, reference tracking etc. Hence, we can select the penalty matrices with focus on minimizing the windup effects regarding Objective 2 and 3 ! [1]

The solution $\mathbf{L}_\delta$ can be used directly in the anti-windup compensator scheme suggested by Teel & Kapoor [52], see Section 4.3.1. When the plant is represented by a state space description, (as in [52]) then the partial states ξ of our polynomial description of the scheme (4.30), are simply the states x_δ. The control signal u_δ

[1] It should, however, be remembered that the solution to the continuous time problem, (5.14)-(5.15) and the solution to the discrete time problem, (5.19)-(5.20) is *optimal* only while the system remains linear ($\psi(u(t)) \equiv u(t)$).

can then be obtained directly as $u_\delta = -\mathbf{L}_\delta x_\delta$.

For the polynomial anti-windup compensator (4.8) the polynomial $\boldsymbol{P}_2$ must be specified and we will show two different ways of how it can be obtained next.

5.2 LQR AWC design: A polynomial approach

The relation between the state-space description (5.3) and the polynomial description of the plant, $\boldsymbol{B}\boldsymbol{A}^{-1}$ in (2.1), can also be expressed as

$$\begin{aligned} \boldsymbol{B}_x\boldsymbol{A}^{-1} &\sim \left[\begin{array}{c|c} \mathbf{F} & \mathbf{G} \\ \hline \mathbf{I} & \mathbf{0} \end{array}\right] \\ \boldsymbol{B} &= \mathbf{C}\boldsymbol{B}_x \ . \end{aligned} \tag{5.21}$$

Here, an output vector $\xi = \boldsymbol{B}_x\boldsymbol{A}^{-1}v$ constitutes partial states of the plant model.

According to (5.12) the polynomial and the state-space loop transfer functions are related as

$$\begin{aligned} (\boldsymbol{P}_2 - \boldsymbol{A})\boldsymbol{A}^{-1} &\sim \left[\begin{array}{c|c} \mathbf{F} & \mathbf{G} \\ \hline \mathbf{L}_\delta & \mathbf{0} \end{array}\right] \\ &\sim \mathbf{L}_\delta\boldsymbol{B}_x\boldsymbol{A}^{-1} \ . \end{aligned} \tag{5.22}$$

Then we have that

$$\begin{aligned} \boldsymbol{P}_2 - \boldsymbol{A} &= \mathbf{L}_\delta\boldsymbol{B}_x \\ &\Longleftrightarrow \\ \boldsymbol{P}_2 &= \mathbf{L}_\delta\boldsymbol{B}_x + \boldsymbol{A} \ . \end{aligned} \tag{5.23}$$

Hence, this way to obtain the polynomial matrix $\boldsymbol{P}_2$ requires the gain matrix $\mathbf{L}_\delta$ from the Riccati-solution in Result 5.3, or in Result 5.4, to be obtained in the continuous-time case or in the discrete-time case respectively.

It can be shown that the LQR-problem (5.13) or (5.18) is also solved by solving the following polynomial spectral factorization equation

$$\overline{\boldsymbol{P}}_2^*\overline{\boldsymbol{P}}_2 = \boldsymbol{B}_x^*\mathbf{Q}\boldsymbol{B}_x + \boldsymbol{A}^*\mathbf{Q}_u\boldsymbol{A} \ . \tag{5.24}$$

Here, the suffix $*$ represents transpose-conjugate, see Remarks on the notations at the beginning of the thesis. A sketch of proof will now be presented for the continuous time case. By assuming that the the signal δ in the system of Result (4.28) is a dirac-pulse applied at time $t = 0$, we can express the cost function (5.13) as

$$J = \int_0^\infty (y_\delta^T(t)\mathbf{Q}y_\delta(t) + u_\delta^T(t)\mathbf{Q}_u u_\delta(t))\,dt$$

(Parseval's formula)

$$\begin{aligned} &= \frac{1}{\pi}\int_0^\infty \boldsymbol{\mathcal{H}}_\delta^*(\omega)\mathbf{Q}\boldsymbol{\mathcal{H}}_\delta(\omega) \\ &+ (\mathbf{I} - (\boldsymbol{\mathcal{L}}_v(\omega)+\mathbf{I})^{-1})^*\mathbf{Q}_u(\mathbf{I} - (\boldsymbol{\mathcal{L}}_v(\omega)+\mathbf{I})^{-1})d\omega \\ &= \left\| \mathbf{Q}^{\frac{1}{2}}\boldsymbol{\mathcal{H}}_\delta \right\|_2^2 + \left\| \mathbf{Q}_u^{\frac{1}{2}}\left(\mathbf{I} - (\boldsymbol{\mathcal{L}}_v+\mathbf{I})^{-1}\right)\right\|_2^2 \end{aligned} \tag{5.25}$$

Insertion of the expressions for $\boldsymbol{\mathcal{H}}_\delta$ and $\boldsymbol{\mathcal{L}}_v$ of Result 4.2 gives

$$J = \left\| \mathbf{Q}^{\frac{1}{2}}\boldsymbol{B}\boldsymbol{P}_2^{-1} \right\|_2^2 + \left\| \mathbf{Q}_u^{\frac{1}{2}}\left(\boldsymbol{A}\boldsymbol{P}_2^{-1} - \mathbf{I}\right)\right\|_2^2. \tag{5.26}$$

Relationship between discrete time polynomial and state space solutions of the LQR problem is discussed in detail in [77].

The polynomial matrix $\boldsymbol{P}_2$ of the anti-windup compensator (4.9), affecting the system according to the expressions in (5.12), can be calculated as

$$\boldsymbol{P}_2 = \mathbf{A}_m(\overline{\mathbf{P}}_{2m})^{-1}\overline{\boldsymbol{P}}_2. \tag{5.27}$$

Here $\overline{\boldsymbol{P}}_2$ is the "stable" solution of (5.24) (i.e. $\overline{\boldsymbol{P}}_2^{-1}$ is stable) and $\mathbf{A}_m$ and $\overline{\mathbf{P}}_{2m}$ are the leading coefficient matrices of $\boldsymbol{A}$ and $\overline{\boldsymbol{P}}_2$ respectively. The scaling of $\overline{\boldsymbol{P}}_2$ in (5.27) is needed in order to obtain a polynomial matrix $\boldsymbol{P}_2$ that fulfils the Requirement 4.3, see Remark 4.5, and the use of the stable solution $\overline{\boldsymbol{P}}_2$ is needed in order for $\boldsymbol{P}_2$ to fulfil Requirement 4.4.

The choice of the penalty matrices $\mathbf{Q},\ \mathbf{Q}_u$ in the criterion (5.26) have, in the end, the same effect on the system as in the state space case discussed in the previous section. We will therefore not repeat the design guidelines here for the polynomial case but refer to them given in the previous section.

Riccati-equation solvers are available in many standard software packages on control, i.e., Control System Toolbox for Matlab, whereas software packages having spectral factorization-equation solvers for polynomial-matrix expressions are less common. However, the polynomial toolbox for Matlab, developed by PolyX [78] provides such solvers, which are both accurate and fast.

5.3 Design for obtaining diagonal loop gain

We now consider the case when $\boldsymbol{A}_o\boldsymbol{P}_1 = \boldsymbol{\alpha}$ (as above), and $\boldsymbol{P}_2 = \mathrm{diag}(P_{2j})$ and $\boldsymbol{A} = \mathrm{diag}(A_j)$ both are selected diagonal. Such choices makes the loop transfer function diagonal, i.e.,

$$\begin{aligned} \boldsymbol{\mathcal{L}}_v &= \mathrm{diag}(\mathcal{L}_j) \\ \mathcal{L}_j &= \frac{P_{2j}}{A_j} - 1. \end{aligned} \tag{5.28}$$

See Section 4.3, in particular Result 4.1 and 4.2 and Property 4.

Thus, the second step of the design of an anti-windup compensator (considering the choice $\boldsymbol{A}_o\boldsymbol{P}_1 = \boldsymbol{\alpha}$ to be the first) is reduced to m scalar designs in which the m elements of the diagonal loop gain matrix $\boldsymbol{\mathcal{L}}_v$ are systematically adjusted by appropriate choices of the scalar polynomials P_{2j} using scalar tools, in particular Nyquist-like methods that will be desrcibed in Section 5.4.2. This makes the design procedure simpler compared to most cases involving MIMO-design. This simplification is, however, accomplished to the price of some loss in performance and it involves the following two potential drawbacks:

- A diagonal loop transfer function $\boldsymbol{\mathcal{L}}_v$ (taken around ψ) decouples saturation events in such a way that when saturation occurs in the component u_i of the vector u, say, then none of the other components of u (operating in the linear region) will respond to this. Hence, none of the other components will help reducing the saturation effects, simply because they are not aware of them.
- The constrained structure of $\boldsymbol{\mathcal{H}}_\delta$ (having a diagonal denominator $\boldsymbol{P}_2$) will in some cases result in slower decay of the saturation effects.

Next we propose a LQR design strategy similar to the one presented in Section 5.2 but modified so that it allows design of the diagonal elements P_{2j}. In Chapter 6 we will discuss heuristic guidelines for the design of SISO AWC:s which are useful also for the design of polynomials P_{2j} in such a "diagonal" MIMO design.

5.3.1 LQR AWC design for MIMO systems with diagonal loop transfer function

By selecting the penalty matrices $\mathbf{Q} = \mathbf{I}$, $\mathbf{Q}_u = \mathrm{diag}(\rho_j)$, the criterion (5.26) will be given by

$$J_p = \left\|\boldsymbol{B}\boldsymbol{P}_2^{-1}\right\|_2^2 + \left\|\mathrm{diag}(\sqrt{\rho_j})\left(\boldsymbol{A}\boldsymbol{P}_2^{-1} - \mathbf{I}\right)\right\|_2^2 . \tag{5.29}$$

Let B_{ij} be the ij-th scalar polynomial element of the plant numerator $\boldsymbol{B}$. The minimum of (5.29), with respect to a diagonal polynomial matrix $\boldsymbol{P}_2$, for a given diagonal penalty matrix $\mathbf{Q}_u = \text{diag}\sqrt{\rho_j}$, is shown in [49] to be attained by solving p separate scalar spectral factorizations

$$\begin{aligned} r_j P_j P_j^* &= \sum_{i=1}^{m} B_{ij} B_{ij}^* + \rho_j A_j A_j^* \\ \boldsymbol{P}_2 &= \text{diag}(P_j) \ . \end{aligned} \tag{5.30}$$

A detailed derivation is presented in Appendix B.3.1. Here r_j is a scaling factor. Equation (5.30) has to be solved for $j = 1, 2....p$, where p is the number of process inputs and m is the number of process outputs.

Note that if $\rho_j \to \infty$, then $P_j \to A_j$ for stable A_j. The jth loop gain $\boldsymbol{\mathcal{L}}_j$ in (5.28) will then contract towards zero and stability is secured if A_j is stable[2]. As a result, repeated saturations will not occur in that loop. However, the windup effects in the plant may decay slowly since the common denominator of the jth column of $\boldsymbol{\mathcal{H}}_\delta$ goes towards the plant dynamics A_j, which may be slow or poorly damped.

At the other extreme, i.e. if ρ_j is selected small, then the dynamics of the jth column of $\boldsymbol{\mathcal{H}}_\delta$ will become fast, while the jth loop gain may become large as measured by $\|\mathcal{L}_j\|_2^2$. This may generate repeated re-saturations and one must therefore select the values of ρ_j properly to obtain an appropriate trade-off.

5.4 Tools for stability analysis

Stability of feedback loops is one of the most basic issues in control theory. In this thesis it is in our interest to be able to predict stability in feedback loops consisting of one linear part, represented by the loop transfer function $\boldsymbol{\mathcal{L}}_v$, and one nonlinear part represented by ψ. Although stability and performance properties of a particular control system solution often in practice are evaluated and approximately established, through numerous simulations, test as well as knowledge, based on analytical stability conditions will be important in some situations. We will therefore in this section present some well known stability criteria.

[2]For stable A_j, the loop gain $\mathcal{L}_j$ vanishes when $\rho_j \to \infty$. It is mostly possible to find adjustments of ρ_j which pushes $\mathcal{L}_j$ outside some avoidance sector. But there are exceptions. If triple or higher order integrators are present in $\mathcal{A}_j$, then a crossing between the loop gain and the describing function cannot be avoided. The intersection point must then be placed so far to the left that no disturbances with reasonable amplitudes will initiate a limit cycle oscillations.

It is well known that the requirements for closed loop stability, placed on $\mathcal{L}_v$ when limiters ψ are present in the loop, see Figure 5.2, are usually more restrictive compared to purely linear closed loop systems. Of course, if a system can be operated so that saturation never occurs, then that system will behave as a stable linear system. But unless saturation can be guaranteed to not occur, there is no guarantee that the system having input limiters will be stable, only because the linear closed loop system ($\psi \equiv \mathbf{I}$) is so.

Stability properties for a closed loop system, consisting of $\mathcal{L}_v$ and memoryless nonlinearities such as σ or γ defined in Chapter 2, have been analyzed by many researchers and several stability results and analysis methods, which apply when memoryless input saturations are present in the loop, have been proposed over the years. Some of these can only be used for the analysis of single-input systems whereas others generalize to analysis of multiple-input systems. The most frequently discussed methods, and probably the most frequently used, are

- the Circle-criterion,
- the Popov-criterion, and
- Nyquist-like analysis.

Discussions on these methods can be found in many standard textbooks on nonlinear control, see e.g. [79], [28]. Some early, and particular important, contributions on the issue of absolute stability can be found in [18].

When using a Nyquist-like analysis, the nonlinear loop is approximated using a *describing function* of the saturation nonlinearity. Since the Nyquist-criterion was originally proposed for analyzing stability in linear feedback systems, the name *Nyquist-like* analysis and design is often used in the case of nonlinear loops, in particular such as the ones discussed in this thesis.

The Circle-criterion and the Popov-Criterion generalize to analysis of MIMO-systems whereas the Nyquist criterion, in combination with the saturation describing function, is most powerful when used in the single-input case. There exist, however, methods for multiple-input describing functions but the gain in simplicity that describing functions imply, may be lost when used for stability analysis of multiple-input systems.

In the single-input case all three stability tests, the Circle, the Popov, and the Nyquist tests, can be carried out graphically in a Nyquist like plot and the anti-windup design can be carried out by using either heuristic loop shaping methods or optimization-based methods, such as the LQR-methods described earlier in this chapter. In the MIMO-case, stability *analysis* can be made graphically whereas *design* is in general more complicated. The reason for this is that the relation between the graphs and the tuning parameters is nontrivial. Of course, one can choose the anti-windup compensators such that the loop gain becomes diagonal, allowing graphical SISO-design methods to be used.

Whenever stability test are performed in the upcoming examples in this thesis, we use either the Nyquist-like criterion, the Circle criterion, or the criteria based on passivity given in [52] for the anti-windup scheme proposed by Teel & Kapoor. Since the Circle criterion can be found in most of the standard texts on nonlinear control, it will not be presented here. A somewhat uncommon, but in our view useful, variant of the Nyquist-like analysis is presented at the end of this section. Special cases of the passivity based criteria outlined in [52] will be presented next.

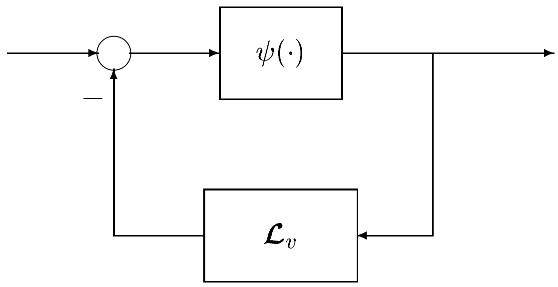

Figure 5.2: Loop transfer function and saturation

5.4.1 Passivity

The loop transfer function $\boldsymbol{\mathcal{L}}_v$ (5.12) is assumed to be a continuous-time state space description, given by

$$\boldsymbol{\mathcal{L}}_v = \mathbf{L}_\delta(s\mathbf{I} - \mathbf{F})^{-1}\mathbf{G} \tag{5.31}$$

Then, a sufficient condition for the feedback loop depicted in Figure 5.2 to be stable, is given in [52] and states, *in particular*, the following:

Lemma 5.1 If ψ is the amplitude limiter σ in (2.5) or the directionally compensated amplitude limiter γ in (2.17), and if $\mathbf{F}$ is critically stable, i.e. if there exists a $\mathbf{P} = \mathbf{P}^T \geq 0$ such that the Lyapunov equation

$$\mathbf{F}^T\mathbf{P} + \mathbf{P}\mathbf{F} \leq 0 \tag{5.32}$$

holds, then

$$\mathbf{L}_\delta \ = \ \mathbf{G}^T\mathbf{P} \tag{5.33}$$

gives a stable system.

5.4.2 Describing functions and Nyquist-like analysis

The method presented in this section is based on the classical Nyquist-criterion used for the analysis of linear feedback systems. By the use of a *describing function* approximation, $N(C,\omega)$, of the input nonlinearity, ψ, the loop transfer function

$$\mathcal{L}_v(\omega)N(C,\omega) \triangleq \overline{\mathcal{L}_v} \tag{5.34}$$

is a linear approximation of the nonlinear function $\mathcal{L}_v\psi(\cdot)$. See e.g. [79].

Describing functions
Rate- as well as amplitude saturations are nonlinear in their nature and can therefore not be described exactly in the frequency domain. The technique of *describing functions* gives, however, approximate frequency-domain models of these, and other, nonlinearities, see e.g. [17],[79],[28],[3]. Hence, a describing function of an input nonlinearity combined (i.e. multiplied) with a linear dynamic model of the SISO loop transfer function, give an approximative linear frequency domain description of the compound system (input saturation and loop transfer function). This allows us to use standard frequency domain methods, such as Nyquist- and Bode methods, for analysis and design of anti-windup compensators, in this and in the next chapter.

The basic definition of the describing function used in this thesis is given next.

Definition 5.1 Describing function
The describing function of a nonlinear element $N(\cdot)$ is given by the complex number

$$
\begin{aligned}
N(C,\omega) &= \frac{1}{C}(b_1 + ja_1) \\
&\text{where} \\
a_1 &= \frac{1}{\pi}\int_{-\pi}^{\pi} \eta(t)\cos(\omega t)d(\omega t) \\
b_1 &= \frac{1}{\pi}\int_{-\pi}^{\pi} \eta(t)\sin(\omega t)d(\omega t).
\end{aligned} \tag{5.35}
$$

Here, the signal $\eta(t)$ is the output from $N(i(t))$ when applying a sinusoid $i(t) = C\sin(\omega t)$ at its input. The integration over one period, $-\pi \to \pi$, shall begin first after that the output has reached a steady-state behavior.

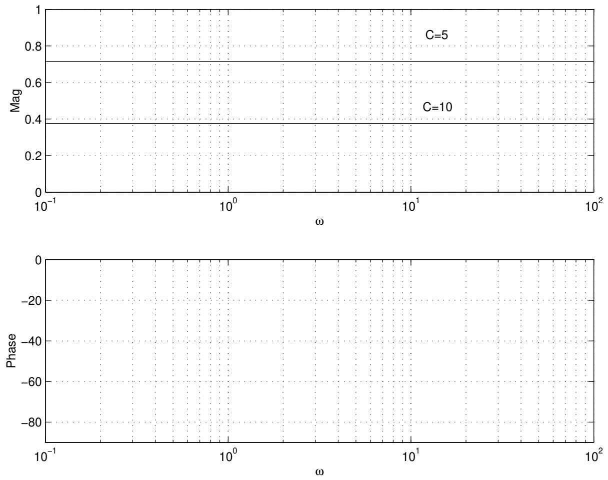

Figure 5.3: Describing function $N(C,\omega)$ of an amplitude limiter σ_{-3}^{+3} for $C = 1,\ 5$ and 10. Note that the amplitude $C = 1$ does not saturate the limiter.

Remark 5.4 The describing function defined in Definition 5.1 is a *first order* describing function. A first order describing function is a *linear* approximation of N. Linear describing functions are undoubtedly the most commonly used and discussed in the automatic control society where they most often are used for stability analysis using Nyquist-like methods.[3]

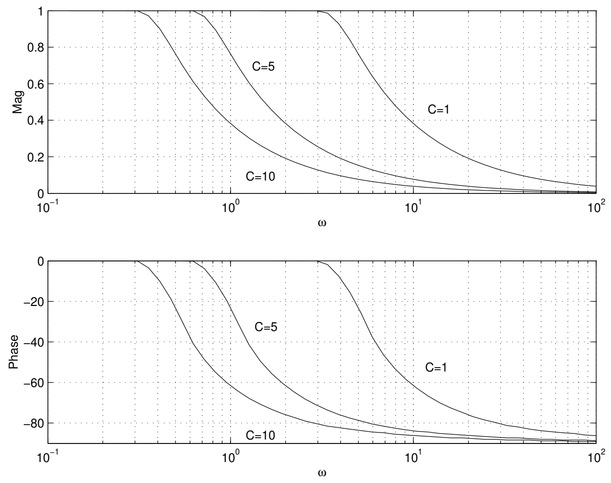

Figure 5.4: Describing function $N(C,\omega)$ of a rate limiter ρ_{-3}^{+3} for $C = 1, \quad 5$ and 10.

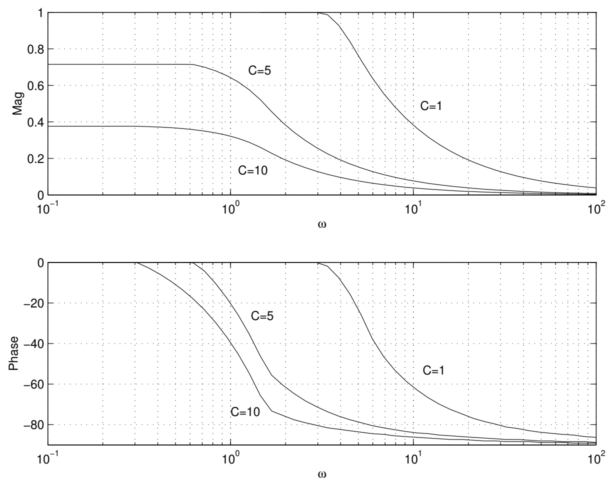

Figure 5.5: Describing function $N(C,\omega)$ of a combined amplitude and rate limiter $\rho_{-3}^{+3}[\sigma_{-3}^{+3}]$ for $C = 1,\ 5$ and 10.

[3] In other field of engineering, e.g. in the field of radio and power amplifiers, higher order describing functions are sometimes used to build simulators.

The describing function of an amplitude limiter σ_{-3}^{+3}, a rate limiter ρ_{-3}^{+3}, and a combined amplitude and rate limiter $\rho_{-3}^{+3}[\sigma_{-3}^{+3}]$, are shown in Figures 5.3, 5.4 and 5.5 respectively. Here, we have estimated the describing functions by the use of experimental evaluation. In should be pointed out, however, that memoryless nonlinearities, e.g. the amplitude limiter, have describing functions that can be expressed by compact mathematical expression. See e.g. Section 5.1 of [79].

While the describing function technique is based on sinusoidal approximations, there exist other methods based on other approximations. One such methods is the method of *stochastic linearization* which is based on a statistical approximation where the properties of a nonlinear element is described in terms of variances. In [29] the researchers present ”An LQR/LQG Theory for Systems With Saturating Actuators” which is based on this idea. Stochastic linearization will, however, not be discussed further in this thesis.

Nyquist-like analysis
We state the following condition:

Approximate condition for limit cycles Limit cycle oscillations can be expected to occur when

$$\mathcal{L}_v(\omega)N(C,\omega) \;=\; -1 \tag{5.36}$$

or, equivalently, if

$$\mathcal{L}_v(\omega) \;=\; -\frac{1}{N(C,\omega)}, \tag{5.37}$$

for any combination of amplitude and frequency (C,ω).

The most commonly discussed graphical analysis technique is carried out by checking wether or not $\mathcal{L}_v(\omega)$ intersects with $-\frac{1}{N(C,\omega)}$, for any combination (C,ω). This technique is well suited for simple nonlinear elements, e.g., the standard amplitude saturation function, having a describing function $N(C)$ which does not depend on ω and, furthermore, which does not involve phase-lag. Since we will analyze also rate limiters, which have describing functions that depend also on ω and give phase-lags, we will here plot the combined loop transfer function $\overline{\mathcal{L}_v}(\omega)$ in (5.34) and check wether it encircles (or stays well away from) the point $(-1,0)$ or not. This technique has at least two advantages compared to checking when $\boldsymbol{\mathcal{L}}_v$ intersects $-\frac{1}{N(C,\omega)}$:

1. It is simpler to analyze more complicated nonlinearities and the ”forbidden region” is the same, namely the neighborhood around the point $(-1, 0)$, for different kinds of describing functions.

2. It allows the use of the property *phase margin* (PM) which is strongly associated with robustness- and damping properties in feedback loops.

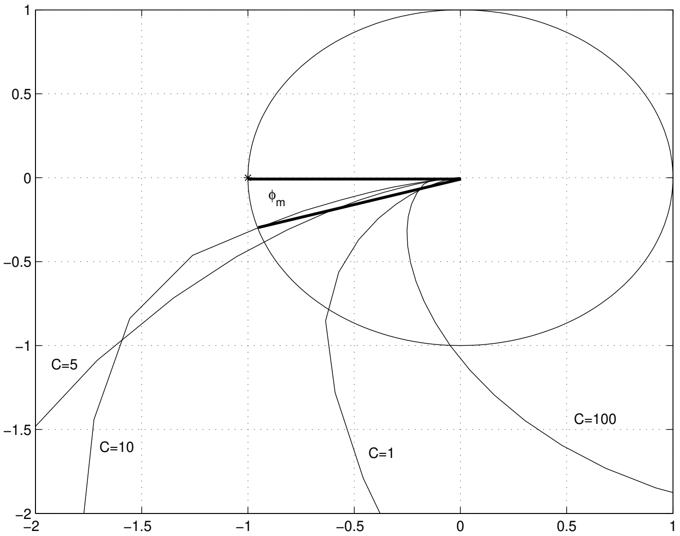

Figure 5.6: Example of Nyquist-loci of $\overline{\mathcal{L}_v} = \mathcal{L}_v(\omega)N(C,\omega)$ *for* $C = 1,\ 5,\ 10,\ 100$. *The worst case phase margin* ϕ_w *is here* $\phi_w \approx 17^o$ *obtained for* $C = 10$.

The phase margin in nonlinear loops is here defined as to be the phase margin for the ”worst-case-amplitude” denoted by ϕ_w. Let us formalize this property next.

Definition 5.2 Worst case phase margin
The worst case phase margin ϕ_w is defined as

$$\phi_w \ = \ \min_C \phi_m(C)$$

where

$$\phi_m(C) \ = \ \pi + \arg \overline{\mathcal{L}}_v(C, \omega_g). \tag{5.38}$$

Here, the *gain cross over frequency* ω_g is the frequency where $|\overline{\mathcal{L}_v}(C, \omega)| \ = \ 1$.

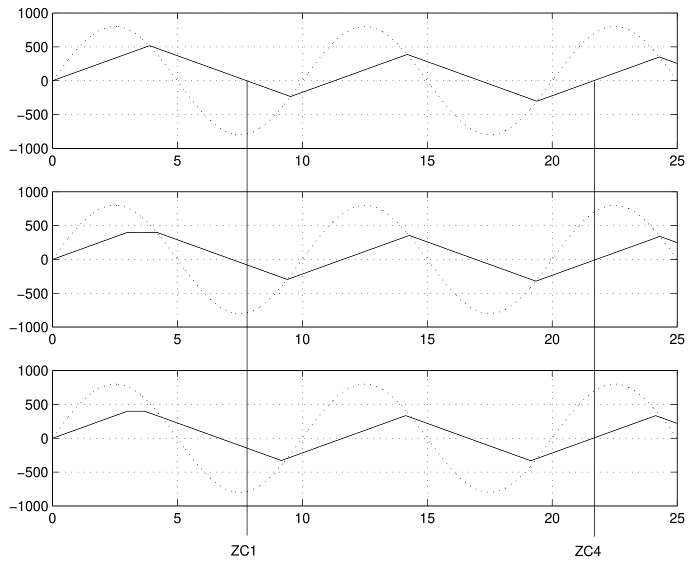

Figure 5.7: Output from a rate limiter N_1 (upper, solid), a combined amplitude- and rate limiter N_2 (mid, solid) and a combined amplitude- and rate limiter having a square-root function at the input N_3 (lower, solid). The input to the nonlinearities is a sinusoid $i(t) = 800\sin(2\pi 0.1t)$ (all, dotted). The time-lag (or phase-lag) at the first "zero crossing" (ZC1) of N_1 (upper, solid) is larger than the time-lag of N_2 (mid, solid) which, in turn, is larger than the time-lag of N_3 (lower, solid). However, in steady-state, which we can consider to be obtained at the fourth "zero-crossing" (ZC4), the time-lags and the amplitude responses are equal.

Remark 5.5 Since the anti-windup dynamics introduced by the anti-windup modification affects the loop only if (or when) saturation occurs, it may seem irrelevant to evaluate and analyze a nonlinear loop in terms of $N(C,\omega)\mathcal{L}_v$ where $\mathcal{L}_v$ is obtained for an *AWC*, for amplitudes that do not saturate N. The answer is that such a stability analysis becomes a little conservative. But this is only so if we know that the saturation limits are constant and known and even if that is the case, the conservatism is quit small compared to many other analysis methods.

It is worth noting that different nonlinearities, having the same (or almost the same) describing function (derived under steady-state conditions according to Definition 5.1) may have quite different initial (or transient) behavior. See Figure 5.7. Although this fact is of no importance for the analysis of predicting limit cycles and stability robustness against model errors, we can however expect it to have large impact on the tendency of the system to overshoot when applying e.g. a step in the reference signal r. For example, the system whose response to a sinusoid is shown in the lower plot of Figure 5.7, can be expected to have an input step response with less tendency of overshooting than the system which response is shown in the upper plot of Figure 5.7. In some situations, it may therefore be of interest to investigate, not only the worst-case phase margin defined in Definition 5.2, but also the lag associated with the response of first period in the derivation of the describing function. If that information is available, of course.

5.5 Design examples

We will now illustrate the ability of the anti-windup design techniques that we have proposed, by the use of examples. These examples, and the systems we consider in them, will be presented next.

Plant 1: Ill-conditioned MIMO(2,2) plant Here we use a plant proposed and discussed in [61]. The same example was later also used by Teel & Kapoor in [52] to illustrate the ability of their concept. The plant considered here has two inputs and two outputs where the inputs are limited in amplitude, i.e., $\psi = \sigma$ (see the description in Example 5.1). Three anti-windup compensators, designed using the LQR-design procedure proposed earlier in this chapter, are discussed below in Example 5.1. In Example 6.3 we evaluate some different OBSAWC:s and some other GLAWC:s. Then, in Example 6.5, each input amplitude limiter is appended with a rate limiter to obtain a combined rate- and amplitude limiter. The purpose is to show the ability of our proposed designs to handle also more difficult situations.

Plant 2: Double integrator MIMO(2,2) plant We have adopted this example from [80]. Three different anti-windup designs, carried out using the LQR design approach proposed in Section 5.1, and one simple OBSAWC will be investigated below in Example 5.2. Other, more heuristic designs of OBSAWC:s and a GLAWC for this system, are presented and discussed in Example 6.4. A completely different type of controller for this system is also proposed and evaluated in Example 9.1.

We have chosen these examples because, together, they illustrate an important family of problems that anti-windup compensators must be able to handle. Furthermore, we can compare our solutions to others proposed in the literature.

Some notations and abbreviations, specific for the examples, are

LQR Whenever an AWC is denoted by ”LQR”, we have used the design method described earlier in this chapter. This means, in particular, that we have selected $\boldsymbol{A}_o\boldsymbol{P}_1 = \boldsymbol{\alpha}$, see Section 4.3, where $\boldsymbol{\alpha} = \boldsymbol{R}\boldsymbol{A} + \boldsymbol{S}\boldsymbol{B}$ is specific for each nominal system under consideration.

OBSAWC Whenever an AWC is denoted by ”OBSAWC”, we have used the controller structure described in Section 4.1.

GLAWC Whenever an AWC is denoted by ”GLAWC”, we have used the controller structure described in Section 4.2.

NOMCON By this notation we mean that a nominal controller (2.2) is used.

Directional compensation (dir.comp.) ”Directional compensation” replaces the standard amplitude saturation function, see Section 2.5.

The examples will primarily compare nominal control, OBSAWC:s and GLAWC:s of Chapter 4. Their properties, in terms of loop gain $\boldsymbol{\mathcal{L}}_v$ and desaturation transient dynamics $\boldsymbol{\mathcal{H}}_\delta$, that were introduced in Chapter 3, are summarized below.

Summary: Loop transfer functions
The loop transfer functions, obtained by nominal control (Section 2.1), OBSAWC (Section 4.1) and GLAWC (Section 4.2) are given by (3.9), (4.7) and (4.16), respectively, i.e.

$$\boldsymbol{\mathcal{L}}_v = \begin{cases} \boldsymbol{R}^{-1}\boldsymbol{\alpha}\boldsymbol{A}^{-1} - \mathbf{I} & \text{nominal control,} \\ \boldsymbol{A}_o^{-1}\boldsymbol{\alpha}\boldsymbol{A}^{-1} - \mathbf{I} & \text{OBSAWC,} \\ \boldsymbol{P}_2\boldsymbol{P}_1^{-1}\boldsymbol{A}_o^{-1}\boldsymbol{\alpha}\boldsymbol{A}^{-1} - \mathbf{I} & \text{GLAWC} \end{cases} \tag{5.39}$$

Summary: Desaturation transient dynamics
The desaturation transient dynamics, obtained by nominal control (Section 2.1), OBSAWC (Section 4.1) and GLAWC (Section 4.2) are given by (3.9), (4.7) and (4.16), respectively, i.e.

$$\boldsymbol{\mathcal{H}}_\delta = \begin{cases} \boldsymbol{B}\boldsymbol{\alpha}^{-1}\boldsymbol{R} & \text{nominal control,} \\ \boldsymbol{B}\boldsymbol{\alpha}^{-1}\boldsymbol{A}_o & \text{OBSAWC,} \\ \boldsymbol{B}\boldsymbol{\alpha}^{-1}\boldsymbol{A}_o\boldsymbol{P}_1\boldsymbol{P}_2^{-1} & \text{GLAWC} \end{cases} \tag{5.40}$$

EXAMPLE 5.1: PLANT 1, NOMINAL SYSTEM AND LQR AWC

Plant 1
The plant has two inputs and two outputs and it is described in continuous time by the model

$$\begin{aligned} y &= \boldsymbol{\mathcal{G}}(s)v \\ &= \frac{1}{s+0.1}\begin{pmatrix} 0.5 & 0.4 \\ 0.4 & 0.3 \end{pmatrix} v \\ v(t) &= \begin{pmatrix} \sigma_{-3}^{3}(u_1(t)) \\ \sigma_{-10}^{10}(u_2(t)) \end{pmatrix} , \end{aligned} \tag{5.41}$$

where the plant inputs v are limited in amplitude (see Section 2.2).

Nominal controller
This plant is controlled by a decentralized PI-controller, given by

$$\begin{aligned} u &= \boldsymbol{\mathcal{K}}(s)(r-y) \\ &= \frac{10(s+0.1)}{s}\begin{pmatrix} 1 & 0 \\ 0 & -1 \end{pmatrix}(r-y) \; . \end{aligned} \tag{5.42}$$

System properties
In the way we represent plants and controllers, we select the polynomial matrices as

$$\begin{aligned} \boldsymbol{B} &= \begin{pmatrix} 0.5 & 0.4 \\ 0.4 & 0.3 \end{pmatrix}, \quad \boldsymbol{A} \;=\; (s+0.1)\mathbf{I} \\ \boldsymbol{S} &= (10s+1)\begin{pmatrix} 1 & 0 \\ 0 & -1 \end{pmatrix}, \quad \boldsymbol{R} \;=\; s\mathbf{I} \\ \boldsymbol{T} &= \boldsymbol{S} \text{ (error feedback)} \; . \end{aligned} \tag{5.43}$$

Notice that

$$\boldsymbol{S} = 10\boldsymbol{A}\begin{pmatrix} 1 & 0 \\ 0 & -1 \end{pmatrix} \; . \tag{5.44}$$

The closed loop denominator matrix, $\boldsymbol{\alpha}$, is, hence, given by

$$\begin{aligned}\boldsymbol{\alpha} &= \boldsymbol{R}\boldsymbol{A} + \boldsymbol{S}\boldsymbol{B} \\ &= \boldsymbol{R}\boldsymbol{A} + 10\boldsymbol{A}\begin{pmatrix}1 & 0\\ 0 & -1\end{pmatrix}\boldsymbol{B} \\ &= \boldsymbol{A}\begin{pmatrix}s+5 & 4\\ -4 & s-3\end{pmatrix} = \begin{pmatrix}s+5 & 4\\ -4 & s-3\end{pmatrix}\boldsymbol{A}\,. \end{aligned} \tag{5.45}$$

The last equality holds because $\boldsymbol{A}$ is a scalar polynomial multiplied by the identity matrix. We introduce the notation

$$\boldsymbol{\alpha}_i \triangleq \begin{pmatrix}s+5 & 4\\ -4 & s-3\end{pmatrix}\,. \tag{5.46}$$

The loop transfer functions (5.39) are then given by

$$\boldsymbol{\mathcal{L}}_v = \begin{cases}\boldsymbol{R}^{-1}\boldsymbol{\alpha}_i - \mathbf{I} & \text{nominal control}\\ \boldsymbol{A}_o^{-1}\boldsymbol{\alpha}_i - \mathbf{I} & \text{OBSAWC}\\ \boldsymbol{P}_2\boldsymbol{P}_1^{-1}\boldsymbol{A}_o^{-1}\boldsymbol{\alpha}_i - \mathbf{I} & \text{GLAWC}\end{cases}\,, \tag{5.47}$$

and the desaturation transient dynamics (5.40) are given by

$$\boldsymbol{\mathcal{H}}_\delta = \begin{cases}\boldsymbol{B}\boldsymbol{A}^{-1}\boldsymbol{\alpha}_i^{-1}\boldsymbol{R} & \text{nominal control}\\ \boldsymbol{B}\boldsymbol{A}^{-1}\boldsymbol{\alpha}_i^{-1}\boldsymbol{A}_o & \text{OBSAWC}\\ \boldsymbol{B}\boldsymbol{A}^{-1}\boldsymbol{\alpha}_i^{-1}\boldsymbol{A}_o\boldsymbol{P}_1\boldsymbol{P}_2^{-1} & \text{GLAWC}\end{cases}\,. \tag{5.48}$$

When all the components of the control signal operate in the linear region of σ, i.e. when $v(t) \equiv u(t)$, the closed loop system is given by the linear relations (2.3) ($\beta \equiv 0$) an the polynomial matrices (5.43). The closed loop linear system is stable since $\det(\boldsymbol{\alpha})$ has all zeros in the left half plane. The system response to a step-change in the reference signal vector r is shown in the two left plots of Figure 5.8.

Let us consider the nominal system for a moment. According to most design guidelines concerning linear controllers in the academic literature, a linear plant such as (5.41) ($\sigma(u) \equiv u$) requires a more advanced controller than the simple *decentralized* controller (5.42). An advanced controller should reduce the cross couplings between the plant outputs, and reduce the overshoots, when applying steps in the reference. See the two left plots of Figure 5.8. However, the reasons for using a seemingly "too" simple linear controller are sometimes justified

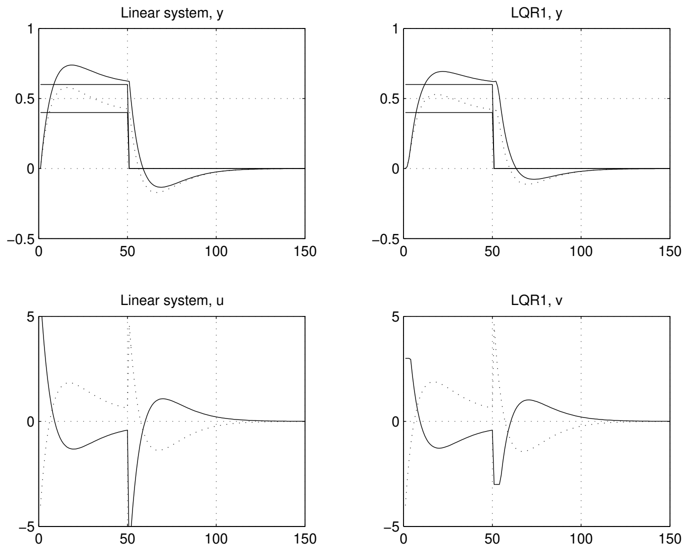

Figure 5.8: Reference step response for the linear system (left) and for the LQR1 (right). The plant outputs y_1 and y_2 are shown in the upper plots as (solid) and (dotted) lines respectively, whereas the plant inputs v_1 and v_2 are shown in the lower plots as (solid) and (dotted) lines respectively.

by factors such as robustness against model errors (especially in ill-conditioned plants such as the one investigated here), available hardware and software and competence. It is therefore difficult for us to value the performance of the nominal controller in the linear system and we will, in the sequel, assume that the closed loop linear response is the best possible. Furthermore, we allow ourself to evaluate anti-windup compensators regardless of whether it is relevant or not to use e.g. a model based LQR AWC for compensation of a system with input limiters, having a simple decentralized and PI-type nominal controller.

Stability analysis of the nominal system

Using (5.43),(5.45) and (5.47), we have that the nominal loop transfer function is given by

$$\begin{aligned}\boldsymbol{\mathcal{L}}_v &= \frac{1}{s}\begin{pmatrix} s+5 & 4 \\ -4 & s-3 \end{pmatrix} - \frac{1}{s}s\mathbf{I} \\ &= \frac{1}{s}\begin{pmatrix} 5 & 4 \\ -4 & -3 \end{pmatrix} .\end{aligned} \tag{5.49}$$

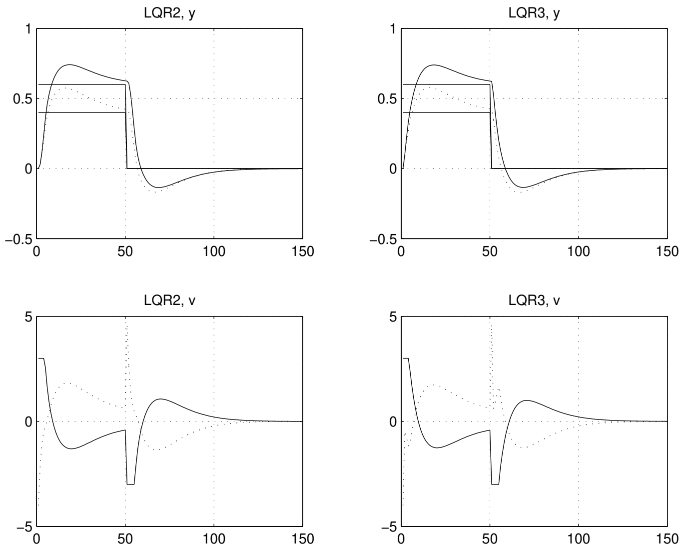

Figure 5.9: Reference step response for the LQR2 (left) and for the LQR3 (right). The plant outputs y_1 and y_2 are shown in the upper plots as (solid) and (dotted) lines respectively, whereas the plant inputs $v1$ and v_2 are shown in the lower plots as (solid) and (dotted) lines respectively.

We will now check stability by using the Circle-criterion. We have that

$$Z \stackrel{\Delta}{=} \boldsymbol{\mathcal{L}}_v + \mathbf{I} \; = \; \frac{1}{s}\begin{pmatrix} s+5 & 4 \\ -4 & s-3 \end{pmatrix} \tag{5.50}$$

and it is easy to show that

$$\begin{aligned} \overline{Z}(j\omega) &\stackrel{\Delta}{=} Z(j\omega) + Z^T(-j\omega) \\ &= \begin{pmatrix} 2 & \frac{8}{j\omega} \\ -\frac{8}{j\omega} & 2 \end{pmatrix} . \end{aligned} \tag{5.51}$$

The eigenvalues of $\overline{Z}(j\omega)$ are given by

$$2 \pm \frac{8}{\omega} \tag{5.52}$$

where, apparently, one eigenvalue is always negative for frequencies $\omega < 4$. According to the Circle-criterion, this indicates that the systems may not be stable. It is verified by the simulations in [61] that the nominal system, obtained when using the nominal controller (5.42) for the control of the plant (5.41), is

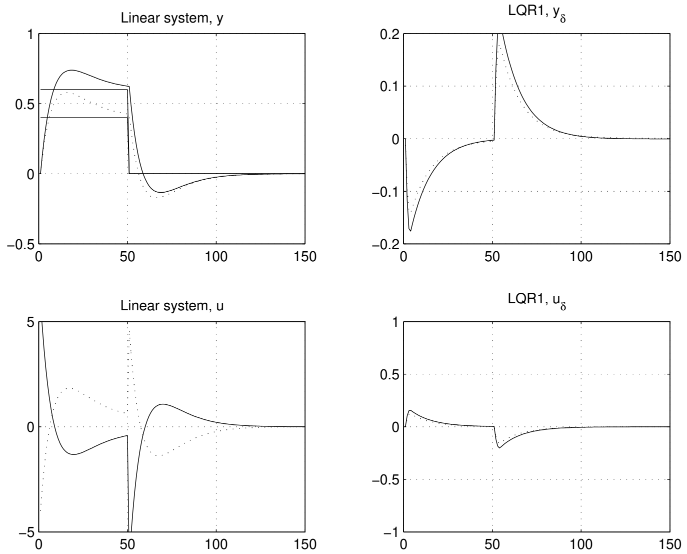

Figure 5.10: Reference step response for the linear system (left) and the windup effects of the plant, and the controller, for the LQR1 (upper right) and (lower right), respectively. Solid and dotted lines represent windup effects in y_1, u_1 and y_2, u_2 respectively.

not asymptotically stable.

Anti-windup compensation: LQR design

The general linear anti-windup compensator (GLAWC) defined by (4.8)-(4.9) and (4.6) is now used. The design of compensators discussed and evaluated here are based on the LQR-optimization procedure described in Section 5.1. Then, according to (5.45)-(5.46) and (4.19)-(4.20) we can select the polynomial matrices $\boldsymbol{A}_o,\ \boldsymbol{P}_1$ as

$$\begin{aligned} \boldsymbol{A}_o &= \alpha_i \\ \boldsymbol{P}_1 &= \boldsymbol{A}\,. \end{aligned} \tag{5.53}$$

The polynomial matrix $\boldsymbol{P}_2$ can be obtained from (5.23), i.e.,

$$\boldsymbol{P}_2 = \mathbf{L}_\delta \boldsymbol{B} + \boldsymbol{A}\,, \tag{5.54}$$

where $\mathbf{L}_\delta$ is calculated according to Result 5.3. Notice that the output vector y represent a state vector x of the plant (5.41). We can therefore select $\boldsymbol{B}_x$ and $\boldsymbol{A}$ in (5.21), and thereby also in (5.23), as to be $\boldsymbol{B}$ and $\boldsymbol{A}$ in (5.43).

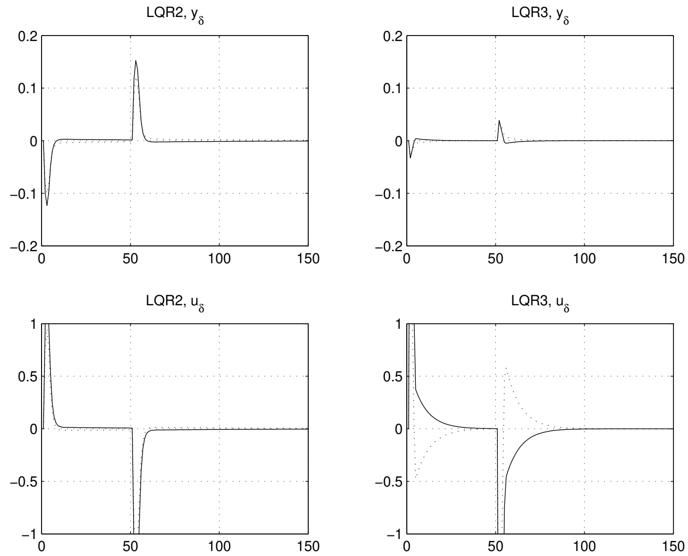

Figure 5.11: Windup effects of the plant and the controller, for the LQR2 (upper left) and (lower left), respectively, and for the LQR3 (upper right) and (lower right), respectively. Solid and dotted lines represent windup effects in y_1, u_1 and y_2, u_2 respectively.

The feedback gain matrix $\mathbf{L}_\delta$, obtained from (5.14) and by solving the Riccati-equation (5.15), is calculated for the following three pairs of penalty matrices

$$\begin{aligned}\text{LQR1: } \mathbf{Q} &= \mathbf{I}, \ \mathbf{Q}_u = \mathbf{I}\\ \text{LQR2: } \mathbf{Q} &= 100\mathbf{I}, \ \mathbf{Q}_u = \mathbf{I}\\ \text{LQR3: } \mathbf{Q} &= 10000\mathbf{I}, \ \mathbf{Q}_u = \mathbf{I}\end{aligned} \tag{5.55}$$

and the result is

$$\begin{aligned}\text{LQR1: } \mathbf{L}_\delta &= \begin{pmatrix} 0.5263 & 0.4588 \\ 0.4588 & 0.2969 \end{pmatrix}\\ \text{LQR2: } \mathbf{L}_\delta &= \begin{pmatrix} 4.3337 & 7.1005 \\ 7.1005 & 0.7835 \end{pmatrix}\\ \text{LQR3: } \mathbf{L}_\delta &= \begin{pmatrix} 27.1289 & 93.1741 \\ 93.1741 & -19.4582 \end{pmatrix} .\end{aligned} \tag{5.56}$$

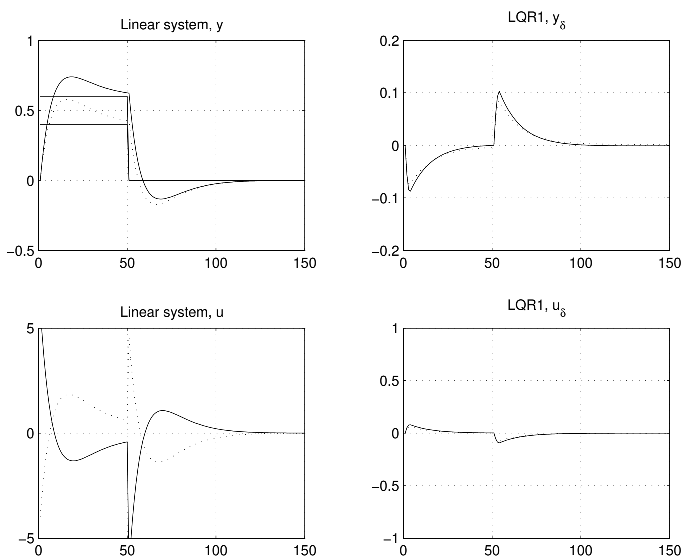

Figure 5.12: Same conditions as in Figure 5.10 with the difference that directionality compensation is used here.

The control signal u_a of the GLAWC (4.8)-(4.9) can be obtained as

$$\begin{aligned} u_a &= (\boldsymbol{P}_1 - \boldsymbol{P}_2)\boldsymbol{P}_1^{-1}(v - u_o) \\ &= -\mathbf{L}_\delta \boldsymbol{B}\boldsymbol{A}^{-1}(v - u_o) \\ &= -\frac{1}{s+0.1}\mathbf{L}_\delta \begin{pmatrix} 0.5 & 0.4 \\ 0.4 & 0.3 \end{pmatrix}(v - u_o) \ . \end{aligned} \tag{5.57}$$

Here, u_o is the output from the OBSAWC (4.6) which, in this example, is given by [4]

$$u_o = \frac{1}{s}\left[\begin{pmatrix} 5 & 4 \\ -4 & -3 \end{pmatrix}(v - u_o) + (10s+1)\begin{pmatrix} 1 & 0 \\ 0 & -1 \end{pmatrix}(r - y)\right] \ . \tag{5.58}$$

According to (4.8), the controller output, u, is obtained as $u = u_o + u_a$.

Stability analysis of the AWC:s

It is straightforward to verify (using a computer) that all three solutions $\mathbf{P}_c$ of the Riccati-equation satisfy the Lyapunov-equation (5.32) and hence, stability is guaranteed for all the three designs LQR1,2 and 3.

[4] Note that the choice $\boldsymbol{A}_o = \alpha_i$ makes the OBSAWC loop transfer function (5.47) become equal to zero in this particular case. As a consequence, we have that $u_o = u_l$ and $u_a = u_\delta$.

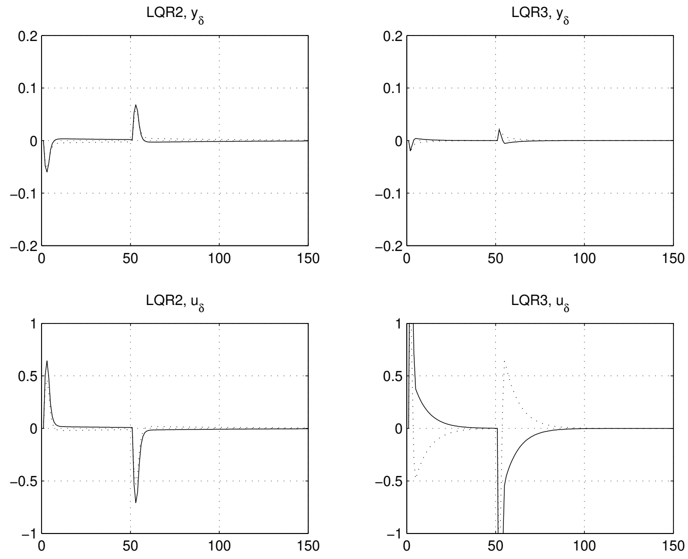

Figure 5.13: Same conditions as in Figure 5.11 with the difference that directionality compensation is used here.

Simulations
The process behavior is evaluated when applying a set-point change having 5 seconds of duration and magnitude $r_1 = 0.6$ and $r_2 = 0.4$. The plots to the left in Figure 5.8 show the response of the linear (ideal) controlled system. The right part of Figure 5.8 and the left and right parts of Figure 5.9, show the response of the controlled system (5.41), (5.57), (5.58) for the AWC design choices LQR1, LQR2 and LQR3 of (5.55), respectively. Figure 5.10 shows the linear response (again) and the saturation effects in the plant, y_δ, and the saturation effects in the controller, u_δ, for the AWC LQR1. The plots in Figure 5.11 show the corresponding effects when using the AWC:s LQR2 and LQR3, respectively. The unacceptable response of the nominal system, shown in [61] to be such that none of the components of y_δ ever decay to zero, is not shown here.

From Figures 5.10 and 5.11 we conclude that the LQR1 design results in a slower decay of the saturation effects in the plant, y_δ, than compared to LQR2 which, in turn, shows a slower decay of the saturation effects in the plant compared to LQR3. On the other hand, when considering the windup effects of the controller, u_δ, the circumstance are reversed. This is in agreement with the penalties (5.55) of y_δ and u_δ in the different cases. The reason why we really obtain these results, apart from the fact that the LQR design aims for it, is that the system has nice stability properties with respect to the saturation nonlinearity. These nice stability properties are, in turn, a result of using reasonable penalties.

The Figures 5.12 and 5.13 show the performance, in terms of windup effects, when introducing the directionality compensator γ in the loop. Notice that in this particular case, and for these AWC designs, LQR1, LQR2 and LQR3, the saturation effects y_δ reduce when introducing γ. The main reason for this is that the instant effect on y_δ caused by the saturation event (in other words the excitation of the saturation effects x_δ) is reduced when introducing the directional compensator into the loop. The linear transient dynamics $\boldsymbol{\mathcal{H}}_\delta$ are, however, the same!

EXAMPLE 5.2: PLANT 2, LQR- AND OBSAWC

Plant 2
The plant is a discrete-time double integrator given by

$$
\begin{aligned}
y(t) &= \boldsymbol{\mathcal{G}}(q)v(t) \\
&= \frac{0.5(q+1)}{(q-1)^2}\mathbf{G}_c v(t) \\
v(t) &= \psi(u(t)) \\
&= \begin{pmatrix} \sigma_{-1}^{1}(u_1(t)) \\ \sigma_{-0.01}^{0.01}(u_2(t)) \end{pmatrix}
\end{aligned}
\tag{5.59}
$$

where

$$
\mathbf{G}_c = \begin{pmatrix} 1 & -0.5 \\ -0.5 & 1 \end{pmatrix}
$$

and

$$
\mathbf{G}_c^{-1} = \frac{2}{3}\begin{pmatrix} 2 & 1 \\ 1 & 2 \end{pmatrix}. \tag{5.60}
$$

Nominal controller
The nominal controller, given by

$$\begin{aligned}
\boldsymbol{R}(q) &= (q-1)(q+0.2062)\,\mathbf{I} \triangleq R(q)\,\mathbf{I} \\
\boldsymbol{S}(q) &= (0.7876q^2 - 1.39q + 0.617)\mathbf{G}_c^{-1} \triangleq S(q)\,\mathbf{G}_c^{-1} \\
\boldsymbol{T}(q) &= 0.36(q-0.8)^2\mathbf{G}_c^{-1} \triangleq T(q)\mathbf{G}_c^{-1}
\end{aligned} \tag{5.61}$$

is assumed to be used. The sampling interval is $h = 1$.

System properties
We choose to parameterize the plant (5.59) as

$$\begin{aligned}
\boldsymbol{B}(q) &= 0.5(q+1)\mathbf{G}_c \triangleq B(q)\mathbf{G}_c \\
\boldsymbol{A}(q) &= (q-1)^2\mathbf{I} \triangleq A(q)\mathbf{I}\,.
\end{aligned} \tag{5.62}$$

Then, according to (5.62) and (5.61), the closed loop denominator $\boldsymbol{\alpha}(q)$ can be expressed as

$$\begin{aligned}
\boldsymbol{\alpha}(q) &= \boldsymbol{R}(q)\boldsymbol{A}(q) + \boldsymbol{S}(q)\boldsymbol{B}(q) \\
&= R(q)A(q)\mathbf{I} + S(q)\mathbf{G}_c^{-1}\mathbf{G}_c B(q) \\
&= (R(q)A(q) + S(q)B(q))\mathbf{I} \\
&= (q^4 - 2.4001q^3 + 2.0801q^2 - 0.7679q + 0.1023)\mathbf{I} \\
&\triangleq \alpha(q)\mathbf{I}\,.
\end{aligned} \tag{5.63}$$

The loop transfer functions and the transient dynamics obtained when using the nominal controller (5.61) (NOMCON), the OBSAWC (4.1) with $\boldsymbol{A}_o = \mathrm{diag}(a_{o1}, a_{o2})$ and the GLAWC (4.8)-(4.9) are given by

$$\boldsymbol{\mathcal{L}}_v(q) = \begin{cases} (\frac{\alpha}{RA} - 1)\mathbf{I} & \text{NOMCON,} \\ \frac{\alpha}{A}\,\mathrm{diag}(\frac{1}{a_{o1}}, \frac{1}{a_{o2}}) - \mathbf{I} & \text{diagonal OBSAWC} \\ \boldsymbol{P}_2\boldsymbol{P}_1^{-1}\boldsymbol{A}_o^{-1}\frac{\alpha}{A} - \mathbf{I} & \text{GLAWC} \end{cases} \tag{5.64}$$

and

$$\boldsymbol{\mathcal{H}}_\delta(q) = \begin{cases} \mathbf{G}_c\frac{BR}{\alpha} & \text{NOMCON,} \\ \mathbf{G}_c\frac{B}{\alpha}\,\mathrm{diag}(a_{o1}, a_{o2}) & \text{diagonal OBSAWC,} \\ \mathbf{G}_c\frac{B}{\alpha}\boldsymbol{A}_o\boldsymbol{P}_1\boldsymbol{P}_2^{-1} & \text{GLAWC .} \end{cases} \tag{5.65}$$

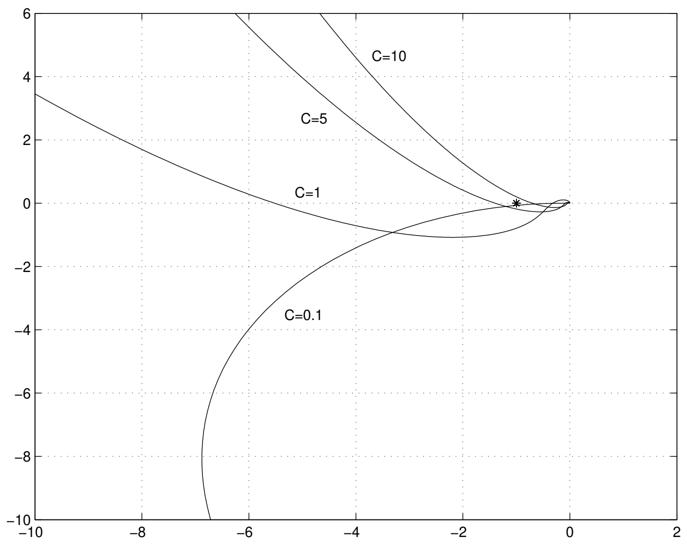

Figure 5.14: Nyquist-loci for the composed loop transfer function $\mathcal{L}_v(\omega)N(C)$ when using the nominal controller without anti-windup. Here $N(C)$ represents the describing function for the standard amplitude limiter given by the limits $a = -b = 1$.

Stability analysis of the nominal system

Since the nominal loop transfer function $\boldsymbol{\mathcal{L}}_v$ is diagonal, and the amplitude limiter σ is decentralized (diagonal), the stability analysis can be carried out by using the Nyquist-like method discussed in Section 5.4.2. Figures 5.14 and 5.15 show the Nyquist-loci of the combined loop transfer function $\overline{\boldsymbol{\mathcal{L}}}_v$, defined in Section 5.4.2, of the first loop where the amplitude limits are ± 1, and of the second loop where the amplitude limits are ± 0.01, respectively. Since the plant is a double integrator, the phase-lag at $\omega = 0$ is, at least, -180^o. The controller integrator makes this lag become -270^o for the loop transfer function obtained when using the nominal controller. Since some of the loci, of both the combined, scalar, loop transfer functions, encircle the point $(-1, 0)$, the system can not be expected to be stable. The simulation result shown in Figure 5.16 confirms this.

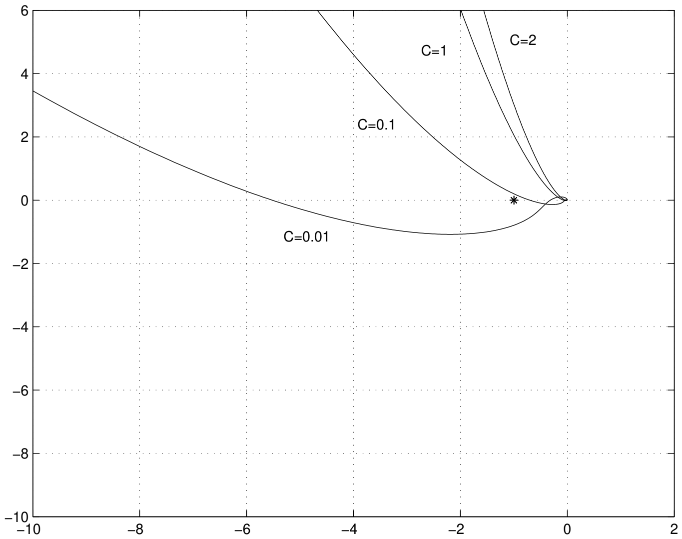

Figure 5.15: The loop transfer function $\boldsymbol{\mathcal{L}}_v$ is the same as in Figure 5.14 but here, the describing function $N(C)$ is given by the amplitude limits $a = -b = 0.01$.

Anti-windup compensation: LQR design

We begin by factorizing $\alpha(q)$ (5.63) as

$$\begin{aligned} \alpha(q) &= \alpha_1(q)\alpha_2(q) \\ &\text{where} \\ \alpha_1(q) &= (q - 0.8064)(q - 0.7929) \\ \alpha_2(q) &= (q - 0.4181)(q - 0.3826)\ . \end{aligned} \tag{5.66}$$

Then, we select the polynomial matrices $\boldsymbol{A}_o$ and $\boldsymbol{P}_1$ of the GLAWC (4.8), (4.9) and (4.6) as

$$\begin{aligned} \boldsymbol{A}_o(q) &= \alpha_1(q)\mathbf{I} \triangleq A_o(q)\mathbf{I} \\ \boldsymbol{P}_1(q) &= \alpha_2(q)\mathbf{I} \triangleq P_1(q)\mathbf{I}\ . \end{aligned} \tag{5.67}$$

See (4.20).

The output u_o of the GLAWC (4.8) (obtained by using the observer based anti-windup compensator structure (4.6)) can be calculated as

$$\begin{aligned} R(q)u_o(t) &= R_o(q)\mathbf{I}(v(t) - u_o(t)) + \mathbf{G}_c^{-1}(T(q)r(t) - S(q)y(t)) \\ R_o(q) \triangleq A_o(q) - R(q) &= -0.8055q + 0.8456 \end{aligned} \tag{5.68}$$

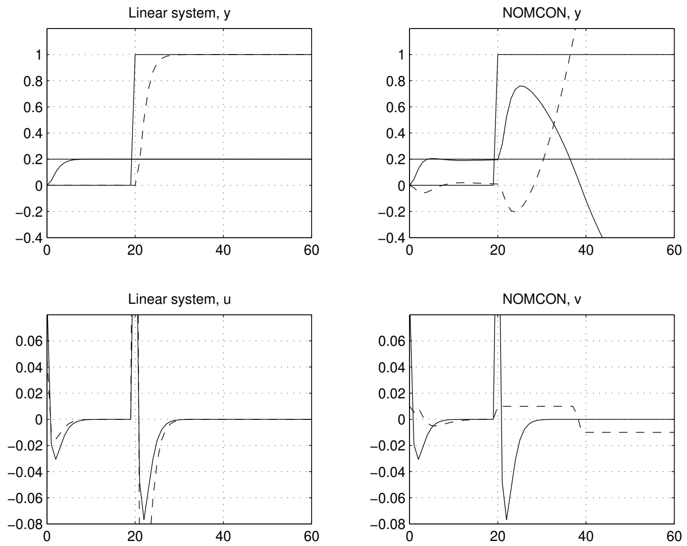

Figure 5.16: Reference step response for the linear system (left) and for the nominally controlled system (right). The plant outputs y_1 and y_2 are shown in the upper plots as (solid) and (dashed) respectively, and the plant inputs $v1$ and v_2 are shown in the lower plots as (solid) and (dashed) lines respectively.

and the output u_a of the GLAWC is obtained as

$$u_a(t) \;=\; \frac{1}{P_1(q)}(P_1(q)\mathbf{I} - \boldsymbol{P}_2(q))(v(t) - u_o(t)) \;. \tag{5.69}$$

Here, the polynomial matrix $\boldsymbol{P}_2$ can be calculated in the following way

$$\begin{aligned} \boldsymbol{P}_2 \;&=\; \mathbf{L}_\delta \boldsymbol{B}_x(q) + A(q)\mathbf{I} \\ &=\; \mathbf{L}_\delta \begin{pmatrix} q & 0 \\ 1 & 0 \\ 0 & q \\ 0 & 1 \end{pmatrix} + A(q)\mathbf{I} \;. \end{aligned} \tag{5.70}$$

See Section 5.2. According to (4.8), the controller output u is obtained as $u = u_o + u_a$.

Three different AWC:s obtained from the LQR-design discussed earlier, defined

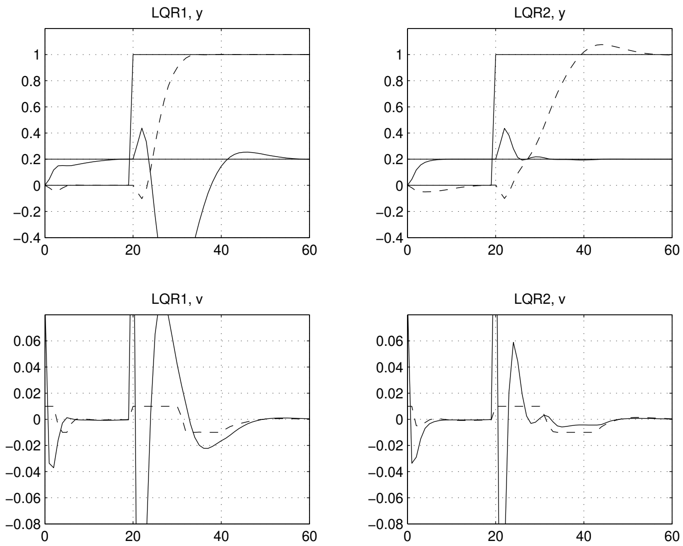

Figure 5.17: Reference step response for the LQR1 (left) and for the LQR2 (right). The plant outputs y_1 and y_2 are shown in the upper plots as (solid) and (dashed) respectively, and the plant inputs $v1$ and v_2 are shown in the lower plots as (solid) and (dashed) lines respectively.

by the design choices

$$\begin{aligned} &\text{LQR1: } \mathbf{Q} = \mathrm{diag}(1, 100), \ \ \mathbf{Q}_u = 100\mathbf{I} \\ &\text{LQR2: } \mathbf{Q} = \mathrm{diag}(100, 1), \ \ \mathbf{Q}_u = 100\mathbf{I} \\ &\text{LQR3: } \mathbf{Q} = \mathbf{I}, \ \ \mathbf{Q}_u = 100\mathbf{I} \end{aligned} \tag{5.71}$$

are evaluated in this example.

The gain matrices $\mathbf{L}_\delta$, obtained from (5.19) and by solving the discrete time Ricatti equation (5.20) are given by

$$\begin{aligned} &\text{LQR1: } \mathbf{L}_\delta = \begin{pmatrix} 0.5546 & -0.4003 & -0.3813 & 0.1865 \\ -0.3813 & 0.1865 & 1.1152 & -0.6745 \end{pmatrix} \\ &\text{LQR2: } \mathbf{L}_\delta = \begin{pmatrix} 1.1152 & -0.6745 & -0.3813 & 0.1865 \\ -0.3813 & 0.1865 & 0.5546 & -0.4003 \end{pmatrix} \\ &\text{LQR3: } \mathbf{L}_\delta = \begin{pmatrix} 0.4242 & -0.3458 & -0.1107 & 0.0749 \\ -0.1107 & 0.0749 & 0.4242 & -0.3458 \end{pmatrix} \end{aligned} \tag{5.72}$$

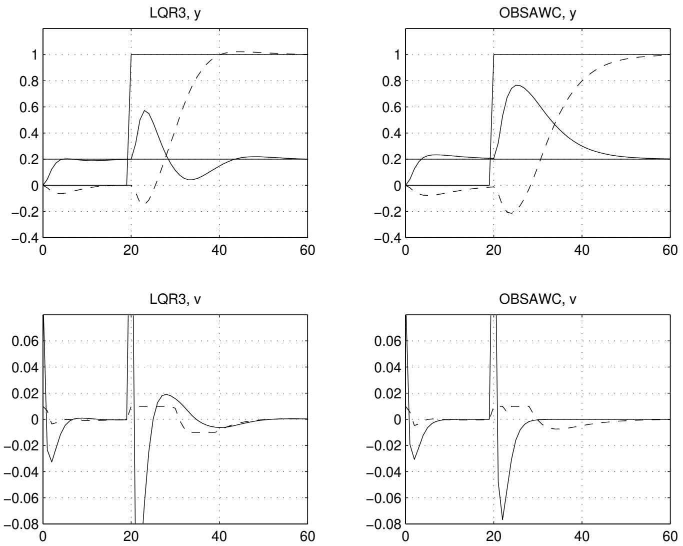

Figure 5.18: Reference step response for the LQR3 (left) and for the OBSAWC (right). The plant outputs y_1 and y_2 are shown in the upper plots as (solid) and (dashed) respectively, and the plant inputs $v1$ and v_2 are shown in the lower plots as (solid) and (dashed) respectively.

Anti-windup compensation: OBSAWC
Here we will evaluate one OBSAWC, given by the simple design choice

$$\text{OBSAWC:} \;\; \boldsymbol{A}_o = (q - 0.4)^2 \mathbf{I} \; . \tag{5.73}$$

The compleat OBSAWC is then given by

$$\begin{aligned} R(q)u_o(t) \; &= \; R_o(q)\mathbf{I}(v(t) - u_o(t)) + \mathbf{G}_c^{-1}(T(q)r(t) - S(q)y(t)) \\ R_o(q) \overset{\Delta}{=} A_o(q) - R(q) \; &= \; -0.0062q + 0.37 \\ u(t) \; &= \; u_o(t) \; . \end{aligned} \tag{5.74}$$

Stability analysis
Notice that for the choice of $\boldsymbol{A}_o$ (5.73) of the OBSAWC, the loop transfer function is given by a scalar transfer function times a (2x2) identity matrix. This allows us to use the Nyquist-like analysis methods in the same way as we did for the nominal system earlier in this example. The two scalar loci of the loop gains $\overline{\mathcal{L}_v}(C, e^{j\omega})$ are plotted in the Figures 5.19 and 5.20, respectively. According to the stability conditions discussed in Section 5.4.2, the system obtained by using

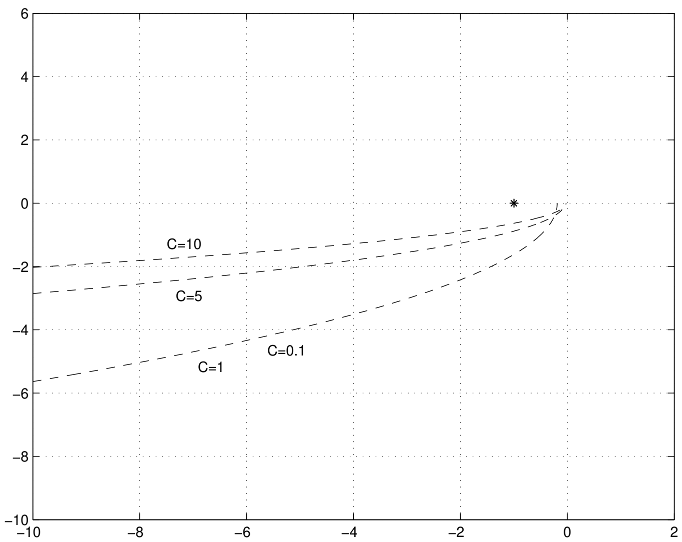

Figure 5.19: Nyquist-loci for the composed loop transfer function $\mathcal{L}_v(\omega)N(C)$ when using the OBSAWC. The situation is otherwise the same as in Figure 5.14.

the OBSAWC can be expected to be stable.

Simulations

In addition to the three LQR-based AWC:s (5.71) and the OBSAWC (5.73), we also evaluated, by simulations, the performance for all of the four designs, when using the directionality compensator γ (2.17). Comments upon these results are provided at the end of the example.

The system is at rest for time $t < 0$ and all initial states are zero. At time $t = 0$ we apply a step $r_1 = 0.2$ which remains for the rest of the test run. At time $t = 20$ a step $r_2 = 1$ is applied and it remains for the rest of the test run.

When designing LQR1 we penalize $y_{\delta 2}$ a hundred times harder than $y_{\delta 1}$ and when designing LQR2 we do the opposite. The penalty on $u_{\delta 1}$ and $u_{\delta 2}$ are equal. In the design of LQR1 we ask the AWC to prioritize minimizing $y_{\delta 2}$ and for the design of LQR2 we ask the AWC to prioritize minimizing $y_{\delta 1}$. The simulation result confirms that this intended effect is achieved when not using the directional compensation.

The large cross interaction on $y_{\delta 1}$ when using LQR1 may be acceptable in some

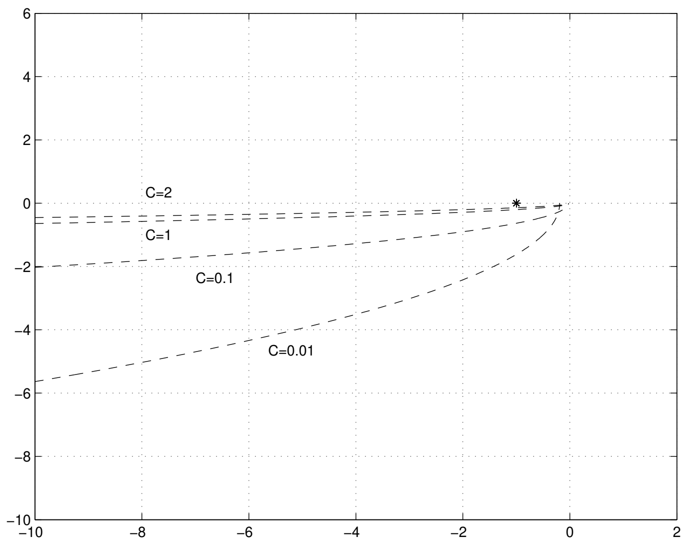

Figure 5.20: The loop transfer function $\mathcal{L}_v$ is the same as in Figure 5.19 but here, the describing function $N(C)$ is given by the amplitude limits $a = -b = 0.01$.

applications, e.g. when $y_{\delta 1}$ is a level in some buffer, whereas in other applications this cross interaction is not acceptable.

The design of LQR3 involves an equal trade-off between the saturation effects $y_{\delta 1}$ and $y_{\delta 2}$ accomplished by equal penalties. The results from the simulation show that the intended effect is achieved to some extent.

The big advantage of the OBSAWC (5.73) is that it can be tuned without a model of the plant. The performance is similar to that of LQR3, however, the decay of saturation effects are somewhat slower. Since the polynomial $(z - 0.4)^2$ has replaced R in the loop transfer function expression, the phase lag is reduced to $-180\,\mathrm{deg}$ at $\omega = 0$. The stability properties improve and the system response is stable.

Notice that since the nominal controller decouples the linear system response from r (and from disturbances acting on the plant output), to the plant output y, directional compensation $v = \gamma u$ preserves this decomposition to some extent. Directional compensation degrades the performance of LQR1 whereas the overall behavior of LQR2 is more or less unchanged. Compare the Figures 5.17 and 5.21.

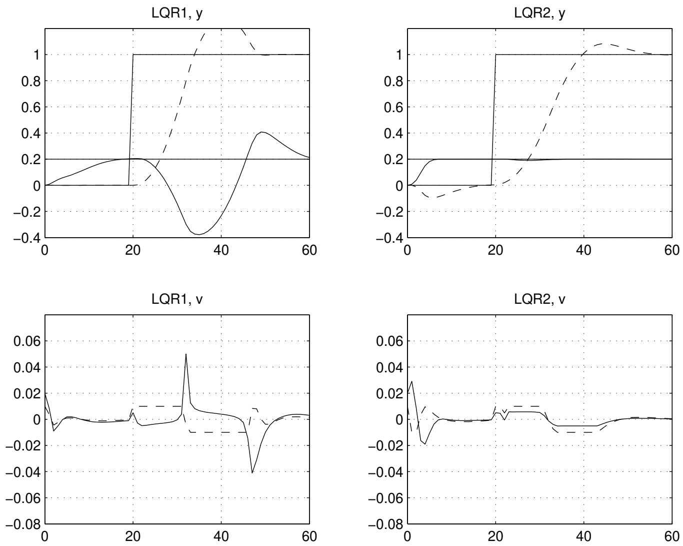

Figure 5.21: Reference step response for the LQR1 (left) and for the LQR2 (right) when using dir.comp. The plant outputs y_1 and y_2 are shown in the upper plots as (solid) and (dashed) respectively, and the plant inputs $v1$ and v_2 are shown in the lower plots as (solid) and (dashed) respectively.

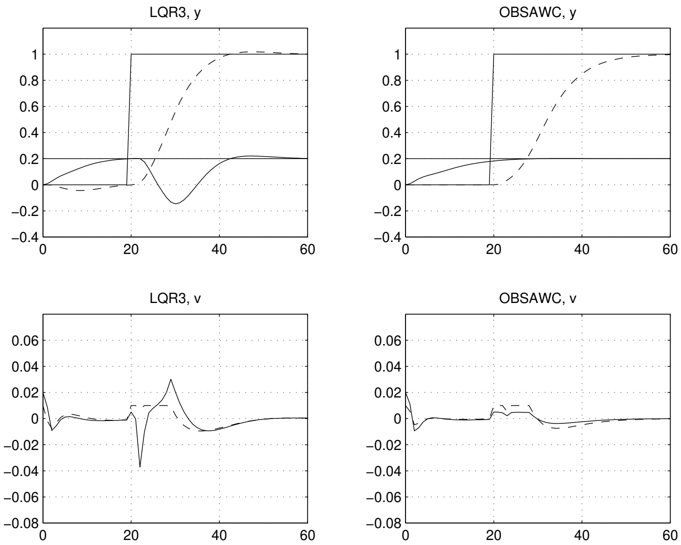

Figure 5.22: Reference step response for the LQR3 (left) and for the OBSAWC (right) when using dir.comp. The plant outputs y_1 and y_2 are shown in the upper plots as (solid) and (dashed) respectively, and the plant inputs $v1$ and v_2 are shown in the lower plots as (solid) and (dashed) respectively.

CHAPTER 6

Guidelines for heuristic design

> I like to keep things as simple as possible, but not simpler
> *Albert Einstein*

In the previous chapter we proposed a design strategy for obtaining fast recovery back to linear performance, after a saturation event. The idea behind the method is to cancel all influence from the nominal controller on the loop transfer function taken around the input limiters and then use available degrees of freedom to alter the properties. By doing this, we can ignore the properties of the nominal controller when analyzing and designing windup compensators. It was argued that the choice of appropriate properties involve trade-offs between stability and fast de-saturation transients. To obtain suitable trade-offs we used LQ-optimization.

In this chapter, we search for

- appropriate polynomials $\boldsymbol{A}_o$ and $\boldsymbol{P}_1,\ \boldsymbol{P}_2$ of the OBSAWC and the GLAWC structures, respectively
- appropriate directionality compensators (artificial limiters) among which the directionality preserver γ is one.

The methodology

- shall be simple to understand
- shall open up the possibility to find simple anti-windup compensators of low order
- shall open up the possibility to use ad-hoc solutions which rely less on models

Such a methodology requires insight and understanding of what parts of the system causes windup problems and, later on, also how the problems can be avoided. For instance, in contrast to the LQ-method, properties of the nominal controller that can contribute to windup when *not* cancelled will be discussed. Earlier work aiming in the same direction can be found in e.g. [56] and [55].

6.1 Anti-windup in SISO-systems

Nominal controllers are designed on the basis of underlying design goals such as disturbance rejection and accurate tracking under varying operating conditions. An anti-windup modification can be seen as a second part of a well performing controller and its task is to change the controller action such that it can handle input saturations better than the nominal linear controller.

The design goals concerning the AWC involve

1. retaining control of the states within the nominal controller e.g. prevent them from growing ”large”, and
2. additional control action that can be used either for increasing or decreasing the control action provided by an OBSAWC.

The first design goal can be fulfilled by using an appropriate OBSAWC whereas the latter requires the use of the GLAWC structure.

When using Nyquist-like methods for the design of an AWC, the design goals can be fulfilled by keeping the Nyquist-loci of the combined loop transfer function $\overline{\mathcal{L}}(C,\omega)$ (5.34) away from the point $(-1,0)$ and see to that the gain $|\overline{\mathcal{L}}(C,\omega)|$ is limited at all frequencies.[1]

[1] This is not possible if the plant contains an integrator. That case will be discussed later in this chapter.

The designer must also keep control of the desaturation transients so that they decay fast. This can be accomplished by selecting the dynamics of $\boldsymbol{\mathcal{H}}_\delta$ properly.

Summary: Loop transfer functions in SISO systems
The loop transfer functions in SISO systems, obtained by nominal control (Section 2.1), OBSAWC (Section 4.1) and GLAWC (Section 4.2) are given by (3.9), (4.7) and (4.16), respectively, i.e.

$$\mathcal{L}_v = \begin{cases} \frac{\alpha}{RA} - 1 & \text{nominal control} \\ \frac{\alpha}{A_o A} - 1 & \text{OBSAWC} \\ \frac{\alpha P_2}{A_o P_1 A} - 1 & \text{GLAWC} . \end{cases} \tag{6.1}$$

Summary: Desaturation transient dynamics in SISO systems
The desaturation transient dynamics in SISO systems, obtained by nominal control (Section 2.1), OBSAWC (Section 4.1) and GLAWC (Section 4.2) are given by (3.9), (4.7) and (4.16), respectively, i.e.

$$\mathcal{H}_\delta = \begin{cases} \frac{BR}{\alpha} & \text{nominal control} \\ \frac{BA_o}{\alpha} & \text{OBSAWC} \\ \frac{BA_o P_1}{\alpha P_2} & \text{GLAWC} . \end{cases} \tag{6.2}$$

The scalar closed loop denominator polynomial α is given by

$$\alpha \;=\; \alpha_1 \alpha_2 \;=\; RA + SB \; . \tag{6.3}$$

Here α_1 is assumed to represent "observer" dynamics which we prefer to interpret as moved poles of the controller (roots of R), whereas α_2 represents the moved poles of the plant (roots of A). More detailed discussions concerning polynomial partitioning of this kind can be found in [56].

In the discussion below we will pinpoint specific properties of controllers and plants that contribute negatively to windup effects in the sense of Definitions 3.1 and 3.2. It is my experience that many systems suffer from more than one of the specified properties and that all of these properties must be dealt with before the system can be expected to behave well.

6.1.1 Windup caused by loop-shaping filters

Consider the loop transfer function (6.1) obtained when using the nominal controller. Problems that may arise due to loop shaping filters, such as integral action[2], can be explained by the fact that the controller polynomial R appears explicitly in the denominator of $\mathcal{L}_v$, see (6.1).

Consider a controller with integral action, i.e. let $R = \Delta\bar{R}$ where Δ represents a differentiator (s in continuous time and e.g. $q-1$ in discrete time). If $\overline{\mathcal{L}_v}(C,\omega)$ does not encircle the point $(-1,0)$, then stability is secured (see Section 5.4.2) but the performance will be degraded because of the infinite DC-gain provided by the Δ-factor. This is the classical and well known integral-windup problem. During a saturation event the integrator will accumulate energy that will be released to the system after desaturation. This will often cause an overshoot.

Not only does integral action result in high loop gain at low frequencies, but also does it provide a phase-lag of -90^o already at $\omega = 0$. This may force $\overline{\mathcal{L}_v}(C,\omega)$ to encircle the point $(-1,0)$. The observer polynomial α_1 will eventually, as the frequency increases, compensate for this lag. But if the observer dynamics are fast, then the phase-lead it contributes with will appear at high frequencies and $\overline{\mathcal{L}_v}(C,\omega)$ may encircle $(-1,0)$ at lower frequencies (for some amplitudes C).

This way of reasoning holds not only for an integrator but also for other loop-shaping filters.

The windup problem described above can be compensated for by using an appropriate OBSAWC and, if no other problems caused by the factor $\frac{\alpha_2}{A}$ are present, then the extra ability provided by the GLAWC is not needed. Design of an appropriate OBSAWC for this problem will be discussed and demonstrated in the examples later in this chapter.

6.1.2 Unstable controllers

Unstable controllers result in unstable modes of R and are simply not acceptable when saturation occurs. As in the previously discussed case concerning integral action the problem of having an unstable controller in a loop with a limiter, can be explained by the fact that the controller denominator R appears as a denominator of $\mathcal{L}$. The controller states may grow unboundedly when saturation occurs. The

[2]Integral action can be seen as a special case of a loop shaping filter where the intended effect is to make the DC-gain in the loop infinite.

problem is however easily avoided by using the OBSAWC discussed in Section 4.1. The designer must select a stable and appropriate A_o such that $\overline{\mathcal{L}_v}(C,\omega)$ stays away from $(-1,0)$ for all C.

6.1.3 Aggressive feedback

By aggressive feedback we here refer to a situation where the poles of the closed loop system (roots of α) are moved far from the poles of the plant (roots of A). Since $\alpha = RA + SB$ such a situation can arise when either the elements of B are large or the elements of the controller polynomial S are selected large. By studying the loop transfer function $\mathcal{L}_v = \frac{\alpha}{A_o A} - 1$, obtained when using the OSBAWC discussed in Section 4.1, we can draw the following conclusions:

The roots of α appear as zeros in $\frac{\alpha}{A_o A}$. Hence, if the poles of the closed loop system (roots of α) are moved far from the plant poles (roots of A), then the phase-lag of $\frac{1}{A_o A}$ will dominate for low frequencies and may force $\overline{\mathcal{L}}(C,\omega)$ to approach, and maybe encircle, $(-1,0)$ before the phase-lead provided by α takes effect. Notice that the best design choice we can make in order to reduce this lag, when using the OBSAWC, is to select the poles of $1/A_o$ as fast as possible so that these poles do not contribute to the phase-lag for low frequencies. But this may not always be sufficient. The GLAWC can, however, be used to solve the problem. Consider the loop transfer function (6.1) obtained when using the GLAWC structure. The polynomial P_2 can be selected so that it contributes with a phase-lead at desired frequencies and the phase-lag of P_1 can be selected to affect the loop at higher frequencies where the gain is small enough, thus preventing $\overline{\mathcal{L}_v}$ to encircle $(-1,0)$[3].

6.1.4 Weak feedback

By weak feedback we here refer to a situation where the desired step response has been obtained mainly by the use of feed forward control. In such systems the roots of α_2 are located close to those of A. Consequently, the loop gain $|\frac{\alpha_2}{A} - 1| \approx |1 - 1| = 0$. The dynamics of $\mathcal{H}_\delta$ are basically equal to the plant dynamics. Hence, the windup effects may decay slowly. Since the transfer function $\mathcal{H}_\delta$ equals the transfer function $\mathcal{H}_\beta$ (describing the influence of input disturbances β on the output y, see (2.1)), this is in agreement with the well know fact that weak feedback attenuates external disturbances poorly.

The GLAWC can be used to reduce the windup effects caused by weak feedback. This is shown in the following example.

[3]Recall the order of P_1 is the same as P_2, see Remark 4.1

EXAMPLE 6.1: FEED-FORWARD CONTROL AND GLAWC

Nominal system

$$\begin{aligned} y &= \frac{B}{A}v = \frac{1}{s+1}v \\ v &= \sigma_{-8}^{8}(u) \\ u &= \frac{T}{R}r = \frac{20(s+1)}{s^2+7s+20} \, . \end{aligned}$$

Notice that the controller polynomial S is zero in a pure feed forward controller. For this nominal system, $\mathcal{L}_v$ and $\mathcal{H}_\delta$ are given by

$$\begin{aligned} \mathcal{L}_v &= \frac{RA}{\alpha} - 1 = \frac{RA}{RA} - 1 = 0 \\ \mathcal{H}_\delta &= \frac{BR}{\alpha} = \frac{BR}{RA} = \frac{B}{A} = \frac{1}{s+1} \end{aligned} \tag{6.4}$$

respectively. Absolute stability is guaranteed since $\mathcal{L}_v = 0$. The transient dynamics described by $\mathcal{H}_\delta$ are, however, slow compared to the compensated system. Using the GLAWC (4.9), for the choices

GLAWC

$$\begin{aligned} P_1 &= A = s+1 \\ P_2 &= s+20 \end{aligned} \tag{6.5}$$

we obtain

$$\begin{aligned} \mathcal{L}_v &= \frac{19}{s+20} \\ \mathcal{H}_\delta &= \frac{BRP_1}{RAP_2} = \frac{B}{P_2} = \frac{1}{s+20} \, . \end{aligned} \tag{6.6}$$

The last equality holds because $P_1 = s+1$ cancels $A = s+1$. Notice that we do not use the control action provided by an OBSAWC which means that the polynomial $A_o = R$. Since $\mathcal{L}_v$ has only one pole, and the limiter is an amplitude limiter, the Nyquist-loci $\overline{\mathcal{L}_v}(C, \omega)$ can never encircle the point $(-1, 0)$. Hence, stability is guaranteed (approximately). We can expect the saturation transient to decay fast since the pole of $\mathcal{H}_\delta$ is twenty times faster than in the nominal case. Furthermore, as a consequence of the larger loop gain, the plant input $\sigma(u)$ obtained when using the GLAWC, can be expected to stay saturated for a longer time compared to what the input of the nominal controller will do. The nominal

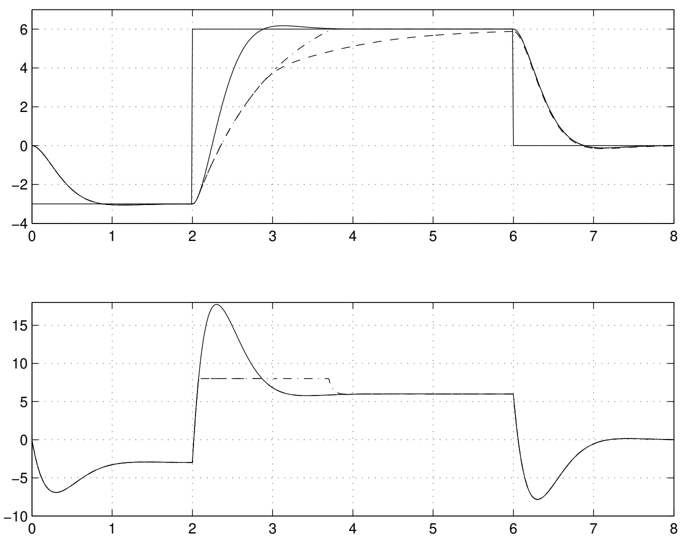

Figure 6.1: The plant output (upper part) and the plant input (lower part) of the linear system response (solid), the response of the nominal system (dashed) and the response of the system with the GLAWC (dash-dotted).

control signal u will be the same as the control signal of the linear system and, hence, it will only saturate when the linear control signal exceeds the saturation limits ± 8.

Figure 6.1 shows the result when applying a reference signal in form of a sequence of steps. The plant input in the nominal system exits saturation at time $t \approx 2.8s$ and follows the linear control signal thereafter. The plant output in the nominal system begins to decrease significantly in growth at time $t \approx 3.1s$ and it takes the whole duration of $4s$ until it reaches the plant output of the linear system at $t \approx 6s$. The plant input of the compensated system, however, stays saturated almost until the plant output reaches the linear response which happens at time $t \approx 3.7s$. Then, both the plant input and the plant output almost immediately follows the corresponding signals of the linear system. The response of the three different systems to the step change from $r = 6$ to $r = 0$, which happens at time $t = 6s$, are almost identical. This is so because none of the control signals saturate. If the optimal performance is to follow the linear plant output, then the system with the GLAWC compensator operates very close to optimum.

6.1.5 State-estimate feedback controllers

In case the nominal controller is a state feedback controller that utilizes an observer to estimate the states, windup problems are most often blamed on incorrect state estimates. What saturation concerns, incorrect state estimates result when the observer uses the controller output u instead of the real plant input $\psi(u)$ when updating the estimates. In a state-estimate feedback controller having an observer which relies much on the plant input, input saturation may result in very poor performance and even instability if the observer uses the control signal u instead of $\psi(u)$ in its updates. Some state-estimate feedback controllers without LTR compensation will rely much on the plant input. The poor stability properties can be analyzed e.g. by studying the properties of the loop transfer function, $\mathcal{L}$, around the saturation nonlinearity, see e.g. Doyle (1979) [81].[4]

The problem can easily be avoided by simply using $\sigma(u)$ in the observer instead of u.

It should be made clear, however, that the problem of incorrect state-estimate, caused by the use of u instead of $\sigma(u)$, may not be the only problem caused by saturation in such a system. Loop shaping filters and high gain feedback may cause severe windup as well. Problems that may arise due to loop shaping filters where discussed above. What the problem of high feedback gain concerns, we suggest two different solutions. One can either decrease the gain of the nominal controller permanently (by de-tuning it) or use the GLAWC to reduce the loop gain only when saturation occur. The technique behind the last mentioned solution appear particularly clear in the scheme proposed by Teel & Kapoor [52]. See also Section 4.3.1. We will, however, demonstrate that simple GLAWC:s of lower order can often be used with satisfactory result. This is demonstrated in some the examples later in this chapter.

6.1.6 Plants with integrator

Having integrators in a loop with saturations will in some cases mean trouble. Problems that will arise due to a *controller integrator* can, as we discussed before, be avoided by using an OBSAWC. Some of the problems that a *plant integrator* may cause in a loop with saturations can, however, no AWC set right. An indication of this fact is that marginally stable factors of the plant denominator polynomial A

[4] If LTR compensation is used, then the estimator does often not rely as much on the plant-input signal as compared to the case when not using LTR. Consequently the estimator becomes less sensitive to which signal u or $\sigma(u)$ is used.

will remain denominator factors of $\boldsymbol{\mathcal{L}}_v$ regardless of how the stable AWC polynomials A_o, P_1, P_2 are selected.

If an external disturbance affects a plant having an integrator, in such a way that the integrator is driven by it, and the disturbance is such that the largest possible control amplitude $\sigma(u)$ does not manage to compensate for it, then the plant integrator state will continue to grow as long as the disturbance remains. This is a physical fact that *no* controller (of any type) can do anything about. What we *can* expect from a well performing controller is that it takes over the control of the system after the disturbance has disappeared (or decreased sufficiently). According to the design strategy advocated in this thesis, this can be obtained by selecting the AWC polynomials such that the dynamics of $\mathcal{H}_\delta$ becomes (or remains) sufficiently fast while keeping the Nyquist-loci $\overline{\mathcal{L}}(C,\omega)$ away from the point $(-1,0)$.

Input saturation does, however, not always imply problems in control systems where the plant contains an integrator. As we pointed out before, large reference steps will often cause controller integrator windup if no AWC is used when the input saturates. When an integrator is present in the plant (and not in the controller), a saturation event caused by a large change in the reference signal will in some systems only slow down the response (compared to the linear ideal system), and some systems would actually operate close to their maximum capacity. The following example illustrates this.

EXAMPLE 6.2: PLANT WITH INTEGRATOR

Consider the following two systems:
System 1 (controller integrator)

$$
\begin{aligned}
y_1 &= \frac{B_1}{A_1}v_1 = \frac{1}{s+1}v_1 \\
v_1 &= \sigma_{-6}^{6}(u_1) \\
u_1 &= \frac{-S_1y_1+T_1r}{R_1} = \frac{-20(0.3s+1)y_1+20r}{s}
\end{aligned} \tag{6.7}
$$

and

System 2 (plant integrator)

$$
\begin{aligned}
y_2 &= \frac{B_2}{A_2} v_2 = \frac{1}{s(s+1)} v_2 \\
v_2 &= \sigma_{-6}^{6}(u_2) \\
u_2 &= \frac{-S_2 y_2 + T_2 r}{R_2} = \frac{-20(0.3s+1)y_1 + 20r}{1}
\end{aligned}
\tag{6.8}
$$

Notice that the plants of the two systems are different. This means that we can not compare their performance. We just want to show that a plant integrator does not always means trouble and, in the same example, we also want to show that controller integrators may be problematic (when not compensated for by an AWC). Notice that the loop transfer functions $\mathcal{L}_v$ are, however, the same and given by

$$
\mathcal{L}_v = \frac{20(0.3s+1)}{s(s+1)} . \tag{6.9}
$$

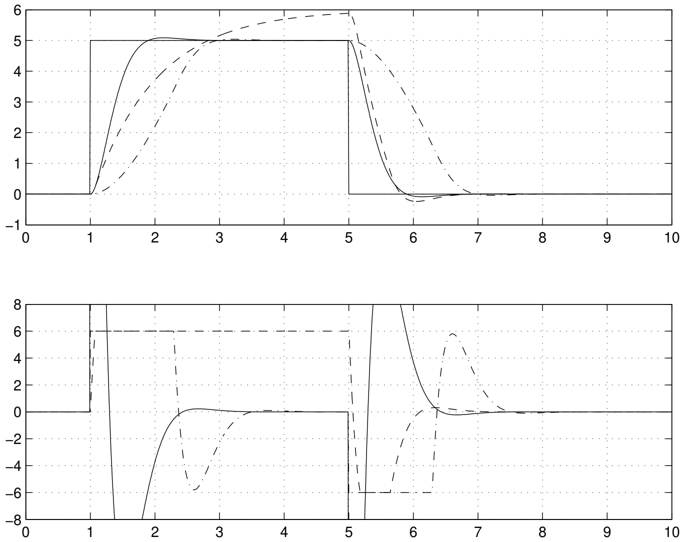

Figure 6.2: The plant output (upper part) and input (lower part) of the linear system response (solid), the response of System 1 (dashed) and the response of System 2 (dash-dotted).

The plant output y_2 of System 2 operates close to its maximum performance (in terms of reference-following). This is indicated by the fact that the control signal u_2 saturates just as long as it can while still avoiding y_2 from overshooting.

The controller integrator in System 1, however, ”winds-up” the control signal u_1 and causes an overshoot in the response of y_1. The ”reference-to-output” step response of the two linear systems ($\sigma(u_i) \equiv u_i,\ i = 1, 2$) are identical. See Figure 6.2.

6.1.7 Unstable plants

Unstable plants can not be stabilized globally when having saturations in the loop. Anti-windup can improve stability compared to the nominal linear controller, but it can never guarantee stability when e.g. large disturbances acts on the system. The discussion in this thesis does not concern unstable systems.

6.2 Anti-windup in MIMO-systems

With respect to performance, feedback of single-input saturating systems is a complicated issue but multiple-input systems are, as usual, even more awkward to deal with. Some properties causing severe windup in control systems can only be found in multiple-input systems and can thereby not be placed in any of the categories discussed in the previous sections concerning windup in SISO-systems. This type of problems have been referred to as *directionality problems* in some works, see e.g [42] and [61]. It should be pointed out that although we chose to discuss these MIMO-specific problems in this chapter concerning heuristic design, the design strategies proposed in Chapter 5 can, of course, also be used to solve them.

In this section we will show how directionality problems can be detected, by using a root-locus like method, and how they can be avoided by using directionality compensation. But first, we must point out shortcomings concerning the transfer function $\boldsymbol{\mathcal{H}}_\delta$ in MIMO systems.

Shortcomings of $\boldsymbol{\mathcal{H}}_\delta$ as a tool for performance analysis in MIMO systems
The transfer function $\boldsymbol{\mathcal{H}}_\delta$, describing the decay of saturation effects, is not a useful tool for analysis of performance (in terms of saturation effects) *during* saturation in some, or all, of the components of the controller output u. The reason for this can be explained in the following way: Assume that u saturates in the component u_i and consider the ”loss” of input power as a ”disturbance” acting on u_i. Then, the disturbance attenuation properties will be given by $\boldsymbol{\mathcal{H}}_\delta$ in the same way as $\boldsymbol{\mathcal{H}}_\beta$ describes attenuation of a normal external disturbance β, in the linear sys-

tem (2.1) and (2.2). The difference is that in the case of saturation, u_i, can not be used to eliminate the "disturbance" during saturation simply *because it saturates*. The degree of performance loss during saturation thus depends on how well the unsaturated components of u can help attenuate the "disturbance". Or more correctly expressed, how well the unsaturated components of u can help compensate the shortcoming that the saturation in u_i implies. If the degree of feedback is reasonable, i.e., if the loop gain $|\boldsymbol{\mathcal{L}}_v|$ is reasonably large, then the system may perform well. The use of directional compensation, see Section 2.5, may also help keeping the performance loss at an acceptable level. This was shown earlier in Examples 5.1 and 5.2 and it is also shown in Examples 6.3 and 6.4 below.

Next, a simple but useful method for analysis of closed loop MIMO-systems with input saturations will be proposed and discussed. Although the method can detect and classify many of the windup problems discussed earlier in this chapter, it is most useful for analysis of directionality problems. We will here demonstrate the idea when using a nominal controller, and an OBSAWC. It is important to point out that the method indicates stability only **approximately**.

6.2.1 Root-locus like analysis for MIMO systems with saturating actuators

For the standard amplitude limiter σ, the components $v_i(t)$ of the plant input vector, $v(t)$, can be described as

$$v_i \;=\; \sigma(u_i) \;=\; \frac{\sigma(u_i)}{u_i}u_i \stackrel{\Delta}{=} \gamma_i u_i \tag{6.10}$$

where $0 < \gamma_i \leq 1$ for $u_i < \infty$. By introducing a diagonal matrix $\Gamma_{p|p}$ having the numbers $\gamma_1, \gamma_2 \ldots \gamma_p$ as diagonal elements, i.e,

$$\Gamma(i,j) \;=\begin{cases}\gamma_i, & i=j\\ 0 & i\neq j\end{cases} \tag{6.11}$$

for $i = 1, 2, \ldots p,\ j = 1, 2, \ldots p$, the plant model (2.1) (for $\beta = 0,\ \psi \equiv \sigma$) can be written as

$$\begin{aligned} y \;&=\; \boldsymbol{B}\boldsymbol{A}^{-1}\sigma(u) \;=\; \boldsymbol{B}\boldsymbol{A}^{-1}\Gamma u\\ &=\; \boldsymbol{B}(\Gamma^{-1}\boldsymbol{A})^{-1}u\ . \end{aligned} \tag{6.12}$$

Notice that Γ^{-1} exist since all the components $u_i < \infty$. We now rewrite the OBSAWC in the same way, i.e.,

$$\boldsymbol{A}_o u \;=\; (\boldsymbol{A}_o - \boldsymbol{R})\Gamma u + \boldsymbol{T}r - \boldsymbol{S}y\ . \tag{6.13}$$

Collecting all u-terms on the left hand side gives

$$(\boldsymbol{A}_o - (\boldsymbol{A}_o - \boldsymbol{R})\Gamma)u \;=\; \boldsymbol{T}r - \boldsymbol{S}y \;. \tag{6.14}$$

By introducing the notations

$$\begin{aligned} \bar{\boldsymbol{R}} \;&=\; (\boldsymbol{A}_o - (\boldsymbol{A}_o - \boldsymbol{R})\Gamma) \\ \bar{\boldsymbol{A}} \;&=\; \Gamma^{-1}\boldsymbol{A} \;, \end{aligned} \tag{6.15}$$

the plant model (6.12) and the OBSAWC (6.13) can be written as

$$\begin{aligned} y \;&=\; \boldsymbol{B}\bar{\boldsymbol{A}}^{-1}u \\ \bar{\boldsymbol{R}}u \;&=\; \boldsymbol{T}r - \boldsymbol{S}y. \end{aligned} \tag{6.16}$$

The closed loop system can then be described by (see the linear system description (2.3))

$$\begin{aligned} y &= \boldsymbol{B}(\bar{\boldsymbol{R}}\bar{\boldsymbol{A}} + \boldsymbol{S}\boldsymbol{B})^{-1}\boldsymbol{T}r \\ &\triangleq \boldsymbol{B}\bar{\boldsymbol{\alpha}}^{-1}\boldsymbol{T}r \;. \end{aligned} \tag{6.17}$$

Approximately, stability can now be investigated by calculating the poles i.e. the roots of $\bar{\boldsymbol{\alpha}}$.

We have that

$$\begin{aligned} \bar{\boldsymbol{\alpha}} \;&=\; \bar{\boldsymbol{R}}\bar{\boldsymbol{A}} + \boldsymbol{S}\boldsymbol{B} \\ &=\; (\boldsymbol{A}_o - (\boldsymbol{A}_o - \boldsymbol{R})\Gamma)\Gamma^{-1}\boldsymbol{A} + \boldsymbol{S}\boldsymbol{B} \\ &=\; (\boldsymbol{A}_o\Gamma^{-1} - (\boldsymbol{A}_o - \boldsymbol{R}))\boldsymbol{A} + \boldsymbol{S}\boldsymbol{B} \\ &=\; \boldsymbol{A}_o\Gamma^{-1}\boldsymbol{A} - \boldsymbol{A}_o\boldsymbol{A} + \boldsymbol{R}\boldsymbol{A} + \boldsymbol{S}\boldsymbol{B} \\ &=\; \boldsymbol{A}_o(\Gamma^{-1} - \mathbf{I})\boldsymbol{A} + \boldsymbol{\alpha} \;. \end{aligned} \tag{6.18}$$

Let us formalize this expression as a result.

Result 6.1 *The closed loop denominator of a system controlled by an OBSAWC, via saturating actuators represented by the matrix Γ, is given by*

$$\bar{\boldsymbol{\alpha}} \;=\; \boldsymbol{A}_o(\Gamma^{-1} - \mathbf{I})\boldsymbol{A} + \boldsymbol{\alpha} \;. \tag{6.19}$$

Note that when none of the components u_i saturate, i.e. $\Gamma = \Gamma^{-1} = \mathbf{I}$, then

$$\bar{\boldsymbol{\alpha}} \;=\; \boldsymbol{A}_o(\mathbf{I}-\mathbf{I})\boldsymbol{A} + \boldsymbol{\alpha} \;=\; \boldsymbol{\alpha}\;. \tag{6.20}$$

and the closed loop transfer function from r to y is given by the linear description (2.3).

Closed loop stability of the system with limiters is indicated if the the roots of $\bar{\boldsymbol{\alpha}}$ are located in the left half plane in the continuous-time case and inside the unit circle in the discrete-time case, when the elements of the diagonal of Γ varies and take values $0 < \gamma_i \leq 1$.

By calculating the roots of $\bar{\boldsymbol{\alpha}}$ for different values of the components γ_i, we will be able to find both critical directions $(\gamma_1, \gamma_2, \ldots, \gamma_p)$ and critical amplitude reductions where stability can no longer be obtained. The result can also help finding appropriate directionality compensators in form of artificial limiters. This will be demonstrated in the example that follows next. In distinction to root-locus analysis, we are only interested in the location of the ”worst-case” pole, i.e., the location of the pole which is closest to the stability boundary in case the systems is stable, or the pole which located most far from the stability boundary in case the system is unstable. Recall that the choice $\boldsymbol{A}_o = \boldsymbol{R}$ makes the OBSAWC become equal to the nominal controller and, hence, also the nominal system can be analyzed by using the expressions derived above.

6.3 Examples

The rest of this chapter is devoted to examples where the analysis and design concepts proposed and discussed earlier in this chapter, we will used for the design of anti-windup compensators.

EXAMPLE 6.3: PLANT 1, HEURISTIC DESIGN

The nominal system under investigation here is the same as in Example 5.1. There, it was argued and shown by stability analysis and simulations, that the nominal system is not stable.

First, we use the root-locus method to analyze stability and to find critical directions. The closed loop denominator $\bar{\boldsymbol{\alpha}}$ (6.19) (containing Γ) is in this case given

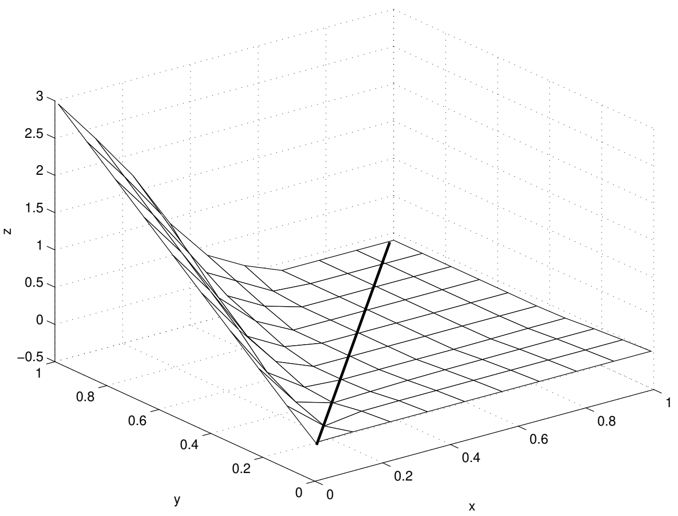

Figure 6.3: Worst case root-locus for the nominal controller. The x-axis represents γ_2 and the y-axis represents γ_1, taking ten values each in the interval $0.01 - 1$. The z-axis represents the maximum value of the real parts of the roots. The system can be expected not to be stable in areas where the surface take positive z-values. The solid line represents the function $\gamma_1 = \gamma_2$ which corresponds to the result obtained from directionality preservation. Since the line is located below $z = 0$ such compensation can be expected to stabilize the system.

by

$$\begin{aligned} \bar{\boldsymbol{\alpha}} &= \boldsymbol{A}_o(\Gamma^{-1} - \mathbf{I})\boldsymbol{A} + \boldsymbol{\alpha} \\ &= \boldsymbol{A}_o(\Gamma^{-1} - \mathbf{I})\boldsymbol{A} + \boldsymbol{\alpha}_i \boldsymbol{A} \\ &= (\boldsymbol{A}_o(\Gamma^{-1} - \mathbf{I}) + \boldsymbol{\alpha}_i)\boldsymbol{A} \ . \end{aligned} \tag{6.21}$$

Nominal system

The nominal case corresponds to $\boldsymbol{A}_o = \boldsymbol{R}$ and gives that

$$\bar{\boldsymbol{\alpha}} = (s(\Gamma^{-1} - \mathbf{I}) + \boldsymbol{\alpha}_i)(s + 0.1) \ . \tag{6.22}$$

We now calculate the roots of $\bar{\boldsymbol{\alpha}}$ in (6.22) when letting γ_1 and γ_2 take the values $[1 \ 3/5 \ 3/7 \ 3/9]$. Since we are interested only in the ”worst-case” root, and since the system is represented in continuous time, we show only the maximum real part of the roots, for each pair $(\gamma_1(j), \gamma_2(i))$. If the maximum real part is positive, then at least one pole is locate in the right half plane and the system can be expected to go unstable in the particular direction. The following matrix

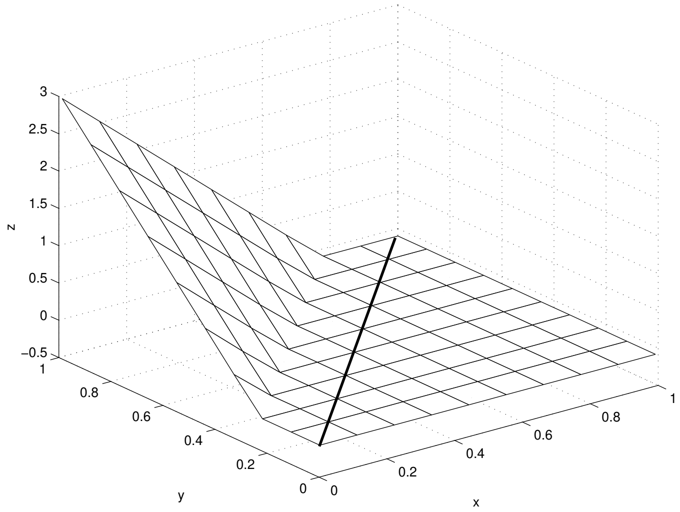

Figure 6.4: Worst case root-locus for a diagonal OBSAWC. The x-axis represents γ_2 and the y-axis represents γ_1, taking ten values each in the interval $0.01 - 1$. The z-axis represents the maximum value of the real parts of the roots. The system can be expected not to be stable in areas where the surface take positive z-values. The solid line represents the function $\gamma_1 = \gamma_2$ which corresponds to the result obtained from directionality preservation. Since the line is located below $z = 0$, such compensation can be expected to stabilize the system.

where obtained in this case

$$\begin{pmatrix} -0.1000 & -0.1000 & -0.1000 & -0.0851 \\ 0 & -0.1000 & -0.1000 & -0.1000 \\ 0.4286 & -0.1000 & -0.1000 & -0.1000 \\ 1.0000 & 0.0667 & -0.1000 & -0.1000 \end{pmatrix} \tag{6.23}$$

Here, the column "i" corresponds to $\gamma_2(i)$ and the row "j" corresponds to $\gamma_1(j)$. We can see that at least one pole is located in the right half plane for some $\gamma_1 < \gamma_2$ (below the diagonal) which corresponds to when u_1 saturates deeper, relatively, than u_2. In Figure 6.3, such a matrix is plotted for γ_1 and γ_2 taking ten values each in the interval $0.01 - 1$.

We will now also show that in this simple case, one can derive an expression for the critical condition. Since the root of $(s + 0.1) = 0$, i.e. -0.1 lies in the left half plane we continue to investigate only the other factor, which can be written

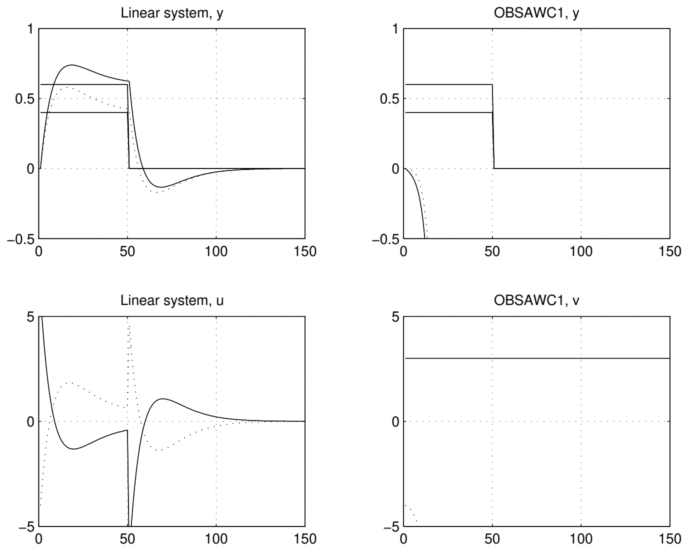

Figure 6.5: Reference step response for the linear system (left) and for the OBSAWC1 (right). The plant outputs y_1 and y_2 are shown in the upper plots as (solid) and (dotted) lines respectively, whereas the plant inputs v_1 and v_2 are shown in the lower plots as (solid) and (dotted) lines respectively.

as

$$\begin{pmatrix} s(\frac{1}{\gamma_1}-1) & 0 \\ 0 & s(\frac{1}{\gamma_2}-1) \end{pmatrix} + \begin{pmatrix} s+5 & 4 \\ -4 & s-3 \end{pmatrix}$$
$$= \begin{pmatrix} \frac{s}{\gamma_1}+5 & 4 \\ -4 & \frac{s}{\gamma_2}-3 \end{pmatrix} . \qquad (6.24)$$

The determinant of this matrix is given by

$$\frac{s^2}{\gamma_1\gamma_2} + (\frac{5}{\gamma_2} - \frac{3}{\gamma_1})s + 1 , \qquad (6.25)$$

and, hence, the poles are given by the roots of

$$s^2 + (5\gamma_1 - 3\gamma_2)s + \gamma_1\gamma_2 = 0 . \qquad (6.26)$$

We can se that all poles are located strictly in the left half plane if and only if

$$\begin{aligned} 5\gamma_1 - 3\gamma_2 &> 0 \\ &\Leftrightarrow \\ \gamma_2 &< \frac{5}{3}\gamma_1 . \end{aligned} \qquad (6.27)$$

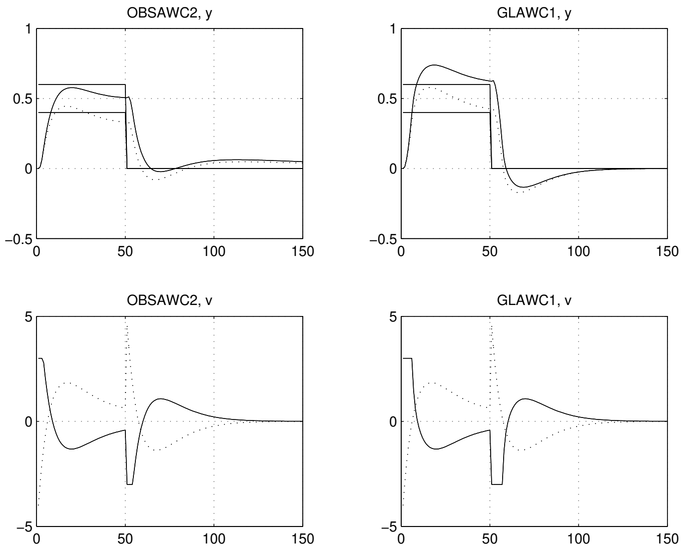

Figure 6.6: Reference step response for the OBSAWC2 (left) and for the GLAWC1 (right). The plant outputs y_1 and y_2 are shown in the upper plots as (solid) and (dotted) lines respectively, whereas the plant inputs v_1 and v_2 are shown in the lower plots as (solid) and (dotted) lines respectively.

It is obvious that saturations in u_1 are critical. However, if γ_2 is forced, by direction compensation, to take values such that the condition (6.27) is fulfilled, stability can be achieved. Saturations in u_2, however, are not critical for stability according to this analysis. This fact can be used when designing a directionality compensator for the system. Using directional preservation makes $\gamma_1 = \gamma_2 = \gamma$ so the stability condition (6.27) holds for all γ. Hence, according to the results obtained from this analysis, direction preservation stabilizes the nominal system. This conclusion can be drawn also from studying the location of the solid line in Figure 6.3, since it is located below $z = 0$.

The nominal controller (5.42) contains an integrator and according to the discussion in Section 6.1.1 an OBSAWC is, at least, needed in order to avoid overshoots. We will investigate two different OBSAWC and also one GLAWC given by the polynomials

$$\begin{aligned}
&\text{OBSAWC1} \quad \boldsymbol{A}_o = (s + a_o)\mathbf{I} \\
&\text{OBSAWC2} \quad \boldsymbol{A}_o = \boldsymbol{\alpha}_i \\
&\text{GLAWC1} \quad \boldsymbol{A}_o = \boldsymbol{\alpha}_i, \;\; \boldsymbol{P}_1 = \boldsymbol{A}, \;\; \boldsymbol{P}_2 = (s+10)\mathbf{I}\,,
\end{aligned} \tag{6.28}$$

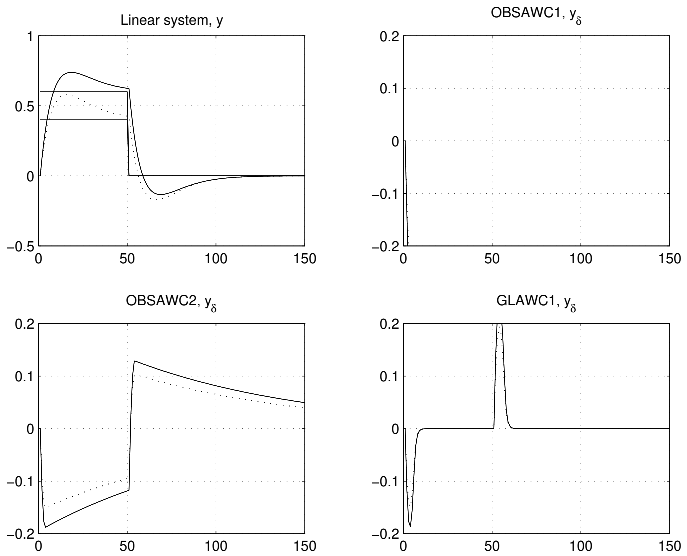

Figure 6.7: Reference step response for the linear system (upper left) and the windup effects of the plant outputs for the OBSAWC1 (upper right), OBSAWC2 (lower left) and for the GLAWC1 (lower right). Solid and dotted lines represent windup effects in $y_1,\ u_1$ and $y_2,\ u_2$ respectively.

where

$$\begin{aligned}\boldsymbol{\alpha}_i &\triangleq \begin{pmatrix} s+5 & 4 \\ -4 & s-3 \end{pmatrix} \\ \boldsymbol{A} &= (s+0.1)\mathbf{I}. \end{aligned} \tag{6.29}$$

See (5.46) and (5.43). The constant a_o will be used as a tuning parameter.

OBSAWC1

It is easy to verify that the loop transfer function obtained by using OBSAWC1 is given by

$$\boldsymbol{\mathcal{L}}_v = \frac{1}{s+a_o}\begin{pmatrix} 5-a_o & 4 \\ -4 & -3-a_o \end{pmatrix}. \tag{6.30}$$

The controller-integrator windup problem is avoided as expected. Let us now investigate the stability properties by using the Circle-criterion as we did in Example 5.1. Here, we make it easy for us by simply investigating $\bar{Z}(j\omega = 0)$. It can be shown that

$$\bar{Z}(0) = \frac{1}{a_o}\begin{pmatrix} 10 & 0 \\ 0 & -6 \end{pmatrix} \tag{6.31}$$

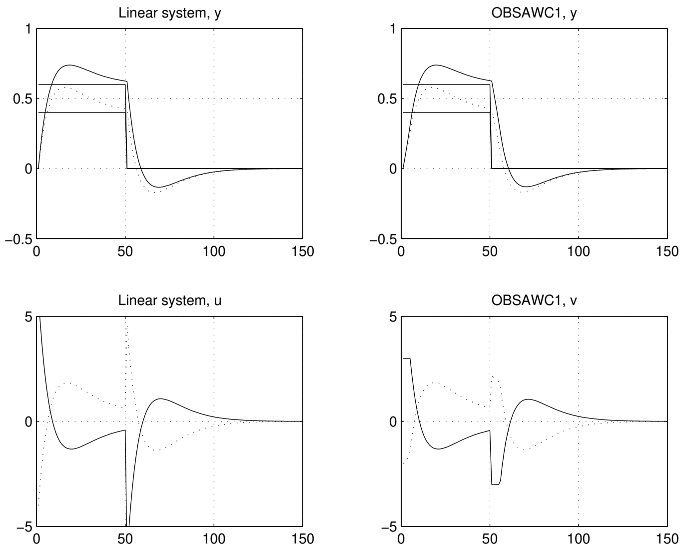

Figure 6.8: Same situation as shown in Figure 6.5 but with directional compensation of u.

which has one negative eigenvalue for any $a_o \neq 0$ (the case $a_o = 0$ corresponds to the nominal case investigated in the Example 5.1). According to the Circle-criterion this indicates that the simple OBSAWC1 will not be able to stabilize the system, an indication which is verified by several simulations one of which is shown in Figures 6.5 and 6.7 respectively.

We will now analyze the special choice $\boldsymbol{A}_o = (s+1)\mathbf{I}$ by using the root-locus like method. For this choice of $\boldsymbol{A}_o$, the matrix (6.23) is given by

$$\begin{pmatrix} -0.1000 & -0.1000 & -0.1000 & -0.1000 \\ 0.3200 & -0.1000 & -0.1000 & -0.1000 \\ 1.6400 & 0.3200 & -0.1000 & -0.1000 \\ 2.9600 & 1.6400 & 0.3200 & -0.1000 \end{pmatrix} . \tag{6.32}$$

Notice that since $\boldsymbol{A}_o$ does not contain an integrator, poles do not move towards zero as γ_2 decreases, as they did in the nominal case where $\boldsymbol{R}$ is a pure integrator (upper-right part of the matrix). The Figure 6.4 shows the worst-case pole as a function of γ_1 and γ_2. Both the matrix (6.32) and the 3-D plot of Figure 6.4 shows that the system is most likely not stable if u_1 saturates deeper than u_2, i.e. when $\gamma_1 < \gamma_2$. Note that this is particularly serious in this system where u_1 saturates at ± 3 whereas u_2 saturates at ± 10.

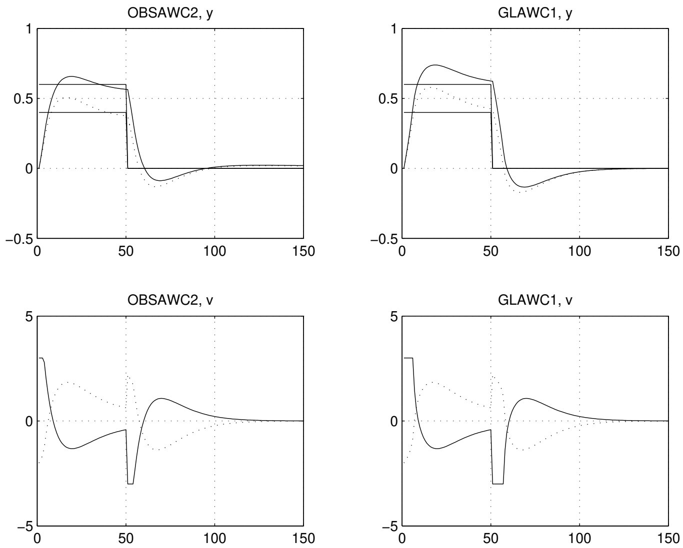

Figure 6.9: Same situation as shown in Figure 6.6 but with directional compensation of u.

Since the diagonal elements of the matrix (6.32) all are negative, directionality preservation will stabilize the system.

OBSAWC2

The loop transfer function obtained by using the OBSAWC2 is given by

$$\boldsymbol{\mathcal{L}}_v \;=\; \mathbf{I} - \mathbf{I} \;=\; 0. \tag{6.33}$$

Since the plant is asymptotically stable, this choice of anti-windup compensator stabilizes the system. The response is shown in Figures 6.6 and 6.7. The desaturation transient is, however, very slow, as we can see in the plot. This can be explained by studying the dynamics $\boldsymbol{\mathcal{H}}_\delta$ which in this case is identical to the plant, i.e.,

$$\boldsymbol{\mathcal{H}}_\delta \;=\; \boldsymbol{B}\boldsymbol{A}^{-1} \;=\; \boldsymbol{B}\frac{1}{s+0.1}. \tag{6.34}$$

Hence, both the transients will decay with a time constant of 10 s which explains the rather slow recovery. According to the discussion in Section 6.1.4 the problem is caused by *weak feedback* and a GLAWC can be used to improve the performance.

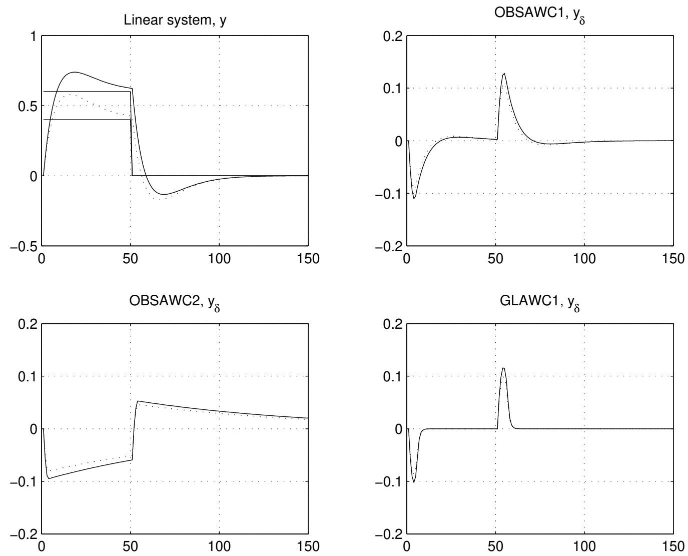

Figure 6.10: Same situation as shown in Figure 6.7 but with directional compensation of u

One can also use the root-locus method proposed above. The choice $\boldsymbol{A}_o = \boldsymbol{\alpha}_i$ gives

$$\begin{aligned}\bar{\boldsymbol{\alpha}} &= (\boldsymbol{\alpha}_i(\Gamma^{-1} - \mathbf{I}) + \boldsymbol{\alpha}_i)(s + 0.1) \\ &= \boldsymbol{\alpha}_i \Gamma^{-1}(s + 0.1) \ ,\end{aligned} \tag{6.35}$$

which has all roots in the left half plane. Hence, this choice results in a stable system.

GLAWC1

The loop transfer function, which by this choice becomes diagonal, is given by

$$\begin{aligned}\boldsymbol{\mathcal{L}}_v &= \boldsymbol{P}_2 \boldsymbol{A}^{-1} - \mathbf{I} \\ &= \frac{(10 - 0.1)}{s + 0.1}\mathbf{I}\end{aligned} \tag{6.36}$$

and the transient dynamics are described by

$$\begin{aligned}\boldsymbol{\mathcal{H}}_\delta &= \boldsymbol{B}\boldsymbol{P}_2^{-1} \\ &= \boldsymbol{B}\frac{1}{s + 10} \ .\end{aligned} \tag{6.37}$$

The time constants of $\boldsymbol{\mathcal{H}}_\delta$ are one hundred times smaller than in (6.34) and we can expect the transients to decay much faster in this case. But before this can be guaranteed, the stability properties must be investigated and since the loop transfer function is diagonal, we will use the Nyquist-like method presented in Chapter 5.4.2. Since ψ is the amplitude limiter and the loop transfer function is of order one, the Nyquist-loci $\overline{\mathcal{L}_v}(C,\omega)$ stays in the right half-plane and can thereby not encircle the point (-1,0). Stability is therefore guaranteed in this case. Simulation results are shown in Figures 6.6 and 6.7.

Directionality compensation

By introducing the directionality preserving limiter γ defined in (2.17) instead of the "standard" amplitude limiter σ defined in (2.5), the behavior of the systems defined by OBSAWC1, OBSAWC2 and GLAWC1, improve and the unstable system obtained when using OBSAWC1 is now stable and behaves well. Simulation results are shown in Figures 6.9 and 6.10.

EXAMPLE 6.4: PLANT 2, HEURISTIC, MODEL-BASED DESIGN OF OBSAWC:S

The polynomial matrix $\boldsymbol{A}_o$ of the OBSAWC will here be selected to be a scalar transfer function A_o times a (2x2) identity matrix. This results in a diagonal loop transfer function having the same diagonal elements. This scalar transfer function is given by

$$\mathcal{L}_v = \frac{\alpha}{A_o A} - 1 \tag{6.38}$$

and the de-saturation transient dynamics are given by

$$\boldsymbol{\mathcal{H}}_\delta = \mathbf{G}_c \frac{B A_o}{\alpha}\ , \tag{6.39}$$

where $A(q),\ B(q)$ and $\mathbf{G}_c$ are defined in (5.59) and (5.62). The closed-loop denominator polynomial α defined in (5.63) can be factorized as

$$\alpha = (q-0.8064)(q-0.7929)(q-0.4181)(q-0.3826). \tag{6.40}$$

We know from the example in the previous chapter that the diagonal OBSAWC defined by $A_o = (q-0.4)^2$ stabilized the system but resulted in a somewhat slow desaturation transient. Figure 5.22 shows simulation results when using the direction preserving limiter γ (2.17). The slow recovery can be explained by the

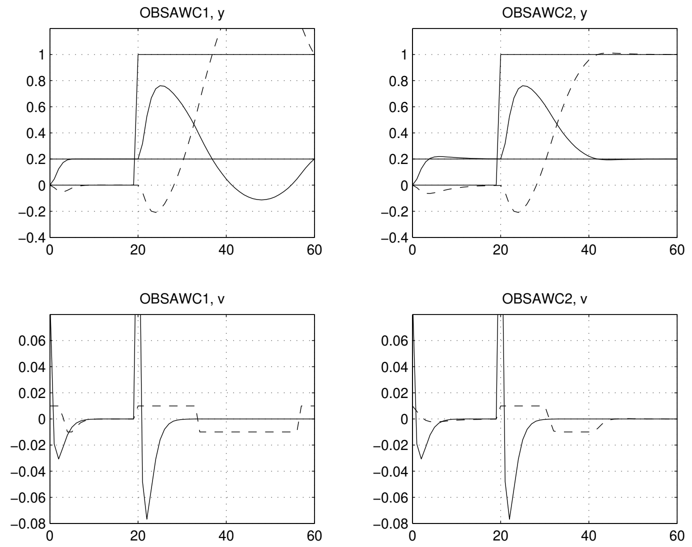

Figure 6.11: Reference step response for the OBSAWC1 (left) and for the OBSAWC2 (right).

fact that the zeros 0.8064 and 0.7929 of α in (6.40) slow down the dynamics of $\boldsymbol{\mathcal{H}}_\delta$. Interpreted in terms of "weak feedback" discussed in Section 6.1.4, the same conclusion can drawn from the fact that these slow roots of α contributes with phase-lead and small gain of $\boldsymbol{\mathcal{L}}_v(\omega)$ at rather low frequencies. By cancellation of these zeros/poles using A_o, the dominating poles of $\boldsymbol{\mathcal{H}}_\delta$ will be "faster" (which also means that the phase-lead of $\boldsymbol{\mathcal{L}}_v(\omega)$ reduces and the gain increases) and hence, the recovery can be expected to become faster. We will here investigate two OBSAWC:s based on the following selection of $\boldsymbol{A}_o$:

$$\begin{aligned} \text{OBSAWC1} \;\; A_o &= (q-0.8064)(q-0.7929) \\ \text{OBSAWC2} \;\; A_o &= q(q-0.8064)\ . \end{aligned} \tag{6.41}$$

Root-locus like analysis: the nominal system

The worst case root-locus for the nominal system is shown in Figure 6.13. Since the surface lies above $+1$ for some γ_1 and γ_2, the nominal system can not be expected to be stable.

Root-locus like analysis: the OBSAWC1

The worst case root-locus for the OBSAWC1 is shown in Figure 6.14. Since the surface lies below $+1$ for all γ_1 and γ_2, the OBSAWC1 can be expected to give a stable system. Since the surface is symmetric with respect to the line $\gamma_1 = \gamma_2$, there are no critical directions in this system. The surface increases in the z-

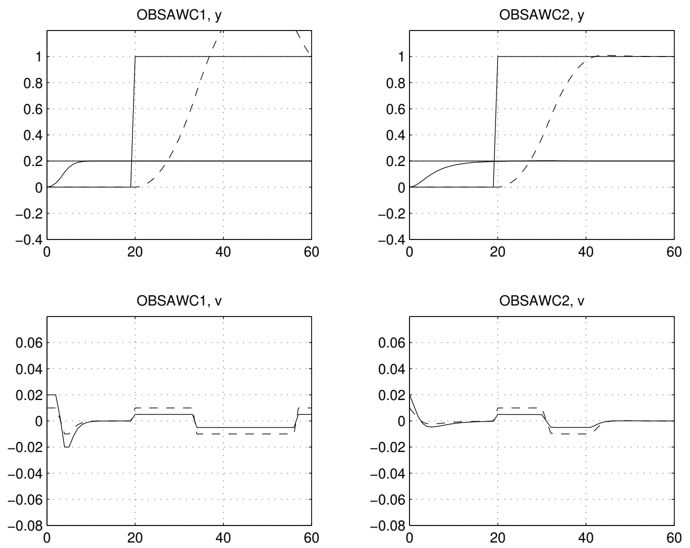

Figure 6.12: Reference step response for the OBSAWC1 (left) and for the OBSAWC2 (right) when using directional compensation.

direction and approaches the value $z = 1$, as γ_1 and γ_2 decreases. This is due to the fact that the plant contains double integrators.

Root-locus like analysis: the OBSAWC2

The worst case root-locus for the OBSAWC2 is shown in Figure 6.15. Since the surface lies below $+1$ for all γ_1 and γ_2, the OBSAWC2 can be expected to give a stable system.

Comments on OBSAWC1 and 2

The OBSAWC1 cancel out both the slow poles of $\mathcal{H}_\delta$ and results in too much phase-lead reduction (i.e. to large phase-lag). A large over shoot is present in the output y_2. The second design, OBSAWC2, cancels only the pole in 0.8064 and adds a much "faster" pole in $q = 0$. The dominating pole of $\mathcal{H}_\delta$ is now the one in 0.7929. The result improves further when using the directional compensator γ.

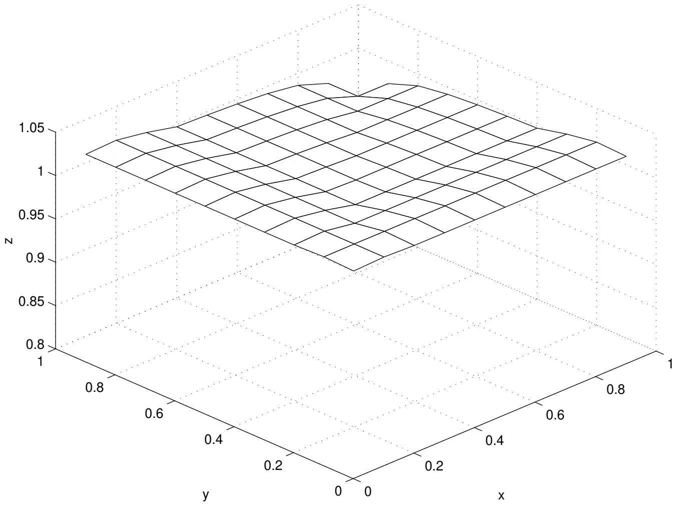

Figure 6.13: Worst case root-locus for the nominal system. The x-axis represents γ_2 and the y-axis represents γ_1, taking ten values each in the interval $0.01 - 1$. The z-axis represents the maximum value among the absolute values of the roots. The system can be expected not to be stable in areas where the surface take values larger than 1.

EXAMPLE 6.5: PLANT 1 WITH COMBINED RATE- AND AMPLITUDE LIMITERS, HEURISTIC DESIGN

In this example, control of the ill-conditioned plant (5.41) is considered. Here, however, combined rate- and amplitude limiters (Figure 2.2) are present at the plant input, which is given by

$$v(t) \;=\; \begin{pmatrix} \rho_{-3}^{+3}[\sigma_{-3}^{+3}(u_1(t))] \\ \rho_{-3}^{+3}[\sigma_{-10}^{+10}(u_2(t))] \end{pmatrix} \;. \tag{6.42}$$

The two OBSAWC:s and the GLAWC (6.28) in Example 6.3, and one additional GLAWC:s will be investigated. The new GLAWC, denoted GLAWC2, is given by

$$\text{GLAWC2}\;\; \boldsymbol{A}_o \;=\; \boldsymbol{\alpha}_2,\;\; \boldsymbol{P}_1 \;=\; \boldsymbol{A},\;\; \boldsymbol{P}_2 \;=\; (s+p_2)\mathbf{I}\;. \tag{6.43}$$

Using the GLAWC:s results in a diagonal $(2x2)$ loop transfer function, which allow us to use Nyquist-like analysis for each one of the two SISO-system elements.

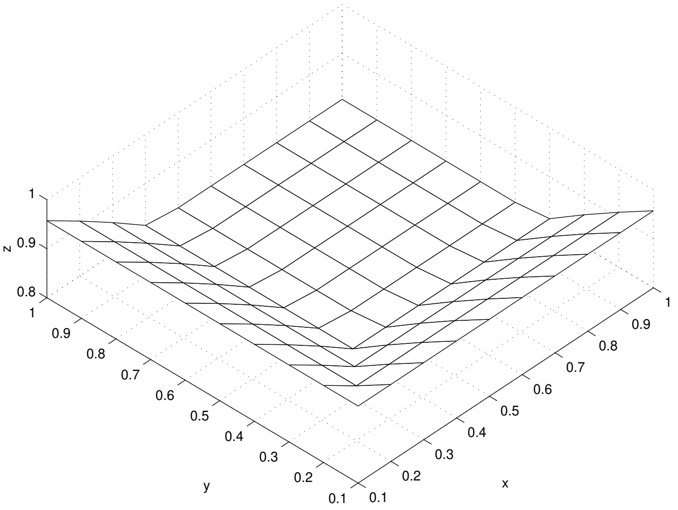

Figure 6.14: Worst case root-locus for the OBSAWC1. The x-axis represents γ_2 and the y-axis represents γ_1, taking ten values each in the interval $0.01 - 1$. The z-axis represents the maximum value among the absolute values of the roots. The system can be expected to be stable since the surface lies below $z = 1$.

Performance of the GLAWC1 In Figures 6.16 and 6.17 Nyquist-loci:s for the combined loop transfer function $\mathcal{L}_v(\omega)N(C,\omega)$ are shown for amplitude and rate limits $a = -b = 3,\ c = -d = 3$, and for amplitude and rate limits $a = -b = 10,\ c = -d = 3$, respectively. Note that the worst case phase margin, ϕ_w, is smaller in the loop having amplitude limits ± 10 than it is in the system where the amplitude limits are ± 3. This makes sense since a rate limiter that operates over a large amplitude range gives larger lags in the input-output response than a rate limiter that operates over a smaller amplitude range.[5]. Since none of the Nyquist-loci:s encircles the point $(-1, 0)$ we can expect the system to be stable. However, the worst case phase margin is small (measured in terms of linear system phase margin) and we can therefore expect overshoots in the step response. The simulation results shown in the left plots of Figure 6.21 confirms the expectation.

[5]This phenomenon can also be seen in the Figure 5.7 at the first zero-crossing ZC1

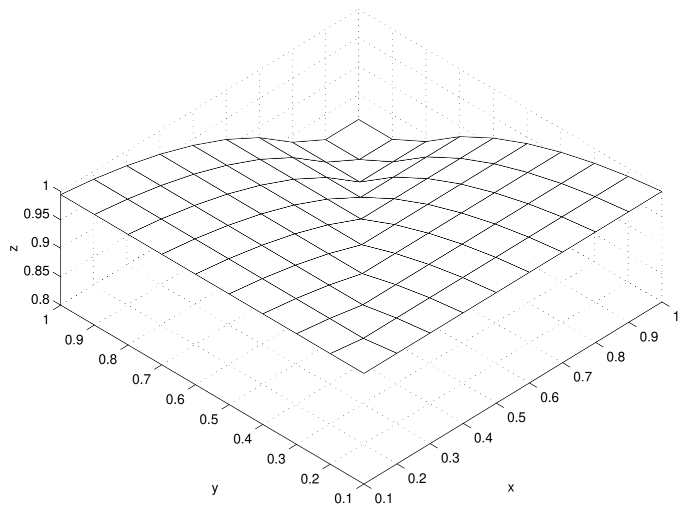

Figure 6.15: Worst case root-locus for the OBSAWC1. The x-axis represents γ_2 and the y-axis represents γ_1, taking ten values each in the interval $0.01 - 1$. The z-axis represents the maximum value among the absolute values of the roots. The system can be expected to be stable since the surface lies below $z = 1$.

Tuning the GLAWC2

Compared to the Nyquist-loci:s obtained from the loop transfer function

$$\mathcal{L}_v = \frac{(10 - 0.1)}{s + 0.1} \tag{6.44}$$

obtained by using the GLAWC1 (see (6.36)), Nyquist-loci:s obtained from the loop transfer function

$$\mathcal{L}_v = \frac{(p_2 - 0.1)}{s + 0.1} \tag{6.45}$$

where p_2 is selected closer to the pole of the plant, 0.1, will contract and the worst case phase margin increases. By trial and error, we found $p_2 = 0.9$ to be an appropriate choice.

Performance of the GLAWC2

The results from the simulation are shown in the right plots of Figure 6.21. Evidently, the GLAWC2 gives much better performance than GLAWC1 does. In Figures 6.18 and 6.19 Nyquist-loci:s obtained when using the GLAWC2 are shown. The phase margin is much larger than compared to when using the GLAWC1. In fact, much larger than what is usually required in a *linear* loop in order to avoid overshoots in the step response. The lesson learned from this must be that absolute limits of the worst case phase margin in nonlinear loops might be difficult to establish.

By studying the results shown in Figure 6.20 we can conclude that the OBSAWC1 is far to aggressive and that the OBSAWC2 is much to slow.

The windup effects in the three systems are shown in Figure 6.22.

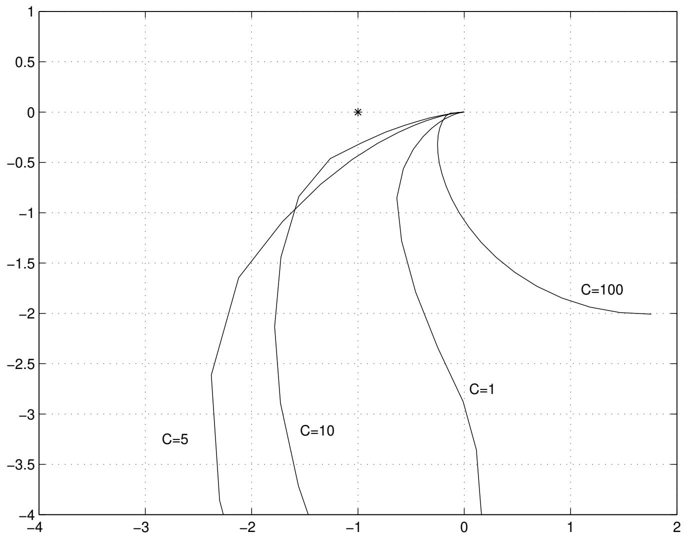

Figure 6.16: Nyquist-loci for the composed loop transfer function $\mathcal{L}_v(\omega)N(C,\omega)$ when using the GLAWC1. Here $N(C,\omega)$ represents the describing function for the combined rate- and amplitude limiter given by the limits $a = -b = 3$ and $c = -d = 3$ for amplitude and rate limits respectively. The worst case phase margin is here $\phi_w \approx 17^o$, obtained for $C = 10$.

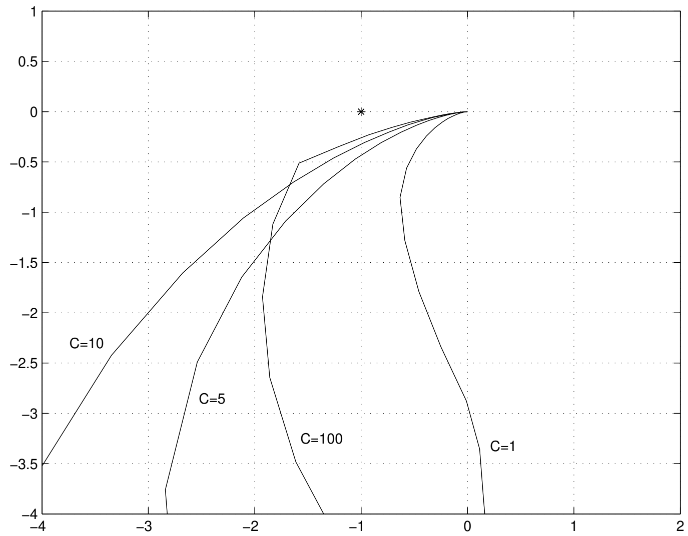

Figure 6.17: The same situation as in Figure 6.16 but here the amplitude limits are $a = -b = 10$. The worst case phase margin is here $\phi_w \approx 14^o$, obtained for $C = 100$. The second worst is $\phi_m = 17^o$ obtained for $C = 10$.

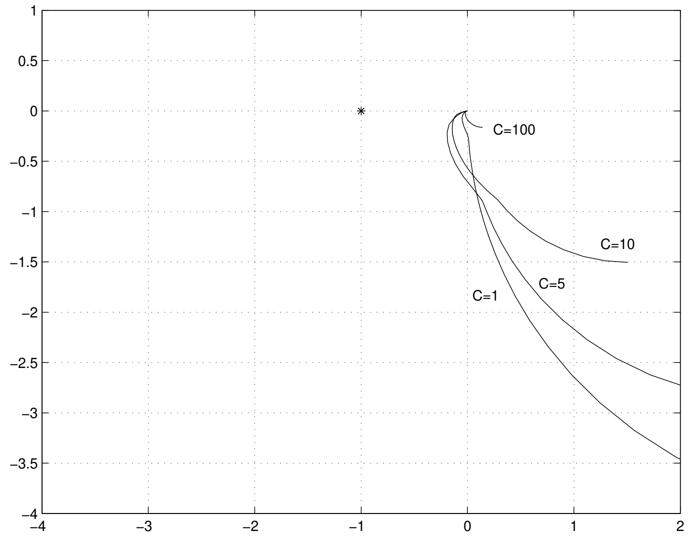

Figure 6.18: The same situation as in Figure 6.16 expect that the GLAWC2 is used here. The worst case phase margin is here $\phi_w \approx 97^o$, obtained for $C = 1$.

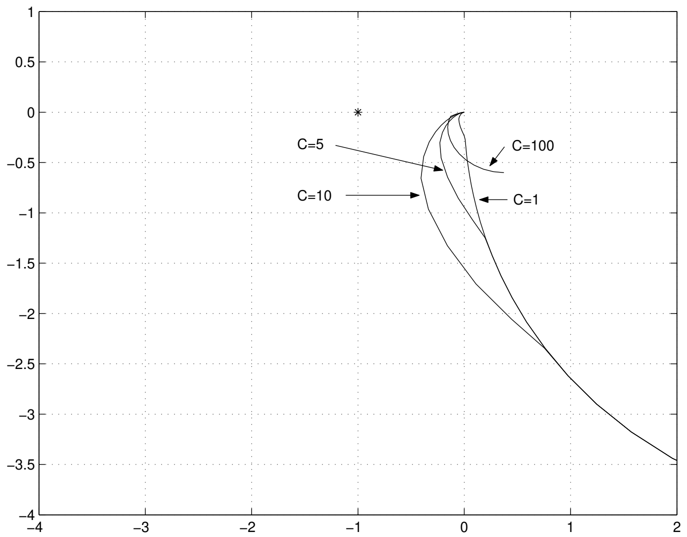

Figure 6.19: The same situation as in Figure 6.17 expect that the GLAWC2 is used here. The worst case phase margin is here $\phi_w \approx 70^o$, obtained for $C = 10$.

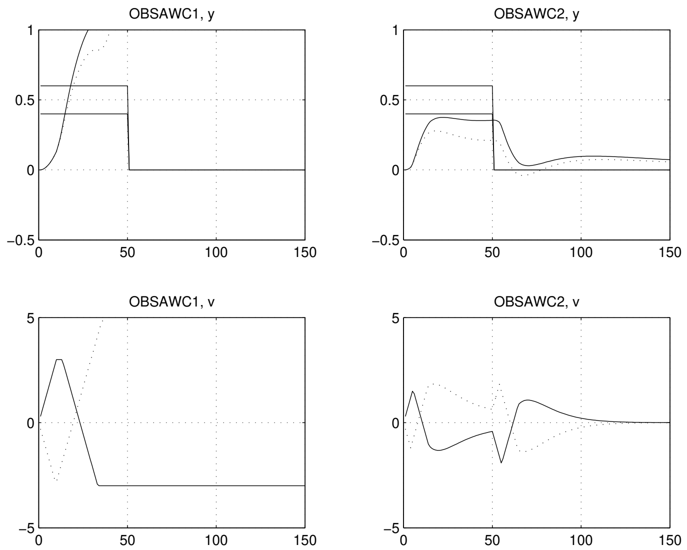

Figure 6.20: Reference step response for the OBSAWC1 (left) and the OBSAWC2 (right) when having both rate- and amplitude limiters at the plant input.

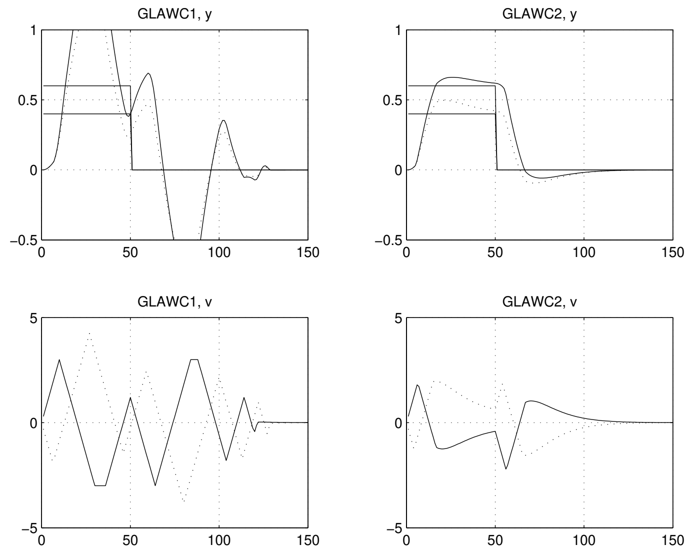

Figure 6.21: Reference step response for the GLAWC1 (left) and for the GLAWC2 (right)

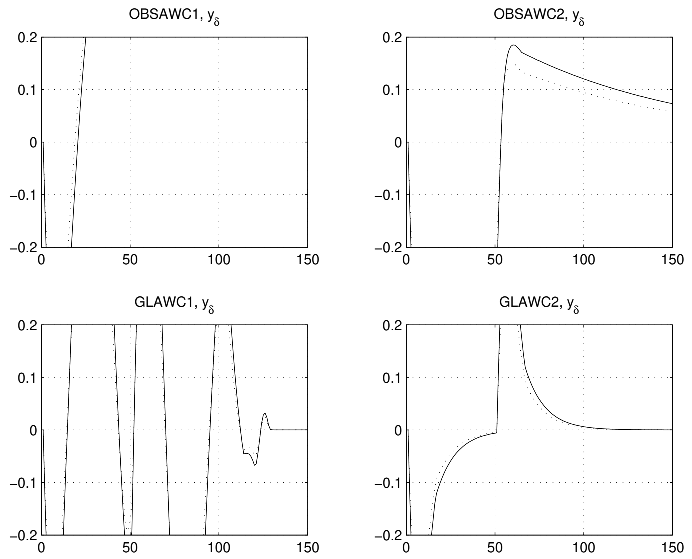

Figure 6.22: Windup effects of the plant outputs for the OBSAWC1 (upper left), OBSAWC2 (upper right), the GLAWC1 (lower left) and for the GLAWC2 (lower right)

CHAPTER 7

Path anti-windup compensation

A shortcoming of linear anti-windup compensation
If it is desirable that the system outputs follow a certain path in a phase portrait rater than a reference $r(t)$ in time, then it may be better to adjust the reference $r(t)$ instead of the controller states when inputs saturate. The following example illustrates this.

EXAMPLE 7.1: CIRCULAR-PATH FOLLOWING

By this simple example I want to show that the definition of windup effects and what is often taken as to be a performance measure of anti-windup, namely how well the real system follows the linear response *in time*, is not always adequate.

Consider simple proportional control of two integrators given by

$$\begin{aligned}
\dot{x}_1 &= k_1 \sigma_{-a}^{a}(u_1(t)) \\
\dot{x}_2 &= k_2 \sigma_{-a}^{a}(u_2(t)) \\
k_1 &= k_2 = 1 \quad \text{nominally} \\
a &= 2\pi
\end{aligned} \tag{7.1}$$

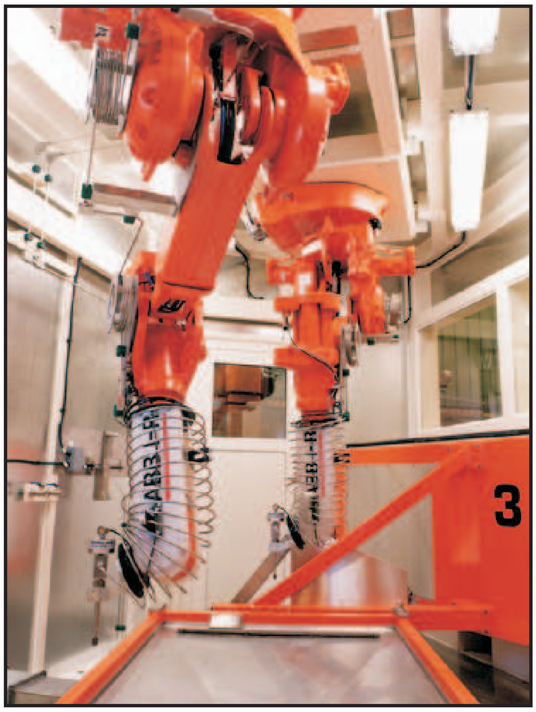

Figure 7.1: Two 6 DOF (degree of freedom) ABB (Asea Brown Boveri) robots cutting holes. It should be pointed out that control of a 6 DOF robot is much more complicated than control of the 2 DOF system considered in the simple example below.

and where the controller is given by

$$\begin{aligned} u_1(t) &= K_{p1}(r_1(t) - x_1(t)) \\ u_2(t) &= K_{p2}(r_2(t) - x_2(t)) \\ K_{p1} &= K_{p2} = 100 \ . \end{aligned} \tag{7.2}$$

Assume that each integrator represents a motor and that the compound servo system, i.e., the two motors operating together, is used for cutting circular holes in a certain material. The reference signals

$$\begin{aligned} r_1(t) &= A\sin(\frac{2\pi t}{T}) \\ r_2(t) &= A\cos(\frac{2\pi t}{T}) \end{aligned} \tag{7.3}$$

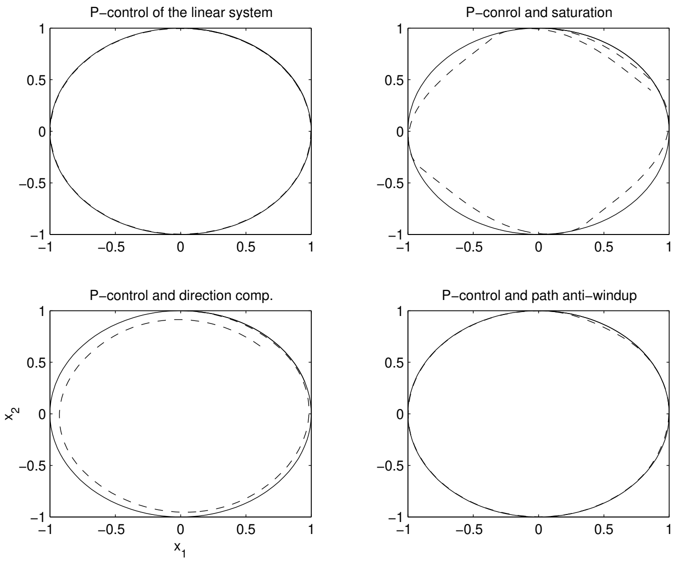

Figure 7.2: Circle-path following of the linear system (upper-left), of the nominal system with P-controller (upper-right), of the directionally compensated system (lower-left) and of the system using the proposed path anti-windup compensator (lower-right).

form a circle in a phase-portrait r_1 versus r_2. Since the controller gains are selected high, the step response is fast which means that a phase portrait of x_1 versus x_2 forms a fairly good circle as long as none of the control signals saturate. If the cycle time is selected as $T = 1$, saturation will not occur, but the system is operating on its limits. Assume that a load disturbance decreases the gains $k_1,\ k_2$ by 20% down to $k_1 = k_2 = 0.8$. Then the control signal will saturate and the response will be affected by this. Figure 7.3 shows the time response and Figure 7.2 shows the resulting path that is supposed to form a circle. The upper-left figure shows the linear response, the upper-right shows the response when the limiters σ are present, and the same P-controller is used, and the lower-left figure shows the response when using directionality preservation (2.17). The response shown in the lower-right figure is obtained by a controller where the reference is changed as a function of the dept of the saturation. The references are generated as in (7.3) with the exception that the cycle-time $T = T(t)$ is no longer constant but changed in the following way:

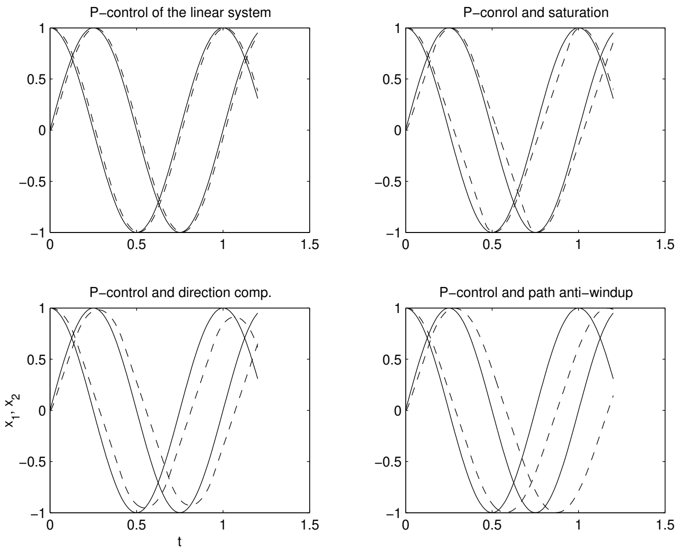

Figure 7.3: The time response of the linear system (upper-left), of the nominal system with P-controller (upper-right), of the directionally compensated system (lower-left) and of the system using the proposed path anti-windup compensator (lower-right).

Path anti-windup compensation

$$\frac{1}{T} = \frac{1}{T_0} - [\Delta f(u_1(t), u_2(t))]_0^{\Delta f_{max}} \tag{7.4}$$

where Δf can be selected, e.g., as to be

$$\begin{aligned} \lambda &= \max\left(|\sigma(u_1(t)) - u_1(t)|, |\sigma(u_2(t)) - u_2(t)|\right) \\ (\dot{\Delta f}) &= \begin{cases} c\lambda & \text{for permanent adjustment,} \\ c\lambda - b(\Delta f) & \text{for decaying adjustment.} \end{cases} \end{aligned} \tag{7.5}$$

Here, c, b and Δf_{max} are tuning parameters.

Nominal proportional control

The use of the two uncompensated proportional controllers results in the smallest deviation from the linear response *in time* of the three solutions. See the upper-right plot in Figure 7.3. However, the resulting path is a rectangle with rounded corners rather than a circle. See the upper-right plot in Figure 7.2. This result would be unacceptable in most real cases.

Proportional control with directional compensation
When using directional compensation, i.e., when replacing the limiters σ by γ, the system eventually makes a circular path. See the lower-left plot in Figure 7.2. However, the radius of this circle is smaller than the wanted and the result is most likely not satisfying.

Proportional control with *path anti-windup compensation*
The proposed controller, where the cycle time T is adjusted according to (7.5), makes an almost perfect circular path immediately in the first cycle and already in the second cycle, it will be almost identical to the desired path. See the lower-right plot in Figure 7.2. The cycle time is, however, longer and the deviation from the liner response in time is the worst of the three solutions. See the lower-right plot in Figure 7.3.

In the proposed path anti-windup compensator, the initial value of the cycle time is $T_0 = 1$ and the maximum allowable adjustment of T is $1/\Delta f_{max}$. The constant b controls the decay back to T_0 and c sets the speed of the adjustment. In a real situation one would most likely come up with a better solution, e.g., perform some kind of re-set after a number of cycles. The purpose of this example is to illustrate the possibility of doing something better than minimizing a linear combination of the states describing the saturation effects, over time.

CHAPTER 8

Control of a Paper Machine Headbox: a case study on anti-windup designs

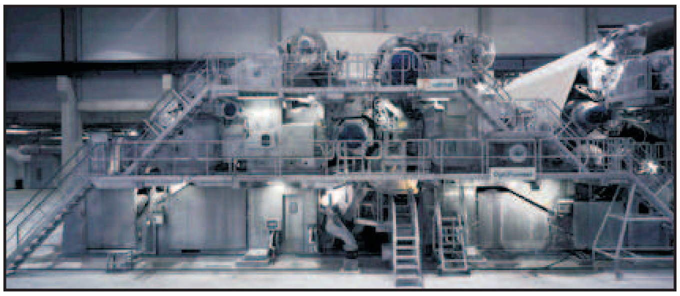

Figure 8.1: Paper machine headbox.

The case study presented in this chapter concerns control of a *paper machine headbox* at AssiDomän Kraftliner in Piteå, Sweden. The function of a headbox is to deliver a uniform jet of furnish having essentially the same width as the paper web to be produced. In the headbox considered here, amplitude saturation in air valves, and rate saturation in the stock-pump system, both cause performance degradation. To obtain good control, anti-windup compensation is needed [82]. Four different designs will be investigated namely two different observer anti-windup designs, an internal-model anti-windup compensator and an LQR design, see Chapters 5 and

6. These designs are tested by simulation experiments with the plant represented by a detailed nonlinear model of this real headbox.[1] The headbox, the headbox model, and the modeling procedure are presented and described in detail in [83].

8.1 The Headbox

The nonlinear plant model has three inputs, ten disturbance inputs, three outputs and eleven states. However, several experiments carried out by staff and students at the Control Group at Luleå Technical University has shown that the nominal controller can be designed based on linearized, reduce order, discrete-time models having two inputs, two outputs and two states. We will use one of these models, obtained at a certain operating point, for the design of our anti-windup compensators. The states of the model, also selected as the outputs, are the total pressure (mVP) at the outlet, here denoted y_1, and the stock level (m) denoted y_2. The inputs are the air valve opening (%) represented by v_1, and the stock-pump speed (rpm) represented by v_2. The nonlinear system model was linearized at $(y_{1o}, y_{2o}) = (4.8, 0.62)$ and the control signals off-set at (y_{1o}, y_{2o}) was $(u_{1o}, u_{2o}) = (30, 527.34)$. The situation is depicted in Figure 8.2.

Stock-pump motor
The speed of the stock pump, the second plant input v_2, is constrained in both amplitude and rate. We will, however, ignore the amplitude limit in the sequel simply because it never saturates under normal circumstances. The rate limitation is caused by a resolution window implemented in the real, pre-existing control system. The purpose of the resolution window is to preserve quantization resolution throughout the whole working range of the stock-pump motor.[2] This rate limiter takes a form that is different from any of the rate limiters discussed in Chapter 2. See the relation between v_2 and u_2 in Figure 8.2. We have therefore used a "$\approx$" in the model (8.1) below.

Air valve
The actuator imposing the amplitude limiter present at the plant input v_1 consists of two air valves, one for the inlet-flow and one for the outlet-flow. Each one of these valves has a maximum opening obtained for $u_1 = \pm 100$ (%) and a minimum

[1] The aim was to evaluate the anti-windup designs on the real plant after testing them by simulations. Since the results obtained from the simulations are promising implementation on the real headbox will be the next step.

[2] The fix is needed to overcome some communication problems between the control system and the stock-pump motor frequency converter.

closeup obtained for $u_1 = \pm 5$ respectively. This means that the control signal u_1 can operate between the limits ± 100 but also that none of the valves close completely. We have therefore used a "$\approx$" in the model (8.1) below.

Model used for controller design
The model used for the design is given by

$$\begin{aligned}
x(t+1) &= \mathbf{F}x(t) + \mathbf{G}v(t) \\
y(t) &= x(t) \\
v &= \begin{pmatrix} v_1 \\ \bar{v}_2 \end{pmatrix} \\
v_1 &\approx \sigma(u_1) \\
v_2 &\approx \rho(u_2) \\
\mathbf{F} &= \begin{pmatrix} 0.75025 & -2.4641 \\ -0.014339 & 0.85559 \end{pmatrix} \\
\mathbf{G} &= \begin{pmatrix} -4.161810^{-4} & 4.860810^{-3} \\ 3.736710^{-6} & 2.842310^{-4} \end{pmatrix} .
\end{aligned} \tag{8.1}$$

The sampling time is $T_s = 0.5s$. The eigenvalues of F,

$$\text{eig}(F) \;=\; 0.6077,\; 0.9981 \;, \tag{8.2}$$

are located inside the unit circle, so the plant is open loop stable.

8.2 Nominal controller

To obtain a controller with integral action, integrating the control error, the two-state model (8.1) was augmented by two integrator states according to

$$\begin{aligned}
\bar{x}(t+1) &= \bar{\mathbf{F}}\bar{x}(t) + \bar{\mathbf{G}}v(t) \\
\bar{y}(t) &= \bar{x}(t) \\
\bar{\mathbf{F}} &= \begin{pmatrix} \mathbf{F} & \mathbf{0} \\ \mathbf{I} & \mathbf{I} \end{pmatrix} \\
\bar{\mathbf{G}} &= \begin{pmatrix} \mathbf{G} \\ \mathbf{0} \end{pmatrix} .
\end{aligned} \tag{8.3}$$

Here, the zero- and identity matrices have dimension (2x2). The nominal controller was obtained from an LQR discrete-time, state-feedback design minimizing

$$J = \text{E}\{\lim_{N\to\infty} \frac{1}{2N} \sum_{t=0}^{N} (\bar{x}^T \mathbf{Q}_{\bar{x}} \bar{x} + u^T \mathbf{Q}_u u)\} \;. \tag{8.4}$$

The penalty matrices that appeared to give the best result, when controlling the system so that the inputs do not saturate, are given by

$$Q_{\bar{x}} = 10^2 \begin{pmatrix} 300 & 200 & 0 & 0 \\ 200 & 200 & 0 & 0 \\ 0 & 0 & 0.7 & 0 \\ 0 & 0 & 0 & 0.8 \end{pmatrix} \tag{8.5}$$
$$Q_u = \begin{pmatrix} 0.0005 & 0 \\ 0 & 0.005 \end{pmatrix} .$$

Here, the elements $(\mathbf{Q}_{\bar{x}}(3,3), \mathbf{Q}_{\bar{x}}(4,4)) = (70, 80)$ penalizes the integrator states. The nominal controller is given by

$$\begin{aligned} u(t) &= (\frac{1}{\Delta}\mathbf{L}_i + \mathbf{L}_x)e \\ &= \frac{1}{\Delta}(\mathbf{L}_i + \Delta\mathbf{L}_x)e \;=\; \mathcal{K}(q)e \\ e &\triangleq r - y = r - x \end{aligned} \tag{8.6}$$

where

$$\begin{aligned} \mathbf{L}_x &= 10^3 \begin{pmatrix} -0.5426 & 6.3356 \\ 0.1108 & 0.1385 \end{pmatrix} \\ \mathbf{L}_i &= \begin{pmatrix} -113.0055 & 333.3285 \\ -0.4773 & 30.6178 \end{pmatrix} \end{aligned} \tag{8.7}$$

is the result obtained from solving (8.3)-(8.4) with (8.5), and were $\Delta = q - 1$. Notice that the controller (8.6) can be regarded as a kind of MIMO-PI controller.

The design of the nominal controller (8.6) was carried out by researchers at the Control Group at Luleå Technical University, Luleå. So, our anti-windup design work begins here and we consider the system model (8.1) the augmented model (8.3) the nominal controller (8.6), resulting from the solution of (8.4), given the penalties (8.5), and the nonlinear model described in [83] as given and not to be changed.

8.3 Anti-windup compensation

Since the given nominal controller is represented on state space form, we will represent also the OBSAWC:s and the GLAWC used in this chapter by state space descriptions. However, in order to show how the polynomial representations and the state space representations of OBSAWC are related, we will also represent the OBSAWC designs in polynomial form.

A polynomial representation of the controller (8.6) is given by

$$\begin{aligned}\boldsymbol{R}(q) &= \Delta\mathbf{I} = (q-1)\mathbf{I}\\ \boldsymbol{S}(q) &= (\mathbf{L}_i + \Delta\mathbf{L}_x)\\ \boldsymbol{T}(q) &= \boldsymbol{S} \text{ (error feedback)} ,\end{aligned} \tag{8.8}$$

where $\boldsymbol{R}^{-1}(q)\boldsymbol{S}(q) = \boldsymbol{\mathcal{K}}(q)$. According to Appendix B.2.2, (8.6) can also be represented by the state space description

$$u = \left[\begin{array}{c|c}\mathbf{I} & \mathbf{L}_i\\ \hline \mathbf{I} & \mathbf{L}_x\end{array}\right] e . \tag{8.9}$$

The OBSAWC1 is designed using the heuristic approach described in Chapter 6. The design of OBSAWC2 is based on the idea presented in [61]. The design of the LQR AWC follows the procedure described in Chapter 5. However, here we use the principle of the scheme suggested by Teel & Kapoor, where the saturation effects of the plant, y_δ, are cancelled before the control error is fed to the controller. See Section 4.3.1 and also Figure 8.2 above.

8.3.1 OBSAWC

For the special choice $\boldsymbol{R}_o \triangleq \boldsymbol{A}_o - \boldsymbol{R} = \mathbf{K}_o$, where $\mathbf{K}_o$ is a constant matrix, we show in the Appendix B.2.2 that the OBSAWC (4.1) can be represented by the state space description

$$\begin{aligned}u_o &= \boldsymbol{A}_o^{-1}(\boldsymbol{S}e + \boldsymbol{R}_o v)\\ &= \left[\begin{array}{c|c}\mathbf{I}-\mathbf{K}_o & [\mathbf{L}_i - \mathbf{K}_o\mathbf{L}_x \;\; \mathbf{K}_o]\\ \hline \mathbf{I} & [\mathbf{L}_x \; \mathbf{0}]\end{array}\right] \begin{pmatrix} e \\ v\end{pmatrix} .\end{aligned} \tag{8.10}$$

This representation will be use for the OBSAWC:s in this chapter. Two different designs will be investigated. These are:

$$\begin{aligned}&\text{OBSAWC1} \;\; \boldsymbol{A}_o = (q-0.4)\mathbf{I}\\ &\text{OBSAWC2} \;\; \boldsymbol{A}_o = \boldsymbol{S}\mathbf{L}_x^{-1} .\end{aligned} \tag{8.11}$$

The corresponding constant matrices $\mathbf{K}_o = \boldsymbol{R}_o \triangleq \boldsymbol{A}_o - \boldsymbol{R}$ are then given by

$$\begin{aligned}\text{OBSAWC1} \;\; \mathbf{K}_o &= (q-0.4-q+1)\mathbf{I} = 0.6\mathbf{I}\\ \text{OBSAWC2} \;\; \mathbf{K}_o &= \boldsymbol{S}\mathbf{L}_x^{-1} - \boldsymbol{R} = (\mathbf{L}_i + \Delta\mathbf{L}_x)\mathbf{L}_x^{-1} - \Delta\mathbf{I}\\ &= \mathbf{L}_i\mathbf{L}_x^{-1} .\end{aligned} \tag{8.12}$$

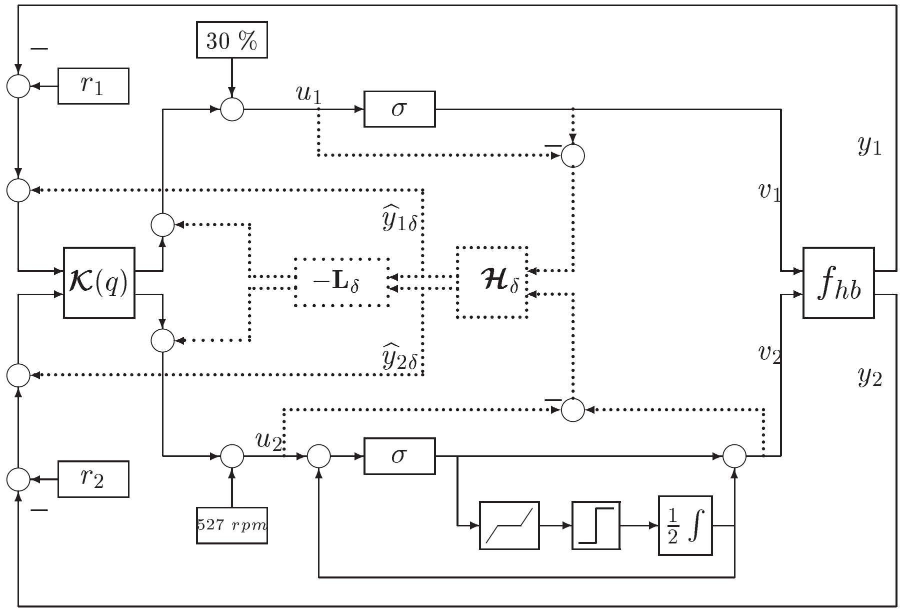

Figure 8.2: A schematic picture of the control system considered. The function f_{hb} represents the nonlinear model of the headbox. The dotted lines and boxes represents the general linear anti-windup compensation. The controller $\mathcal{K}(q) = \boldsymbol{R}^{-1}(q)\boldsymbol{S}(q)$ is designed to give a satisfactory control of the system when control signals u_1, u_2 do not saturates. The state-feedback matrix $\mathbf{L}_\delta$, used in the GLAWC, is tuned according (8.13) and (8.14) and is used for control of saturation effects. Notice that the OBSAWC structure does not fit into the anti-windup scheme shown here. The function from u_2 to v_2 constitutes a window used to maintain quantization resolution throughout the whole working range of the pump motor. It ramps-up the pump motor speed and functions almost as a rate limiter.

The compensator OBSAWC2 has the special property that the controller states are no longer driven by the control error e when saturations occur. This idea was proposed by Campo & Morari in [61]. Although it is not clear to me why this should be a desired property, the compensator seems to perform well in some situations.

As will be shown below, this is the case here. This type of compensator is also discussed in [5].

When selecting the polynomial matrix $\boldsymbol{A}_o$ of the OBSAWC1 as in (8.11), we reasoned in the following way: Since the plant is stable (8.2) and the controller is not unstable and has full state information, we can expect that windup effects are caused by either strong or weak feedback, the controller integral action or some MIMO related problems. See Sections 6.1 and 6.2. Assume that experiments have been carried out using the nominal controller and that the results shown in Figure 8.4 are available. Then we know that the nominal system is stable although it shown a somewhat sluggish behavior. If we are lucky, this sluggish behavior is caused mainly by the controller integrator. The simplest solution is then to select $\boldsymbol{A}_o$ in such a way that $\boldsymbol{R}_o = \boldsymbol{A}_o - \boldsymbol{R}$ becomes a constant matrix, e.g. $\boldsymbol{A}_o = (q - a_o)\mathbf{I}$ as in (8.11). The value of the constant a_o can be obtained from a "trial an error" procedure.

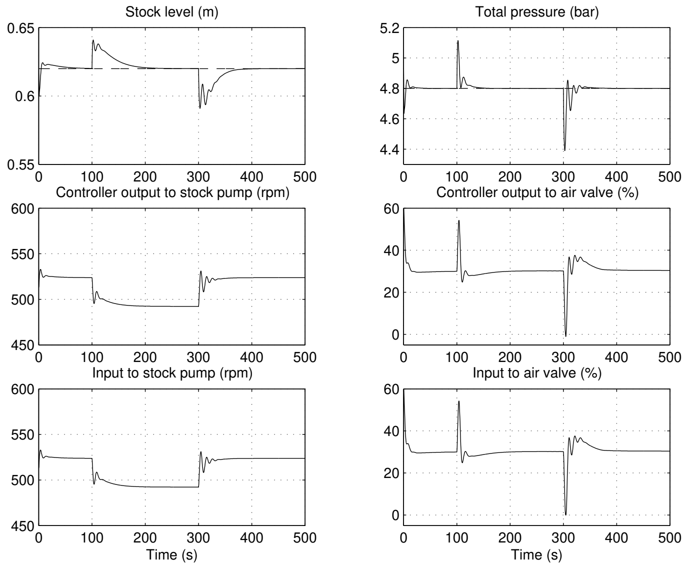

Figure 8.3: Response of the system without input limiters. The plant outputs y_1 and y_2 are the stock level and the total pressure, respectively. The plant inputs, v_1 and v_2 are stock pump speed and air valve opening, respectively.

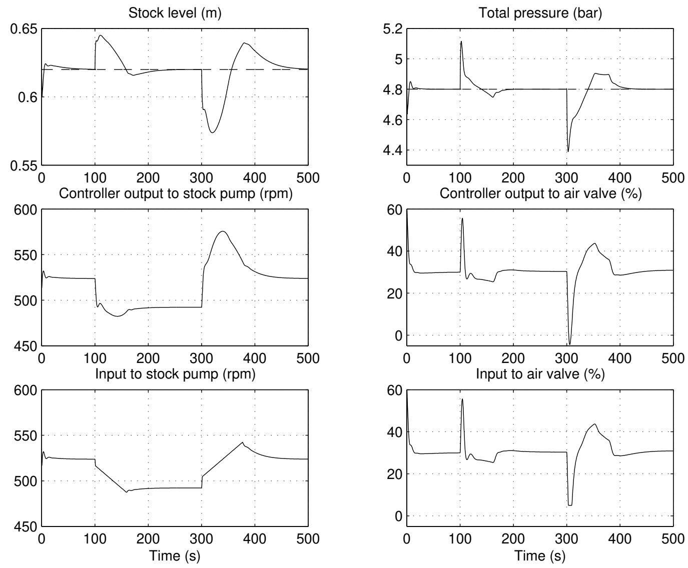

Figure 8.4: Response of the nominal system with input limiters but without anti-windup compensation. The plant outputs, y_1 and y_2, are the stock level and the total pressure, respectively. The plant inputs, v_1 and v_2 are stock pump speed and air valve opening, respectively.

8.3.2 GLAWC: LQR and IMC

For the LQR design of $\mathbf{L}_\delta$, the criterion

$$J = \mathrm{E}\{\lim_{N\to\infty} \frac{1}{2N} \sum_{t=0}^{N} (x^T \mathbf{Q}_{y_\delta} x + u^T \mathbf{Q}_{u_\delta} u)\} \tag{8.13}$$

is minimized. The penalties are here selected as

$$\begin{aligned} Q_{y_\delta} &= \begin{pmatrix} 300 & 200 \\ 200 & 200 \end{pmatrix} \\ Q_{u_\delta} &= 10^{-5}\mathbf{Q}_u \end{aligned} \tag{8.14}$$

respectively. Note that the penalties (8.14) are equal to the ones used in the nominal design, multiplied by a scalar. By making this choice, the experience gained from the tuning of the nominal controller is utilized. Note also that we use the original state space model (8.1) when designing the LQR AWC and not the augmented model with integrators.

The IMC anti-windup compensator is simply obtained by selecting $\mathbf{L}_\delta \equiv \mathbf{0}$.

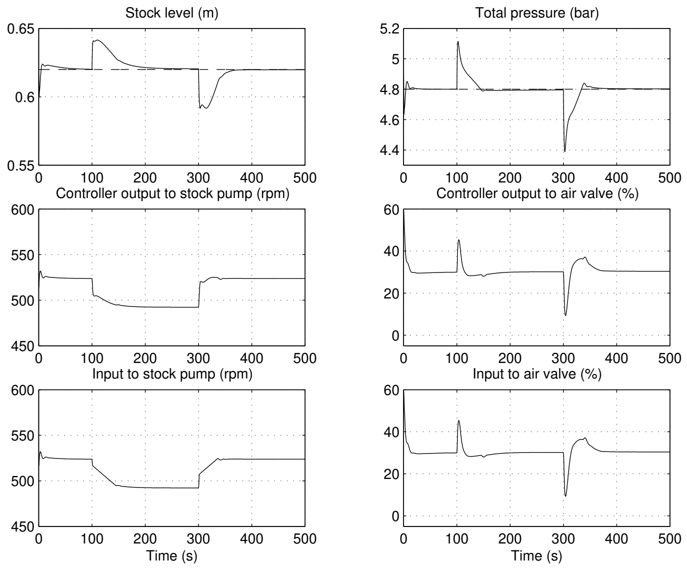

Figure 8.5: Response of the system when using the IMC AWC. The plant outputs y_1 and y_2 are the stock level and the total pressure, respectively. The plant inputs, v_1 and v_2 are stock pump speed and air valve opening, respectively.

8.4 Simulations

Operating conditions

The headbox is started at $t = 0$ s by speeding up the stock pump motor to 527 rpm, and by opening the air valve 30%. At time $t = 100$ s the lip is closed 3mm and at $t = 300$ s the lip opens 3mm.[3] This operation affects both the stock level and the total pressure inside the headbox and from the viewpoint of the level- and pressure controller, this operation can be regarded as a disturbance . The window-rate limiter saturates at both instants whereas the air valve saturate only when the lip closes at $t = 300$ s .

Comments and conclusions

The response of the (ideal) system without input limiters is shown in Figure 8.3. When the lip close at $t = 100$ s both the stock level and the total pressure grow larger that the desired reference values. However, the level is controlled back to the desired value in less than 100 s and the pressure in less than 50 s. When the lip opens up again at $t = 300$ s the course of events are reversed but otherwise similar.

[3]The lip is used for controlling the amount of stock that flows on to the paper machine.

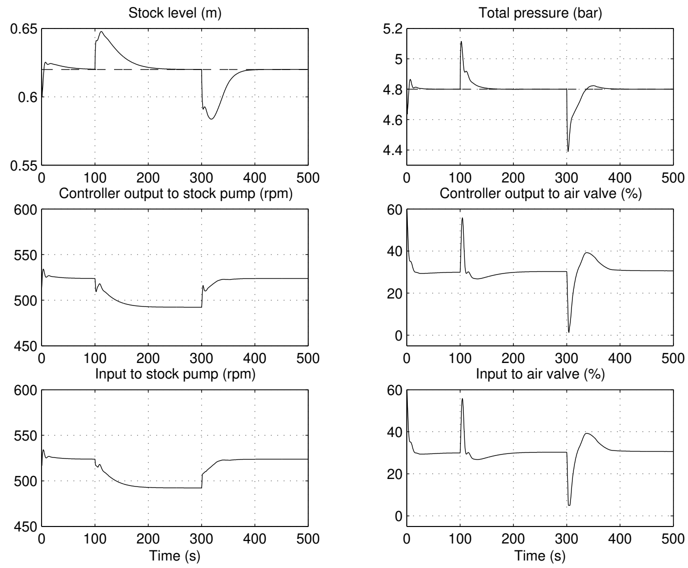

Figure 8.6: Response of the system when using the OBSAWC1. The plant outputs y_1 and y_2 are the stock level and the total pressure, respectively. The plant inputs, v_1 and v_2 are stock pump speed and air valve opening, respectively.

According to Definitions 3.1 and 3.2, we consider this behavior as normal and desired and windup effects, caused by input saturations, are defined as the deviations from this behavior. As in the examples studied in Chapters 5 and 6, the goal is to keep the windup effects $y_{1\delta},\ y_{2\delta}$, present in the plant, small.

The response of the nominal system, i.e. the system with input limiters but without anti-windup compensation, is shown in Figure 8.4 and the windup effects, $y_{1\delta},\ y_{2\delta}$ are shown i Figure 8.10. It is clear from the plots in Figure 8.4 that this system behaves worse than the one without limiters. The question is how much the performance can be improved by using anti-windup compensation? The immediate impact which slows down the system may not be possible to affect, whereas the overshoots, which can be expected to be caused by any of the properties that contribute negatively to windup listed and discussed in Sections 6.1 and 6.2, can probably be reduce. This hunch is based on the fact that the plant is asymptotically stable. The results obtained when using anti-windup compensation confirm the hunch.

It is clear from the Figures 8.5-8.8 that all the anti-windup compensators improve the performance compared to the nominal system, and the windup effects reduce,

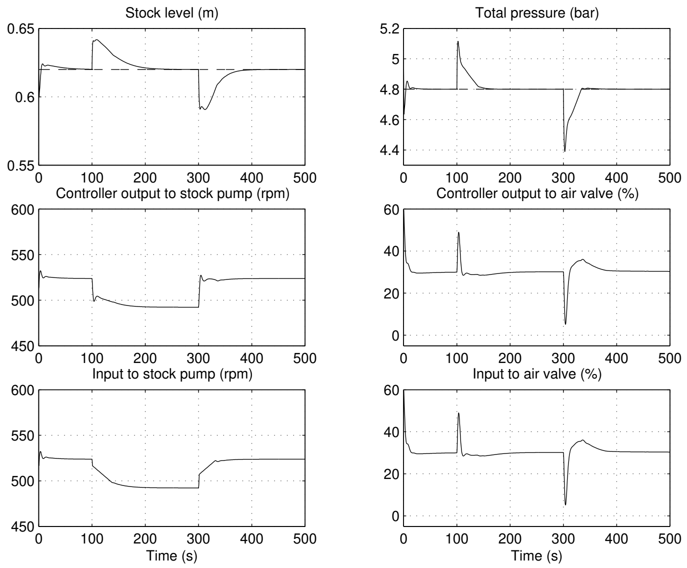

Figure 8.7: Response of the system when using the OBSAWC2. The plant outputs y_1 and y_2 are the stock level and the total pressure, respectively.

see Figure 8.10 and compare to Figures 8.11-8.14. Note, however, that the anti-windup compensators all give similar performance. See Figures 8.5-8.8. In order to see any differences we show only the time intervals $100 - 200$ s and $300 - 400$ s in the Figures 8.10-8.14. In these figures, we have also scaled the $y - axis$ so that the windup effects appear clearer. Note that the LQR AWC and the OBSAWC2 show almost equal performance although the decay of $y_{1\delta}$ (left plots) is somewhat faster for the LQR AWC. This decay is slowest when using the OBSAWC1. On the other hand, the windup effects $y_{2\delta}$ present immediately after $t = 100$ (upper-right plot in Figure 8.12) are the smallest when using the OBSAWC1. This trade off *seem* to be an unavoidable fact in this system.

The anti-windup problem turned out to be quite easy to solve in this case and if we look for the main cause of windup effects among the properties discussed in Sections 6.1 and 6.2, we will find that the integral action of the nominal controller is the main cause.

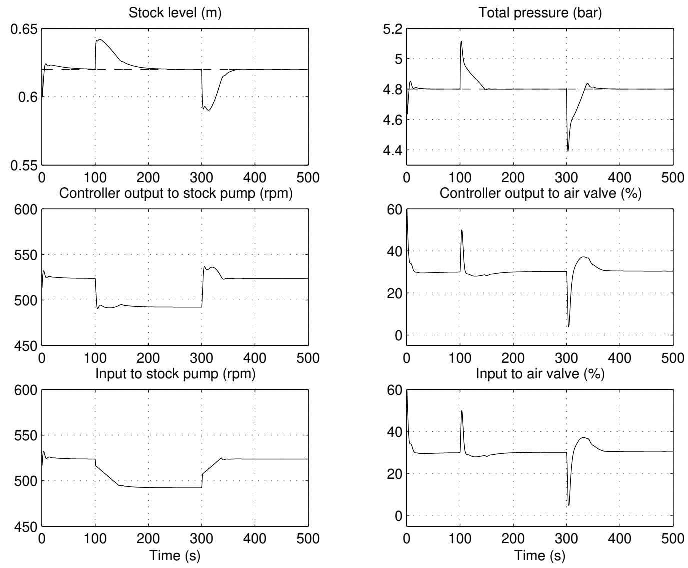

Figure 8.8: Response of the system when using the LQR AWC. The plant outputs y_1 and y_2 are the stock level and the total pressure, respectively. The plant inputs, v_1 and v_2 are stock pump speed and air valve opening, respectively.

Meas	nom	IMC	OBS1	OBS2	LQ
$\parallel y_{\delta 1} \parallel_2$	20.6	5.36	12.0	5.53	5.61
$\parallel y_{\delta 2} \parallel_2$	1.05	0.866	0.713	0.855	0.846
$\parallel y_{\delta 1} \parallel_1$	2.66	0.559	1.32	0.558	0.475
$\parallel y_{\delta 2} \parallel_1$	10.6	7.65	5.00	6.11	6.23
$\parallel y_{\delta 1} \parallel_\infty$	3.09	1.47	2.08	1.63	1.66
$\parallel y_{\delta 2} \parallel_\infty$	0.304	0.287	0.269	0.283	0.281
$\parallel y_\delta^T \mathbf{Q}_{y_\delta} y_\delta \parallel_2$	2.95	1.68	1.29	1.65	1.63

Figure 8.9: The performance measures of: the nominal system (nom), internal model control anti-windup (IMC), two different observer-based anti-windup solutions (OBS1,2) and a general linear anti-windup compensator designed using the LQR approach. The measured values in the first- and the fifth row should be multiplied by 10^{-2} and the values in the last row by 10^2.

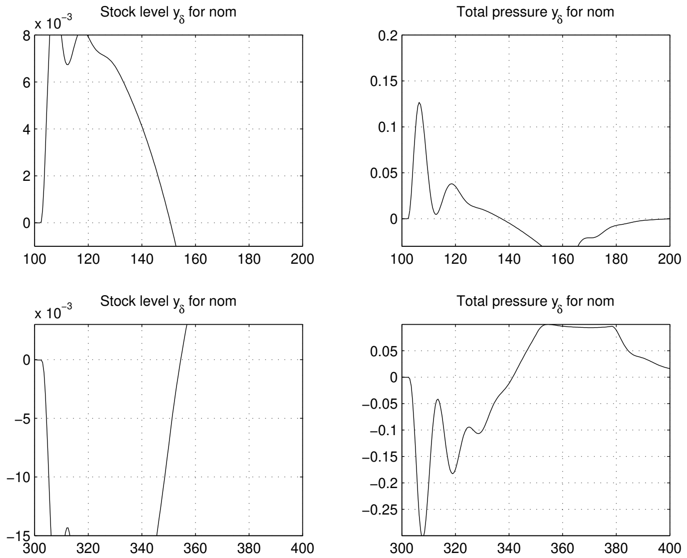

Figure 8.10: Windup effects present in the plant of the nominal system. The left plots show $y_{1\delta}$ in the time intervals $t = 100 - 200$ s and $t = 300 - 400$ s, respectively. The right plots show $y_{2\delta}$ in the same intervals.

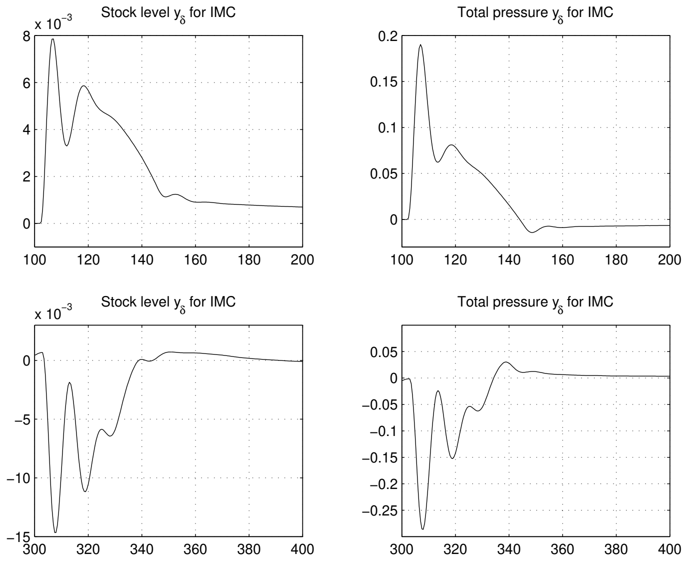

Figure 8.11: Windup effects present in the plant of the system using IMC AWC. The left plots show $y_{1\delta}$ in the time intervals $t = 100 - 200$ s and $t = 300 - 400$ s, respectively. The right plots show $y_{2\delta}$ in the same intervals.

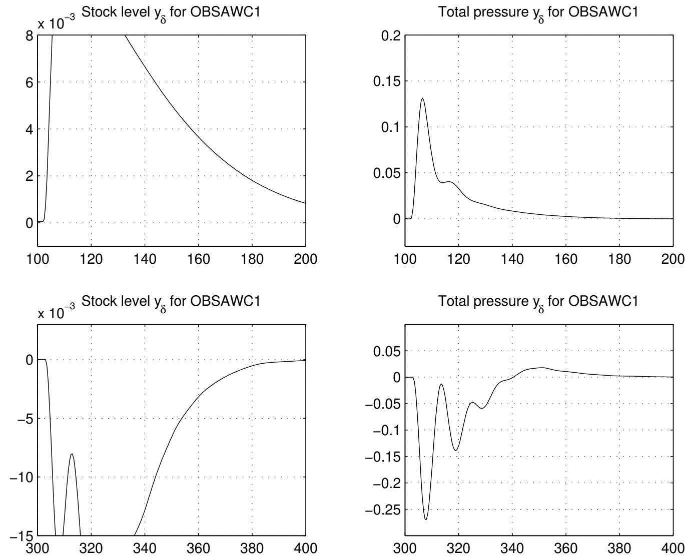

Figure 8.12: Windup effects present in the plant of the system using OBSAWC1. The left plots show $y_{1\delta}$ in the time intervals $t = 100 - 200$ s and $t = 300 - 400$ s, respectively. The right plots show $y_{2\delta}$ in the same intervals.

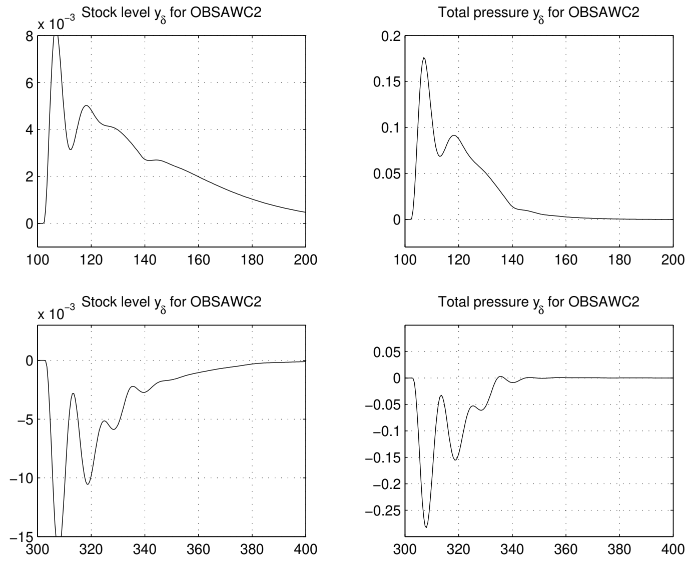

Figure 8.13: Windup effects present in the plant of the system using OBSAW2. The left plots show $y_{1\delta}$ in the time intervals $t = 100 - 200$ s and $t = 300 - 400$ s, respectively. The right plots show $y_{2\delta}$ in the same intervals.

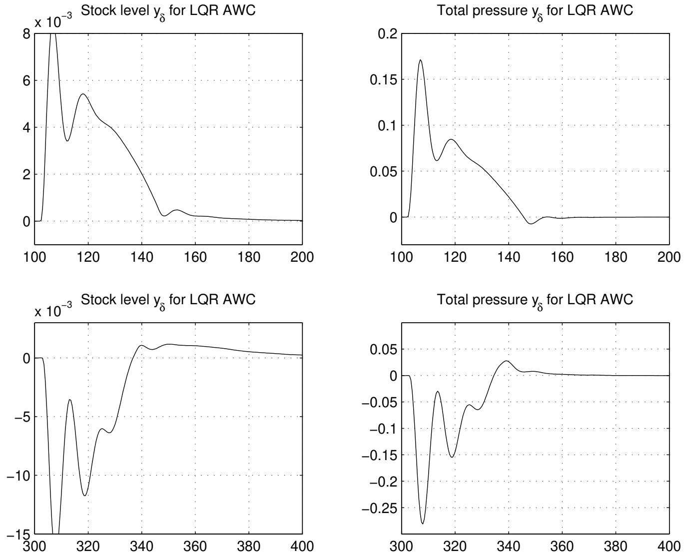

Figure 8.14: Windup effects present in the plant of the system using LQR AWC. The left plots show $y_{1\delta}$ in the time intervals $t = 100 - 200$ s and $t = 300 - 400$ s, respectively. The right plots show $y_{2\delta}$ in the same intervals.

CHAPTER 9

Control of the double integrator via saturating inputs

In the previous chapters we have discussed and shown what linear anti-windup can accomplish to improve performance in input saturating systems. In this chapter we will discuss control of a double integrator process with amplitude limited inputs. Control laws, which are modified versions of the time-optimal controller for this process, are proposed. It will also be shown that time-optimal control of a double integrator via an amplitude limiter is equivalent to time-optimal control of a single integrator via a rate limiter, a fact indicating that the suggested controller can be useful in many industrial applications. In fact, these control laws were developed for the control of hydraulic cylinders used in container crane systems. This application is discussed separately in Chapter 10. This chapter also includes a comparative study along the lines of [67]. Two of the best performing controllers in [67] are here compared to different version of the proposed approximate time-optimal controller. The results show that the proposed controller outperforms the best controllers of [67] and that it attains a performance close to the superior performance obtained by time-optimal control under ideal circumstances, but with the nice robustness properties of the simple PD-controller when operating under non-ideal conditions.

9.1 The double integrator

The double integrator is given by

$$\begin{aligned} \dot{x}_1 &= x_2 \\ \dot{x}_2 &= \frac{\sigma_a(u)}{m} \,. \end{aligned} \tag{9.1}$$

In this description (the same as in [67]), the system is a body with the mass *m*, that moves with the speed $x_2(t)$, located at the position $x_1(t)$, at time t. The notation σ_a will be used in the following whenever the saturation limits are symmetric and given by $\pm a$ (i.e. $\sigma_a = \sigma_{-a}^{a}$). The time index t will most often be omitted.

9.2 Time-optimal control

To begin with, we consider time-optimal control to the origin, $(x_1, x_2) = (0, 0)$, of the process (9.1) for $m = 1$. Such a time-optimal controller is of bang-bang type, see e.g. [84][79]. This means that the control signal, u, switches between the limits $\pm a$ of σ and the switching conditions are given by

$$u = \begin{cases} +a; & x \,\epsilon\, \Sigma^{+} \,\cup\, \Gamma^{+} \\ -a; & x \,\epsilon\, \Sigma^{-} \,\cup\, \Gamma^{-} \end{cases} \tag{9.2}$$

where

$$\Sigma^{+} = \{x : x_1 + \frac{1}{2a} x_2 |x_2| < 0\}; \quad \Sigma^{-} = \{x : x_1 + \frac{1}{2a} x_2 |x_2| > 0\} \,, \tag{9.3}$$

with switching borders given by the parabolic semi-arcs Γ^{+} and Γ^{-}, see Figure 9.1. The time-optimal response of the double integrator in (9.1), using the controller (9.2)-(9.3), is illustrated in the phase portrait in Figure 9.1.

9.2.1 Control synthesis

First, note that a relay function (a switch) can be obtained by multiplying the input u to the amplitude limiter by a large number. Now, according to the time-optimal strategy, u should be equal to $u = +a$ whenever $x_1 + \frac{1}{2a} x_2 |x_2| < 0$ and $u = -a$ whenever $x_1 + \frac{1}{2a} x_2 |x_2| > 0$. Hence, multiplying $x_1 + \frac{1}{2a} x_2 |x_2|$ by a large *negative* constant and feed the result to the amplitude limiter σ_a, will result in a time-optimal feedback controller, see Figure 9.2. Thus, time-optimal control of the

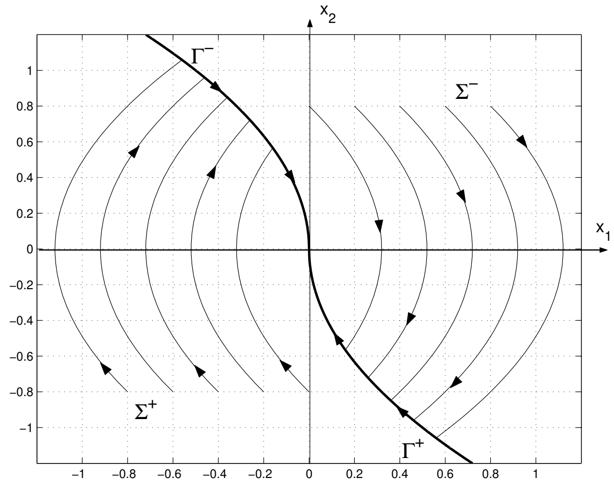

Figure 9.1: Phase portrait for time-optimal control of the double integrator

double integrator (9.1) is obtained by using the controller

$$u = -Kx_1 - Kg(x_2)$$
$$g(x_2) = \frac{1}{2a}x_2|x_2| \tag{9.4}$$

for $K \to \infty$. Another, and for our purpose even more useful synthesization, is the one obtain by multiplying $\operatorname{sgn}(-x_1)\sqrt{2a|x_1|} - x_2$ by a large *positive* constant and then feeding the result through the saturation σ_a, see Figure 9.3. Such a controller is given by

$$\begin{aligned} u &= -Kx_2 + Kf(x_1) = K(f(x_1) - x_2) \\ f(x_1) &= \operatorname{sgn}(-x_1)\sqrt{2a|x_1|} \end{aligned} \tag{9.5}$$

for $K \to \infty$. Note that the controller (9.5) takes the form of a cascade control scheme where the inner (speed) loop is closed by a constant "high" gain feedback and where the outer (position) loop is closed by a nonlinear square-root function. See Figure 9.3. The output from the position control loop, $f(x_1)$, fed to the inner loop, serves as a reference for the speed, x_2.

Note that for infinite (or large) K, the inner loop system constitutes a *rate limiter*, see Figure 9.4 and also Section 2.2. This means that (9.5) is a time-optimal con-

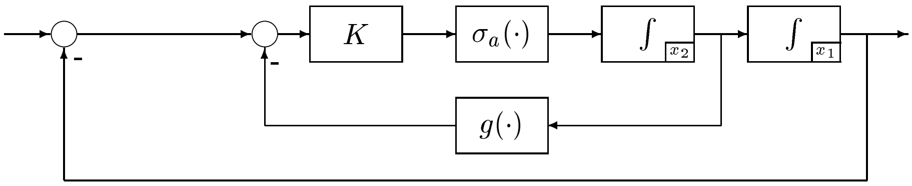

Figure 9.2: Controller synthesizing time-optimal control of the double integrator system by using nonlinear feedback in the inner-loop

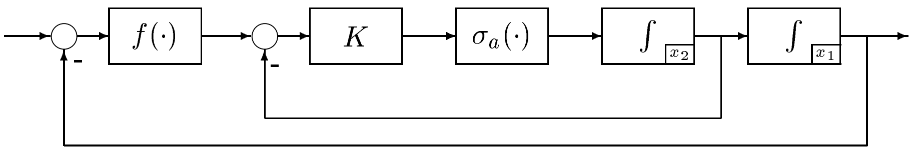

Figure 9.3: Cascade controller synthesizing time-optimal control of the double integrator system by using a nonlinear feedback in the outer-loop

troller not only for a double integrator with amplitude-limited input, but also for a single integrator with rate-limited input. We will discuss and use this result later.

9.3 Time optimal control and speed saturation

When both the input u and the state x_2 (speed) of the double integrator (9.1) are constrained and may saturate in amplitude, the time optimal performance will be slower, whenever x_2 saturates, compared to the case when only the input saturates.

By studying the phase portrait in Figure 9.6, one can see that control to the origin, from any initial state, is described by either of two situations:

1. The speed limit is never exceeded and the behavior will be identical to that of the unconstrained-state system, see the phase portrait in Figure 9.1.

2. The behavior is described by the following three phases of motion:

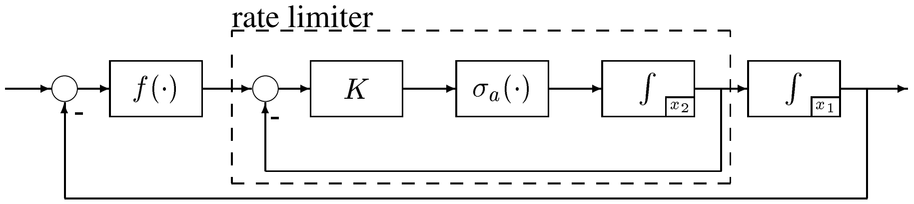

Figure 9.4: The inner closed-loop constitutes a rate limiter

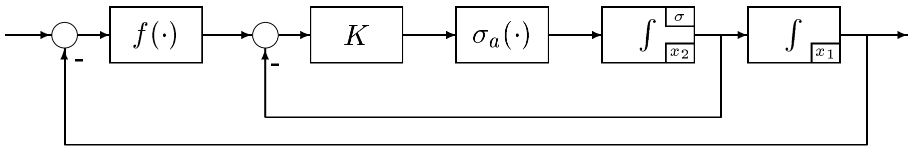

Figure 9.5: Time-optimal control of a double integrator with constrained input and constrained state x_2 (speed).

phase (1) maximum acceleration until x_2 saturates (which means maximum and saturated speed)

phase (2) maximum speed until Γ^- (or Γ^+) is reached

phase (3) maximum retardation until the origin $(x_1, x_2) = (0, 0)$ is reached.

The controller (9.5) is, thus, still a time-optimal controller for the system, see Figures 9.5 and 9.6. Note that if x_2 has limited amplitude, then the inner loop will function as a combined *rate- and amplitude limiter*. See Figure 9.7 and also Section 2.2. This means than the controller (9.5) is a time-optimal controller also for a single integrator controlled via a combined rate- and amplitude limiter. Such an application is discussed in Chapter 10. We formalize the property in the following way:

Property 5 The scheme for time-optimal control of a double integrator having amplitude constrained input and speed is equivalent to the scheme of time-optimal control of a single integrator having rate- and amplitude limited input.

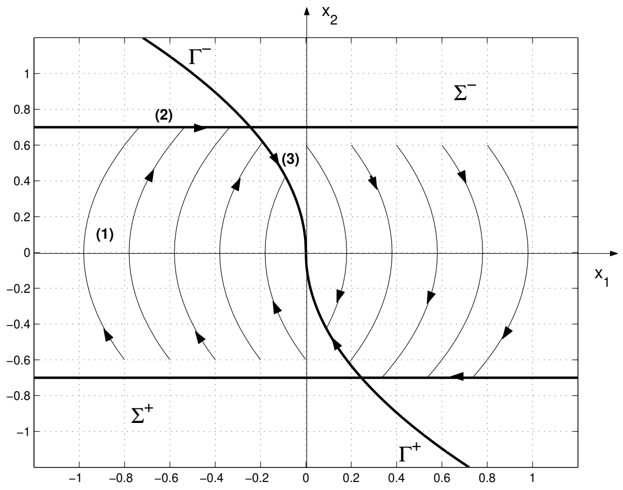

Figure 9.6: Phase portrait for time-optimal control of a double integrator having both the input and the state x_2 (speed) limited in amplitude.

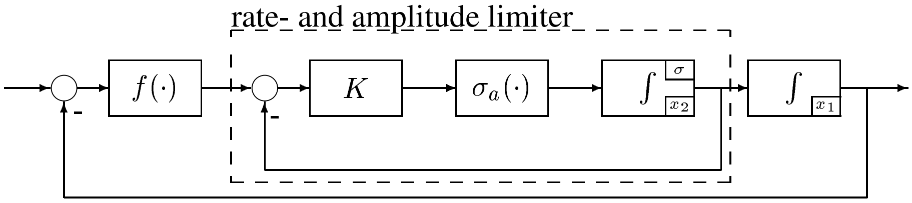

Figure 9.7: The inner loop will function as a combined rate- and amplitude limiter

9.4 Robust almost time-optimal control

The bang-bang controller (9.5) discussed above can be inappropriate to use in many real applications. The main reason is poor robustness against deviations of the real plant from the model (9.1). In order to make the time-optimal controller more robust, and more useful in real applications, I propose the following modifications of (9.5):

Position reference
In practice we must be able to control the system to a point $(x_1, x_2) = (x_1^{ref}, 0)$, and not only to the origin. To obtain time-optimal control to the position $x_1 = x_1^{ref}$, we must add x_1^{ref} to $-x_1$ in the controller (9.5). In the modified controller (9.15) below, we have introduced the controller error $e = x_1^{ref} - x_1$, instead of $-x_1$ as in (9.5).

Not unity mass
We must, of course, be able to control systems where the parameter $m \neq 1$. Note that the maximum obtainable (saturated) acceleration, $\dot{x}_2^{max}$, is given by

$$\dot{x}_2^{max} = \max\left(\frac{\sigma_a(u)}{m}\right) = \frac{a}{m} \, . \tag{9.6}$$

The minimum obtainable acceleration is $-\frac{a}{m}$. Now, since the control signal of the time-optimal controller switches between the limits $\pm a$, the acceleration will always be either $\pm\frac{a}{m}$, or 0 when x_2 saturates. Hence, the mass, m, can be incorporated into the model of the input limiter, where the new limits are $\pm\frac{a}{m}$. The system model is then given by

$$\begin{aligned} \dot{x}_1 &= x_2 \\ \dot{x}_2 &= \sigma_{\frac{a}{m}}(u) \, . \end{aligned} \tag{9.7}$$

The saturation limit a in the controller (9.5) has therefore been replaced by $\frac{a}{m}$ in the proposed controller (9.15) below.

Not unity gain between $\dot{x}_1$ and x_2
In many applications concerning control of a single integrator via a rate limiter, the gain K_v in the relation $\dot{x}_1 = K_v x_2$ is not unity. The time optimal controller for such systems will contain the parameter K_v and it appear as in the controller (9.15). A motivation for this is given next. This motivation can in fact be taken as a simple proof of the time optimal controller as such.

The process is assumed to be given by

$$\begin{aligned} \dot{x}_1 &= K_v x_2 \\ x_2 &= \rho_a[\sigma_1(f(e))] \, , \end{aligned} \tag{9.8}$$

where $f(e)$, in agreement with Property 5, comes from the time optimal controller. Consider the step response in Figure 9.8 where the solid line represents x_1 and the dashed line represents x_2. Now, consider only the phase of retardation which takes

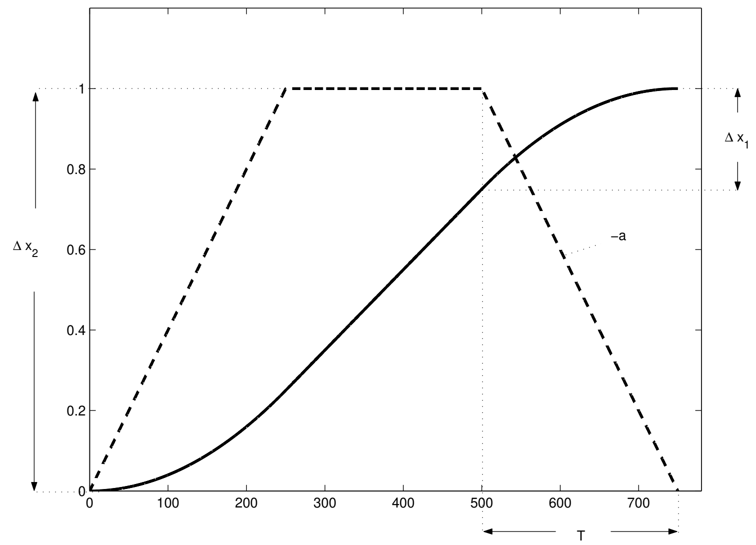

Figure 9.8: Time optimal response to a step-change in x_1^{ref}. The solid line represents the response of x_1 and the dashed line the response of x_2 where $\dot{x}_1 = K_v x_2$.

place during the time interval T. The change of the position Δx_1 is related to the change of the output Δx_2 from the rate- and amplitude limiter, as

$$\Delta x_1 \;=\; K_v \frac{T|\Delta x_2|}{2} \; . \tag{9.9}$$

Note that $\frac{T|\Delta x_2|}{2}$ is the area of the triangle with the base T and the hight $|\Delta x_2|$, which equals the value of

$$\int x_2(t) \text{ dt} \tag{9.10}$$

taken over the time interval T. The slope $-a$ by which the rate limiter ramps down the signal x_2 can be express as

$$-a \;=\; \frac{\Delta x_2}{T} \tag{9.11}$$

which means that

$$T \;=\; \frac{\Delta x_2}{-a} \; . \tag{9.12}$$

Insertion of this expression of T into (9.9) gives that

$$\Delta x_1 \;=\; K_v \frac{T|\Delta x_2|}{2} \;=\; K_v \frac{(\Delta x_2)^2}{2a}. \tag{9.13}$$

The retardation can then be expressed as

$$\Delta x_2 = \sqrt{\frac{2a\Delta x_1}{K_v}}. \tag{9.14}$$

Compare this expression to the one on the second row of (9.5) where $f(x_1)$ functions as a reference for speed, see also the text that follows directly after the expression (9.5). This ends the motivation for why K_v appears in the way it does in (9.15).

Approximation of the relay function

It is often (but not always) possible, and desirable, to replace the relay function by a saturation function so that the system can operate in a linear region for small control signals. This gives a smoother control action and it improves the robustness properties of the controller. Since our relay function is obtained by the use of an amplitude limiter, replacing the relay function by an amplitude limiter so that linear control is obtained for small u, is simply obtained by selecting the constant K finite. In the proposed controller (9.15) below, the infinite gain K is replaced by the finite gain $d * k_2$. The reason why we introduce two constants, d and k_2, is that the constant k_2 corresponds to a parameter of the PD-controller that will be compare to our proposed controller later in Section 9.6, in an illustrative way.

Limited gain of the square root function

The standard square root function $\sqrt{z}$ has infinite gain, $\sqrt{(z)}/z$, for small z. It is therefore wise to limit the gain of $\sqrt{2a|e|}$ in (9.5) for small control errors e. Figure 9.9 illustrates the situation for the standard square root function $f(z) = \sqrt{z}$. Introducing such a limitation of the square root function into the controller (9.5), results in a switching event at e_0 in the proposed controller (9.15) below. Notice that this modification makes the controller (9.5) become a simple PD-controller, for small errors e. See also Figure 9.10.

Aim window and adjustable gain

As a consequence of the proposed modifications of limiting the gain of the square root function, and replacing the relay by an amplitude limiter σ, the response of the inner loop will become slower than the corresponding response obtain by using the true time-optimal controller (9.5). The gain in the position feedback loop (outer) must therefore be reduced. Otherwise, the now slower retardation will take place to late, which results in a position overshoot. In the proposed controller (9.15) below, the constant c is used to adjust the gain in the outer (position) loop.

For reasons explained below, we also introduce an ”aim at” window in order to reduce the tendency of the position x_1 to overshoot. This modification is obtained by

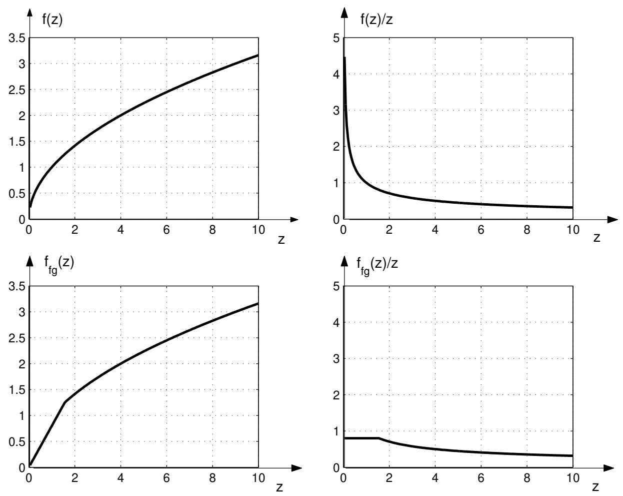

Figure 9.9: Output from, and gain of: the square root function (upper-left and upper right respectively) and of the limited-gain square root function (lower-left and lower-right respectively)

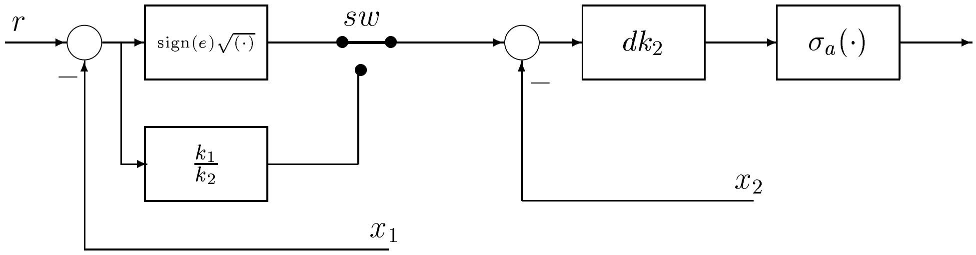

Figure 9.10: Limiting the gain $f(e)/e$ results in a switched control action where, for a small error e, the controller becomes a simple PD controller.

replacing e under the square root function of $f(e)$, by the dead zone $\sigma_0^\infty(|e| - w_2)$. Interpreted in the phase portrait and in terms of the phases of motion described in Section 9.3, the effect of this modification is that the retardation takes place (slightly) before the system trajectory reaches the borders Γ^+ and Γ^-, respectively. This reduces the risk of getting position overshoots, at the cost of a slightly slower response. In the application discussed in Chapter 10, for which the controller (9.15) was originally developed, increasing the size of the window w_2 has a similar effect on the system behavior as decreasing the constant c has. In that application, it turned out, however, that by using the window ($w_2 > 0$) in combination with tuning of $c < 1$, we could tune the system so that a faster response was obtain under somewhat ideal condition, as well as acceptable response under less favorable conditions, than compared to when the window w_2 was not used ($w_2 = 0$).

Which strategy that works best could be expected to depend on the actual application so, I do not give the reader any advises here.

Turn-off control

In some applications it is desirable to set the speed to zero when a sufficiently small error e is reached. We therefore set $f(e) = 0$ for $|e| < w_1$ in the proposed controller (9.15) below.

Integral action

For better attenuation of disturbances, one can add integral action to the controller. We suggest that such an integrator is active only for $|e| < e_0$. The controller then becomes a ”standard” PID-controller for position errors smaller than e_0. Notice that the value of the integrator-state will, of course, affect the continuality conditions mentioned in Remark 9.3 below. For a given fix value of e_0, we can always adjust the state of the integrator so that u becomes continuous when switching *to* the PID-controller. However, this is not possible when switching *from* the PID-controller, simply because the controller we switch to lacks adjustable states. This may, or may not, be important for a given application. An example of how integral action can be introduced is presented in Chapter 10.

The proposed SQRT-controller

The modified and more robust, "almost" time-optimal controller is given by

$$
\begin{aligned}
u &= dk_2(f(e) - x_2) && (9.15)\\
f(e) &= \begin{cases} \mathrm{sign}(e)\sqrt{\frac{a}{m}\frac{1}{K_v}2c\sigma_0^{\infty}(|e| - w_2)} & |e| \geq e_0 \\ \frac{k_1}{k_2}e & w_1 < |e| < e_0 \\ 0 & |e| < w_1 \end{cases}\\
e &= x_1^{ref} - x_1\\
&0 \leq w_1 < e_0 && (9.16)\\
&0 \leq w_2 < e_0 \ . && (9.17)
\end{aligned}
$$

Remark 9.1 Selecting the tuning parameters as

$$
\begin{aligned}
c &= 1\\
w_1 &= w_2 = e_0 = 0\\
dk_2 &= K \to \infty \qquad (9.18)
\end{aligned}
$$

makes the controller (9.15) become a true time-optimal controller for the process (9.1) and also the process (9.8).

Remark 9.2 Assume that the turn-off function is disabled, i.e. $w_1 = 0$. Then, for given values of the tuning parameters $c,\ d,\ k_2,\ w_2$, the control signal u will be continuous for a certain value of e_0. This property may, or may not, be important for a given application.

Remark 9.3 Switching between different controllers, as in (9.15), may in some systems result in trouble such as chattering or trapping the system in undesired states of rest, or in stable limit cycles. An exact mathematical analysis is non-trivial. This is so even in the, in reality unusual, case where every parameter is constant and known. In practice, a more passable way is testing and more testing. Some application are such that problems will most likely not occur and in others they may. If some scattering problems should occur, selecting $w_2 = 0$ and reducing the gain c *could* solve the problem.

9.5 Control of the MIMO(2,2) double integrator

Next, we will show that our proposed controller performs well even when used for control of the MIMO(2,2) double integrator (Plant 2) defined in Example 5.2.

EXAMPLE 9.1: PLANT 2, SQRT-CONTROL

This example concerns control of the MIMO(2,2) discrete time double integrator (5.59), by the use of the proposed SQRT-controller (9.15). In this example, however, we consider a MIMO(2,2) plant with cross couplings between the inputs and the outputs. Therefore, we will here use the same principle as the nominal controller (5.61) is based on, namely the principle of decoupling. Furthermore, we use the direction compensated limiter γ (2.17). The scheme is depicted in Figure 9.11. Note that we need two SQRT controllers, one for each decoupled loop.

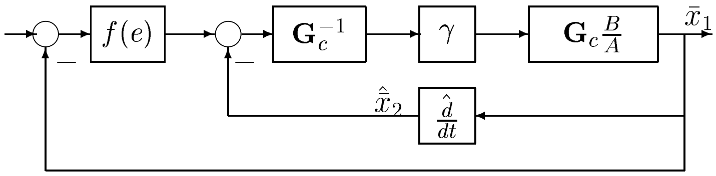

Figure 9.11: Decoupled MIMO double integrator with direction compensated input limiter γ, controlled by the proposed SQRT-controller (9.15).

The following set of controller parameters are used in both the SQRT controllers:

SQRT

$$\begin{aligned} w_1 &= 0,\ w_2 = 0.04 \\ e_0 &= 0.05,\ c = 0.65 \\ a &= 0.01,\ m = 1 \\ K_v &= 1. \end{aligned} \tag{9.19}$$

Since the controller (9.15) is developed for control of *one* double integrator, its is not straightforward to find corresponding plant parameters, such as the mass m, the amplitude limit a and the gain K_v, in the MIMO plant (5.59). Therefore, we select the parameters in a rather ad-hoc manner in this example. The results from the simulation are shown in Figure 9.12.

The (MIMO) SQRT controller performs much better than the OBSAWC. In fact, it probably performs better than all the other controllers that we have evaluated for the control of Plant 2 in this thesis.[1]

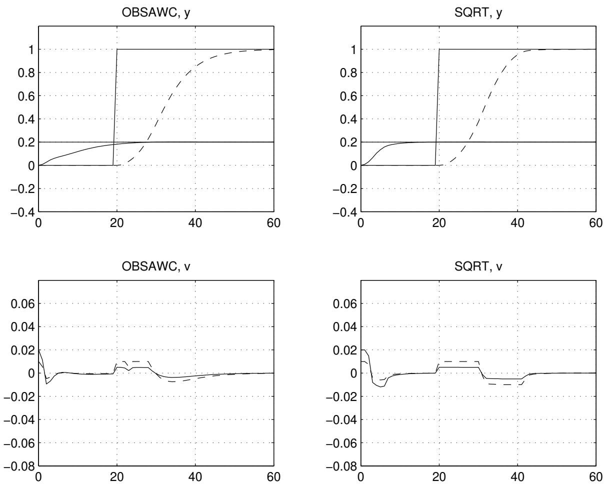

Figure 9.12: Reference step response for the for the SQRT (right) and for the OBSAWC1 (left).

9.6 Comparative study

This section is concerned with comparison tests where the best performing controllers investigated in [67] are compared to the controller (9.15) for three different sets of parameters.

9.6.1 Controllers

Three differently tuned controllers, denoted SQRT_1, SQRT_2 and SQRT_3, defined by the control law (9.15) for the following three sets of parameters

$$\begin{aligned}
&\text{SQRT}_1 \;\; w_2 = 0, \;\; d = 1 \\
&\text{SQRT}_2 \;\; w_2 = 0, \;\; d = 2 \\
&\text{SQRT}_3 \;\; w_2 = 0.8, \;\; d = 3 \\
&\text{SQRT}_{1,2,3} \;\; w_1 = 0, \;\; c = 0.7, \;\; e_0 = 1, \;\; k_1 = 1, \;\; k_2 = 1.25 \; ,
\end{aligned} \tag{9.20}$$

[1]The reason for why I say ”probably” is that performance measures varies from one application to another.

will be investigated. Each one of them will be compared to two of the best performing controllers tested in the investigation [67], namely the *Saturation controller* proposed by Teel in [24] given by
Saturation controller (SAT)

$$u = -\mathrm{sat}_{u_{max}}[x_2 + \sigma_{0.49}(x_1 + x_2)], \tag{9.21}$$

and a simple PD controller,
PD controller (PD)

$$u = -k_2(\frac{k_1}{k_2}x_1 - x_2) \ . \tag{9.22}$$

The values of the tuning parameters are the same here as above, namely $k_2 = 1.25$ and $k_1 = 1$. Note that the controller SQRT1 equals the PD controller in (9.22) for $|x_1| < 1$ ($x_1^{ref} = 0$).

9.6.2 Process subject to unknown variations

The process to be controlled is a double integrator subject to unknown variations. It is given by

Process subject to unknown variations

$$\begin{aligned} \dot{x}_1 &= x_2 \\ \dot{x}_2 &= -\omega^2 x_1 - 2\xi\omega x_2 + \frac{\sigma_1(u)}{m} \\ x_1^{meas}(t) &= x_1(t - t_d), \ \ x_2^{meas}(t) \ = \ x_2(t - t_d) \ , \end{aligned} \tag{9.23}$$

where the parameters, which are assumed to be unknown to us when designing the controllers, varies in the following way:

$$\begin{aligned} \text{(I)} \ & m \in [0.05, \ 0.5, \ 1, \ 1.5, \ 2] \\ \text{(II)} \ & \omega \in [0, \ 2, \ 4, \ 6] \\ \text{(III)} \ & \omega \in [0.2, \ 0, \ -0.03, \ -0.05], \ \text{for } \xi = 1 \\ \text{(IV)} \ & t_d \in [0.1, \ 0.2, \ 0.3, \ 0.4, \ 0.5, \ 0.6] \ . \end{aligned} \tag{9.24}$$

Note that the system (9.23) is, in fact, a true double integrator only for $\omega = \xi = 0$. The mass variation (I) varies the gain, (II) introduces poles on the imaginary axis, (III) introduces poles on the real axis (stable and unstable) and (IV) introduce time delays t_d seconds in both the measurement channels (speed and position). If nothing else is stated, the nominal values $\xi = \omega = t_d = 0$ and $m = 1$ are used.

Nominal process
We define the *nominal process*, in the following way:

$$\begin{aligned} \dot{x}_1 &= x_2 \\ \dot{x}_2 &= \sigma_1(u)\ . \end{aligned} \tag{9.25}$$

9.6.3 Experiments

The ability of the investigated controllers are evaluated by carrying out the following experiments:

Step response of the nominal process (9.25) when applying steps x_1^{ref} of the magnitudes $1,\ 5,\ 10$. The results are presented in Figures 9.14, 9.17 and 9.22.

Control to the origin of the process (9.23) from 10 different initial points (x_{10}, x_{20}) evenly distributed on a circle with radius $rad = 5$ in the phase portrait. The performance is measured in terms of settling time which is here defined as the time it takes the state-trajectory to reach, and then stay inside, a circle with radius 0.01. The *achieved settling time* (AST) is taken as to be the largest settling time out of the 10. The results are presented in the phase portraits of Figures 9.15, 9.18 and 9.23, and in plots of achieved settling times as functions of the unknown variations in Figures9.16, 9.19 and 9.24.

For the controller SQRT_2, the PD controller, and the saturation controller, phase portraits and achieved settling times as functions of the unknown variations are shown also for initial states lying on a circle with radius $rad = 10$. See Figures 9.20 and 9.21. Achieved settling times obtained for the nominal system, for each and every one of the controllers, are also presented in Table 1.

9.6.4 Comments and conclusions

Controller	**AST**, $rad = 5$	**AST**, $rad = 10$
SAT	36.0	117.5
PD	23.2	58.5
SQRT_1	19.4	31.8
SQRT_2	15.6	28.1
SQRT_3	15.9	28.6

Table 1.

The test in [67] shows that the achieved settling time for true time-optimal control of the nominal double integrator is $13.9s$ for $rad = 5$.

Comparisons between the SQRT controllers
The controller SQRT_1 has the lowest gain $d = 1$ among the proposed SQRT controllers. A small gain dk_2 results in a slow inner loop. As we argued before, this increases the tendency of x_1 to overshoot under nominal conditions. This tendency is clear from the step responses of Figure 9.14. Compare with the step responses of Figure 9.17 and Figure 9.22 obtained for SQRT_2 and SQRT_3, respectively. The difference between these three controllers what concerns the tendency of overshooting is clear also from the lower phase portraits of Figures 9.15, 9.18 and 9.20, and 9.23 obtain for SQRT_1, SQRT_2 and SQRT_3, respectively.

The achieved settling times (AST) obtain under unknown variations, presented in Figures 9.16, 9.19 and 9.21, and 9.24, are similar for the three controllers. However, under nominal conditions the AST obtained for SQRT_1 is typically somewhat longer than for the other two SQRT controllers. On the other hand, the conditions are reversed when having ”large” and unknown time delays in the measurement equipment, see the lower-right plots of Figures 9.16, 9.19 and 9.24. The achieved settling times obtained under nominal conditions are presented in Table 1.

Comparisons between the SQRT controllers and the PD and SAT controllers
The controllers SQRT_2 and SQRT_3 outperforms the PD controller and the SAT controller, under nominal conditions. See e.g. Table 1. This is not remarkable since the SQRT controllers are approximations of the time-optimal solution. What is remarkable, however, is that they are robust against the variations *as well*. See the Figures 9.19, 9.21 and 9.24. The only situations where SQRT_2 and SQRT_3 show less favorable performance than the PD and the SAT controller, is for large unknown time delays. The relatively high gain in the speed loop is the cause of this. The controller SQRT_1 which has a lower gain in the speed loop, handles large time delays well.

By comparing the results obtained when the initial states are located on a circle with radius $r = 5$, shown in Figure 9.19, by the results obtained when the initial states are located on a circle with radius $r = 10$, shown in Figure 9.21, we can see that the SQRT_2 controller performs even better in the latter case.

Conclusions
The results from the Example 9.1 but, most of all, the results from this sections comparative study, show that the proposed controller (9.15) has a great potential to become the most suitable controller that can be used for the control of double integrators with inputs constrained in amplitude, and for the control of single integrator

with rate- and amplitude constrained inputs. In the next chapter we will demonstrate its potential further by using it for the control of container crane spreaders.

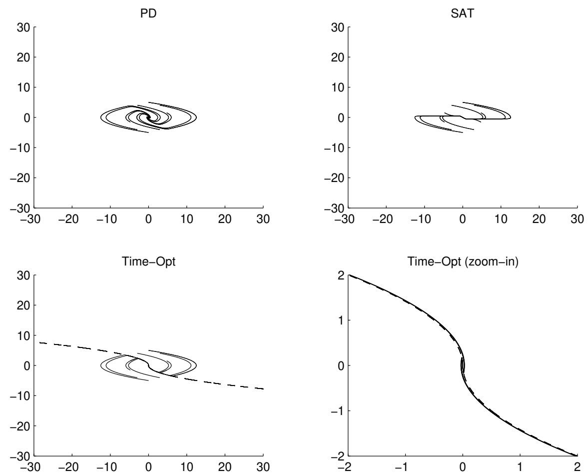

Figure 9.13: Phase portraits for the control to the origin of the nominal process, with initial states located on a circle with radius $rad = 5$, using the SAT (upper right), the PD (upper left) and the true time optimal controller (lower) controller. The dashed curves in the lower plots are the semi-arcs for the true time-optimal controller.

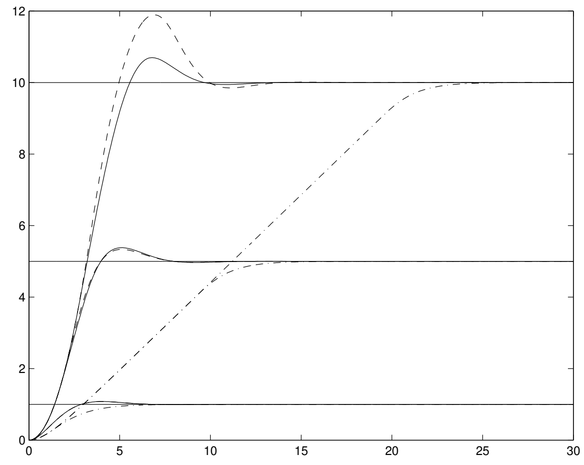

Figure 9.14: Step response for the SAT (dash-dot), the PD (dashed) and the SQRT$_1$ (solid) controller

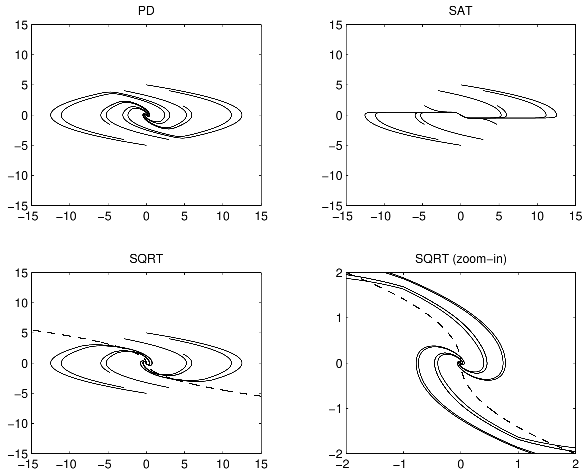

Figure 9.15: Phase portraits for the control to the origin of the nominal process, with initial states located on a circle with radius $rad = 5$, using the SAT (upper right), the PD (upper left) and the SQRT$_1$ (lower) controller. The dashed curves in the lower plots are the semi-arcs for the true time-optimal controller.

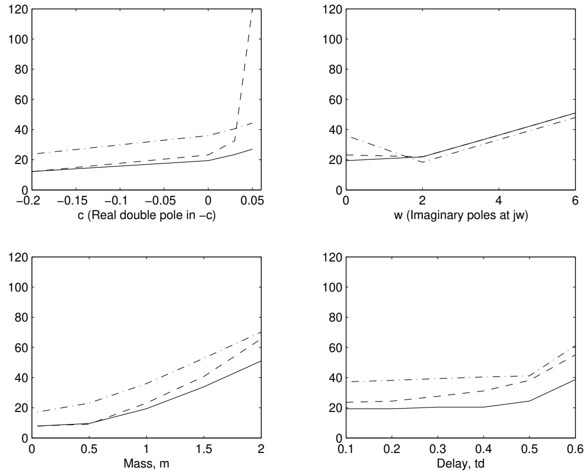

Figure 9.16: The achieved settling time, AST, for the control to the origin of the process subject to different unknown variations, when using the SAT (dash-dot), the PD (dashed) and the SQRT$_1$ (solid) controller. The initial states are located on a circle with radius $rad = 5$.

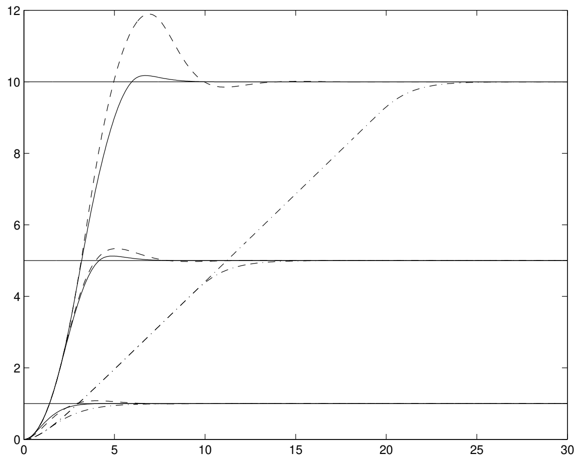

Figure 9.17: Step response for the SAT (dash-dot), the PD (dashed) and the $SQRT_2$ (solid) controller

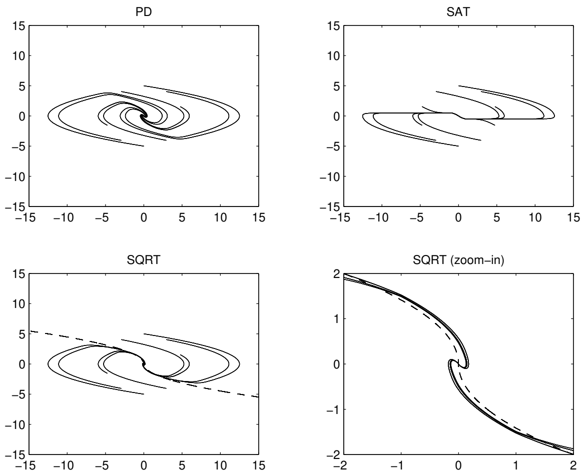

Figure 9.18: Phase portraits for the control to the origin of the nominal process, with initial states located on a circle with radius $rad = 5$, using the SAT (upper right), the PD (upper left) and the $SQRT_2$ (lower) controller. The dashed curves in the lower plots are the semi-arcs for the true time-optimal controller.

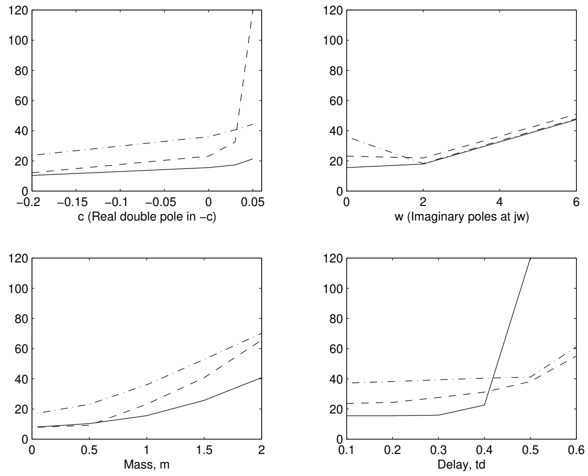

Figure 9.19: The achieved settling time, AST, for the control to the origin of the process subject to different unknown variations, when using the SAT (dash-dot), the PD (dashed) and the $SQRT_2$ (solid) controller. The initial states are located on a circle with radius $rad = 5$.

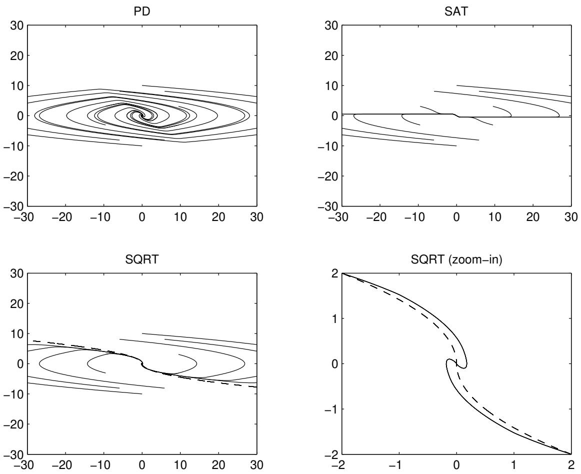

Figure 9.20: Phase portraits for the control to the origin of the nominal process, with initial states located on a circle with radius $rad = 10$, using the SAT (upper right), the PD (upper left) and the $SQRT_2$ (lower) controller. The dashed curves in the lower plots are the semi-arcs for the true time-optimal controller.

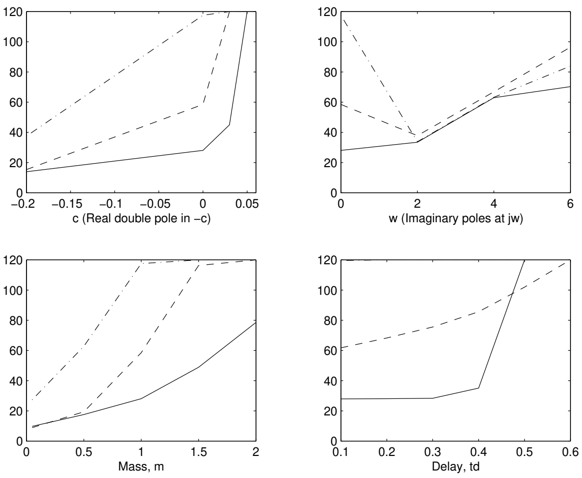

Figure 9.21: The achieved settling time, AST, for the control to the origin of the process subject to different unknown variations, when using the SAT (dash-dot), the PD (dashed) and the SQRT$_2$ (solid) controller. The initial states are located on a circle with radius $rad = 10$.

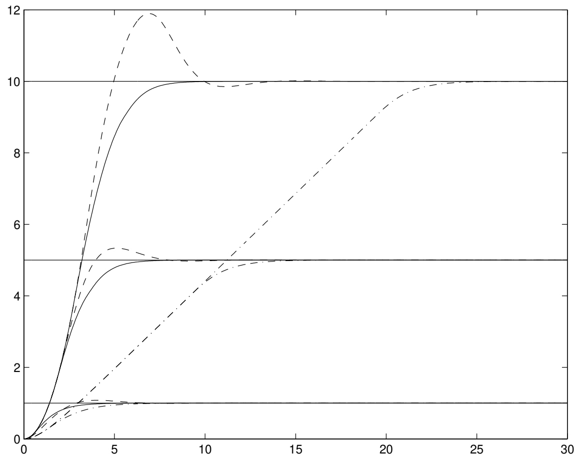

Figure 9.22: Step response for the SAT (dash-dot), the PD (dashed) and the SQRT$_3$ (solid) controller

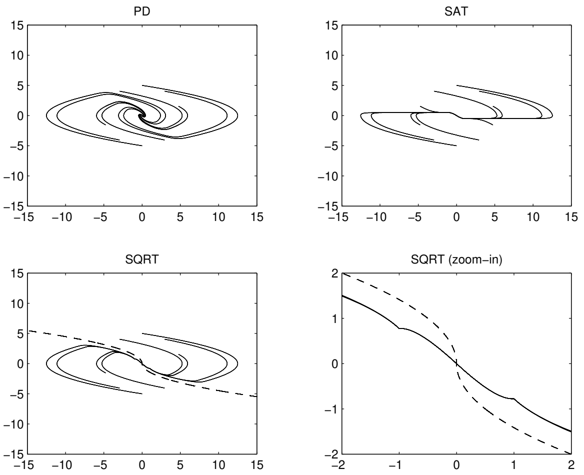

Figure 9.23: Phase portraits for the control to the origin of the nominal process, with initial states located on a circle with radius $rad = 5$, using the SAT (upper right), the PD (upper left) and the SQRT$_3$ (lower) controller. The dashed curves in the lower plots are the semi-arcs for the true time-optimal controller.

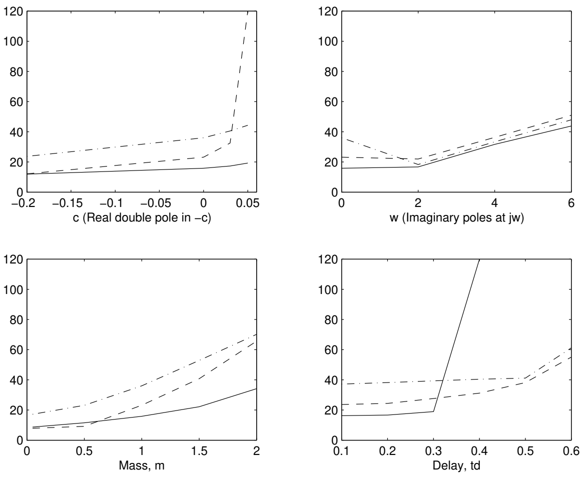

Figure 9.24: The achieved settling time, AST, for the control to the origin of the process subject to different unknown variations, when using the SAT (dash-dot), the PD (dashed) and the SQRT$_3$ (solid) controller. The initial states are located on a circle with radius $rad = 5$.

CHAPTER 10

Control of Hydraulic Cylinders in a Container Handling System

Figure 10.1: Spreader (hanging in a crane) for handling a single container.

In this chapter, an industrial project which concerns development of new control strategies for position- and speed control of a container handling system, is presented and discussed. [1] The control problem concerns individual as well as synchronous position- and speed control of hydraulic cylinders, under imposed acceleration limits. The cylinders are, among other things, used for adjust the position of containers, attached to a *spreader* which, in turn, is hanging in crane, see Figure 10.1. The acceleration limit is imposed in order to limit the forces acting on the ropes.

The reader may find the discussion in some parts of this chapter incomplete, especially the parts that concern technical details of the cranes and the hydraulic systems. For several reasons e.g. secrecy and my lack of knowledge, many technical details have been left out in the discussion. Yet, I hope that reader shall find the discussion concerning control interesting, and gain some insights from it.

Figure 10.2: Spreader (left) standing on the ground under the crane (right). Containership at quay (background). Author downloading the controller software (middle).

[1]This project was carried out during 2001-2002 in co-operation with staff from CC-systems and Bromma Conquip. The final test and implementation of the controller was made in July 2002 in one of the most automated harbors in the world located in Hamburg, Germany. The controller is, today, implemented in a total of fifty cranes.

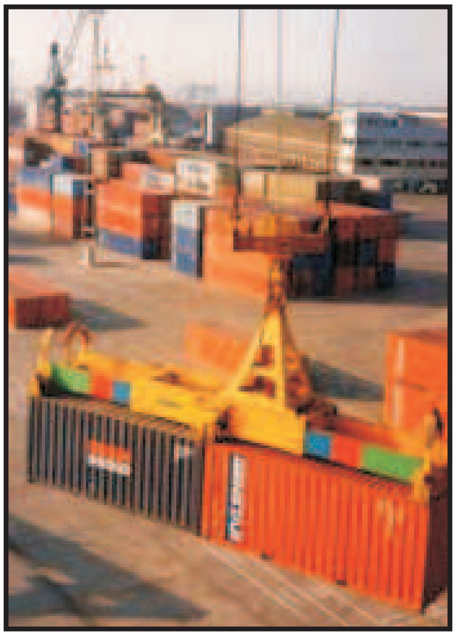

Figure 10.3: Twin-Lift Jib Crane Spreader

10.1 Container cranes and spreaders

Spreaders are used for lifting containers and they usually hang in ropes attached to a crane, see Figure 10.1. The beams of the spreader can be moved in and out so that it can handle containers of different size. The spreaders considered here acquire this movement by hydraulic cylinders.

The crane itself can move to a certain position, with a certain accuracy, where a container is to be placed or picked-up. In order to obtain better accuracy, some spreaders have moveable links in which the ropes are attached to the spreader. These links can be moved (shorter distances) with a higher accuracy than the crane itself. The motion of the links are acquired by hydraulic cylinders. Such micro motion defines the problem addressed in this chapter.

In some application, it is favorable to move cylinders synchronously [68], e.g. in order to prevent twisting oscillations. Control for synchronized micro motions will be discussed in Section 10.3.

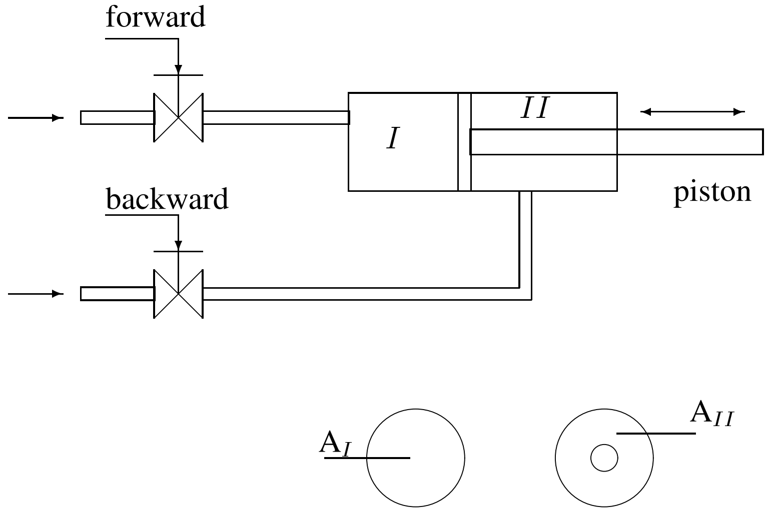

Figure 10.4: A simple description of the hydraulic cylinder actuated by valves. The cylinder moves by letting a flow of hydraulic liquid through its chambers. For motion forward the flow goes into Chamber I and out of Chamber II, and the reverse way for motion backwards. The flow comes from a pump and is controlled by valves. The lower part of the figure shows cross-sections of the two chambers, where the areas of the cross-sections are denoted by A_I and A_{II}, respectively. The fraction of maximum obtainable speed forward/backward is equal to the fraction A_{II}/A_I. Here, $A_{II} < A_I$ because the cross-section area of the piston.

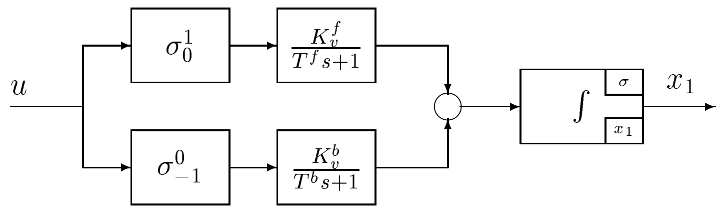

Figure 10.5: A simple model of the hydraulic system in Figure 10.4, after valve compensation.

10.1.1 Hydraulic cylinders

Consider the simple picture of the hydraulic cylinder in Figure 10.4. The cylinder moves by letting a flow of hydraulic liquid through its chambers. For motion forward the flow goes into Chamber I and out of Chamber II, and the reverse way for motion backwards. The flow comes from a pump and is controlled by valves. The valves are actuated via electromagnets. The electromagnet is controlled by a *Pulse-Width Modulated* PWM-signal. The static relation between the pulse-width and the valve opening is fairly linear. The pulse generate a current ranging from 0 up to 2500 mA and the pulse-width is here assumed to be scaled so that it takes real values in the interval $0 - 1$. The dynamics of the valves can be modelled by first order systems having time-constants T^f and T^b, respectively. Housings and the electromagnetic actuator are the parts of the system that contributes most to these dynamics.

The relation between the PWM-signal and the flow is, however, nonlinear and there is much to gain from linearizing it. Such a linearization was carried out by using one of the methods mentioned in Section 2.6. The compensation allows us to model the valve in the way it is depicted in Figure 10.5.

The size of the forward and backward gains, $K_v^f,\ K_v^b$ are given by the capacity of the hydraulic system. The relation between them are given by the cross-section areas A_I and A_{II} as

$$\frac{K_v^f}{K_v^b} = \frac{\mathrm{A}_{II}}{\mathrm{A}_I} < 1 \,, \tag{10.1}$$

see Figure 10.4. Hence, the maximum obtainable speed of the cylinder is always faster in the backward direction.

10.2 Control of a single cylinder

In this section we will show that Property 5 of Section 9.3 allows us to use the SQRT-controller (9.15) for the control of cylinders with imposed acceleration limits. The controller must, however, be adapted to some new conditions.

Valve pre-compensation
As mentioned above, the nonlinear characteristics of the valves must be compensated for before successful control can be obtained. The static relation between the valve input and the speed of the cylinder is modelled by a polynomial equation, see Section 2.6. The inverse of this equation is then implemented in the software between the controller and the valve. [2]

[2]The procedure is carried out automatically in the real cylinder control system.

Valve dynamics
When the position controller ramps-down the valve-input signal, in order to retard the motion of the cylinder, the valve dynamics cause a somewhat slower response. This increases the cylinders tendency to overshoot in position when operating in closed loop. However, the dynamics are fast compared to how the system will be operated and will therefore be ignored in the model used for controller design. Problems that may occur due to this simplification can be avoided by using the ”aim at” window proposed in Section 9.4.

The pre-compensation of the valves along with the fact that we can ignore the valve dynamics, knowing that the aim-at window can be used to overcome problems that these approximations may cause, allow us to model the cylinder in the following way:

$$\begin{aligned} \dot{x}_1 &= K_v \sigma_1(u) \\ K_v &= \begin{cases} K_v^f & \text{forward motion} \\ K_v^b & \text{backward motion .} \end{cases} \end{aligned} \tag{10.2}$$

The valves for backward and for forward motion are here considered as to be one actuator with symmetric saturation limits ± 1. Note that in (10.2) the limited operating range of x_1 (denoted by a small σ-sign in the upper corner of the integrator in Figure 10.4) is ignored. This is possible because the system is operated so that the cylinder always stays within its limits.

Next, we list some performance requirements and operating conditions that must also be taken into account. These are the following:

Requirements and operating conditions

1. The acceleration of the cylinder must be constrained
2. Disturbances and inaccuracy of the valves require integral action of the position controller
3. The cylinder is not, at any time during a movement from one point to another, allowed to move against the desired direction
4. The gain K_v can vary significantly from one movement to another, as due to the fact that containers have different weights

5. Numerical problems caused by limited word-length in the microprocessor must be avoided

6. The computational capacity is substantially constrained

7. Position overshoots are not accepted

Since the input to an integrator is proportional speed, $\dot{x}_1$, the first requirement, constrained acceleration, can be met by letting the control signal u pass through a rate limiter before it operates on the process. Introducing the rate limiter into the model (10.2) gives the new model

Model used for controller design

$$\begin{aligned} \dot{x}_1 &= K_v \rho_a(\sigma_1(u)) \\ K_v &= \begin{cases} K_v^f & \text{forward motion} \\ K_v^b & \text{backward motion} \end{cases} \end{aligned} \tag{10.3}$$

where the function $\rho_a(\sigma_1(u))$ is a combined rate- and amplitude limiter, see (2.4) and Figure 2.2. Recall that the amplitude limiter σ_1 in (10.3) represents the limits of the *real physical* valves whereas the rate limiter, that constrains the speed of which the valve can be opened/closed and thereby the acceleration of the cylinder, must me implemented in the controller software. However, we implement the combined rate- and amplitude limiter in the software, where the amplitude limits correspond to the real limits of the valve and where the rate limit a are set by the user. The parameter a represents the desired opening/closing speed of the valve. For example if we want the valve to go from closed to fully opened in 4 seconds, say, then $a = \frac{1}{4}$ is the correct choice.

Now, according to the Property 5 the proposed ”almost” time-optimal SQRT-controller (9.15) can be used for position of the cylinder (10.3).

Consider position control of the system (10.3) using the SQRT controller (9.15). Such a system is shown in Figure 10.6. We will now, step by step, adapt the controller (9.15) to the requirements and operating conditions listed above.

Point 1 This requirement is already met by introducing the soft rate limiter.

Point 2 When $|e| < e_0$, where $e_0 > w_2$, a PI-controller will take over. See the next point.

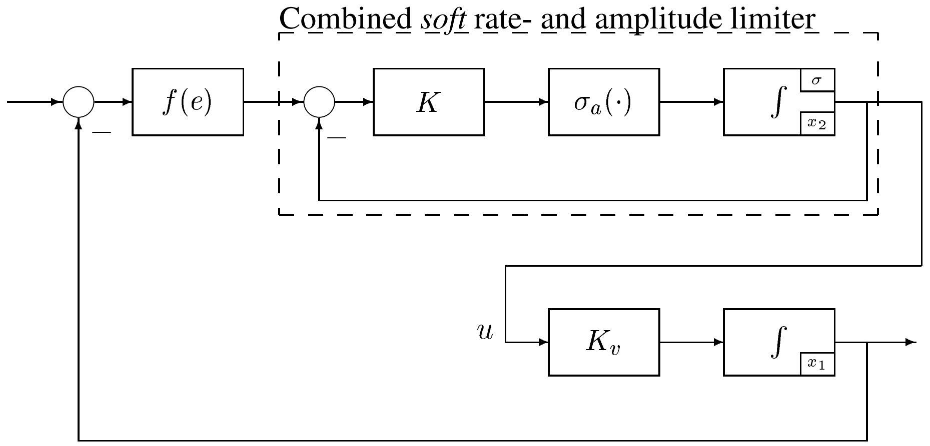

Figure 10.6: The controller scheme. In this description, the gain of the cylinder, K_v, is different in the forward and in the backward directions. See (10.2). In this block diagram we have moved the amplitude limiter representing the valves, into the soft *limiter. The soft limiter thereby becomes a combined rate- and amplitude limiter, see (2.4) and Figure 2.2.*

Point 3 What may violate this requirement is the PI-controller. If the integrator-state is set to zero at the switching event, the proportional part (that has derivative action on the differentiated signal) will work against the movement and may change the direction of the cylinder, at least for a short time. Therefore, we must se to that the output from the PI-controller, u_{PI} saturates downwards at zero when the control-error is positive, and saturates upwards at zero when the control-error is negative. The controller is shown in (10.6) below.

Point 4 The best performance would probably be obtained if K_v^b and K_v^f could be estimated every time a new container is to be moved. That was not considered as an option in this case. Therefore, K_v^b and K_v^f are estimated only at certain occasions, and then kept fixed. The estimation strategy is discussed under Point 7 below.

Point 5 In order to avoid numerical overflow and to obtain the best possible resolution, the control error is limited upwards to 250. The length of the cylinders are in some cases 1000 mm so the error will sometimes be 1000. The reason for setting the limit to 250 comes from the fact that

$$\min\left(\frac{2a}{K_v}\right) \approx 5000 \tag{10.4}$$

This means that the maximum valve opening, which corresponds to $u = 1000$ in the real control system, is reached for $|e| - w_2 \approx 200$. A typical size of w_2 was 20 mm and hence, $e_{max} = 250$ will be sufficient.

Point 6 The complete controller (10.5) is fairly easy to compute. The heaviest part is the square root operation, which we therefore implemented as a look-up table in the real controller.

Point 7 The choice of the *controller* parameters K_v^b and K_v^f, have significant effect on the tendency of the cylinder to overshoot. Too small values of K_v, used by the controller, will result in overshoots. Therefore, we estimate K_v^b and K_v^f when moving an empty container since this gives the highest values of K_v^b and K_v^f in a given system.

Recall from the discussion in the previous chapter that the SQRT-controller (9.15) is appropriate for avoiding overshoots, and so is the controller (10.5) proposed here, when tuned properly.

The complete controller is given by

Position controller

$$\begin{aligned}
u_{pos} &= f(e) \\
f(e) &= \begin{cases} \text{sign}(e)\sqrt{\frac{a}{K_v} 2c\sigma_0^{\infty}(|e| - w_2)} & |e| \geq e_0 \\ u_{PI} & w_1 < |e| < e_0 \\ 0 & |e| < w_1 \end{cases} \\
K_v &= \begin{cases} K_v^f & \text{unloaded, forward motion} \\ K_v^b & \text{unloaded, backward motion} \end{cases} \\
& e = \sigma_{-250}^{+250}(x_1^{ref} - x_1) \\
& 0 \leq w_2 < e_0 \ ,
\end{aligned} \tag{10.5}$$

where u_{PI} is given by

$$\Delta u_{PI}(t) = \begin{cases} K_p(\Delta e(t) + K_i T_s e(t)) & w_1 < |e| < e_0 \\ 0 & \text{otherwise} \end{cases}$$
$$u_{PI}(t) = \begin{cases} \text{sat}_0^{1000}(u_{PI}(t-1) + \Delta u_{PI}(t)) & e \geq 0 \\ \text{sat}_{-1000}^{0}(u_{PI}(t-1) + \Delta u_{PI}(t)) & e < 0\ . \end{cases} \tag{10.6}$$

10.2.1 Speed control

The spreader is not always maneuvered in terms of desired position but also desired speed. This means that the cylinders must have speed controllers as well as position controllers. Two different control strategies were considered initially:

1. Open loop control, where the output to the valve given in $\%$ will result in $\%$ of maximum obtainable speed and,

2. feedback control where the speed is estimated by taking the derivative of the measured position.

When deciding what strategy would be best, the fact that maximum obtainable speed (in terms of the gain K_v) is not known, must be taken into consideration. The fact that K_v is unknown and that it will change every time a new container is handled the maximum obtainable speed is unknown and varying. For the crane operator, who maneuvers the system using a joystick, the two different control strategies result in the following effects:

Open loop control
For a given and fixed joystick angle, i.e. for a given and fixed speed-reference, this strategy would typically not result in the desired speed of the cylinder. Furthermore, for a given and fixed joystick angle this strategy would not result in same cylinder speed for different values K_v. On the other hand, the maximum speed would be obtained for maximum possible angle of the joystick and the operator has ”contact” throughout the range of the joystick.

Feedback control
Feedback control gives the same speed for the same joystick angle even when the maximum obtainable speed is different. However, the operator do not know the joystick angle that corresponds to maximum obtainable speed and he will eventually reach a joystick angle where the speed saturates. He will then lose contact with the movement when increasing the joystick angle further.

The open loop control strategy for speed was considered to be the best strategy for this application and it is therefore used in the real control system. Open loop control of speed is simply obtained by replacing $f(e)$ from the position controller, by the desired speed reference in terms of $\%$ of maximum obtainable speed. Another reason for using feed forward is explained in Remark 10.3 and concerns synchronizing control.

10.2.2 Why not linear design appended with anti-windup

The first approach taken was to control the position of the cylinders using a PI controller having anti-windup compensation. This controller never fulfilled the specified requirements. It could not be tuned so that both small as well as large steps i position, result in a satisfactory performance. The imposed soft rate-limiter is the cause of this.

10.3 Synchronous control of two cylinders

In some situations, and applications, and for several reasons, the movement of two cylinders must be synchronized so that the deviation in the positions of two cylinders e_{1-2} do not exceed a maximum allowable limit e_{1-2}^{max}. The discussion in this section concerns synchronous control of two cylinders.

The control system must be able to handle the following situations and conditions well.

Requirements and operating conditions

1. All the requirements and conditions concerning control of one cylinder listed in Section 10.2, must be fulfilled.
2. The difference in position of the two cylinders, $e_{1-2} \triangleq x_1 - x_2$ must be kept smaller than 10 mm.
3. The controller is not allowed to move any of the cylinders backwards, see the condition 3 of Section 10.2.
4. The maximum obtainable speed of one cylinder can vary up to 300% when moving different containers and it may vary independently of the other cylinder, i.e., $K_{v1} \neq K_{v2}$. This is an unavoidable consequence when cylinders meet different resistance, e.g when handling two containers of different weights.

The requirements must be fulfilled both in case of speed, as well as position, control.

Point 1

We use the SQRT controller (10.5) for the control of each one of the two cylinders and then we add a *synchronizer*.

Points 2, 3 and 4

The proposed synchronizer operates so that it decreases the speed of the fastest cylinder when it is ahead of the slower one. The synchronizer operates by multiplying the control signal from the SQRT controller by a scalar $z(t) \in (0, 1]$. See Figure 10.7. The strongest synchronizing control action corresponds to $z \to 0$ and will stop one of the cylinders completely. Note that $\mathrm{sign}(zu) = \mathrm{sign}(u)$ which means that the synchronizer can not move any of the cylinders against the desired direction.

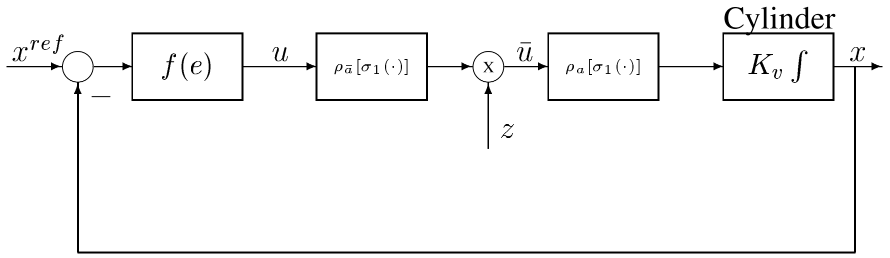

Figure 10.7: The synchronizer multiplies the possibly rate- and amplitude limited control signal u from either the position controller or the speed controller, by a number, z, which takes real values in the interval $(0, 1]$.

The proposed synchronizing controller is given by

Multiplicative synchronizing control action

$$\begin{aligned} \bar{u}_1(t) &= z_1(t)\rho_a[\sigma_1(u_1(t))] \\ \bar{u}_2(t) &= z_2(t)\rho_a[\sigma_1(u_2(t))] \end{aligned} \tag{10.7}$$

where u_1 and u_2 are either u_{pos} of (10.5) in case of position control, or the open loop feed forward control signal u_{spd} in case of speed control (see Section 10.2.1), used for the control of Cylinders 1 and 2, respectively. The synchronizer from which z_1 and z_2 are obtained is given by

Synchronizer

$$\begin{aligned}
z_1(t) &= 1 - [u_{sync}(t)]_0^1 \\
z_2(t) &= 1 + [u_{sync}(t)]_{-1}^0 \\
u_{sync}(t) &= I_{sync}(t) + P_{sync}(t) \\
P_{sync}(t) &= k_p e_{1-2}(t) \\
I_{sync}(t) &= \begin{cases} 0 & \text{reset instants} \\ \sigma_b(I_{sync}(t-1) + k_p k_i T_s) & \text{otherwise} \end{cases} \\
e_{1-2}(t) &= \begin{cases} (x_1 - x_2) & \text{if forward motion} \\ -(x_1 - x_2) & \text{if backward motion} \\ 0 & \text{if } e_1 \text{ or } e_2 \text{ inside window } w_1 \end{cases}
\end{aligned} \tag{10.8}$$

Remark 10.1 The reason why we introduce a second rate- and amplitude limiter in each loop (the ones in (10.7) that appears before the multiplication between u and z in Figure 10.7), is that it gives to a more gentle synchronizing control action in the phase of acceleration.

Remark 10.2 Note that the control error e_{1-2} in (10.8) is always positive when x_1 is ahead of x_2, irrespective of the direction of the motion. In this way, the integrator state I_{sync} built up during a movement in one direction, does not have to drain and build up a value of opposite sign, in case the direction of the motions is changed. Without this modification, synchronization will lost when changing direction.

The Figures 10.9 and 10.10 show simulations where the synchronizer is disabled and enabled, respectively. The Figure 10.11 show results obtained from experiments carried out on a real system. The Figure 10.12 show the difference between the positions of the two cylinders under the movement shown in Figure 10.11. Note that the second requirement listed above, which requires that the difference must be smaller that 10 mm, is, by far, met in this case.

Remark 10.3 Note that the multiplicative control strategy (10.7) would not work in case cylinder speed was controlled by feedback (which is not the case). If it was, the effect of the speed-decreasing action from the synchronizing controller would be effectively compensated for by the speed-feedback controller. Feed forward control will, however, not notice that the speed has decreased. This is, of course, a highly desirable property in this case. In case the multiplicative effect would

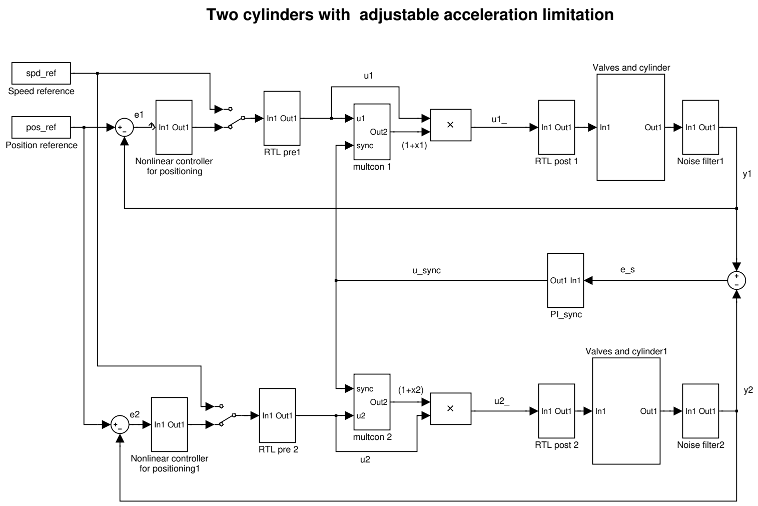

Figure 10.8: Synchronous controller scheme.

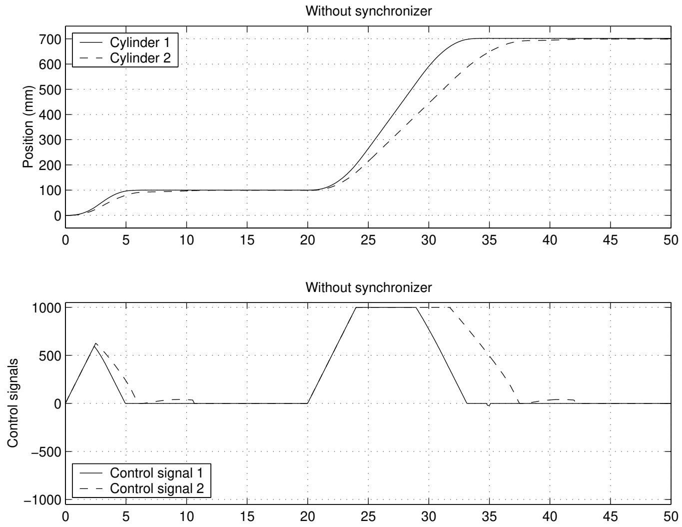

Figure 10.9: Synchronous control turned OFF.

be applied at the speed-reference input, in case of speed feedback, the unknown maximum speed level would cause a dead-zone in synchronizing control. This is due to the fact that the reference might exceed the maximum possible (unknown) speed. Thus, the multiplicative reduction of speed would not take effect until the reduced speed reference reaches the actual maximum value.

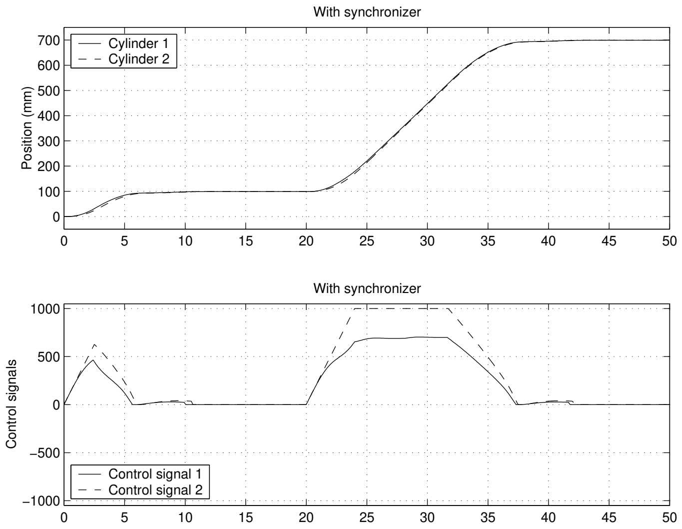

Figure 10.10: Synchronous control turned ON.

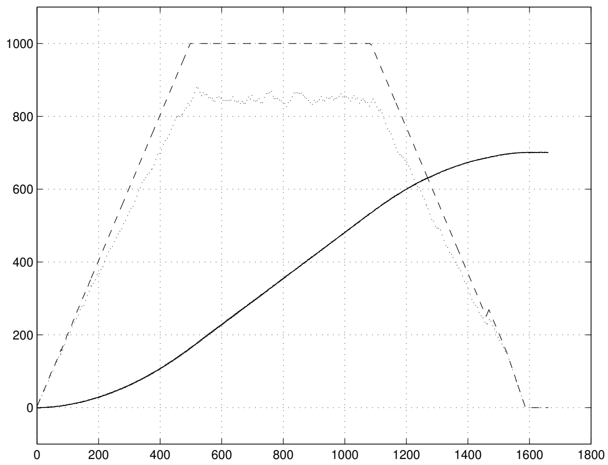

Figure 10.11: Synchronous control of a pair of real cylinders. The dotted line represent the output from the rate- and amplitude limiter operating on $\bar{u}_1$ and the dashed line represent the output from the rate- and amplitude limiter operating on $\bar{u}_2$. The positions x_1 and x_2 of the cylinders are almost equal. The difference $x_1 - x_2$ is shown in Figure 10.12 below.

Remark 10.4 In some application it might be desirable to move the two cylinders different distances, from different start-positions to different end-positions. This can be obtained by adding a reference, $r_{diff} \neq 0$, to the position error $x_1 - x_2$.

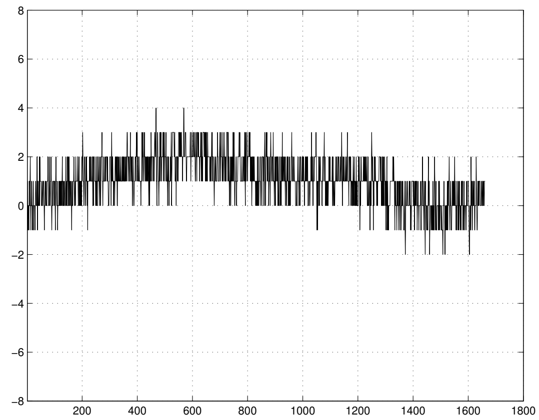

Figure 10.12: Difference in positions, $x_1 - x_2$ (mm). See Figure 10.11.

Such a solution is used in the real control system.

It is interesting to note that when two cylinders move with the same speed due to the fact that the synchronizer operates on one of them, then we have that

$$\begin{aligned} \dot{x}_1 &= K_{v1}\rho_a[\sigma_1(\bar{u}_1)] \\ &= \dot{x}_2 = K_{v2}\rho_a[\sigma_1(\bar{u}_2)] \ . \end{aligned} \tag{10.9}$$

The fraction K_{v1}/K_{v2} can then be calculated as

$$\frac{K_{v1}}{K_{v2}} = \frac{\rho_a[\sigma_1(\bar{u}_2)]}{\rho_a[\sigma_1(\bar{u}_1)]} \ . \tag{10.10}$$

This result can be seen as some kind of reversed adaptive control where good control is obtain first, by a multiplicative control action, and then the fraction of gains can be estimated from the control signals. This estimate can be useful in situations where it corresponds to some unknown but interesting physical property of the controlled system.

10.4 Simulations under varying conditions

The proposed controller given by (10.5) and (10.7)-(10.8) will here be used for control of a pair of cylinders subject to unknown variations. We will compare the results by the results obtained from using what can be considered as a MIMO (2x2) PI-controller with observer-based anti windup. The two inputs to this controller are: the difference in positions, $x_1 - x_2$ and the sum of the positions divided by 2, i.e. $(x_1 + x_2)/2$, respectively. We will therefore denote this controller by ”SUMDIFF” in this section. This controller was used in the real system at an early stage but since it failed to fulfill the requirements, a new controller was developed. This new controller is the one given by (10.5) and (10.7)-(10.8) and it will be denoted by ”SQRTSYNC” in this section.

Process variations
Descriptions of the variations we consider here is given next. Table 10.4 shows how they vary between different simulations.

acc-lim Here, the rate limit a is varied and since a is a parameter of the soft rate limiter, this variation in not unknown. The rest of variations listed below are, however, considered to be unknown. Nominally, we select both the rate limits (one for each cylinder) to be $(a_1, a_2) = (2, 2)$. This means that it will take 2 s to move the valve from closed to fully opened.

dyn Valve dynamics are introduced, see Figure 10.5. The nominal condition is $(2, 2)$ which means that the valves of both the cylinders have first order dynamics with time constants $T^f = T^b = 2$ s.

gain The process gains are given by

$$\begin{aligned} K_{v1}^f &= g_1 \cdot 66,\ K_{v1}^b = g_1 \cdot 101 \\ K_{v2}^f &= g_2 \cdot 66,\ K_{v2}^b = g_2 \cdot 101\ , \end{aligned} \tag{10.11}$$

where (g_1, g_2) are varied between the simulations. Nominally we have $(g_1, g_2) = (1, 0.8)$.

noise Band-limited white noise is added to the measured positions. The nominal condition is $(0, 0)$, i.e. noise free measurements.

dist Pulse-disturbances act at the cylinder inputs every 8:th second with a duration of 0.02 seconds. The amplitude varies according to Table 10.4. The nominal value of the amplitude is $(0, 0)$, i.e. no disturbances.

init-pos Here, we let the cylinders have different initial positions when the simulation starts. This test put extra high requirements on the synchronizing action of the controllers. The nominal condition is that both cylinders are in the position $(0, 0)$ initially.

Cond	**acc-lim**	**dyn**	**gain**	**noise**	**dist**	**init-pos**
nom	2	(0.2 0.2)	(1 0.8)	(0 0)	(0 0)	(0 0)
dyn0	nom	(0 0)	nom	nom	nom	nom
dyn05	nom	(0.5 0.5)	nom	nom	nom	nom
gain11	nom	nom	(1 1)	nom	nom	nom
gain78	nom	nom	(0.7 0.56)	nom	nom	nom
noise	nom	nom	nom	(0.1 0.1)	nom	nom
inpdist	nom	nom	nom	nom	(70% 0)	nom
intpos200	nom	nom	nom	nom	nom	(20 0)
intpos020	nom	nom	nom	nom	nom	(0 20)
acclim01	(0.1 0.1)	nom	nom	nom	nom	nom
acclim6	(6 6)	nom	nom	nom	nom	nom
allpos	(6 6)	(0.5 0.5)	(0.7 0.56)	nom	(70% 0)	(0 20)
allpos0d	(6 6)	(0.5 0.5)	(0.7 0.56)	nom	(0 0)	(0 20)
poschange	nom	(0.5 0.5)	(0.7 0.56)	nom	(0 0)	(0 20)

Comments and conclusions From the results of the simulations shown in Figures 10.13-10.26 we can conclude that the proposed controller (10.5), (10.7)-(10.8) here denoted SQRTSYNC, show exceptional performance in all the different situations. The controller SUMDIFF on the other hand performs, assuredly, well in some situations but fails completely in other. Under the conditions ”allpos” and ”allpos0d” (see Table 10.4), the use of the controller SUMDIFF gives an unstable system.

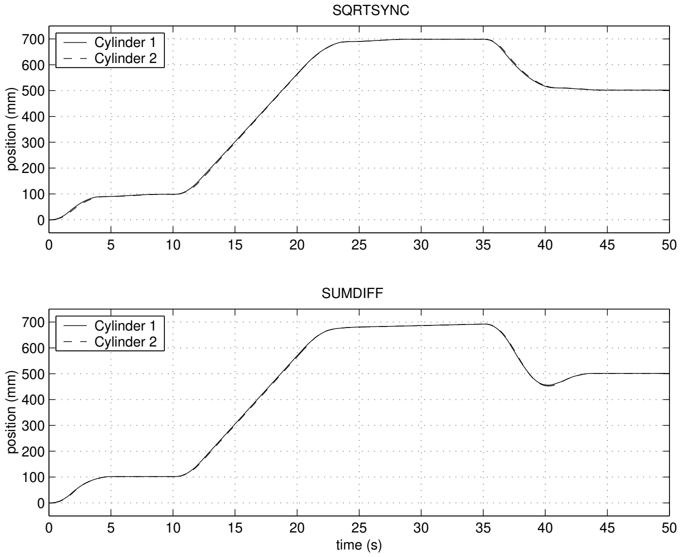

Figure 10.13: Synchronous control under nominal conditions

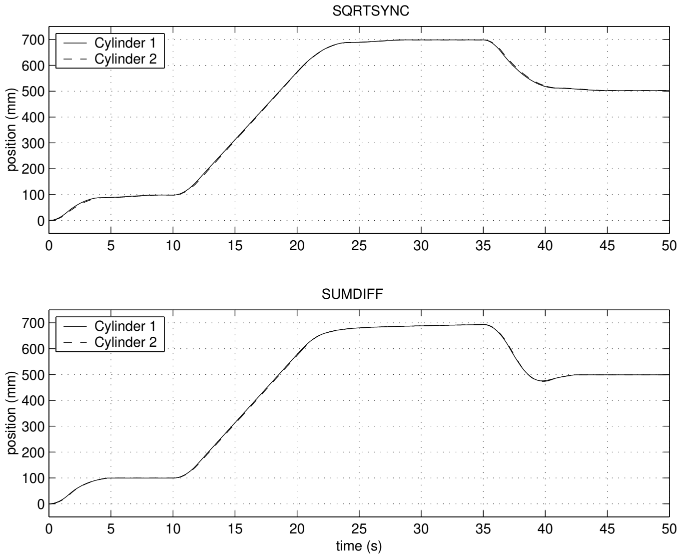

Figure 10.14: Synchronous control under dyn0 conditions

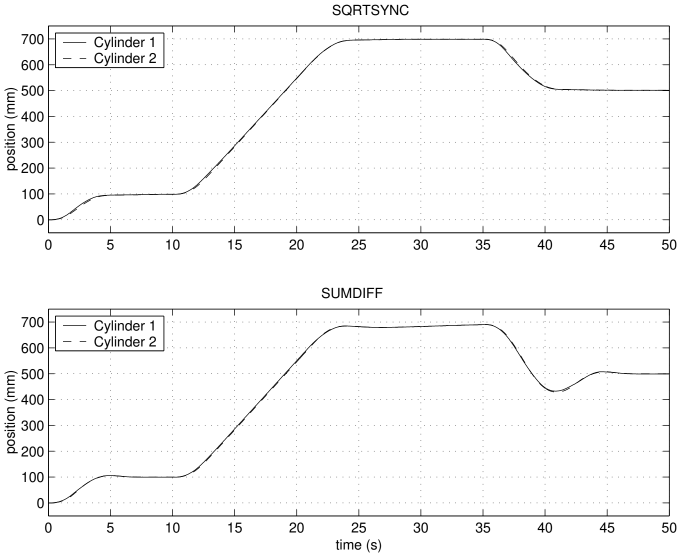

Figure 10.15: Synchronous control under dyn05 conditions

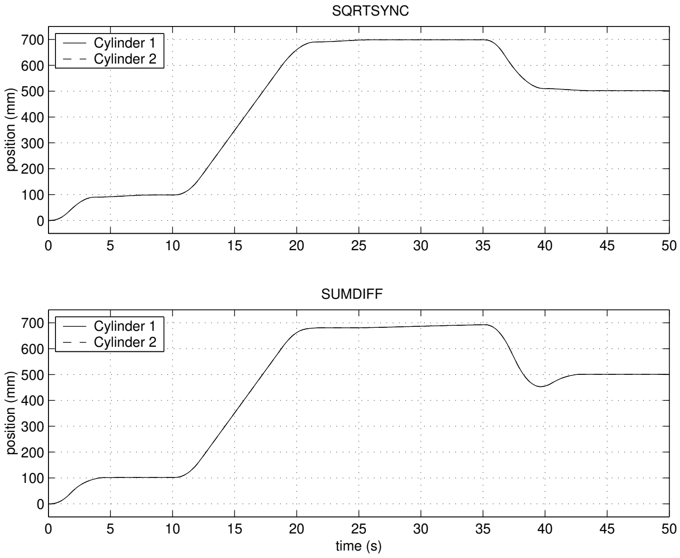

Figure 10.16: Synchronous control under gain11 conditions

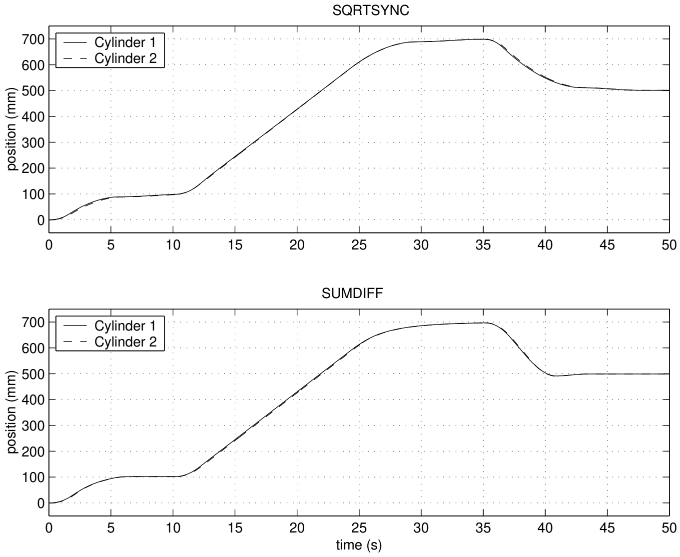

Figure 10.17: Synchronous control under gain 78 conditions

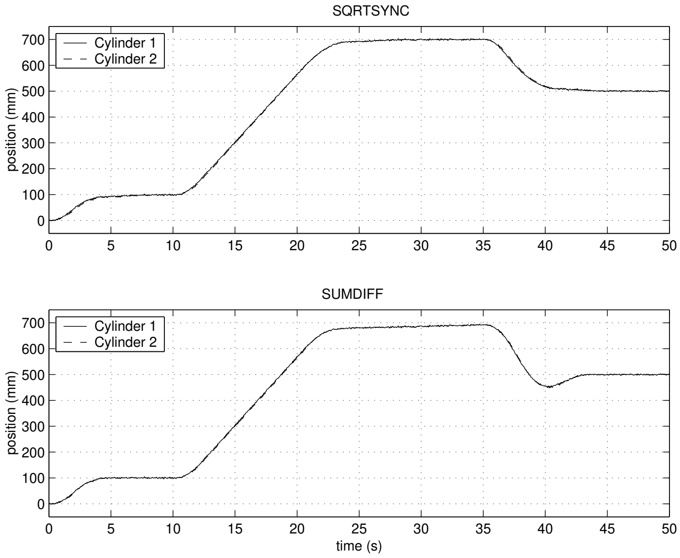

Figure 10.18: Synchronous control under noise conditions

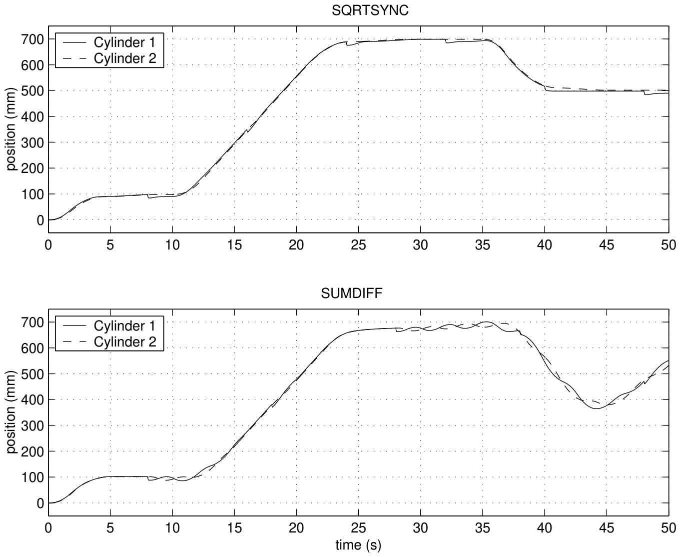

Figure 10.19: Synchronous control under inpdist conditions

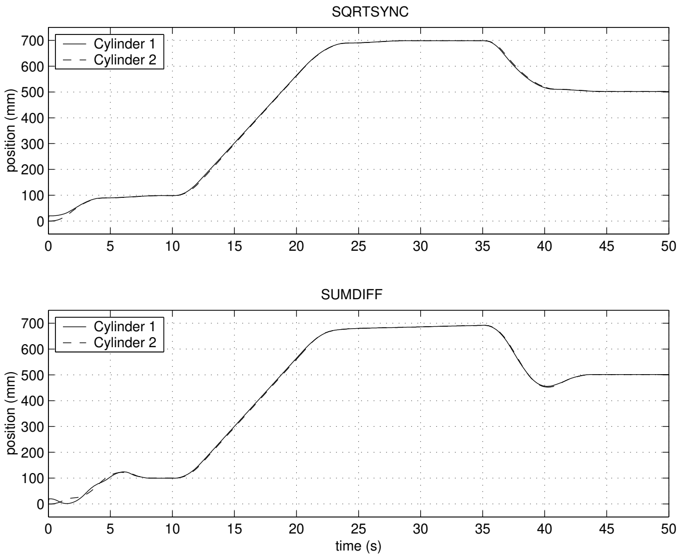

Figure 10.20: Synchronous control under intpos200 conditions

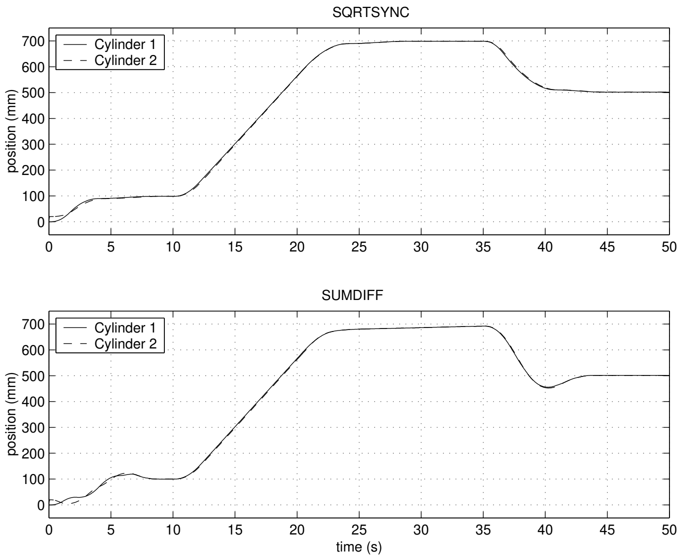

Figure 10.21: Synchronous control under intpos020 conditions

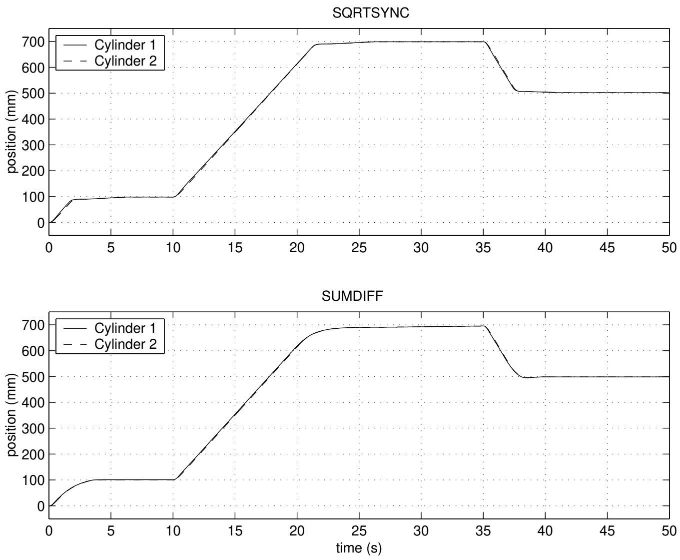

Figure 10.22: Synchronous control under acclim01 conditions

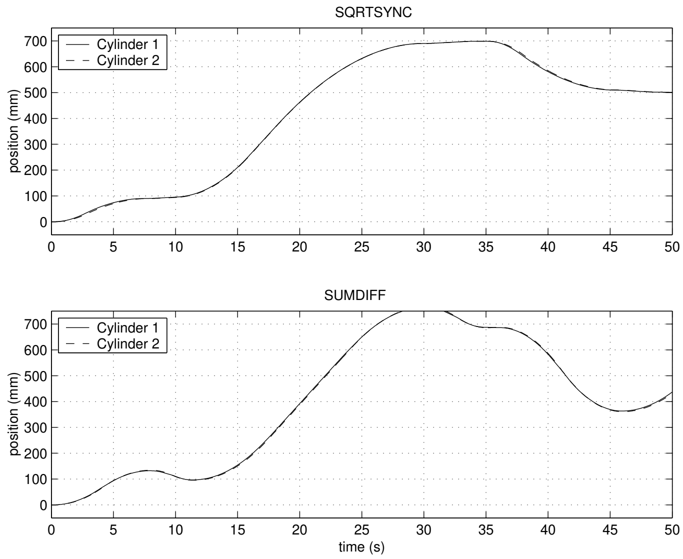

Figure 10.23: Synchronous control under acclim6 conditions

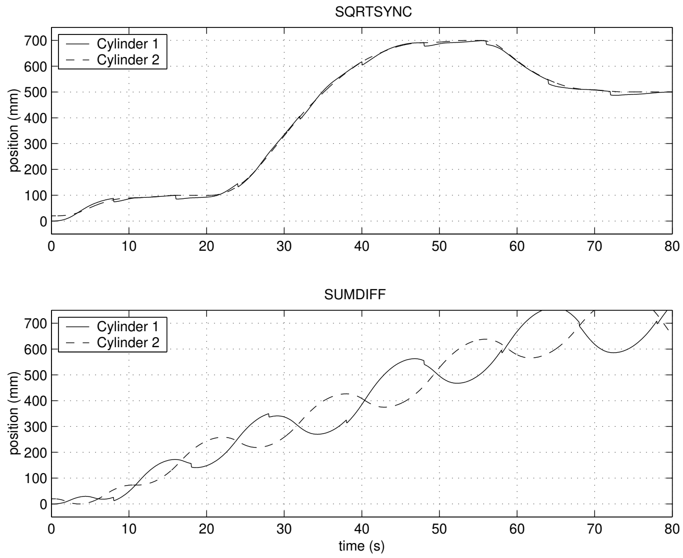

Figure 10.24: Synchronous control under allpos conditions

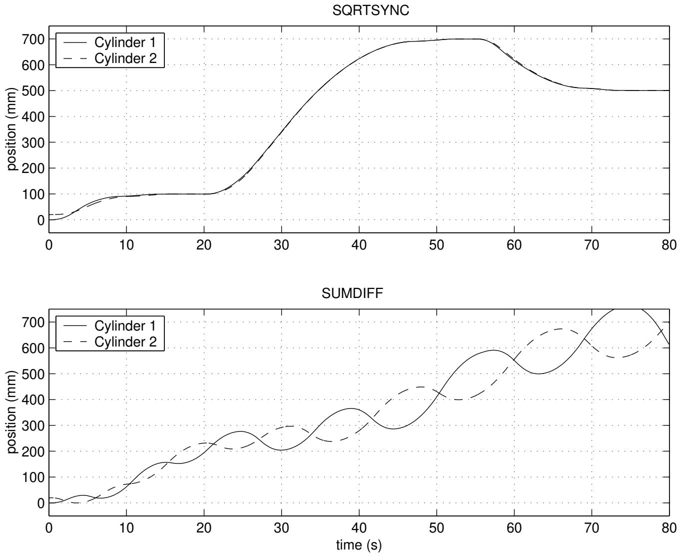

Figure 10.25: Synchronous control under allpos0d conditions

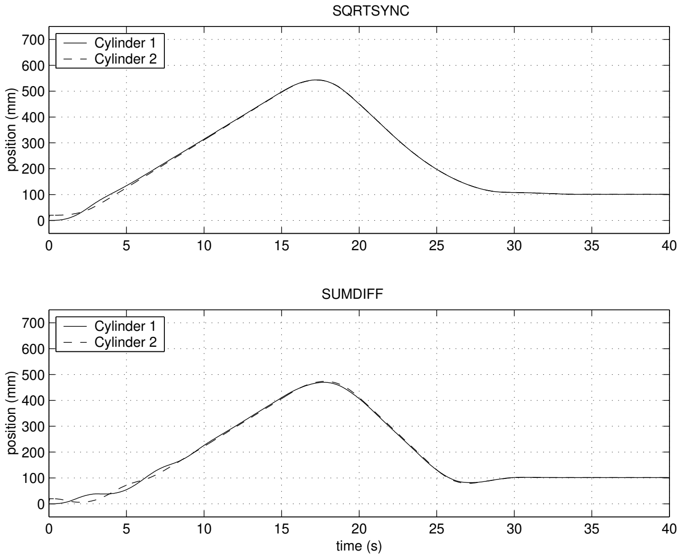

Figure 10.26: Synchronous control under poschange conditions

CHAPTER 11

Suggestions for future work

Many researchers in the academic community leer at the industry in order to find new interesting applications for their methods, tools and solutions and also in order to find new problems to work on. This is, in my opinion, sound. However, one can also look for solutions in the industry! Solutions that often lie outside the standard concepts used by researchers and students in the academic community and that can be, not only interesting solutions as such, but also embryos of new concepts. My recommendation for future research is the following: Find out what company or institution could be your potential partner and give them a call. Now! And do not hesitate to contact companies that do not have strong research traditions. I am confident that you will find not only problems and applications of interest but also *solutions* that may be that embryo of a new solution, new concept or even a new research field.

APPENDIX A

Derivations in Chapter 2

A.1 Derivations in Chapter 2

A.1.1 Linear system

The plant output of the linear system ($\psi \equiv 0$) is given by

$$y = \boldsymbol{B}\boldsymbol{A}^{-1}(u_l + \beta)\ . \tag{A.1}$$

Here, the controller output u_l from the linear, nominal controller, is given by

$$\begin{aligned}
\boldsymbol{R}u_l &= \boldsymbol{T}r - \boldsymbol{S}y && \text{(A.2)}\\
&= \boldsymbol{T}r - \boldsymbol{S}\boldsymbol{B}\boldsymbol{A}^{-1}(u_l + \beta) && \text{(A.3)}\\
&= \boldsymbol{T}r - \boldsymbol{S}\boldsymbol{B}\boldsymbol{A}^{-1}\beta - \boldsymbol{S}\boldsymbol{B}\boldsymbol{A}^{-1}u_l && \text{(A.4)}
\end{aligned}$$

Collecting the u_l-terms on the right hand side gives

$$\begin{aligned}
(\boldsymbol{R} + \boldsymbol{S}\boldsymbol{B}\boldsymbol{A}^{-1})u_l &= \boldsymbol{T}r - \boldsymbol{S}\boldsymbol{B}\boldsymbol{A}^{-1}\beta && \text{(A.5)}\\
(\boldsymbol{R}\boldsymbol{A} + \boldsymbol{S}\boldsymbol{B})\boldsymbol{A}^{-1})u_l &= \boldsymbol{T}r - \boldsymbol{S}\boldsymbol{B}\boldsymbol{A}^{-1}\beta && \text{(A.6)}\\
\boldsymbol{\alpha}\boldsymbol{A}^{-1}u_l &= \boldsymbol{T}r - \boldsymbol{S}\boldsymbol{B}\boldsymbol{A}^{-1}\beta && \text{(A.7)}
\end{aligned}$$

and hence

$$u_l = \boldsymbol{A}\boldsymbol{\alpha}^{-1}(\boldsymbol{T}r - \boldsymbol{S}\boldsymbol{B}\boldsymbol{A}^{-1}\beta). \tag{A.8}$$

We will now derive the closed loop transfer functions from the reference signal vector r, and the disturbance signal vector β, to the output y. Notice that from (A.8) we have that

$$\boldsymbol{A}^{-1}u_l \;=\; \boldsymbol{\alpha}^{-1}(\boldsymbol{T}r - \boldsymbol{S}\boldsymbol{B}\boldsymbol{A}^{-1}\beta). \tag{A.9}$$

Adding the term $\boldsymbol{A}^{-1}\beta$ to this expression gives

$$\begin{aligned}\boldsymbol{A}^{-1}(u_l+\beta) \;&=\; \boldsymbol{\alpha}^{-1}(\boldsymbol{T}r - \boldsymbol{S}\boldsymbol{B}\boldsymbol{A}^{-1}\beta) + \boldsymbol{A}^{-1}\beta \\ &=\; \boldsymbol{\alpha}^{-1}\boldsymbol{T}r + (\mathbf{I} - \boldsymbol{\alpha}^{-1}\boldsymbol{S}\boldsymbol{B})\boldsymbol{A}^{-1}\beta \\ &=\; \boldsymbol{\alpha}^{-1}\boldsymbol{T}r + \alpha^{-1}(\alpha - \boldsymbol{S}\boldsymbol{B})\boldsymbol{A}^{-1}\beta\,. \end{aligned} \tag{A.10}$$

Since $\alpha \;=\; \boldsymbol{R}\boldsymbol{A} + \boldsymbol{S}\boldsymbol{B}$, the term $(\alpha - \boldsymbol{S}\boldsymbol{B}) \;=\; \boldsymbol{R}\boldsymbol{A}$. Then we have that

$$\boldsymbol{A}^{-1}(u_l+\beta) \;=\; \boldsymbol{\alpha}^{-1}\boldsymbol{T}r + \alpha^{-1}\boldsymbol{R}\beta\,. \tag{A.11}$$

Finally, we can express the output $y = y_l$ in the following way

$$y_l \;=\; \boldsymbol{B}\boldsymbol{A}^{-1}(u_l+\beta) \;=\; \boldsymbol{B}\boldsymbol{\alpha}^{-1}\boldsymbol{T}r + \boldsymbol{B}\alpha^{-1}\boldsymbol{R}\beta\,. \tag{A.12}$$

A.1.2 Amplitude limiter

According to (2.6) we have that

$$\sigma_a^b(v_1+u_2) \;=\; \max[a, \min(b, v_1+u_2)] \tag{A.13}$$

where

$$\min(b, v_1+u_2) \;=\; \min(b-v_1, u_2) + v_1\,. \tag{A.14}$$

Insertion of (A.14) into (A.13) gives

$$\begin{aligned}\max[a, \min(b-v_1, u_2)+v_1] \;&=\; \max[a-v_1, \min(b-v_1, u_2)] + v_1 \\ &=\; \sigma_{a-v_1}^{b-v_1}(u_2) + v_1\,. \end{aligned} \tag{A.15}$$

This ends the proof.

A.1.3 Combined rate- and amplitude limiter

The expressions

$$\begin{aligned} v(t) \;&=\; \sigma_a^b(v(t-1) + T_s u_i(t)) \\ u_i(t) \;&=\; \sigma_c^d\Big(\frac{(u(t)-v(t-1))}{T_s}\Big)\,. \end{aligned} \tag{A.16}$$

are given. Here

$$u = u_{fb} + v_{ff} \tag{A.17}$$

where the feed-forward control signal v_{ff} passes through the limiter (A.16) unaltered, i.e.,

$$v(t) = v_{ff}(t) + v_{fb}(t)\ . \tag{A.18}$$

Here v_{fb} represents the limited value of the feedback control signal u_{fb}. Hence, (A.16) can be written as

$$\begin{aligned} v(t) &= \sigma_a^b(v_{ff}(t-1) + v_{fb}(t-1) + T_s u_i(t)) \\ u_i(t) &= \sigma_c^d\left(\frac{(u_{fb}(t) + v_{ff}(t) - v_{ff}(t-1) - v_{fb}(t-1))}{T_s}\right)\ . \end{aligned} \tag{A.19}$$

We define

$$\Delta v_{ff}(t) \triangleq v_{ff}(t) - v_{ff}(t-1)\ . \tag{A.20}$$

Expanding the expression for u_i in (A.19) after inserting (A.18) gives

$$\begin{aligned} u_i(t) &= \sigma_c^d\left(\frac{u_{fb}(t) + \Delta v_{ff}(t) - v_{fb}(t-1)}{T_s}\right) \\ &= \max[c, \min(d, \frac{u_{fb}(t) + \Delta v_{ff}(t) - v_{fb}(t-1)}{T_s})]\ . \end{aligned} \tag{A.21}$$

Subtracting $\frac{\Delta v_{ff}(t)}{T_s}$ from the arguments in the "min"-function gives

$$u_i(t) = \max[c, \min(d - \frac{\Delta v_{ff}(t)}{T_s}, \frac{u_{fb}(t) - v_{fb}(t-1)}{T_s}) + \frac{\Delta v_{ff}(t)}{T_s}] \tag{A.22}$$

and then, subtracting $\frac{\Delta v_{ff}(t)}{T_s}$ from the arguments in the max-function gives

$$\begin{aligned} u_i(t) &= \max[c - \frac{\Delta v_{ff}(t)}{T_s}, \min(d - \frac{\Delta v_{ff}(t)}{T_s}, \frac{u_{fb}(t) - v_{fb}(t-1)}{T_s})] + \frac{\Delta v_{ff}(t)}{T_s} \\ &= \sigma_{c - \frac{\Delta v_{ff}(t)}{T_s}}^{d - \frac{\Delta v_{ff}(t)}{T_s}}\left(\frac{u_{fb}(t) - v_{fb}(t-1)}{T_s}\right) + \frac{\Delta v_{ff}(t)}{T_s} \end{aligned} \tag{A.23}$$

Hence

$$\begin{aligned} u_i(t) &= \sigma_{\bar{c}(t)}^{\bar{d}(t)}\left(\frac{u_{fb}(t) - v_{fb}(t-1)}{T_s}\right) + \frac{\Delta v_{ff}(t)}{T_s} \\ \bar{c}(t) &\triangleq c - \frac{\Delta v_{ff}(t)}{T_s} \\ \bar{d}(t) &\triangleq d - \frac{\Delta v_{ff}(t)}{T_s}\ . \end{aligned} \tag{A.24}$$

The output v can then be written as

$$\begin{aligned} v(t) &= \sigma_a^b(v(t-1) + T_s\sigma_{\bar{c}(t)}^{\bar{d}(t)}(\frac{u_{fb}(t) - v_{fb}(t-1)}{T_s}) + T_s\frac{\Delta v_{ff}(t)}{T_s}) \\ &= \sigma_a^b(v(t-1) + T_s\sigma_{\bar{c}(t)}^{\bar{d}(t)}(\frac{u_{fb}(t) - v_{fb}(t-1)}{T_s}) + \Delta v_{ff}(t)) \ . \end{aligned} \tag{A.25}$$

Using (A.18) and (A.20) we have that

$$\begin{aligned} v(t) &= \sigma_a^b(v_{ff}(t-1) + v_{fb}(t-1) + T_s\sigma_{\bar{c}(t)}^{\bar{d}(t)}(\frac{u_{fb}(t) - v_{fb}(t-1)}{T_s}) + v_{ff}(t) - v_{ff}(t-1)) \\ &= \sigma_a^b(v_{ff}(t) + v_{fb}(t-1) + T_s\sigma_{\bar{c}(t)}^{\bar{d}(t)}(\frac{u_{fb}(t) - v_{fb}(t-1)}{T_s})) \ . \end{aligned} \tag{A.26}$$

From the proof concerning the amplitude limiter in A.1.2 (substituting v_1 for v_{ff}) we have that

$$v(t) = \sigma_{a-v_{ff}(t)}^{b-v_{ff}(t)}(v_{fb}(t-1) + T_s\sigma_{\bar{c}(t)}^{\bar{d}(t)}(\frac{u_{fb}(t) - v_{fb}(t-1)}{T_s})) + v_{ff}(t) \ . \tag{A.27}$$

This ends the proof.

APPENDIX B

Derivations in Chapters 3, 4 and 5

B.1 Derivations in Chapter 3

B.1.1 The de-saturation transient dynamics of the nominal control system

We want to derive the transfer function from $\delta \triangleq v - u$ to y. This can be done by first add and then subtract u at the plant input, i.e.,

$$\begin{aligned} y &= \boldsymbol{BA}^{-1}(v + \beta) \\ &= \boldsymbol{BA}^{-1}(v - u + u + \beta) \\ &= \boldsymbol{BA}^{-1}(\delta + \beta + u) \ . \end{aligned} \tag{B.1}$$

The plant is controlled by the nominal controller in (2.2)

$$\boldsymbol{R}u = \boldsymbol{T}r - \boldsymbol{S}y \ . \tag{B.2}$$

Notice that δ enters the plant input in the same way as β . This means that the transfer function we are seeking will be the same as the one for β, namely $\boldsymbol{B}\alpha^{-1}\boldsymbol{R}$, which we derived earlier in Appendix A.1.1. Hence, we have that

$$y_\delta = \boldsymbol{B}\alpha^{-1}\boldsymbol{R}\delta \ . \tag{B.3}$$

B.2 Derivations in Chapter 4

B.2.1 Objective 1 for the OBSAWC

When the loop is intact, i.e. $v \equiv u$, we have that

$$\begin{aligned} u_o &= \boldsymbol{A}_o^{-1}(\boldsymbol{A}_o - \boldsymbol{R})u_o + \boldsymbol{A}_o^{-1}(-\boldsymbol{S}y + \boldsymbol{T}r) \\ &= (\mathbf{I} - \boldsymbol{A}_o^{-1}\boldsymbol{R})u_o + \boldsymbol{A}_o^{-1}(-\boldsymbol{S}y + \boldsymbol{T}r) \end{aligned} \tag{B.4}$$

and collecting all the u-terms on the right hand side gives

$$\boldsymbol{A}_o^{-1}\boldsymbol{R}u = \boldsymbol{A}_o^{-1}(-\boldsymbol{S}y + \boldsymbol{T}r)\ . \tag{B.5}$$

Due to the Requirement 4.1, we have, after a transient, that

$$\boldsymbol{R}u(k) = -\boldsymbol{S}y(k) + \boldsymbol{T}r(k)\ . \tag{B.6}$$

This expression is equivalent to (2.2). Notice that before saturation ever occur, $\boldsymbol{A}_0$ has no influence on u and hence, the control action will always be identical to that in (2.2).

B.2.2 Controllers and OBSAWC:s in state-space form

When discussed in the literature the OBSAWC is often represented by a state space description. We will therefore provide the reader with connections between polynomial- and state space descriptions of anti-windup compensators. For an explanation of the nomenclature see the Remarks on the notations at the beginning of the thesis.

The nominal controller (2.2) is assumed to be represented by the following state space description

$$\begin{aligned} u &= \boldsymbol{R}^{-1}(\boldsymbol{T}r - \boldsymbol{S}y) \\ &\sim \left[\begin{array}{c|c} \mathbf{A}_c & \mathbf{B}_c \\ \hline \mathbf{C}_c & \mathbf{D}_c \end{array}\right] \begin{pmatrix} r \\ y \end{pmatrix}\ . \end{aligned} \tag{B.7}$$

Here $\mathbf{B}_c = [\mathbf{B}_{cr}\ \mathbf{B}_{cy}]$ and $\mathbf{D}_c = [\mathbf{D}_{cr}\ \mathbf{D}_{cy}]$ where the matrices inside the brackets represent the entries for r and y respectively. Hence, $\mathbf{B}_c$ and $\mathbf{D}_c$ are entries for the stacked vector $[r\ y]^T$.

For the special choice $\boldsymbol{R}_o = \mathbf{R}_o \in \Re^{pxp}$ is a constant matrix, the observer-based anti-windup compensated controller in (4.6) can be represented by

$$\begin{aligned} u_o &= \boldsymbol{R}^{-1}(\boldsymbol{T}r - \boldsymbol{S}y + \boldsymbol{R}_o(v-u_o)) \\ &\sim \left[\begin{array}{c|c} \mathbf{A}_c & [\mathbf{B}_c\,\mathbf{K}_o] \\ \hline \mathbf{C}_c & [\mathbf{D}_c\,\mathbf{0}] \end{array}\right] \begin{pmatrix} r \\ y \\ v-u_o \end{pmatrix} \end{aligned} \tag{B.8}$$

where $\mathbf{K}_o$ is the entry for $v - u_o$. In a similar way, the controller in (4.5) can be represented by

$$\begin{aligned} u_o &= \boldsymbol{A}_o^{-1}(\boldsymbol{T}r - \boldsymbol{S}y + \boldsymbol{R}_o v) \\ &= \left[\begin{array}{c|c} \mathbf{A}_c - \mathbf{K}_o\mathbf{C}_c & [\mathbf{B}_c - \mathbf{K}_o\mathbf{D}_c\ \ \mathbf{K}_o] \\ \hline \mathbf{C}_c & [\mathbf{D}_c\,\mathbf{0}] \end{array}\right] \begin{pmatrix} r \\ y \\ v \end{pmatrix} \end{aligned} \tag{B.9}$$

see, e.g., [3]. As we pointed out earlier the control actions, of (B.8) and (B.9) are identical although their state space representations are different.

The two (alternative) additional anti-windup compensators in (4.9), that makes the OBSAWC a GLAWC, can, of course, also be represented by state space descriptions. Given a state space representation of the first compensator in (4.9)

$$(\boldsymbol{P}_1 - \boldsymbol{P}_2)\boldsymbol{P}_2^{-1} \sim \left[\begin{array}{c|c} \mathbf{A}_p & \mathbf{B}_p \\ \hline \mathbf{C}_p & \mathbf{0} \end{array}\right] \tag{B.10}$$

then, the other compensator of (4.9) can be expressed as

$$(\boldsymbol{P}_1 - \boldsymbol{P}_2)\boldsymbol{P}_1^{-1} \sim \left[\begin{array}{c|c} \mathbf{A}_p - \mathbf{B}_p\mathbf{C}_p & \mathbf{B}_p \\ \hline -\mathbf{C}_p & \mathbf{0} \end{array}\right]\ . \tag{B.11}$$

Error feedback

In case the input to the nominal controller is the difference between the reference and the measured plant output, i.e., $e = r - y$ (error feedback), the controller in (B.7) can be rewritten is a more simple form. In case of error feedback, we have that

$$\begin{aligned} [\mathbf{B}_{cr}\ \mathbf{B}_{cy}] \begin{pmatrix} r \\ y \end{pmatrix} &= \mathbf{B}_e(r-y) \\ \mathbf{B}_{cr} = -\mathbf{B}_{cy} &= \mathbf{B}_e \end{aligned} \tag{B.12}$$

and

$$
\begin{aligned}
[\mathbf{D}_{cr}\ \mathbf{D}_{cy}] \begin{pmatrix} r \\ y \end{pmatrix} &= \mathbf{D}_e(r-y) \\
\mathbf{D}_{cr} = -\mathbf{D}_{cy} &= \mathbf{D}_e \ .
\end{aligned}
\tag{B.13}
$$

The nominal controller (B.7) can then be written in the following way

$$
\begin{aligned}
u &= \boldsymbol{R}^{-1}\boldsymbol{S}(r-y) \\
&= \left[\begin{array}{c|c} \mathbf{A}_c & \mathbf{B}_e \\ \hline \mathbf{C}_c & \mathbf{D}_e \end{array}\right](r-y).
\end{aligned}
\tag{B.14}
$$

It is straight forward to rewrite the OBSAWC according to this, and it will not be done here.

We have discussed connections between polynomial representations and state-space representations of anti-windup compensators. An important factor that one must consider when building controllers (or AWC:s), may it be in reality or in simulators, is controller realization. This is due to numerical aspects. For practical guidelines on this topic, see e.g. [3].

B.2.3 Alternative representation of the GLAWC

The GLAWC defined by (4.1), (4.8) and the first line of (4.9) is given by

$$
\begin{aligned}
u &= u_o + (\boldsymbol{P}_1 - \boldsymbol{P}_2)\boldsymbol{P}_2^{-1}(v-u) \\
\boldsymbol{A}_o u_o &= (\boldsymbol{A}_o - \boldsymbol{R})v + \boldsymbol{T}r - \boldsymbol{S}y \ .
\end{aligned}
\tag{B.15}
$$

We will show that this controller can be written on the form of (4.15). First, we multiply the first line in (B.15) by $\boldsymbol{A}_o$ which gives that

$$
\begin{aligned}
\boldsymbol{A}_o u &= \boldsymbol{A}_o u_o + \boldsymbol{A}_o(\boldsymbol{P}_1 - \boldsymbol{P}_2)\boldsymbol{P}_2^{-1}(v-u) \\
&= \boldsymbol{A}_o u_o + (\boldsymbol{A}_o\boldsymbol{P}_1\boldsymbol{P}_2^{-1} - \boldsymbol{A}_o)(v-u) \\
&= \boldsymbol{A}_o u_o + (\boldsymbol{A}_o\boldsymbol{P}_1\boldsymbol{P}_2^{-1} - \boldsymbol{A}_o)v - (\boldsymbol{A}_o\boldsymbol{P}_1\boldsymbol{P}_2^{-1} - \boldsymbol{A}_o)u \ .
\end{aligned}
\tag{B.16}
$$

Collecting all u-terms to the left gives

$$
\boldsymbol{A}_o\boldsymbol{P}_1\boldsymbol{P}_2^{-1}u = \boldsymbol{A}_o u_o + (\boldsymbol{A}_o\boldsymbol{P}_1\boldsymbol{P}_2^{-1} - \boldsymbol{A}_o)v \ . \tag{B.17}
$$

According to (4.15), $\boldsymbol{A}_o\boldsymbol{P}_1\boldsymbol{P}_2^{-1} = \boldsymbol{\mathcal{W}}^{-1}$ which allows us to rewrite (B.17) as

$$
\boldsymbol{\mathcal{W}}^{-1}u = \boldsymbol{A}_o u_o + (\boldsymbol{\mathcal{W}}^{-1} - \boldsymbol{A}_o)v \ . \tag{B.18}
$$

Now, we substitute $\boldsymbol{A}_o u_o$ on the right hand side of (B.18) by the second line of (B.15) which allows us to rewrite (B.18) as

$$\begin{aligned}\boldsymbol{\mathcal{W}}^{-1}u &= (\boldsymbol{A}_o - \boldsymbol{R})v + \boldsymbol{T}r - \boldsymbol{S}y + (\boldsymbol{\mathcal{W}}^{-1} - \boldsymbol{A}_o)v \\ &= (\boldsymbol{A}_o - \boldsymbol{R} + \boldsymbol{\mathcal{W}}^{-1} - \boldsymbol{A}_o)v + \boldsymbol{T}r - \boldsymbol{S}y \\ &= (\boldsymbol{\mathcal{W}}^{-1} - \boldsymbol{R})v + \boldsymbol{T}r - \boldsymbol{S}y \ . \end{aligned} \tag{B.19}$$

Finally, we multiply both sides from the left by $\boldsymbol{\mathcal{W}}$ to obtain the final expression

$$u = (\mathbf{I} - \boldsymbol{\mathcal{W}}\boldsymbol{R})v + \boldsymbol{\mathcal{W}}(\boldsymbol{T}r - \boldsymbol{S}y) \ . \tag{B.20}$$

This ends the proof.

B.2.4 Loop transfer function: OBSAWC

Since the OBSAWC can be obtained by selecting $\boldsymbol{P}_1 \equiv \boldsymbol{P}_2$ $(= \mathbf{I}$ e.g.$)$ in the GLAWC structure, we will here use the results presented in Section B.2.5 concerning the GLAWC. Then, it is straightforward to show that the loop transfer function is given by

$$\boldsymbol{\mathcal{L}}_v = \boldsymbol{A}_o^{-1}\boldsymbol{\alpha}\boldsymbol{A}^{-1} - \mathbf{I} \tag{B.21}$$

when using the OBSAWC. See Section B.2.5.

B.2.5 Loop transfer function: GLAWC

In order to keep the expressions clear, we will use the controller (4.15), i.e.,

$$u = (\mathbf{I} - \boldsymbol{\mathcal{W}}\boldsymbol{R})v + \boldsymbol{\mathcal{W}}(\boldsymbol{T}r - \boldsymbol{S}y) \tag{B.22}$$

in the derivation. By substituting y for the expression of the plant output (2.1), we have that

$$\begin{aligned}u &= (\mathbf{I} - \boldsymbol{\mathcal{W}}\boldsymbol{R})v - \boldsymbol{\mathcal{W}}\boldsymbol{S}\boldsymbol{B}\boldsymbol{A}^{-1}v \\ &\quad + \boldsymbol{\mathcal{W}}\boldsymbol{T}r - \boldsymbol{\mathcal{W}}\boldsymbol{S}\boldsymbol{B}\boldsymbol{A}^{-1}\beta \\ &= (\mathbf{I} - \boldsymbol{\mathcal{W}}(\boldsymbol{R} + \boldsymbol{S}\boldsymbol{B}\boldsymbol{A}^{-1})v + \boldsymbol{\mathcal{W}}(\boldsymbol{T}r - \boldsymbol{S}\boldsymbol{B}\boldsymbol{A}^{-1}\beta) \\ &= -(\boldsymbol{\mathcal{W}}\boldsymbol{\alpha}\boldsymbol{A}^{-1} - \mathbf{I})v + \boldsymbol{\mathcal{W}}(\boldsymbol{T}r - \boldsymbol{S}\boldsymbol{B}\boldsymbol{A}^{-1}\beta)\end{aligned} \tag{B.23}$$

Selecting $\boldsymbol{\mathcal{W}} = (\boldsymbol{A}_o\boldsymbol{P}_1\boldsymbol{P}_2^{-1})^{-1} = \boldsymbol{P}_2\boldsymbol{P}_1^{-1}\boldsymbol{A}_o^{-1}$ gives

$$\boldsymbol{\mathcal{L}}_v = \boldsymbol{P}_2\boldsymbol{P}_1^{-1}\boldsymbol{A}_o^{-1}\boldsymbol{\alpha}\boldsymbol{A}^{-1} - \mathbf{I} \ . \tag{B.24}$$

B.2.6 Desaturation transient dynamics: OBSAWC

Since the OBSAWC can be obtained by selecting $\boldsymbol{P}_1 \equiv \boldsymbol{P}_2$ ($= \mathbf{I}$ e.g.) in the GLAWC structure, we here use the results derived in Section B.2.7 for the GLAWC. Then, it is straightforward to show that the output y can be expressed as

$$\begin{aligned} y &= y_l + \boldsymbol{\mathcal{H}}_\delta \delta \\ \boldsymbol{\mathcal{H}}_\delta &= \boldsymbol{B}\boldsymbol{\alpha}^{-1}\boldsymbol{A}_o \end{aligned} \tag{B.25}$$

when using the OBSAWC. See Section B.2.7.

B.2.7 Desaturation transient dynamics: GLAWC

We will show that plant output y can be expressed in the following way:

$$\begin{aligned} y &= y_l + \boldsymbol{\mathcal{H}}_\delta \delta \\ \boldsymbol{\mathcal{H}}_\delta &= \boldsymbol{B}\boldsymbol{\alpha}^{-1}\boldsymbol{\mathcal{W}}^{-1} = \boldsymbol{B}\boldsymbol{\alpha}^{-1}\boldsymbol{A}_o\boldsymbol{P}_1\boldsymbol{P}_2^{-1} . \end{aligned} \tag{B.26}$$

In order to keep the expressions clear, we will use the controller representation (4.15), and thereby the transfer function $\boldsymbol{\mathcal{W}} = \boldsymbol{P}_2\boldsymbol{P}_1^{-1}\boldsymbol{A}_o^{-1}$, in the derivation.

Recall that the plant output y was expressed as

$$\begin{aligned} y &= \boldsymbol{B}\boldsymbol{A}^{-1}v + \boldsymbol{B}\boldsymbol{A}^{-1}\beta \\ v &= \psi(u) \end{aligned} \tag{B.27}$$

when we first introduced the description of the plant in (2.1) of Chapter 2.

By the use of the last line of (B.23), i.e.,

$$u = -(\boldsymbol{\mathcal{W}}\boldsymbol{\alpha}\boldsymbol{A}^{-1} - \mathbf{I})v + \boldsymbol{\mathcal{W}}(\boldsymbol{T}r - \boldsymbol{S}\boldsymbol{B}\boldsymbol{A}^{-1}\beta) , \tag{B.28}$$

we have that

$$u = -\boldsymbol{\mathcal{W}}\boldsymbol{\alpha}\boldsymbol{A}^{-1}v + v + \boldsymbol{\mathcal{W}}(\boldsymbol{T}r - \boldsymbol{S}\boldsymbol{B}\boldsymbol{A}^{-1}\beta) . \tag{B.29}$$

Subtracting v from both sides, and then multiply by -1, gives that

$$-(u - v) = \delta = \boldsymbol{\mathcal{W}}\boldsymbol{\alpha}\boldsymbol{A}^{-1}v - \boldsymbol{\mathcal{W}}(\boldsymbol{T}r - \boldsymbol{S}\boldsymbol{B}\boldsymbol{A}^{-1}\beta) \tag{B.30}$$

or, equivalently,

$$\boldsymbol{\mathcal{W}}\boldsymbol{\alpha}\boldsymbol{A}^{-1}v = \delta + \boldsymbol{\mathcal{W}}(\boldsymbol{T}r - \boldsymbol{S}\boldsymbol{B}\boldsymbol{A}^{-1}\beta) . \tag{B.31}$$

Multiplying both sides from the left by first $\boldsymbol{\mathcal{W}}^{-1}$ and then by $\boldsymbol{\alpha}^{-1}$ gives that

$$\boldsymbol{A}^{-1}v \;=\; \boldsymbol{\alpha}^{-1}\boldsymbol{\mathcal{W}}^{-1}\delta + \boldsymbol{\alpha}^{-1}(\boldsymbol{T}r - \boldsymbol{SBA}^{-1}\beta)\;. \tag{B.32}$$

By substituting $\boldsymbol{A}^{-1}v$ in (B.27) by the expression in (B.32) we have that the output y can be described by

$$\begin{aligned} y \;&=\; \boldsymbol{BA}^{-1}v + \boldsymbol{BA}^{-1}\beta \\ &=\; \boldsymbol{B\alpha}^{-1}\boldsymbol{\mathcal{W}}^{-1}\delta + \boldsymbol{B\alpha}^{-1}\boldsymbol{T}r - \boldsymbol{B\alpha}^{-1}\boldsymbol{SBA}^{-1}\beta + \boldsymbol{BA}^{-1}\beta\;. \end{aligned} \tag{B.33}$$

According to the definition of the linear closed loop system output y_l in (2.3), it remains to show that the following holds for the "β-term":

$$\begin{aligned} &- \boldsymbol{B\alpha}^{-1}\boldsymbol{SBA}^{-1}\beta + \boldsymbol{BA}^{-1}\beta \\ &=\; \boldsymbol{B\alpha}^{-1}\boldsymbol{R}\beta\;. \end{aligned} \tag{B.34}$$

We begin by extracting $\boldsymbol{B\alpha}^{-1}$ to the left as

$$\boldsymbol{B\alpha}^{-1}(\boldsymbol{\alpha A}^{-1} - \boldsymbol{SBA}^{-1})\;. \tag{B.35}$$

Since $\boldsymbol{\alpha} = \boldsymbol{RA} + \boldsymbol{SB}$, the β-term can be written as

$$\begin{aligned} &\boldsymbol{B\alpha}^{-1}(\boldsymbol{RAA}^{-1} + \boldsymbol{SBA}^{-1} - \boldsymbol{SBA}^{-1}) \\ &= \boldsymbol{B\alpha}^{-1}\boldsymbol{R}\;. \end{aligned} \tag{B.36}$$

This ends the derivation.

B.2.8 Realization of α

The derivation will be carried out for the discrete time case where polynomials are given in the forward-shift operator q.

The nominal controller denominator $\boldsymbol{R}(q)$ is then given by

$$\boldsymbol{R}(q) \;=\; \mathbf{R}_n q^n + \mathbf{R}_{n-1}q^{n-1} + \ldots + \mathbf{R}_0 \tag{B.37}$$

and the plant denominator $\boldsymbol{A}(q)$ is given by

$$\boldsymbol{A}(q) \;=\; \mathbf{A}_m q^m + \mathbf{A}_{m-1}q^{m-1} + \ldots + \mathbf{A}_0 \tag{B.38}$$

respectively. If the plant is strictly causal/proper, then the closed loop denominator $\boldsymbol{\alpha}(q)$ is then given by

$$\boldsymbol{\alpha}(q) \;=\; \mathbf{R}_n\mathbf{A}_m q^{n+m} + \ldots + (\mathbf{R}_0\mathbf{A}_0 + \mathbf{S}_0\mathbf{B}_0). \tag{B.39}$$

Notice that neither $\boldsymbol{B}(q)$ nor $\boldsymbol{S}(q)$ enter into the leading coefficient matrix of $\boldsymbol{\alpha}(q)$. This is a consequence of having a strictly causal/proper plant model.

The polynomial matrices $\boldsymbol{\alpha}_1(q),\ \boldsymbol{\alpha}_2(q)$ in factorization $\boldsymbol{\alpha}_1(q)\boldsymbol{\alpha}_2(q) = \boldsymbol{\alpha}(q)$ can then be selected as

$$
\begin{aligned}
\boldsymbol{\alpha}_1(q) &= \mathbf{R}_n q^n + \ldots + \boldsymbol{\alpha}_1 \\
\boldsymbol{\alpha}_2(q) &= \mathbf{A}_m q^m + \ldots + \boldsymbol{\alpha}_2 \qquad \text{(B.40)} \\
&\qquad ;. \qquad \text{(B.41)}
\end{aligned}
$$

Hence, the choice $\boldsymbol{A}_o(q) = \boldsymbol{\alpha}_1(q)$ in (4.20) is consistent with the Requirement 5.2.

According to (4.20) and the fact that $\boldsymbol{\alpha}_2(q)$ has the same leading coefficient matrix as $\boldsymbol{A}(q)$ puts the requirement on $\boldsymbol{P}_1(q)$ to also have the same leading coefficient matrix as $\boldsymbol{A}(q)$. This, in turn, restricts $\boldsymbol{P}_2(q)$ to also have the same leading coefficient matrix as $\boldsymbol{A}(q)$. This is due to the Requirement 5.3.

B.3 Derivations in Chapter 5

B.3.1 Diagonal loop $\boldsymbol{H}_2$-optimal design

To keep expressions clear we will denote the polynomial (polynomial matrix) $\boldsymbol{P}_2$ simply by $\boldsymbol{P}$. By insertion of the constant diagonal weight matrix

$$
\mathbf{Q} = \begin{pmatrix} \sqrt{\rho_1} & & \mathbf{0} \\ & \ddots & \\ \mathbf{0} & & \sqrt{\rho_m} \end{pmatrix} \qquad \text{(B.42)}
$$

into (5.29), the criterion can be rewritten as

$$
J = \left\| \boldsymbol{B}\boldsymbol{P}^{-1} \right\|_2^2 + \left\| \mathbf{Q}\left(\boldsymbol{A}\boldsymbol{P}^{-1} - \mathbf{I}\right) \right\|_2^2 \qquad \text{(B.43)}
$$

where

$$
\mathbf{Q}\left(\boldsymbol{A}\boldsymbol{P}^{-1} - \mathbf{I}\right) = \operatorname{diag}\left\{ \sqrt{\rho_j}\left(\frac{A_j}{P_j} - 1\right) \right\} \qquad \text{(B.44)}
$$

$$
\boldsymbol{B}\boldsymbol{P}^{-1} = \begin{pmatrix} \dfrac{\boldsymbol{B}_1}{P_1} & \ldots \dfrac{\boldsymbol{B}_m}{P_m} \end{pmatrix} \qquad \text{(B.45)}
$$

and where $\boldsymbol{B}_1 \dots \boldsymbol{B}_m$ are the columns of $\boldsymbol{B}$. Now, (B.44) and (B.45) allow us to express (B.43), using *Parsevals formula*, as

$$\begin{aligned}
J &= \left\| \begin{pmatrix} \frac{\boldsymbol{B}_1}{P_1} & \frac{\boldsymbol{B}_2}{P_2} & \dots & \frac{\boldsymbol{B}_m}{P_m} \end{pmatrix} \right\|_2^2 + \left\| \operatorname{diag}\left\{ \sqrt{\rho_j} \left(\frac{A_j}{P_j} - 1 \right) \right\} \right\|_2^2 \\
&= \frac{1}{2\pi} \oint_{|z|=1} \operatorname{tr} \left\{ \begin{pmatrix} \frac{\boldsymbol{B}_1}{P_1} & \frac{\boldsymbol{B}_2}{P_2} & \dots & \frac{\boldsymbol{B}_m}{P_m} \end{pmatrix} \begin{pmatrix} \frac{\boldsymbol{B}_1}{P_1} & \frac{\boldsymbol{B}_2}{P_2} & \dots & \frac{\boldsymbol{B}_m}{P_m} \end{pmatrix}^* \right\} \frac{dz}{z} \\
&+ \frac{1}{2\pi} \oint_{|z|=1} \operatorname{tr} \left\{ \left(\operatorname{diag}\left\{ \sqrt{\rho_j} \left(\frac{A_j}{P_j} - 1 \right) \right\} \right) \left(\operatorname{diag}\left\{ \sqrt{\rho_j} \left(\frac{A_j}{P_j} - 1 \right) \right\} \right)^* \right\} \frac{dz}{z} \\
&= \frac{1}{2\pi} \oint_{|z|=1} \operatorname{tr} \left\{ \frac{\boldsymbol{B}_1 \boldsymbol{B}_1^*}{P_1 P_1^*} + \frac{\boldsymbol{B}_2 \boldsymbol{B}_2^*}{P_2 P_2^*} + \dots + \frac{\boldsymbol{B}_m \boldsymbol{B}_m^*}{P_m P_m^*} \right\} \frac{dz}{z} \\
&+ \frac{1}{2\pi} \oint_{|z|=1} \operatorname{tr} \left\{ \operatorname{diag}\left\{ \rho_j \left(\frac{A_j}{P_j} - 1 \right) \left(\frac{A_j}{P_j} - 1 \right)^* \right\} \right\} \frac{dz}{z} \quad .
\end{aligned} \tag{B.46}$$

The expression (B.46) can be decomposed into a sum of m separate pairs of integrals

$$J = \sum_{j=1}^{m} \left(\frac{1}{2\pi} \oint_{|z|=1} \frac{\operatorname{tr}\left\{ \boldsymbol{B}_j \boldsymbol{B}_j^* \right\}}{P_j P_j^*} \frac{dz}{z} + \frac{1}{2\pi} \oint_{|z|=1} \rho_j \left(\frac{A_j}{P_j} - 1 \right) \left(\frac{A_j}{P_j} - 1 \right)^* \frac{dz}{z} \right) \tag{B.47}$$

Each term of the sum is influenced by a separate ρ_j and a separate P_j for $j = 1, 2 \dots m$. Thus, the criterion (B.43) can be rewritten as a sum of m quadratic criteria which may be minimized separately with respect to P_j, i.e.

$$J = \sum_{j=1}^{m} J_j \quad , \tag{B.48}$$

where J_j is given by

$$J_j = \frac{1}{2\pi} \oint_{|z|=1} \frac{\sum_{i=1}^{p} B_{ij} B_{ij}^*}{P_j P_j^*} \frac{dz}{z} + \frac{1}{2\pi} \oint_{|z|=1} \rho_j \left(\frac{A_j}{P_j} - 1 \right) \left(\frac{A_j}{P_j} - 1 \right)^* \frac{dz}{z} \quad . \tag{B.49}$$

In (B.49) we used that the numerator inside the first integral in (B.47) can be expressed as

$$\operatorname{tr}\{\boldsymbol{B}_j \boldsymbol{B}_j^*\} = \sum_{i=1}^{p} B_{ij} B_{ij}^* \tag{B.50}$$

where p is the number of process outputs and B_{ij} is the ijth element of $\boldsymbol{B}$.

Minimizing (B.48) will thus be the same as minimizing m separate criteria, each of which will be minimized by solving a spectral factorization. Minimizing (B.43) with respect of the elements of $\boldsymbol{P}$ for a given matrix $\mathbf{Q}$, will consequently require m scalar spectral factorizations. The optimal choice of the stable transfer operator $P_j(q)$ is then obtained from the scalar rational spectral factorization equation,

$$\boxed{rP_jP_j^* = \textstyle\sum_{i=1}^{p} B_{ij}B_{ij}^* + \rho_j A_j A_j^*} \tag{B.51}$$

which has to be solved for $j = 1, 2....m$, where m is the number of process inputs.

Bibliography

[1] T. Kailath, *Linear Systems*. Englewood Cliffs, NJ: Prentice-Hall, Inc, 1980.

[2] K. J. Åström and B. Wittenmark, *Computer Controlled Systems: Theory and Design*. Englewood Cliffs, NJ: Prentice-Hall, Inc, second edition, 1984.

[3] K. J. Åström and B. Wittenmark, *Computer Controlled Systems: Theory and Design*. Upper Saddle River, NJ: Prentice-Hall, Inc, third edition, 1997.

[4] G. F. Franklin, J. D. Powell, and M. Workman, *Digital Control of Dynamic Systems*. Menlo Park, CA: Addison Wesley Longman, Inc, third edition, 1997.

[5] G. C. Goodwin, S. F. Graebe, and M. E. Salgado, *Control System Design*. Upper Saddle River, NJ: Prentice-Hall, Inc, 2001.

[6] G. F. Franklin, J. D. Powell, and A. Emami-Naeini, *Feedback Control of Dynamic Systems*. Upper Saddle River, NJ: Prentice-Hall, Inc, fourth edition, 2002.

[7] K. Ogata, *Modern Control Engineering*. Upper Saddle River, NJ: Prentice-Hall, Inc, fourth edition, 2002.

[8] H. Kwakernaak and R. Sivan, *Linear Optimal Control Systems*. New York: Wiley, 1972.

[9] M. J. Grimble and M. A. Johnson, *Optimal Control and Stochastic Estimation*, vol. 1: Wiley Ltd, 1988.

[10] M. J. Grimble and M. A. Johnson, *Optimal Control and Stochastic Estimation*, vol. 2: Wiley Ltd, 1988.

[11] B. D. O. Anderson and J. B. Moore, *Optimal Control: Linear Quadratic Methods*. Englewood Cliffs, NJ: Prentice-Hall, Inc, 1989.

[12] J. M. Maciejowski, *Multivariable Feedback Design*: Addison-Wesley Ltd, 1989.

[13] S. Skogestad and I. Postlethwaite, *Multivariable Feedback Control*. West Sussex, England: Wiley, 1996.

[14] K. Åström and T. Hägglund, *PID Controllers: Theory, Design, and Tuning*. Research Triangle Park, NC: Instrument Society of America, 1995.

[15] D. S. Bernstein and A. N. Michel, "Chronological bibliography on saturating actuators," *Int. Journal of Robust and Nonlinear Control*, vol. 5, pp. 375–380, 1995.

[16] A. Stoorvogel and A. Saberi, "Special issue on control problems with constraints," *Int. Journal of Robust and Nonlinear Control*, vol. 9, 1999.

[17] J. E. Gibson, *Nonlinear Automatic Control*. New York, NJ: McGraw-Hill, 1963.

[18] K. S. Narendra and J. H. Taylor, *Frequency Domain Criteria for Absolute Stabity*. New York and London: Academic Press, 1973.

[19] D. P. Atherton, *Nonlinear Control Engineering*. Molly Millar's Lane, Wokingham, Berks: Van Nostrand Reinhold Company Limited, 1975.

[20] I. Horowitz, "A synthesis theory for a class of saturating systems," *Int. Journal of Control*, vol. 38, pp. 169–187, 1983.

[21] P. Gutman and P. Hagander, "A new design of constrained controllers for linear systems," *IEEE Transactions on Automatic Control*, vol. 30, pp. 22–33, 1985.

[22] H. Krishnan and M. Vidyasagar, "Bounded input feedback control of linear systems with application to the control of a flexible beam," in *Proceedings of 27th Conference on Decision and Control*, Austin, TX, 1988, pp. 1619–1626.

[23] P. Kapasouris, M. Athans, and G. Stein, "Design of feedback control systems for stable plants with saturating actuators," in *Proceedings of 27th Conference on Decision and Control*, Austin, TX, 1988, pp. 469–479.

[24] A. R. Teel, "Global stabilization and restricted tracking for multiple integrators with bounded controls," *Syst. Contr. Lett.*, vol. 18, pp. 165–171, 1992.

[25] A. R. Teel, "Linear systems with input nonlinearities: global stabilization by scheduling a family of H_∞-type controllers," *Int. Journal of Robust and Nonlinear Control*, vol. 5, pp. 399–411, 1995.

[26] D. S. Bernstein and W. M. Haddad, "Nonlinear controllers for positive real systems with arbitrary input nonlinearities," *IEEE Transactions on Automatic Control*, vol. 39, pp. 1513–1517, 1994.

[27] A. Saberi, Z. Lin, and A. R. Teel, "Control of linear systems with saturating actuators," *IEEE Transactions on Automatic Control*, vol. 41, pp. 368–378, 1996.

[28] H.K. Khalil, *Nonlinear Systems*. Upper Saddle River, NJ: Prentice-Hall, Inc, 1996.

[29] C. Gökcek, P. T. Kabamba, and S. M. Meerkov, "LQR/LQG theory for systems with saturating actuators," *IEEE Transactions on Automatic Control*, vol. 46, pp. 1529–1542, 2001.

[30] T. Hu and Z. Lin, *Control systems with actuator saturation: analysis and design*. Boston: Birkhäuser, 2001.

[31] S. J. Qin and T. A. Badgwell, "An overview of industrial model predictive control technology," *Chemical Process Control - Amer. Inst. Chem. Eng.*, vol. 93, pp. 232–256, 1997.

[32] P. D. Roberts, "A brief overview of model predictive control," in *IEE Two-Day Workshop (Ref. No. 1999/C95)*, April 1999.

[33] R. R. Bitmead, M. Gevers, and V. Wertz, *Adaptive Optimal Control: The Thinking Man's GPC*. Australia: Prentic-Hall, 1990.

[34] A. Bemporad, F. Borelli, and M. Morari, "Model predictive control based on linear programming-the explicit solution," *IEEE Transactions on Automatic Control*, vol. 47, pp. 1974–1985, 2002.

[35] J. A. De Doná and G. C. Goodwin, "Elucidation of the state-space regions wherein model predictive control and anti-windup strategies achieve identical control policies," in *Proceedings of the ACC*, Chicago, Illinois, June 2000, pp. 1924–1928.

[36] G. F. Wredenhagen and P. R. Belanger, "Piecewise-linear LQ control for systems with input constraints," *Automatica*, vol. 30, pp. 403–416, 1994.

[37] İ. E. Köse and F. Jabbari, "Scheduled controllers for linear systems with bounded actuators," *Automatica*, vol. 39, pp. 1377–1387, 2003.

[38] H. A. Fertik and C. W. Ross, "Direct digital control algorithm with anti-windup feature," *Instrument Society of America*, vol. Preprint, no. 10-1-1CQS-67, 1967.

[39] R. Hanus, "A new technique for preventing control windup," *Journal A*, vol. 21, no. 1, pp. 15–20, 1980.

[40] R. Hanus, "The conditioned control: a new technique for preventing windup nuisances," in *Proceedings of the International Federation for Information Processing - Automation for Safety in Shipping and Offshore Petroleum Operations*, Trondheim, 1980, pp. 221–224.

[41] A. H. Glattfelder and W. Schaufelberger, "Stability analysis of single loop control systems with saturation and antireset-windup circuits," *IEEE Transactions on Automatic Control*, vol. 28, pp. 1074–1081, 1983.

[42] J. C. Doyle, R. S. Smith, and D. F. Enns, "Control of plants with input saturation nonlinearities," in *Proceedings of the 1987 American Control Conference*, Minneapolis, MN, 1987, pp. 1034–1039.

[43] K. J. Åström and L. Rundqwist, "Integrator windup and how to avoid it," in *Proceedings of the 1989 American Control Conference*, 1989.

[44] K. S. Walgama and J. Sternby, "Inherent observer property in a class of anti-windup compensators," *Int. Journal of Control*, vol. 52, pp. 705–724, 1990.

[45] S. Rönnbäck, K. S. Walgama, and J. Sternby, "An extension to the generalized anti-windup compensator," in *Proceedings of the 13th IMACS World Congress on Computation and Applied Mathematics,*, Dublin, Ireland,3,, 1991, pp. 1192–1196.

[46] L. Rundqwist. *Anti-reset windup for PID controllers*, PhD thesis, Lund Institute of Technology, Lund, Sweden, 1991.

[47] M. Sternad and S. Rönnbäck, "A frequency domain approach to anti-windup compensator design,", Technical report, Department of Technology, Uppsala Universitet, Uppsala, Sweden, 1993, Technical report: UPTEC 93024R.

[48] M. V. Kothare, M. Morari P. J. Campo, and C.N. Nett, "A unified framework for the study of anti-windup designs," *Automatica*, vol. 30, pp. 1869–1883, 1994.

[49] J. Öhr, *Systematic Anti-Windup Compensator Design for Multivariable Systems*: Department of Technology, Uppsala Universitet, Uppsala, Sweden, 1995, M.Sc. Thesis, Technical report: UPTEC 95150E.

[50] J. Öhr, M. Sternad, and A. Ahlén, "Anti-windup compensators for multivariable systems," in *Proceedings of the Fourth ECC*, Brussels, Belgium., July 1997.

[51] A. R. Teel and N. Kapoor, "Uniting local and global controllers," in *Proceedings of the Fourth ECC*, Brussels, Belgium., July 1997.

[52] A. R. Teel and N. Kapoor, "The ℓ_2 - anti-windup problem: Its definition and solution.," in *Proceedings of the Fourth ECC*, Brussels, Belgium., July 1997.

[53] C. Edwards and I. Postlethwaite, "Anti-windup schemes with closed-loop stability considerations," in *Proceedings of the Fourth ECC*, Brussels, Belgium., July 1997.

[54] N. Kapoor, A. R. Teel, and P. Daoutidis, "An anti-windup design for linear systems with input saturation," *Automatica*, vol. 34, pp. 559–574, 1998.

[55] P. Hippe and C. Wurmthaler, "Systematic closed-loop design in the presence of input saturations," *Automatica*, vol. 35, pp. 689–695, 1999.

[56] S. Rönnbäck. *Linear Control of Systems with Actuator Constraints*, PhD thesis, Luleå Univerity of Technology, Luleå, Sweden, 1993.

[57] M. V. Kothare. *Control of Systems Subject to Constraints*, PhD thesis, California Institute of Technology, Pasadena, CA, USA, 1997.

[58] M. Bak. *Control of Systems with Constraints*, PhD thesis, Technical University of Denmark, Lyngby, Denmark, 2000.

[59] R. Hanus, M. Kinnaert, and J.L. Henrotte, "Conditioning technique, a general anti-windup and bumpless transfer method," *Automatica*, vol. 23, pp. 729–739, 1987.

[60] K. S. Walgama, S. Ronnbäck, and J. Sternby, "Generalization of conditioning technique for anti-windup compensators,", vol. 139, no. 2, pp. 109–118, 1992.

[61] P. J. Campo and M. Morari, “Robust control of processes subject to saturation nonlinearities,” *Computers & Chemical Engineering*, vol. 14, no. 4/5, pp. 343–358, 1990.

[62] S. Rönnbäck, K. S. Walgama, and J. Sternby, “An extension to the generalized anti-windup compensator,” *In P. BOBNE et al., Eds., Mathematics of the Analysis and Design of Process Control*, pp. 275–285, 1992.

[63] J. Öhr, S. Rönnbäck, and M. Sternad, “h_2-optimal anti-windup performance in siso control systems,” in *Proceedings of the SIAM’98*, Jacksonville, FL, 1998.

[64] S. F. Graebe and A. L. B. Ahlén, “Dynamic transfer among alternative controllers and its relation to anti-windup controller design,” *IEEE Transactions on Control Systems Technology*, vol. 4, pp. 92–99, 1996.

[65] C. Edwards and I. Postlethwaite, “Anti-windup and bumpless transfer schemes,” *Automatica*, vol. 34, pp. 199–210, 1998.

[66] L. Zaccarian and A. R. Teel, “A common framework for anti-windup, bumpless transfer and reliable designs,” *Automatica*, vol. 38, pp. 1735–1744, 2002.

[67] V. G. Rao and D. S. Bernstein, “Naive control of the double integrator,” *Control Systems Magazine*, vol. 21, pp. 86–97, 2001.

[68] A. Lewis, *Personal Communication*. Bromma Conquip, Vällingby, Sweden, 2003.

[69] L. Rundqwist and K. Ståhl-Gunnarsson, “Phase compensation of rate limiters in unstable aircraft,” in *Proceedings of the 1996 IEEE International Conference on Control Applications,*, Dearborn, MI, September 1996, pp. 19–24.

[70] R. H. Middleton and G. C. Goodwin, *Digital Control and Estimation - A Unified Approach*. London: Prentice-Hall International, 1990.

[71] L. Rundqwist, *Personal Communication*. SAAB Military Aircraft, Linköping, Sweden, 2002.

[72] S. Skogestad, M. Morari, and J. C. Doyle, “Robust control of ill-conditioned plants: High-purity distillation,” *IEEE Transactions on Automatic Control*, vol. 33, no. 12, pp. 1092–1105, 1988.

[73] K. J. Åström and B. Wittenmark, *Adaptive Control*: Addison-Wesley, second edition, 1995.

[74] P. Lundqvist, *Personal Communication*. NAF AB, Linköping, Sweden, 2000.

[75] A. Bemporad, A. R. Teel, and L. Zaccarian, "ℓ_2 - anti-windup via receding horizon optimal control," in *Proceedings of the ACC*, Anchorage, AK, May 2002.

[76] A. Bemporad, M. Morari, V. Dua, and E.N. Pistikopoulos, "The explicit linear quadratic regulator for constrained systems," *Automatica*, vol. 38, pp. 3–20, 2002.

[77] M. J. Grimble, "Relationship between polynomial and state-space solutions of the optimal regulator problem," *Systems & Control Letters*, vol. 8, pp. 411–416, 1987.

[78] PolyX, *Online*. www.polyx.com, 2003.

[79] J-J. E. Slotine and W. Li, *Applied Nonlinear Control*. Englewood Cliffs, NJ: Prentice-Hall, Inc, 1991.

[80] K. S. Walgama and J. Sternby, "Conditioning technique for multiinput-multioutput processes with input saturation," *Control Theory and Applications, IEE Proceedings D [see also IEE Proceedings-Control Theory and Applications]*, vol. 140, no. 4, pp. 231–242, 1993.

[81] J. C. Doyle, "Robustness with observers," *IEEE Transactions on Automatic Control*, vol. 24, pp. 607–611, 1979.

[82] J. Öhr, "Control of a paper machine headbox with saturating inputs," in *Proceedings of the First Europoly Workshop on Polynomial Systems Theory and Applications*, Glasgow, UK, April 1999, pp. 127–129.

[83] J. E. Larsson, *On Paper Machine Headbox Control*: Division of Automatic Control, Luleå University of Technology, Luleå, Sweden, 1997, Lic. Thesis.

[84] E. P. Ryan, *Optimal Relay and Saturating Control System Synthesis*. Stevenage, UK, and New York: IEE, Peter Peregrinus Ltd, 1982.